Application of micro-computed tomography towards a taxonomic and palaeobiological reassessment of Huxley and Wright's (1867) tetrapods from the Jarrow Assemblage (Langsettian, Pennsylvanian), Co. Kilkenny, Ireland.

Ph.D. Thesis

2020

Aodhán Ó Gogáin

Trinity College Dublin
Coláiste na Tríonóide, Baile Átha Cliath
The University of Dublin

I declare that this thesis has not been submitted as an exercise for a degree at this or any other university and it is entirely my own work.

I agree to deposit this thesis in the University's open access institutional repository or allow the library to do so on my behalf, subject to Irish Copyright Legislation and Trinity College Library conditions of use and acknowledgement.

Aodhán Ó Gogáin

Signature_____

Summary.

The Jarrow assemblage of Co. Kilkenny, Ireland preserves a diverse assortment of fish and tetrapods from the earliest Pennsylvanian (Langsettian). The Pennsylvanian was an important period in tetrapod evolution, during which many forms were evolving to occupy new ecological niches. This makes the Jarrow assemblage an important fossil site for investigating early tetrapod evolution and ecology as it preserves the earliest example of a coal swamp assemblage. But despite its importance, it is relatively poorly understood compared to later similar assemblages at Linton, Ohio, Nýřany, Czech Republic and Newsham, England. While fossils from all four assemblages are highly compressed, specimens from Jarrow stand out as being poorer in appearance. In unprepared specimens, the boundary between the body fossil and the matrix is difficult to make out. Even in manually prepared specimens this is the case. Additionally, many specimens have been degraded as a result of pyrite disease.

The application of micro-computed tomography (µCT) has become the normal method for aiding in descriptive palaeontology. Particularly it has had widescale use when investigating early tetrapods in recent years. X-ray imaging has been used on specimens from Jarrow, but no papers applying µCT to these specimens have been published to date. The main body of this thesis will deal with applying µCT to five of the seven tetrapods originally described by Huxley and Wright from Jarrow in 1867, in order to redescribe their morphology.

Chapter 2 of the thesis deals with the depositional model and palaeoecology of the Jarrow assemblage. This is in order to better understand the sort of environment the tetrapods lived in and were preserved in. It also provides a list of all identified tetrapods and fish from the assemblage (including tetrapods identified in this thesis). Chapter 3 looks at the preservation of the bone material and how that might affect µCT results.

Chapters 4, 5, 6 and 7 form the main body of the thesis and included all the descriptive work aided by the µCT slices. Chapter 4 focuses on the aïstopod *Ophiderpeton brownriggii* and provides a detailed description of several specimens. A new species of aïstopod is described from one of the syntypes of *O. brownriggii* as *Peisterpeton milnerorum*. Huxley's second aïstopod species, "*Dolichosoma*" *emersoni* is described from a single specimen in Chapter 5. Its troublesome taxonomic issues are resolved and is formally placed into the genus *Dolichosomatites*. Chapter 6 deals with the Urocordylidae nectrideans from Jarrow, *Urocordylus wandesfordii* and *Lepterpeton dobbsii*. Additional cranial and mandibular elements are identified in each. The holotype of *Ichthyerpeton bradleyae* is redescribed in

Chapter 7. Issues of the affinity between *I. bradleyae* and either colosteids or the embolomeres are resolved, with an association between both groups not being supported.

Chapter 8 acts as conclusion chapter and places this study in a larger context highlighting both the benefits and limitations that applying µCT to Jarrow specimens has for understanding early tetrapod evolution and ecology. Despite certain limitations, it is hoped this study will aid in our understanding of the problematic Jarrow assemblage.

Acknowledgments.

A thesis is never the work of a single individual, and in this case the list of thanks I owe is near endless. This is just a brief mention, which cannot convey my full gratitude.

Firstly, I'd like to thank Matthew Parkes who was always willing to give me access and borrow any of the Jarrow material from the NMI, not to forget the many lifts to the museum storage in Swords. I'd also like to thank the geology technicians at the Department of Geology, TCD. Frank, Maura, Noel and Cora were always willing to help in whatever way they could to make sure things went smoothly. Mags Duncan gets a special thanks for all the palaeo-talk.

Thomas Davies and Brett Clark are thanked for carrying out many of the CT scans in this work at the University of Bristol and the NHM respectively. I cannot mention CT scanning without mentioning Richard Coull who got me on two CT training courses and allowed me a free period of access to the CT scanner in the TCD Amber Lab. I'm for ever grateful for the experience and data I got from this. While on the point I must also thank Balz Kamber who put me in contact with the Amber lab and who also encouraged looking at geochemistry of the fossils. I'd also like to thank David Chew who allowed me access to equipment to carry this out.

I'd like to thank Andrew and Angela Milner who were always happy to answer my emails and meet me in person to discuss the Jarrow biota. This was hugely beneficial.

A huge thanks is owed to Una Farrell, who helped me learn about running the museum and who made demonstrating enjoyable. I'd also like to thank my PhD panel members Robbie Goodhue and Chris Nicholas.

The Department of Geology at Trinity has a bustling PhD community and without these I would not have made it through my PhD. To mention a few, I'm forever grateful to Maurice, Hilde, Tadhg, Foteni, Siobhán, Eoghan, Paul, Clare, Caro, James, Lucy and Niamh. You all made every day more enjoyable than the next. I would like to specially thank Brendan and Gary who helped me with the geochemical work.

I am most grateful to my supervisor, Patrick N. Wyse Jackson. Ever since I did my undergraduate course at Trinity he has acted as a supervisor and a mentor, encouraging me to pursue palaeontological research. I was delighted to have the opportunity to return to Trinity to work with him on a project I found highly interesting. Without Patrick's guidance, this project would not have even been able to get off its feet.

I would also like to thank Marcello Ruta and George Sevastopulo who examined my work and provided helpful and constructive criticisms and made valuable suggestions. This thesis is much richer as a result of their help,

Finally, I'd like to thank my father and late mother Ray and Martha Goggin, who have always encouraged and fostered my love of the natural world.

Table of Contents.

Chapter 1: Introduction and aims.

1.1 History of Research

Coal mining in the Jarrow Coal Seam began in 1853 and since that time vertebrate fossils - "large lizards" - accompanied by plant fossils were reported (Baily, 1881; Milner, 2019). Vertebrate fossils were first collected and brought to the scientific community's attention in 1864 by William Bookey Brownrigg (Wyse Jackson *et al*., 2011) who noted at least six forms of what were termed 'reptiles' (Brownrigg, 1865). However, Brownrigg's claim and contribution to the fossil assemblage was side-lined by the then Professor of Zoology at Trinity College Dublin, E.P. Wright, who invited T.H. Huxley from London to describe the specimens (DeArce *et al.,* 2011). Prior to Huxley viewing the Jarrow specimens, William Hellier Baily, who was Acting Palaeontologist working at the Geological Survey of Ireland, produced a watercolour figure of the tetrapod *Keraterpeton galvani* in November 1865 (Wyse Jackson and Parkes, 2009, fig. 11). Etheridge (1866) and Wright and Huxley (1866) reported, in the same volume of the *Geological Magazine*, on the presence of new genera of fish and tetrapods (Table 1.1), but did not accompany them with figures or thorough descriptions. Therefore, although many of the tetrapods were first described from Jarrow by Huxley and Wright (1867), the first use of many of the taxonomic names are either in Etheridge (1866) (who credited Huxley for naming the taxa) or in Wright and Huxley (1866), with the former having precedence. The first figured description of the Jarrow specimens was by Huxley and Wright (1867), and included seven species of tetrapod/tetrapodomorphs and alluded to three other tetrapods, two of which were named, and a genus of sarcopterygian. Despite being dated 1867, Huxley and Wright's paper did not appear in print until 1871. The naming of one of the figured tetrapods in Huxley and Wright (1867), *K. galvani*, has generally been credited to Huxley, yet this could not have been the case because Baily used this name for his watercolour figure. Therefore, it is likely that credit for that name really lies with Baily or Brownrigg, the latter of whom appears to have successfully suggested names for the tetrapods described by Huxley (DeArce *et al*., 2011) Initially Brownrigg appeared content with the arrangement that Huxley would describe the specimens (Wyse Jackson *et al.,* 2011), yet the fact that he was cut out of the picture when it came to writing up the Jarrow fauna made him relinquish geology and in 1870 he sold his collection of Jarrow material to the Natural History Museum, London (DeArce *et al.,* 2011). Although the early years of research on the Jarrow tetrapods give a good insight into the history of interactions and dilemmas between competing naturalists, it has hampered resolving the

taxonomy of these tetrapods, with the genera and species variously being credited to Etheridge (1866), Wright and Huxley (1866) and Huxley and Wright (1867) (Table 1.1).

Jarrow Taxa by 1867	First Publication of Genus	First Publication of Species
Keraterpeton galvani	Etheridge 1866	Wright and Huxley 1866
Urocordylus wandesfordii	Wright and Huxley 1866	Wright and Huxley 1866
Lepterpeton dobbsii	Etheridge 1866	Wright and Huxley 1866
Ophiderpeton brownriggii	Etheridge 1866	Wright and Huxley 1866
Dolichosoma emersoni	Huxley and Wright 1867	Huxley and Wright 1867
Ichthyerpeton bradleyae	Etheridge 1866	Wright and Huxley 1866
Erpetocephalus rugosus	Huxley and Wright 1867	Huxley and Wright 1867
Discospondylus sp.	Huxley and Wright 1867	
Brachyscelis sp.	Huxley and Wright 1867	
Campylopleuron sp.	Etheridge 1866	

Table 1.1. The seven tetrapods described by Huxley (*Keraterpeton galvani* to *Erpetocephalus rugosus*), the two additional tetrapods mentioned by Huxley, *Discospondylus* and *Brachyscelis*, and the sarcopterygian *Campylopleuron* mentioned by Huxley, with the first appearance in the literature of each genus and species name.

Baily secured additional funding from the British Association for the Advancement of Science to collect more material from Jarrow (DeArce *et al.* 2011) and described the unnamed tetrapod, mentioned in Huxley and Wright (1867), as *Anthracosaur edgei* (Baily, 1876, 1879, 1884). Lydekker (1890, 1891a) produced catalogues of fossils housed at the British Museum and the Science and Art Museum, Dublin (now the National Museum of Ireland). In that catalogue he placed the Jarrow taxon *Erpetocephalus rugosum* (Huxley in Huxley and Wright, 1867), which was described from a cranium, in synonomy with *Ichthyerpeton bradleyae* (Huxley in Wright and Huxley, 1866) which is known only from post-cranial material. An association between the two was based on a new specimen containing a skull that resembled *E. rugosum* that had post-cranial elements similar to *I. bradleyae*. Lydekker (1891b) also described a second species of *Ichthyerpeton* from a single cranium as *Ichthyerpeton hibernicum*. Although descriptions of fish material were not as commonly undertaken during this time, Traquair (1893) described a new "palaeoniscid" as *Myriolepis hibernicus*. Additional material, collected by Robertson of *K. galvani* from Jarrow, was described by Woodward (1897). Woodward's paper was the last paper dealing specifically with material from Jarrow until the 1970s.

The 1970s to the 1990s witnessed a renewed interest in the Pennsylvanian tetrapod-bearing coal deposits of Euramerica. Ph.D. theses by Angela Milner and Kathleen Bossy dealt with the diplocaulid and the urocordylid nectrideans from Jarrow, respectively (Bossy, 1976; Milner, 1978). Beaumont (1977) identified and named the baphetid *Megalocephalus pachycephalus*, marking it as the first newly identified tetrapod/tetrapodomorph from the assemblage since the 1890s. This was followed by the publication of radiographs of a possible microbrachid "microsaur" from Jarrow produced by Rainer Zangerl in Carroll and Gaskill (1978). Milner (1980) assigned *E. rugosum* and *I. hibernicum* to the new temnospondyl species *Dendrerpeton rugosum*. That same year, a review of all nectrideans, including the three species from Jarrow was published (Milner, 1980). A list of tetrapod groupings from the Jarrow fauna was included by Milner (1987) in a comparison with other "Westphalian" tetrapod assemblages. The aïstopod *Ophiderpeton brownriggii* was partially redescribed by Milner (1993) and a second temnospondyl *Procochleosaurus jarrowensis* was described by Sequira (1996). Figured descriptions of the Jarrow aïstopods and nectrideans also appeared in the Encyclopaedia of Paleoherpetology Part 1 Lepospondyli (Bossy and Milner, 1998; Carroll, 1998). The latest paper on Jarrow material was by Milner (2019) who published a monograph on *K. galvani*.

There are currently 219 specimens from the Jarrow assemblage, the majority of which are housed in the National Museum of Ireland and the Geological Museum of Trinity College, Dublin. Joseph Dobbs, a manager of Jarrow colliery, donated specimens from his personal collection to the National Museum of Ireland (DeArce, *et al.* 2011) and to the University of Manchester Museum. In 1883 the Warwickshire Natural History and Archaeological Society bought six specimens from Jarrow (now at the Warwickshire Museum) and in 1889 Robertson donated his personal collection of 10 specimens to the Royal School of Mines (DeArce, *et al*. 2011). The NHM Jarrow holdings comprise Brownrigg's specimens (mentioned above). Jarrow specimens have also been incorporated into the collections of the British Geological Survey, Sedgwick Museum (Department of Earth Sciences, University of Cambridge), Landesmuseum Darmstadt, National Museums Scotland, Edinburgh and the Museum of Comparative Zoology, University of Harvard (Milner pers. comms.). The Jarrow material at the Geological Museum of Trinity College, Dublin were transferred to the National Museum of Ireland in 1959 (Wyse Jackson and Monaghan, 1995) as the future of the former museum was uncertain. Thankfully the Geological Museum of Trinity College, Dublin has survived to the present day and Jarrow material was scheduled to return in 1995, but this did not actually occur until 2016. A by-product of the transfer of Jarrow material throughout Irish, British, American and German institutes has meant that no catalogues of all the Jarrow material have been

published and it has not really been studied as a whole. A catalogue raisonné of all of the museum holdings of the Jarrow biota is a worthwhile project for the future.

1.2 Thesis Aims

The diverse assemblage of tetrapods preserved in the coal shales directly above the Jarrow Seam plays an important role in the understanding of early tetrapod evolution and ecology during the early part of the Pennsylvanian. The specimens are unique in preserving complete skeletons in articulation with soft body and scalation outlines. The Jarrow assemblage marks the first occurrence of important Late Palaeozoic clades such as the nectrideans (Milner, 1980, 2019) and the first occurrence of more than one species of aïstopod in the same assemblage (Carroll, 1998). It is also the oldest of the Pennsylvanian coal swamp assemblages (Milner, 1987). Yet despite its importance, it is relatively understudied compared to other similar later coal swamp assemblages such as Linton, Ohio, Nýřany, Czech Republic and Newsham, England (Milner, 1987) and other Pennsylvanian tetrapod bearing localities such as Joggins, Nova Scotia (Falcon-lang *et al.*, 2006). This is probably the result of the appearance of the fossils which are highly compressed and are coated in a layer of matrix making the separation between the body fossil and the matrix difficult to identify. Even when manually prepared the separation can be uncertain (Milner, 2019). As a result, the specimens from Jarrow have been termed "ghost fossils" due to their faint appearance (Huxley and Wright, 1867). The poor appearance of the specimens was thought to be a result of acidic bottom waters in the environment in which the Jarrow assemblage was preserved (Rayner, 1971). This acidic water remobilised the calcium phosphate of the bone and allowed for its partial replacement with bituminous material (Rayner, 1971). As a result, traditional preparation methods for coal swamp tetrapods, including acid etching (Baird, 1955), are considered to be impractical.

Methods that have been used for preparing and visualising specimens from the Jarrow assemblage include matrix removal using abrasion with sodium bicarbonate (Milner, 2019), coating the specimens with ammonium chloride sublimate to bring out texture and the use of X-ray imaging to produce radiographs of specimen (Sequeira, 1996). The first of these methods is not ideal as it may damage them. Micro-computed tomography (µCT) has become a widely utilised method in visualising fossils. It has aided in describing small early tetrapods providing data that are key to resolving their evolutionary relationships. The main aim of this thesis was to apply µCT to the majority of Huxley and Wright's (1867) tetrapods from Jarrow. Two taxa, *Keraterpeton galvani* and *Dendrerpeton rugosum* (originally *Erpetocephalus rugosus*), are not discussed here as they have been recently described in detail (Milner, 1980; Milner, 2019). Prior to scanning, the chemical composition of the Jarrow material was assessed to establish if

µCT is a feasible technique for imaging the material. Additionally, the palaeoenvironment of the Jarrow assemblage was investigated. The aims of Chapters 2-7 are briefly outlined below:

Chapter 2: The aim of this chapter was to put the Jarrow assemblage into a geological context and to assess the possible palaeoenvironment and palaeoecology of the assemblage. The extent of the coal underlaying the assemblage was mapped from previous reports (Higgs and O'Connor, 2005) and the section containing the assemblage was logged from a core in order to interpret the depositional environment. A taxon list including all vertebrates was compiled including new taxa identified by the author.

Chapter 3: This chapter deals with the taphonomy of the Jarrow assemblage. Cathodoluminescence (CL) and Laser-Ablation Inductively Coupled Mass-Spectrometry (LA-ICP-MS) was applied to body fossil material from the Jarrow assemblage in order to determine the degree of bone replacement and to investigate the processes of preservation in Jarrow specimens (Rayner, 1971). It was also important for this study in order to investigate what sort of limitations µCT might have when trying to distinguish fossil hard tissues from the surrounding matrix in the Jarrow specimens.

Chapter 4: This is the first of two chapters dealing with a description of the aïstopods originally described by Huxley and Wright (1867). Here µCT was applied to specimens of *Ophiderpeton brownriggii,* including one of the syntypes, a skull previously described by Milner (1993) and additional previously undescribed material. The aim was to provide a comprehensive description of both cranial and post-cranial material as a basis for a novel diagnosis and an exhaustive comparison of Jarrow aïstopods with other species in the clade.

Chapter 5: This second chapter on the Jarrow aïstopods deals with the enigmatic "*Dolichosoma*" *emersoni* which is less well known than *O. brownriggii*. This is probably because the holotype has been destroyed by pyrite disease and because of its small size making descriptions difficult. It was described from a single specimen identified in the Jarrow collection at the NHM. The aim of the chapter was to resolve the taxonomic problem with this aïstopods (the original generic name is preoccupied by that of a Recent beetle) and to compare it to the derived "narrow-snout aïstopods" (Anderson, 2002, 2003) to analyse whether it records the first geological occurrence of these derived forms or whether it has a more basal phylogenetic position.

Chapter 6: The Jarrow biota contains the earliest known occurrence of the Urocordylidae nectrideans with two taxa, *Urocordylus wandesfordii* and *Lepterpeton dobbsii*. These taxa, in turn, represent basal members of two separate subfamilies, the Urocordylinae and the Sauropleurinae respectively (Bossy and Milner, 1998). Understanding each taxon is important in interpreting internal relationships of these groups. This chapter reports the use µCT to describe these Jarrow nectrideans in more detail. In particular the focus was on cranial anatomy as it is poorly known in each taxon (Bossy and Milner, 1998).

Chapter 7: *Ichthyerpeton bradleyae* is one of the more problematic taxa described by Huxley and Wright (1867), due to the fact that it was originally described from a single specimen including the posterior trunk region, the pelvic region and part of the caudal region, all of which are covered in a dense coating of scales. Its affinities to other tetrapods are not known. It has been considered to be an embolomere (Panchen, 1970) or a colosteid (Clack and Milner, 2015). Some of these proposed affinities are based on material other than the holotype, which has been ignored. In this chapter, µCT was applied to the holotype in order to investigate whether it is an embolomere, a colosteid or whether it shows closer affinities to other tetrapods.

1.3 References

ANDERSON, J. S. 2002. Revision of the aïstopod genus Phlegethontia (Tetrapoda: Lepospondyli), *Journal of Paleontology*, **76**, 1029–1046. doi: 10.1017/s0022336000057851.

— 2003. A new Aïstopod (Tetrapoda:Lepospondyli) from Mazon Creek, Illinois. *Journal of Vertebrate Paleontology*, **23**, 79–88.

BAILY, W. H. 1876. Description of a new species of labyrinthodont Amphibia from the coal at Jarrow colliery, near Castlecomer, County Kilkenny. *Reports of the British Association for the Advancement of Science*, **45**, 62–63.

— 1879. Notice of some additional labyrinthodont Amphibia and fish from the coal of Jarrow solliery, County of Kilkenny, Ireland. *Reports of the British Association for the Advancement of Science*, **48**, 530.

— 1881. Remarks on the fossils. 23–26. *In* HARDMAN, E. T. (ed). *Memoirs of the Geological Survey of the United Kingdom*. Stationery Office, London.

— 1884 Some additional notes on *Anthracosaurus edgei* (Baily sp.), a large sauro-batrachian from the lower Coal Measures, Jarrow colliery, near Castlecomer, County Kilkenny. *Reports of the British Association for the Advancement of Science*, **54**, 496–497.

BAIRD, D. 1955. Latex micro-molding and latex-plaster molding mixture. *Science*, **122**, 202.

BEAUMONT, E. H. 1977. Cranial Morphology of the Loxommatidae (Amphibia: Labyrinthodontia). *Philosophical Transactions of the Royal Society B: Biological Sciences*, **280**, 29–101. doi: 10.1098/rstb.1977.0099.

BOSSY, K. V. H. 1976. Morphology, paleoecology and evolutionary relationships of the Pennsylvanian urocordylid nectrideans (Subclass, Lepospondyli, Class Amphibia). Unpublished PhD thesis, Yale University–Disertation abstracts, **37**, 2731.

— and MILNER, A. C. 1998. Order Nectridea Miall 1875. 73–131. *In* WELLNHOER (ed). *Encyclopedia of Paleoherpetology*. Verlag Dr.Friedrich Pfeil, München, 206 pp.

BROWNRIGG, W. B. 1865. Notes on part of the Leinster Coal Field, with a record of some fossils therein. *Journal of the Royal Geological Society of Ireland*, **1**, 145–147.

CARROLL, R. L. 1998. Order Aïstopoda Miall 1875. 163–182. *In* WELLNHOER (ed). *Encyclopedia of Paleoherpetology*. Verlag Dr.Friedrich Pfeil, München, 206 pp.

— and GASKILL, P. 1978. *The order Microsauria*. American Philosophical Society, Philadelphia, 211 pp.

CLACK, J. A. and MILNER, A. R. 2015. *Handbook of Paleoherpetology, Part 3A1: Basal Tetrapoda.* Verlag Dr.Friedrich Pfeil, München, 92 pp.

DEARCE, M., MONAGHAN, N. T. and WYSE JACKSON, P. N. 2011. The uneasy correspondence between T. H. Huxley and E. P. Wright on fossil vertebrates found in Jarrow, Co. Kilkenny (1865-67). *Notes and Records of the Royal Society*, **65**, 253–271. doi: 10.1098/rsnr.2010.0081.

ETHERIDGE, R. 1866. On the discovery of several new Labyrinthodont reptiles in the coal measures of Ireland. *Geological Magazine*, **3**, 4–5.

FALCON-LANG, H. J., BENTON, M. J., BRADDY, S. J. and DAVIES, S. J. 2006. The Pennsylvanian tropical biome reconstructed from the Joggins Formation of Nova Scotia, Canada. *Journal of the Geological Society*, **163**, 561–576.

HIGGS, K. T. and O'CONNOR, G. 2005. Stratigraphy and palynology of the Westphalian strata of the Leinster Coalfield, Ireland. *Irish Journal of Earth Sciences*, **23**, 65–84.

HUXLEY, T. H. and WRIGHT, E. P. 1867. Royal Irish Academy On a Collection of Fossil Vertebrata , from the Jarrow Colliery, County of Kilkenny, Ireland. *Transactions of the Royal Irish Academy*, **24**, 351–370.

LYDEKKER, R. 1890. *Catalogue Of The Fossil Reptilia and Amphibia in the British Museum (Natural History), Part IV. Containing the orders Anomodontia, Ecaudata, Caudata, And Labyrinthodontia; And Supplement*. British Museum (Natural History), London.

— 1891a. A labyrinthodont skull from the Kilkenny coal-measures. *Quarterly Journal of the Geological Society, London*, **47**, 343–347.

— 1891b. *Catalogue of Fossil Mammals, Birds, Reptiles, and Amphibians in the Science and Art Museum: Dublin, Science and Art Museum*. British Museum (Natural History), London.

MILNER, A. C. 1978. *Carboniferous Keraterpetontidae and Scincosauridae (Nectridea: Amphibia) – a review*. Unpublished PhD thesis, University of Newcastle upon Tyne.

— 1980. A review of the Nectridea (Amphibia). 377–405. *In* PANCHEN, A. L. (ed). *The terrestrial environment and the origin of vertebrates*. Academic Press, London.

— 1993. The aïstopod amphibian from the Viséan of East Kirkton, West Lothian, Scotland. *Transactions of the Royal Society of Edinburgh: Earth Sciences*, **84**, 363–368. doi:

10.1017/S0263593300006167.

— 2019. A morphological revision of *Keraterpeton*, the earliest horned nectridean from the Pennsylvanian of England and Ireland. *Earth and Environmental Science Transactions of the Royal Society of Edinburgh*, **109**, 237–253. doi: 10.1017/S1755691018000579.

MILNER, A. R. 1980. The temnospondyl amphibian Dendrerpeton from the Upper Carboniferous of Ireland. *Palaeontology*, **23**, 125–141.

— 1987. The Westphalian tetrapod fauna; some aspects of its geography and ecology. *Journal of the Geological Society*, **144**, 495–506. doi: 10.1144/gsjgs.144.3.0495.

PANCHEN, A. L. 1970. *Handbuch der Palaoherpetologie / Encyclopedia of Paleoherpetology Teil 5 / Part 5 Batrachosauria Teil A / Part A Anthracosauria.* Verlag Dr.Friedrich Pfeil, München.

RAYNER, D. H. 1971. Data on the environment and preservation of Late Palaeozoic tetrapods. *Proceedings of the Yorkshire Geological Society*, **38**, 437–495.

SEQUIRA, S. E. K. 1996. A cochleosaurid amphibian from the Upper Carboniferous of Ireland. *Special Papers in Palaeontology*, **52**, 65–80.

TRAQUAIR, R. H. 1893. On a new Palaeoniscid fish, *Myriolepis hibernicus*, sp. nov. from the Coal-measures, Co. Kilkenny, Ireland. *Geology Magazine*, **10**, 54–56.

WOODWARD, A. S. 1897. On a new specimen of the stegocephalan *Ceraterpeton galvani* Huxley from the Coal Measures of Castlecomer, Kilkenny, Ireland. *Geological Magazine*, **4**, 293–98.

WRIGHT, E. P. and HUXLEY, T. H. 1866. On a collection of fossils from the Jarrow Colliery Kilkenny, Ireland. *Geological Magazine*, **3**, 165–171.

WYSE JACKSON, P. N. and MONAGHAN, N. T. 1995. Transfer of the Huxley and Wright (1867) Carboniferous amphibian and fish material to Trinity College, Dublin from the National Museum of Ireland. *Journal of Paleontology*, **69**, 602–603.

— and PARKES, M. 2009. William Hellier Baily (1819-1888): forever an Acting Palaeontologist with the Geological Survey of Ireland. *The Geological Curator*, **9** 57–84.

— DEARCE, M. and MONAGHAN, N. T. 2011. A letter from William Bookey Brownrigg to Thomas Henry Huxley, dated 29 November 1865, authorising him to describe his fossil vertebrates from Jarrow Colliery, Co. Kilkenny and giving details of his find. *Irish Journal of Earth Sciences*, **29**, 19-22. doi: 10.3318/IJES.2011.29.19.

Chapter 2: Geological setting, faunal composition and palaeoenviromental analysis.

2.1 Introduction

The Leinster Coalfield is as an elevated plateau spanning parts of counties Kilkenny, Carlow and Laois in south east Ireland (Fig. 2.1A-B) encompassing a roughly oval area of approximately 250 km^2 (Higgs and O'Connor, 2005). This makes it the second largest area of Pennsylvanian strata in Ireland after north west Co. Clare. The Coolbaun Fault cuts through the coalfield along a north-east to south-west orientation. In total, the Pennsylvanian succession is 320 m thick and comprises three conformable formations with eight separate coal seams. According to Higgs and O'Connor (2005), the Jarrow Seam, also termed the No.4 Coal, was deposited in a semi-circular abandoned channel now located towards the centre of the coalfield. The Jarrow assemblage, which yielded tetrapod fossils, is reputed to have been collected from the roof shales and coals of the Jarrow Channel (Sevastopulo, 2009; Milner, 2019), yet there are no detailed records of their provenances.

The Jarrow channel has been considered to have been deposited in an abandoned oxbow lake (Hook and Ferm, 1988). This interpretation is based primarily on observations from the similar, approximately coeval Pennsylvanian (Asturian) tetrapod-bearing coal seams of Linton, Ohio (Hook and Ferm, 1985; Hook and Baird, 1988). Hook and Ferm (1985, 1988) found that the Linton tetrapod assemblage was preserved towards the base of semi-circular channel containing silts and coal. This led to the interpretation of the Linton coals as forming in abandoned channels and oxbow lakes. Using old mining maps of the Jarrow channel, Hook and Ferm (1988) suggested that the Jarrow seam was deposited in a similar fashion to the Linton coals.

The Jarrow assemblage is the oldest of the four classic Westphalian tetrapod coal swamp assemblages (Milner, 1987). The other three assemblages are those of Newsham, England (Duckmantian) (Boyd, 1984), Linton, Ohio (Asturian) (Hook and Baird, 1988) and Nýřany, Czech Republic (Asturian) (Milner, 1980a). Jarrow, Linton and Newsham all appear to fit the model of locally thickened coal formation in a channel proposed by Hook and Ferm (1988). The Nýřany biota includes tetrapods from laterally expansive coals and silts, indicating a more lacustrine environment (Milner, 1980a). Fish and tetrapod faunal compositions have been listed for the Newsham (Boyd, 1984), Linton (Hook and Baird, 1988) and Nýřany (Milner, 1980a) biotas. A faunal list for the Jarrow coal was published in Milner (1987) and

Sequeira, (1996), though these works only dealt with the tetrapod composition and lacked up to date information.

There are currently two competing ecological models for the Jarrow assemblage. The first model suggests that the fauna of Jarrow (and Linton) represents animals that lived within the oxbow lake and in its immediate surroundings (Hook and Ferm, 1988), with the oxbow lake waters showing distinctive zonation having oxygenated water at the top and an anoxic zone towards the bottom. This model also provides an explanation for the high level of preservation seen at Jarrow. Animals that swam close to and on the surface waters would sink after death into the anoxic water below, thus inhibiting scavenging and favouring preservation. The second model takes into account the faunal composition and differentiation between the different classic Westphalian tetrapod bearing coal assemblages. This model suggests that the channel coal tetrapod assemblages of Jarrow and Linton represented estuarine faunas which were washed into an abandoned channel and eventually preserved (Milner, 1987).

In this chapter the Jarrow channel is placed in a geological context. Logging of a core from the Leinster Coalfield and palynofacies analysis of samples from it and from outcrop samples and museum specimens of Jarrow fossils were used to interpret the depositional environment of the Jarrow assemblage. The palaeoenvironment in which the tetrapods of Jarrow was also investigated. A complete faunal list of the fish and tetrapods from the assemblage was compiled. This allows comparison with other Pennsylvanian tetrapod assemblages.

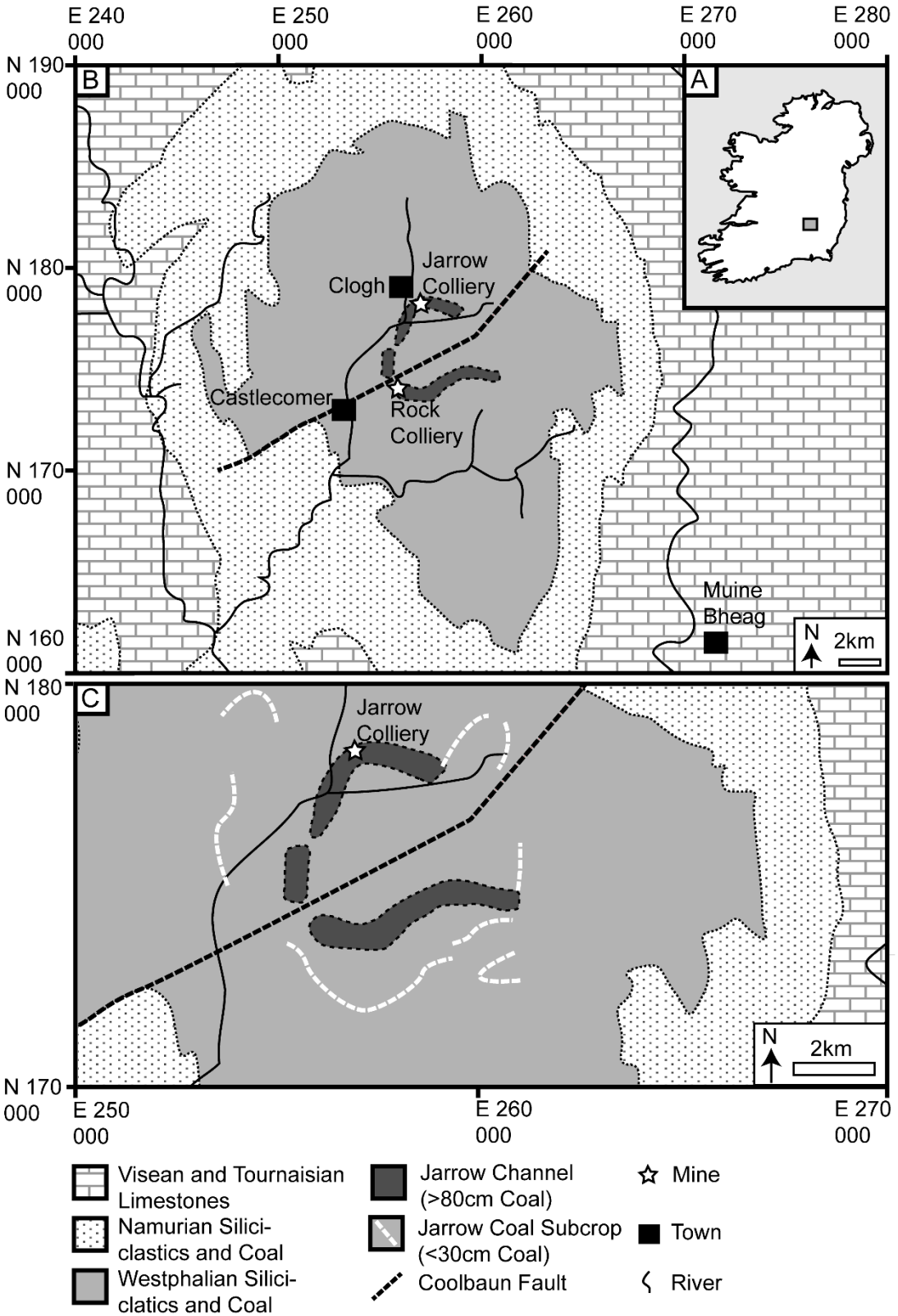

Figure 2.1 Geological map of the Leinster Coalfield showing (A), location in Ireland, (B), extent of the Westphalian deposits in the Coalfield and (C) the Jarrow channel in the subsurface and the subcrop of the thinner Jarrow coal and location of the Jarrow colliery (Base map modified from OSI Sheet 60 (2007); geology adapted from GSI map 137 (1858) and Higgs and O'Connor (2005)).

2.2 Material and Methods

The core taken from Coolbaun Borehole GSI-85-3 (now housed at the Geological Survey of Ireland) through the Coolbaun Coal Formation was logged (Fig. 2.4).

Micro-computed tomography was carried out on NHMUK.R8466 to image microconchids using the Nikon Metrology HMX ST 225 at the Imaging and Analysis Centre, Natural History Museum, London. NHMUK.R8466 was scanned at: 160 kV, 125 uA with a 1 mm Cu filter. Resulting CT-slices were converted to PNG files and imported to the freeware 3D rendering software SPIERS (Sutton *et al.*, 2012) and virtually separated using the masking function.

Ten sites/locations were sampled for palynofacies. Sites/locations included five samples from the core GSI-85-3 (see fig. 2.6 for location), from an outcrop of the Jarrow seam south of the Coolbaun Fault (grid reference: N173,500, 255,300) and from two matrix samples from the Jarrow assemblage collected near Clogh (TCD.38367 and TCD.T87). Samples were dissolved in hydrofluoric acid and palynological strews mounted on slides at the Department of Geology, Trinity College Dublin. Two slides were prepared for each sample. Imaging of the prepared samples was undertaken using a Nikon DS-Ri2 attached to a Nikon Eclipse LV100 microscope. Point counting of Amorphous Organic Matter (AOM), palynomorphs and phytoclasts was carried out using JMicroVision 1.2.7. (Nicolas Roduit, 2008). Two hundred specimens were counted per slide. This allowed for the plotting of Tyson plots (Tyson, 1995).

A list of all Jarrow specimens from the Geological Survey of Ireland, National Museum of Ireland, Natural History Museum, London and TCD Geological museum was compiled (Appendix 1).

Museum abbreviations are: BGS, British Geological Survey, CAMSM, Sedgewick Museum, University of Cambridge, GSI, Geological Survey Ireland, HLMD, Hessische Landesmuseum, Darmstadt, MCZ, Museum of Comparative Zoology, MM, University of Manchester Museum, NHMUK, Natural History Museum, London, NMI, National Museum of Ireland, NMS National Museums of Scotland, Edinburgh, TCD, Geological Museum, Trinity College Dublin, WARMS, Warwickshire Museums Service.

2.3 Stratigraphy

The Westphalian (Langsettian; equivalent to the Bashkirian Stage of the Pennsylvanian) strata of the Leinster Coalfield are approximately 320 m thick and consist of three conformable formations: in ascending order, the Moyadd Coal Formation, the Clay Gall

Sandstone Formation and the Coolbaun Coal Formation (Higgs and O'Connor, 2005) (Fig. 2.2). Bedding generally dips towards the centre of this Pennsylvanian outlier with the youngest stratigraphic units located towards the centre and progressively older beds towards the edge of the plateau. Outcrop is poor and limited to stream sections, quarries and old mine entrances.

The base of the 100 m thick Moyadd Coal Formation is marked by the No.1 Coal (Fig. 2.2) which lies conformably on the Bregaun Flagstone Formation. The formation contains three distinct marine bands, the second of which contains the goniatite *Gastrioceras subcrenatum* which marks the base of the Langsettian (Higgs and O'Connor, 2005). The No.2 Coal underlies the third marine band. The overlying Clay Gall Sandstone Formation comprises massive sandstone beds, containing shale rip-up clasts (clay galls), and ranges in thickness from 50m in the south-west to 30m in the north-east part of the coalfield (Higgs and O'Connor, 2005).

The Coolbaun Coal Formation, approximately 170 m thick, is the thickest of the formations and is located towards the centre of the plateau. The base is marked by the Wards Seam, a thin laterally expansive anthracite that occurs throughout the coalfield (O'Meara, 1964). This is the first of the six coal seams present in this formation (Fig. 2.2). Two non-marine bivalve horizons are present between the Wards Seam and the Swan Sandstone Member, which is composed of massive sandstone beds similar to the Clay Gall Formation, only lacking the rip up clasts (Higgs and O'Connor, 2005). Between the Swan Sandstone Formation and the Jarrow Seam (No. 4 Coal) there are two marine bands, the Fairy Mount Marine Band, containing the goniatite *Gastrioceras* sp. and the bivalve *Dunbarella* sp., and the second marine band containing *Lingula*. This *Lingula* marine band, which is approximately 65m below the Jarrow Seam (Higgs and O'Connor, 2005) is the youngest recorded marine band in the Leinster Coalfield, although the presence of microconchids associated with the Jarrow biota may suggest a younger 'brackish marine band' (see below). Between the non-marine and marine bands there are two beds of clay or fireclay which make up the Double Fireclay Member. Above the fireclay is the boundary between the *Triquitrites sinani-Cirratriradites saturni* (SS) Miospore Biozone and the *Radiizonates aligerens* (RA) Miospore Biozone (Higgs and O'Connor, 2005), with all younger strata, including the Jarrow Seam, being part of the RA biozone.

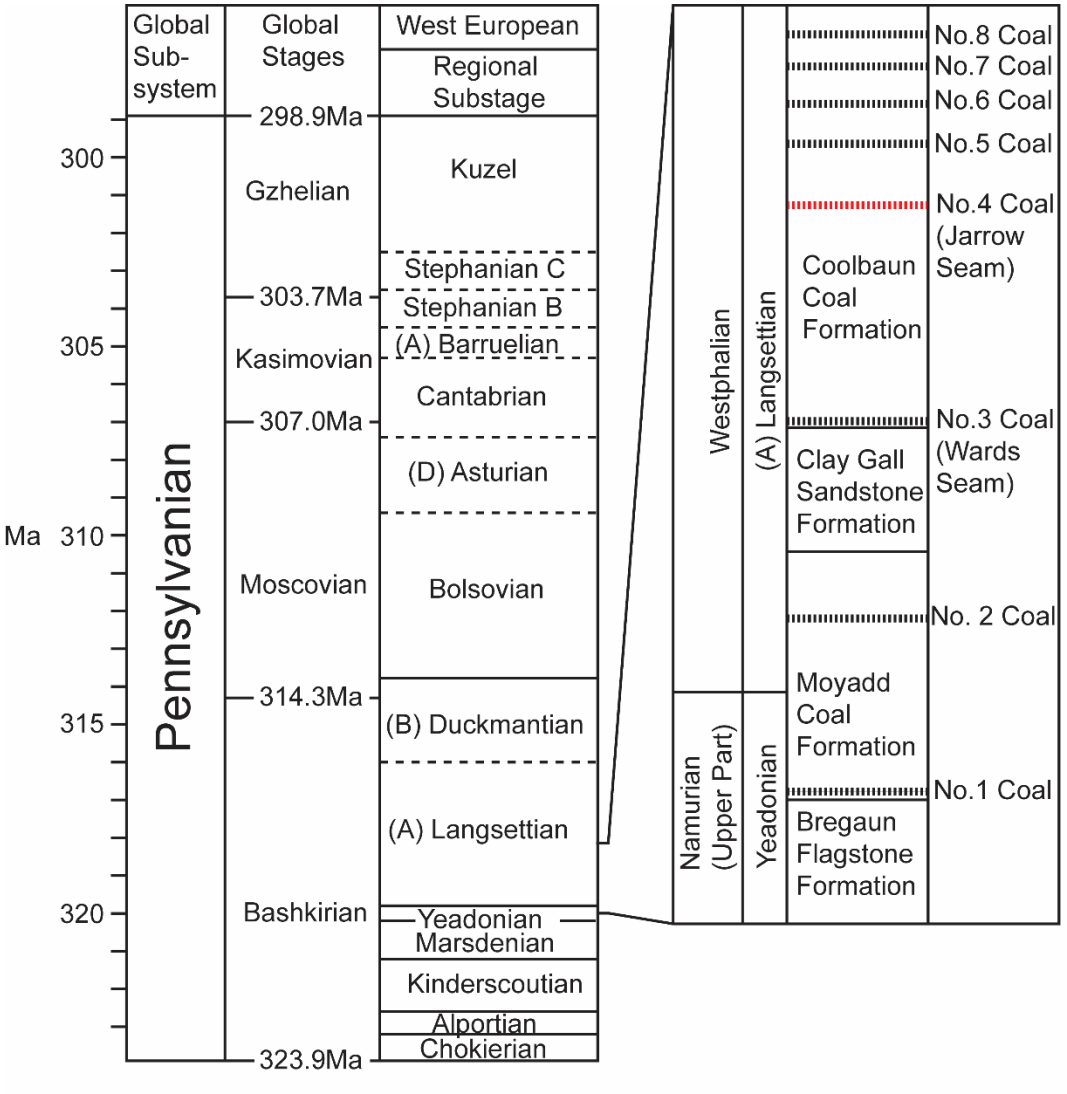

Figure 2.2 Stratigraphic column showing the placement of the Westphalian formations and their associated coal seams in the Leinster Coalfield. The coal seam from which the Jarrow Assemblage was collected is marked in red. Modified from Heckel and Clayton, (2006), Pointon *et al*. (2012) and Cohen, *et al*. (2013).

The Jarrow Seam is located towards the centre of the coalfield on both sides of the Coolbaun Fault. It has a thickness of 0.2-0.3 m except in an area, known as the Jarrow Channel (Fig. 2.1C), where it thickens to between 0.91 m (Higgs and O'Connor, 2005) and 1.67 m (Huxley and Wright, 1867). The Jarrow Channel is semi-circular in plan view (Figure 2.1). Away from the channel, the Jarrow Seam consists of a single homogenous coal. The Jarrow channel in contrast has been recorded as containing at least five different types of coal (Huxley and Wright, 1867) (Fig. 2.3). The Jarrow Channel lies approximately 64 m below the surface so mining was carried out by shaft mining (Huxley and Wright, 1867). All pits have been infilled, so the channel is now inaccessible. This means that the exact location of the Jarrow assemblage

within the channel cannot be readily determined. The assemblage is generally considered to be from the overlying roof shales and coals (Sevastopulo, 2009; Milner, 2019).

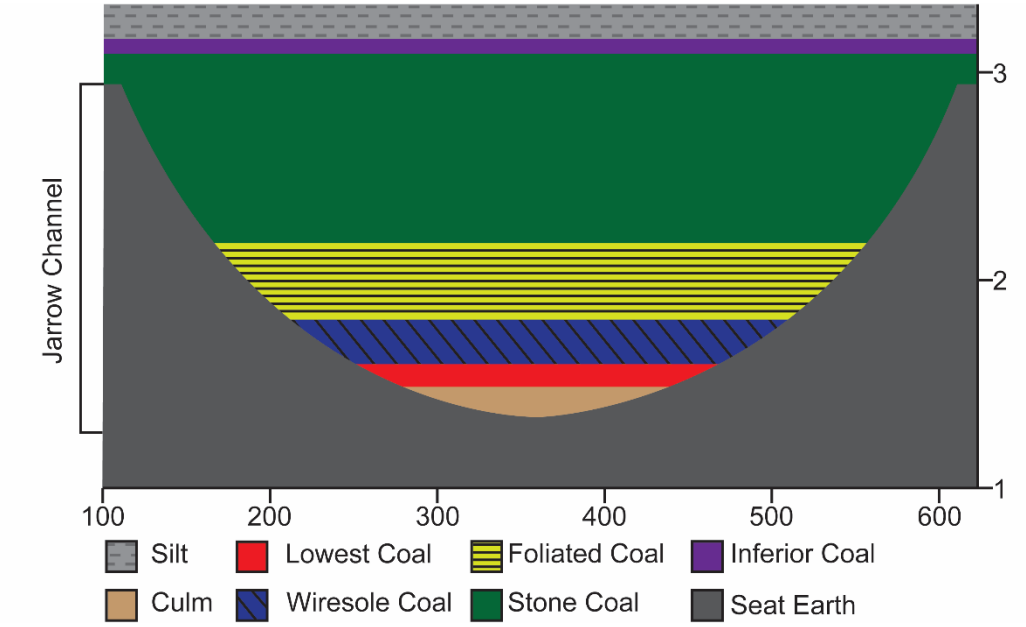

Figure 2.3 Cross-section of the Jarrow Channel based on the description in Huxley and Wright (1867). Scale is in metres for both axes.

The Jarrow Seam is succeeded by shales and sandstones, with a single non-marine bivalve band containing *Carbonicola proversa* and *C. bellula* (Eagar, 1974) which is followed by the Old Three Foot Coal (No. 5 Coal). This is the thickest continuous seam in the coalfield, averaging 0.91 m (Higgs and O'Connor, 2005). The following three coal seams only appear in a quarry in the central part of the coalfield on the south side of the Coolbaun Fault. They contain the non-marine bivalve *Athroconaia modiolaris* which spans the Langsettian/Duckmantian boundary. No younger formations overlying the Coolbaun Coal Formation have been preserved. A Langsettian (equivalent to the Bashkirian global stage) age makes the Jarrow assemblage the oldest of the four well known assemblages of tetrapods from Westphalian coal deposits.

2.4 Deposition, Palaeoenvironment and Palaeoecology

The Leinster Coalfield was deposited in a paralic basin on the microcontinent Avalonia. It records an overall regressive trend, marked with transgressive-regressive cyclothems. Marine bands show a faunal differentiation between the north and south of the coalfield. Southern marine band assemblages tend to consist of benthic fauna including

brachiopods, while northern assemblages are dominated by nektonic ammonoids and pectinoid bivalves (Nevill, 1956). This suggests a deeper environment in the north of the coalfield. This is also supported by palaeoflow indicators in the fluvial Clay Gall Sandstone Formation, suggesting flow towards the north north-west (Sevastopulo, 2009). Therefore, it is likely that marine flooding during transgressive system tracts was from a northerly direction.

The core from borehole GSI-85-3 records the laterally extensive Jarrow Seam (c 0.20 m thick) but not the channel itself. 6.27 m below the Jarrow Seam in the core there are medium sandstones beds (Fig. 2.4A). These beds contain rip up clasts near their bases and trough cross bedding. The medium sandstones fine upwards near the top of the beds. Above these sandstones are thinner medium sandstone beds separated by beds of siltstone. These are then proceeded by siltstones containing plant material and disarticulated insect wings (pers. obvs). Above the siltstones is a 1 m bed of seat earth. This seat earth thins to 0.13 m in the Jarrow Channel (British Consultancy Report, 1982). The seat earth is succeeded by the Jarrow Seam which has a thickness of 0.20 m in the core. Directedly above the Jarrow Seam in ascending order are bioturbated siltstones, siltstones containing actinopterygian scales and flaser beds of siltstone and very fine sandstone.

Information of the sedimentology of the Jarrow Seam is limited to the core from borehole GSI-85-3 and mining reports (British Consultancy Report, 1982). This is a result of poor outcrop and because previously cored material from the Leinster Coalfield has since been disposed of. This in turn limits the interpretation of the depositional environment. Medium sandstones with rip up clasts and trough cross bedding are consistent with a fluvial depositional model. An environmental change to a lower energy environment is marked by the overlying siltstones. This would then be followed by a period of sub-aerial soil formation, producing the seat earth. The formation of the Jarrow Channel is uncertain. The channel may represent an erosion feature, which created accommodation space for the Jarrow Coal. Or coal in the Jarrow Channel may have been deposited at the same time as the seat earth on either side and may represent a localised area where there was a higher concentration of plant matter being deposited. One problem with this later scenario is that it would also suggest a localised body of water as a sub-aqueous environment is necessary for coal formation (Eble and Grady, 1988). Thickening of the Jarrow Seam in the channel is also attributed to a high supply of wash in material (British Consultancy Report, 1982). Overlying flaser bedded siltstones share similar morphology to tidalites seen in Kvale *et al*. (1989). This suggests they may have been deposited in a tidal influenced environment. Though this is not indicative of an environment with marine salinity.

Sedimentology of the Jarrow Seam and its associated sediments is consistent with glacioeustatic cyclothems. The Pennsylvanian was a period of glacial induced transgression and regression cycles (Heckel, 1986, 1997; Heckel *et al*., 1998). This produced cyclothemic deposits, including the Coolbaun Coal Formation. Periods of low sea level in cyclothem deposits are marked by erosional bases (Falcon-Lang and DiMichele, 2010). A likely scenario is that the fluvial channels were formed during a period of low sea level (Fig. 2.4B), accommodating the deposition of medium sandstones. Transgression led to a rise in the water table allowing for lower energy deposition of siltstones within the fluvial basin. This was followed by the formation of a palaeosol. Rising sea levels would continue to increase the water table, eventually causing flooding in the fluvial basins leading to the formation of a flooded forest mire (Falcon-lang and DiMichele, 2010) (Fig. 2.4C). This allowed for the formation of the Jarrow Coal on top of the seat earth. Continued transgression led to the formation of tidal influenced siltstones and sandstones in a tidal flat environment (Fig. 2.4D).

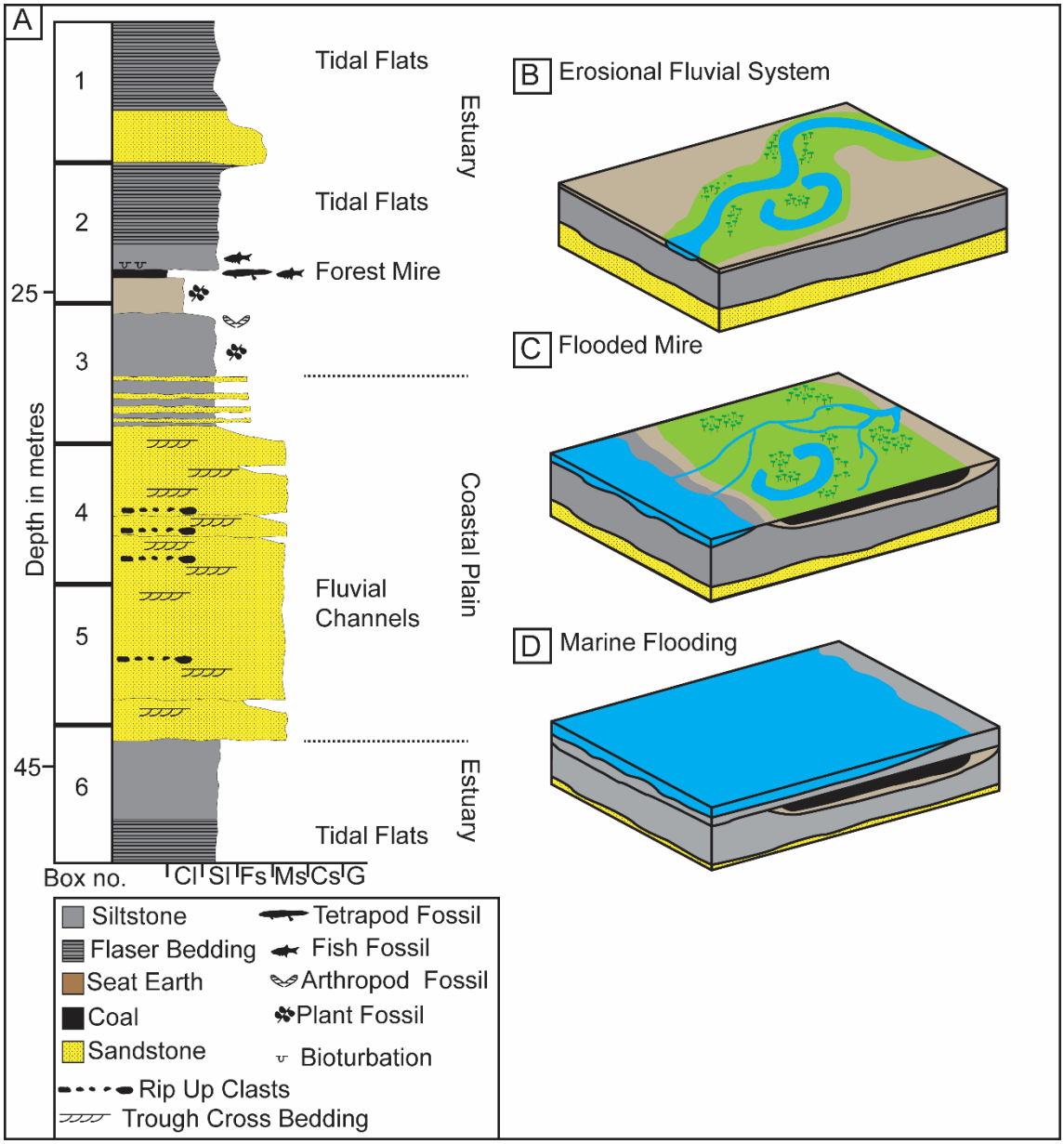

Figure 2.4 Sedimentary log and palaeoenvironmental reconstructions showing (A) a log of the Jarrow Coal seam constructed from GSI-85-3, (B) erosional fluvial system during a falling system tract forming an oxbow lake (Jarrow Channel), (C) mire and "coal swamp" formation in the oxbow lake and surrounding area and (D) continued transgression flooding of the area leading to a marine influenced environment.

Xiphosurans have been reported from the siltstones associated with the Jarrow assemblage but not from the Jarrow Coal. The only invertebrate fossil material found associated with the Jarrow tetrapod assemblage is two microconchid "spirorbids" on specimen NHMUK.R8466 (Fig. 2.5). The microconchids are preserved as spiral calcareous shells. They were traditionally considered to be polychaete annelids, similar to Recent *Spirorbis* (Gierlowski-kordesch and Cassle, 2015). A revision of the palaeoecology and relationship of all pre-mid-Jurassic spirorbids found that they are phorononids, a phylum closely related to

brachiopods and bryozoans. They have now been classified as the Order Microconchida (Gierlowski-Kordesch and Cassle, 2015). Extant phoronids are strictly marine (Gierlowski-kordesch and Cassle, 2015). The presence of microconchid spirorbids in "freshwater" paralic deposits such as at Jarrow represents marine wash in and are characteristic of brackish environments. The presence of only two individuals identified from all the Jarrow specimens is enigmatic. Where present in a sediment, microconchids tend to be very frequent (Gierlowski-kordesch and Cassle, 2015) as in the case of the Linton assemblage where microconchids are present "in millions" (Newberry, 1874 see Hook and Baird for reference). Although microconchids at Jarrow are rare, it suggests that the environment was close to the sea; their presence at in the Linton assemblage indicates that this assemblage was also brackish and represents wash in material *contra* Hook and Ferm (1988).

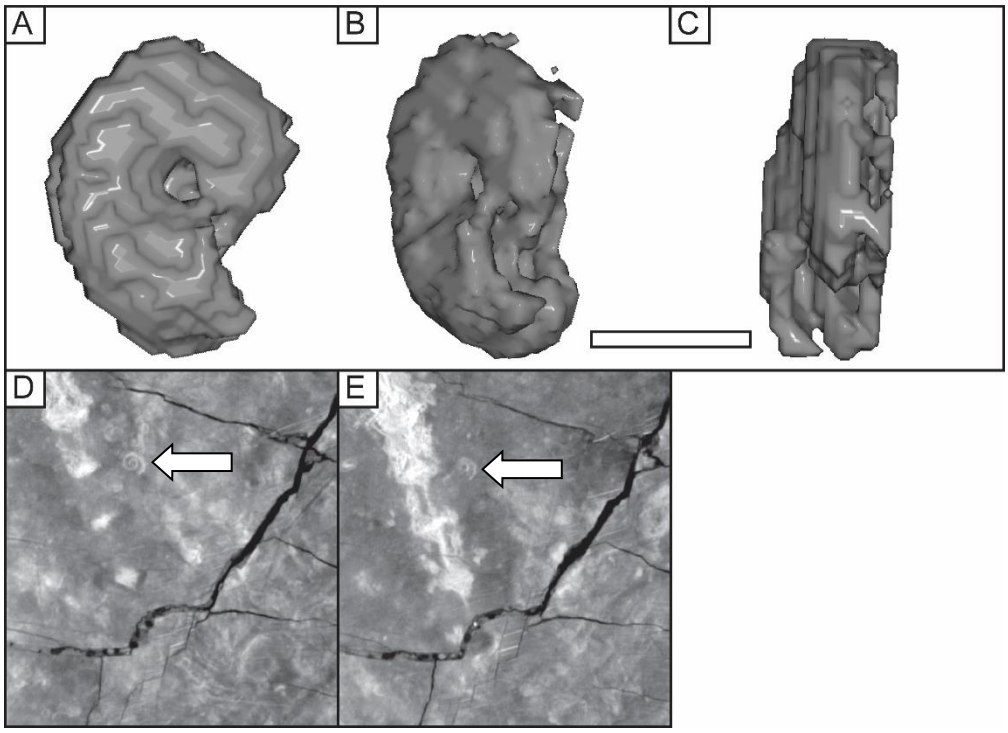

Figure 2.5 NHMUK.R8466 microconchid "spirorbid" from Jarrow (A-E), showing 3D rendering of a microconchid "spirorbid" in (A), lateral view, (B), latero-apertural view and (C) in apertural view, and CT slices (D-E). Scale bar = 1mm for A-C and 14mm for D-E.

Milner (1987) suggested that the presence of the actinistian *Rhabdoderma* in the Jarrow assemblage indicates a brackish assemblage. The Jarrow assemblage does contain fish taxa typical of the Pennsylvanian cosmopolitan fish communities from eastern North American and western to central Europe. These include the Gyracanthidae, the chondrichthyan *Ageleodus pectinatus* and the xenacanthiformes, and the sarcopterygians *Sagenodus*, *Megalichthys* and *Rhizodopsis*, all of which known to be euryhaline (Carpenter *et al.*, 2011, 2014, 2015; Ó

Gogáin *et al.*, 2016). This suggests that the Jarrow fish assemblage at least represents a community with access to the sea and thus is not characteristic of a closed oxbow lake. It could be argued that the Jarrow fish community represents a community that was cut off from the marine/fluvial system when the Jarrow Channel was first excavated (in the oxbow lake scenario), but this is unlikely because the fossils are considered to appear towards the top of the channel (Milner, 2019). Given the amount of time it would have taken for the channel to be filled, while sustaining an isolated community of large fish (e.g. *Megalichthys*), it is unlikely that the assemblage represents an autochthonous community. Therefore, it is more likely that the Jarrow assemblage represents an estuarine fauna, which was washed into the Jarrow Channel and preserved. Specimens were probably transported over a short distance which would explain the articulated nature of most of the specimens. It would not be surprising that the biota was a brackish faunal assemblage because of the presence of euryhaline adaptations in many of the tetrapod clades found at Jarrow (Laurin and Soler-Gijón, 2010).

The Jarrow assemblage is considered to be restricted to just above the Jarrow channel (Milner, 2019). However, given the lateral expansion of the Jarrow seam towards the top of the channel (Fig. 2.3), it might be reasonable to assume that tetrapod material could be found there too. Palynofacies analysis was undertaken on matrix from a tetrapod specimen (TCD.T87) and a fish specimen (TCD.38367), and samples from the Jarrow seam away from the channel and the surrounding rock. No palynomorphs were recovered from any of the palynological samples. A higher frequency of amorphous organic material (AOM) was found in coal samples from the tetrapod (TCD.T87) and the fish (TCD.38367) (Fig. 2.6), compared to all the other coal samples. TCD.T87 and TCD.38367 are the only samples collected from the Jarrow channel. All other samples are nearly exclusively composed of phytoclasts. These include samples taken from the Jarrow Seam away from the channel and associated roof shales. This is consistent with the higher degree of preservation of vertebrate material within the Jarrow Channel and also supports the interpretation that the Jarrow Channel was deposited in an anoxic environment (Tyson, 1995). Therefore, it is likely that fossil material from Jarrow is restricted to the Jarrow Channel.

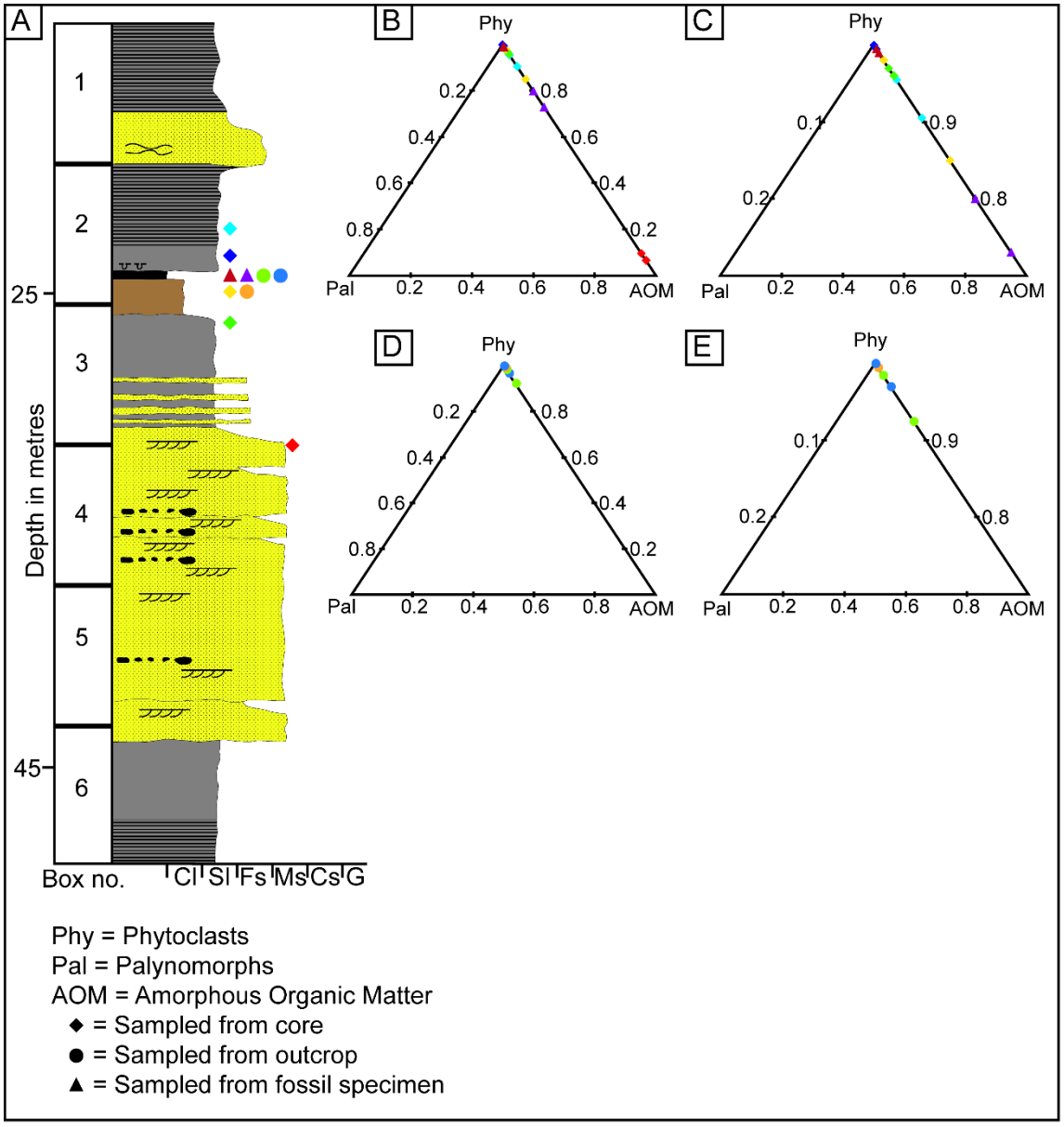

Figure 2.6. Sedimentary log and Tyson plots for palynofacies analysis showing (A) the sedimentary log from Fig. 2.4 showing the relative and real positions of samples, (B) Tyson plot for samples taken from the core GSI-85-3 and from fossil specimens TCD.38368 and TCD.T87, (C) close up of Tyson plot from B showing the upper 30%/70% for palynomorphs/AOM, (D) Tyson plot of samples collected from the outcrop of the Jarrow seam south of the Coolbaun Fault and E) close up of Tyson plot from D showing the upper 30%/70% for palynomorphs/AOM.

It is worth noting that the matrix in which the Jarrow specimens are preserved appears to differ slightly from coaly shales, which preserve the chondrichthyan *Ageleodus pectinatus* (NMI F.16844) and the nectridean *Lepterpeton dobbsii* (TCD.T85b), to the "blocky" unlaminated coal which preserves the sarcopterygian *Rhizodopsis* sp. (TCD.38366). This indicates that the Jarrow assemblage is probably made up of more than one biological assemblage separated by time and/or environment. For ease throughout the thesis, the Jarrow assemblage will refer to all specimens collected from the roof coals and shales.

2.5 Faunal Composition

This study is based on Jarrow specimens collected since the 1860s (DeArce *et al*., 2011; Wyse Jackson, *et al.* 2011) now in various institutions. These include the GSI, NMI and TCD in Ireland, the BGS, CAMSM, MM, NMS, NHMUK in the UK, the HLMD in Germany and the MCZ in the USA. The majority of specimens are housed at TCD, the NMI and the NHM.

The Jarrow Pennsylvanian fauna is dominated by specimens of sarcopterygians (four genera), aïstopods (three genera) and nectrideans (three genera) (Table 2.1). In the latter group, the majority of specimens belong to *Keraterpeton galvani*, with only a single specimen of *Lepterpeton dobbsii*. Spines of the acanthodian *Gyracanthus* and disarticulated anthracosaur/embolomere elements are also common. Rarest of all are baphetids, which are only represented by a single skull of *Megalocephalus pachycephalus* (Beaumont, 1977), and the temnospondyls with two monotypic genera, *Procochleosaurus jarrowensis* (Sequeira, 1996) and *Dendrerpeton rugosum* (Milner, 1980b); these are represented by a single skull and two skulls respectively. *Dendrerpeton* was the only terrestrial tetrapod in the assemblage.

As Milner (1987) indicated, the Jarrow biota shares a similar faunal composition with the Linton biota, being dominated by aïstopods, nectrideans and with colosteids, while temnospondyls are rarer faunistic components. This is in contrast to the fauna at Nýřany, which does contain aïstopods and nectrideans, but is dominated by temnospondyls and lacks colosteids (Milner, 1980a). The Nýřany biota preserves tetrapods in a widespread unit of siltstones and coal, considered to have been deposited in a lacustrine setting (Milner, 1980a). Milner (1987) suggested that the faunal differences between Nýřany and the channel coal deposits of the Jarrow and Linton assemblages represents proximity to marine environments of the latter. The Jarrow and Linton biotas would represent estuarine assemblages (supported by brackish indicators noted above) while the Nýřany assemblage represents upstream freshwater environments. This is marked by the lack of colosteids and the increase in frequency of temnospondyls in Nýřany. The Newsham tetrapod coal assemblage in Northumberland, England is taxonomically the most similar to Jarrow, including the aïstopod *Ophiderpeton* (Boyd, 1982, Chapter 4), the nectridean *Keraterpeton* (Milner, 2019), the baphetid *Megalocephalus pachycephalus* (Boyd, 1984). The palaeoenvironment of Newsham however seems to be more complex than that of Jarrow. Although it shows a locally thickened coal, it does not fit within a channel (Boyd, 1984). Again, fossils appear to be associated with this area of thickening, but the coal seam does not appear to represent a channel infill.

The key difference between the faunal composition of the Jarrow (and the Newsham) assemblage and those of Linton and Nýřany is the apparent absence of crown amniotes, which

are represented by *Anthracodromeus longipes* and *Brouffia orientalis* in the Linton and Nýřany biotas respectively (Carroll and Baird, 1972). Possible amniote material from Jarrow might be RSM 1967 13.2, microbranchid indet., the only specimen of a "microsaur" from the assemblage.

CLASS	ORDER	GENUS	TAXA
Chondrichthyes	Xenacanthiformes		**Xenacanthiformes indet.**
Chondrichthyes		*Ageleodus*	***Ageleodus pectinatus***
Acanthodii		*Gyracanthus*	***Gyracanthus* sp.**
Actinopterygii		*Myriolepis*	***Myriolepis hibernica***
Sarcopterygii	Dipnoi	*Sagenodus*	***Sagenodus* sp.**
Sarcopterygii		*Rhabdoderma*	***Rhabdoderma* sp**
Tetrapodomorpha		*Rhizodopsis*	***Rhizodopsis* sp.**
Tetrapodomorpha		*Campylopleuron*	***Campylopleuron* sp.**
Tetrapodomorpha		*Megalichthys*	***Megalichthys hibberti***
Tetrapodomorpha	Aïstopoda	*Ophiderpeton*	***Ophiderpeton brownriggii***
Tetrapodomorpha	Aïstopoda	*Peisterpeton*	***Peisterpeton milnerorum***
Tetrapodomorpha	Aïstopoda	*Dolichosomatites*	***Dolichosomatites emersoni***
Tetrapodomorpha		*Ichthyerpeton*	***Ichthyerpeton bradleyae***
Tetrapodomorpha			**Colosteidae indet.**
Tetrapodomorpha			***Megalocephalus pachycephalus***
Tetrapoda	Temnospondyli	*Procochleosaurus*	***Procochleosaurus jarrowensis***
Tetrapoda	Temnospondyli	*Dendrerpeton*	***Dendrerpeton rugosum***
Tetrapoda	Nectridea	*Keraterpeton*	***Keraterpeton galvani***
Tetrapoda	Nectridea	*Urocordylus*	***Urocordylus wandesfordii***
Tetrapoda	Nectridea	*Lepterpeton*	***Lepterpeton dobbsii***
Tetrapoda	Embolomeri	*Anthracosaurus*	***Anthracosaur edgei***
Tetrapoda			**Embolomeri indet.**
Tetrapoda	Tuditanomorpha		**Microbrachidae indet.**

Table 2.1. List of Vertebrata from the Jarrow Assemblage. Class column also includes super-,infra and sub- classes. Order column contains suborder.

2.6 Conclusion

Information on the deposition of the Jarrow Seam is limited to previous reports (British Consultancy Report, 1982), the core from borehole GSI-85-3 and from specimens from the Jarrow Assemblage. The traditional model of the Jarrow Assemblage representing an autochthonous fauna within an abandoned oxbow lake is not here supported. The tetrapod assemblage is considered to be from the top of the Jarrow Seam, where the coal is laterally expansive and not restricted to the Jarrow Channel. Further work needs to be done on the sedimentology of the Jarrow Seam, particularly in the localised Jarrow Channel. Despite deriving from the part of the coal not restricted to the Jarrow Channel, it is suggested that vertebrate fossils are found only in coal above the channel. This is supported by a higher preservation of amorphous organic material (AOM) from above the channel, compared to the

same coal to the sides of the channel. It is unsure why coal above the Jarrow Channel shows better preservation.

A faunal list of vertebrates compiled from collections at the NHM, NMI and TCD indicates that the Jarrow fauna consists of 14 tetrapods, five sarcopterygians, one actinopterygian, one acanthodian and two chondrichthyans. The Jarrow fauna is here considered to represent a euryhaline community that lived in an estuarine environment. This is supported by the presence of microconchids which are an indicator of brackish environments (Gierlowski-kordesch and Cassle, 2015). Therefore, the Jarrow Assemblage preserves an estuarine community which was washed into an area above the Jarrow Channel and preserved. The Jarrow Assemblage does not represent a single assemblage and further work needs to be done to distinguish the different lithologies the specimens are preserved in.

2.7 References

BEAUMONT, E. H. 1977. Cranial Morphology of the Loxommatidae (Amphibia: Labyrinthodontia). *Philosophical Transactions of the Royal Society B: Biological Sciences*, **280**, 29–101. doi: 10.1098/rstb.1977.0099.

BOYD, M. J. 1982. Morphology and relationships of the Upper Carboniferous aïstopod amphibian *Ophiderpeton nanum*. *Palaeontology*, **25**, 209–214.

— 1984. The Upper Carboniferous tetrapod assemblage from Newsham, Northumberland. *Palaeontology*, **27**, 367–392.

BRITISH MINING CONSULTANTS LTD. 1982. *Report on Irish coal*. Unpublished report to the Minister for Industry and Energy, Republic of Ireland, vols 1-3.

CARPENTER, D. K., FALCON-LANG, H. J., BENTON, M. J. and NELSON, W. J. 2011. Fishes and tetrapods from the Pennsylvanian (Kasimovian) Cohn Coal Member of the Mattoon Formation, Illinois, USA: systematics, palaeoecology and palaeoenvironments. *Palaios*, **26**, 639–658.

— — — and HENDERSON E. 2014. Carboniferous (late Tournaisian) fish assemblages from the Isle of Bute, Scotland: systematics and palaeoecology. *Palaeontology*, **57**, 1215–1240.

— — — and GREY M. 2015. Early Pennsylvanian (Langsettian) fish assemblages from the Joggins Formation, Canada, and their implications for palaeoecology and palaeogeography. *Palaeontology*, **58**, 661–690.

CARROLL, R. L. and BAIRD, D. 1972. Carboniferous stem-reptiles of the family Romeriidae. *Bulletin of the Museum of Comparative Zoology, Harvard University*, **143**, 321–364.

COHEN, K.M., FINNEY, S.C., GIBBARD, P.L. and FAN, J.-X. 2013. *The ICS International Chronostratigraphic Chart*, **36**, 199-204

DEARCE, M., MONAGHAN, N. T. and WYSE JACKSON, P. N. 2011. The uneasy correspondence between T. H. Huxley and E. P. Wright on fossil vertebrates found in Jarrow, Co. Kilkenny (1865-67). *Notes and Records of the Royal Society*, **65**, 253–271. doi: 10.1098/rsnr.2010.0081.

EAGAR, R. M. C. 1974. Neure arbeiten über das Westfal in Ireland. *Zentralblatt für Geologie und Paläontologie Stuttgart*, **1**, 291-309.

EBLE, C.F. and GRADY, W.C. 1988. Palynologic petrographic and coal-quality characteristics of Middle and Upper Pennsylvanian coal beds: A comparison. *American Association of Petroleuom Geologists Bulletin*, **72**, 906.

FALCON-LANG, H. J. and DIMICHELE, W. A. 2010. What happened to the coal forests during Pennsylvanian phases? *PALAIOS*, **25**, 611–617.

GIERLOWSKI-KORDESCH, E. H. and CASSLE, C. F. 2015. The "*Spirorbis*" problem revisited: Sedimentology and biology of microconchids in marine-nonmarine transitions, *Earth Science Reviews*, **148**, 209–227.

HECKEL, P. H. 1986. Sea level curve for Pennsylvanian eustatic marine transgressive-regressive depositional cycles along Midcontinent outcrop belt, North America. *Geology*, **14**, 330–334.

— 1997. Origin of phosphatic black shale facies in Pennsylvanian cyclothems of mid-Continent North America. *Bulletin of the American Association of Petroleum Geologists*, **61**, 1045–1068.

— GIBLING, M. R. and KING, N. R. 1998. Stratigraphic Model For Glacial-Eustatic Pennsylvanian Cyclothems in Highstand Nearshore. *The Journal of Geology*, **106**, 373–384.

— and CLAYTON, G. 2006. The Carboniferous System. Use of the new official names for the subsystems, series, and stages. *Geologica Acta*, **4**, 403–407.

HIGGS, K. T. and O'CONNOR, G. 2005. Stratigraphy and palynology of the Westphalian strata of the Leinster Coalfield, Ireland. *Irish Journal of Earth Sciences*, **23**, 65–84.

HOOK, R. W. and FERM, J. C. 1985. A depositional model for the Linton tetrapod assemblage (Westphalian D, Upper Carboniferous) and its palaeoenvironmental significance. *Philosophical Transactions of the Royal Society B: Biological Sciences*, **311**, 101–109.

— — 1988. Paleoenivronmental controls on vertebrate bearing abandoned channels in the Upper Carboniferous. *Palaeogeography, Palaeoclimatology, Palaeoecology*, **63**, 159–181.

— and and BAIRD, D. 1988. An overview of the Upper Carboniferous Fossil Deposit at Linton, Ohio. *The Ohio Journal of Science*, **88**, 55–60.

HUXLEY, T. H. and WRIGHT, E. P. 1867. Royal Irish Academy On a Collection of Fossil Vertebrata , from the Jarrow Colliery, County of Kilkenny, Ireland. *Transactions of the Royal Irish Academy*, **24**, 351–370.

KVALE, E. P., ARCHER, A. W. and JOHNSON, H. R. 1989. Daily, montly, and yearly tidal cycles within laminated siltstones of the Mansfield Formation (Pennsylvanian) of Indiana. *Geology*, **17**, 365-368.

LAURIN, M. and SOLER-GIJÓN, R. 2010. Osmotic tolerance and habitat of early stegocephalians: indirect evidence from parsimony, taphonomy, palaeobiogeography, physiology and morphology. *Geological Society, London, Special Publications*, **339**, 151–179.

MILNER, A. C. 2019. A morphological revision of *Keraterpeton*, the earliest horned nectridean from the Pennsylvanian of England and Ireland. *Earth and Environmental Science Transactions of the Royal Society of Edinburgh*, **109**, 237–253. doi: 10.1017/S1755691018000579.

MILNER, A. R. 1980a. The tetrapod assemblage from Nýřany, Czechoslovakia. 439–496. *In* Panchen, A. L. (ed). *The terrestrial environment and the origin of vertebrates*. Academic Press, London.

— 1980b. The temnospondyl amphibian Dendrerpeton from the Upper Carboniferous of Ireland. *Palaeontology*, **23**, 125–141.

— 1987. The Westphalian tetrapod fauna; some aspects of its geography and ecology. *Journal of the Geological Society*, **144**, 495–506.

NEVILL, W. E. 1956. The millstone grit and lower coal measures of the Leinster Coalfield, *Proceedings of the Royal Irish Academy*, **58**, 1–16.

Ó GOGÁIN, A., FALCON-LANG, H. J., CARPENTER, D. K., MILLER, R. F., BENTON, M. J., PUFAHL, P. K., RUTA, M., DAVIES, T. G., HINDS, S. J. and STIMSON, M. R. 2016. Fish and tetrapod communities across a marine to brackish salinity gradient in the Pennsylvanian (early Moscovian) Minto Formation of New Brunswick, Canada, and their palaeoecological and palaeogeographical implications. *Palaeontology*, **59**, 689–724. doi: 10.1111/pala.12249.

O'MEARA, M. 1964. *Unpublished report on the diamond dnlling programme 1959-1963 carried out in the Leinster Coalfield Dublin Department of Industry and Commerce*.

POINTON, M. A., CHEW, D. M., OVTCHAROVA, M., SEVASTOPULO, G. D. and CROWLEY, Q. G. 2012. New high-precision U–Pb dates from western European Carboniferous tuffs; implications for time scale calibration, the periodicity of late Carboniferous cycles and stratigraphical correlation. *Journal of the Geological Society*, **169**, 713-721.

SEQUEIRA, S. E. K. 1996. A cochleosaurid amphibian from the Upper Carboniferous of Ireland. *Special Papers in Palaeontology*, **52**, 65–80.

SEVASTOPULO, G. D. 2009. Carboniferous: Mississippian (Serpukhovian) and Pennsylvanian. 175–215. *In* HOLLAND, C. H. and SANDERS, I. S. (eds). *The Geology of Ireland*. *Second edition*. Dunedin, Edinburgh, 568 pp.

SUTTON, M. D., *GARWOOD, R. J., SIVETER, D. J. and SIVETER, D. J.* 2012. SPIERS and VAXML; A software toolkit for tomographic visualisation and a format for virtual specimen interchange. *Palaeontologia Electronica*, **15**, 1–14.

TYSON, R. V. 1995. *Sedimentary organic matter, organic facies and palynofacies*. Chapman and Hall, London, 615 pp.

WYSE JACKSON, P. N., DEARCE, M. and MONAGHAN, N. T. 2011. A letter from William Bookey Brownrigg to Thomas Henry Huxley, dated 29 November 1865, authorising him to describe his fossil vertebrates from Jarrow Colliery, Co. Kilkenny and giving details of his find. *Irish Journal of Earth Sciences,* **29**, 19-22. doi: 10.3318/IJES.2011.29.19.

Chapter 3: Preservation of the tetrapods from the Jarrow Assemblage.

3.1 Introduction

The Jarrow assemblage preserves an important diverse assemblage of early tetrapods with nearly complete articulated skeletons preserving body outlines. This potential wealth of information is however masked by the poor state of the specimens. Since their first description, the preservation of the Jarrow tetrapods has been remarked upon. Huxley and Wright (1867) mentioned that the "the specimens resemble casts in soft wax, which look their best at a distance, and rather lose than gain in clearness by close examination". The boundary between the skeletons and the matrix is difficult to distinguish. Bone instead appears to blend into the matrix. This was generally attributed to a layer of matrix masking the fossils (Huxley and Wright, 1867). The difficulty of distinguishing features in the Jarrow tetrapods has led to them being relatively understudied compared to the other similar coal swamp assemblages from Linton, Ohio (Hook and Baird, 1988) and Nýřany, Czech Republic (Milner, 1980).

Huxley and Wright (1867) suggested that bone is hard to distinguish from the matrix as it has been coalified, being replaced with bituminous material. Rayner, (1971) sectioned a spine of the acanthodian *Gyracanthus* from Jarrow (specimen GSM 12106), which showed replacement of hydroxyapatite (collophane) with "large" carbonate crystals. In areas of the spine which showed a higher degree of compression, a groundmass of apatite was found to replace the original bone material (Rayner, 1971). Rayner (1971) also mentioned that the vertebrae of *Ophiderpeton brownriggii* contain small apatite crystals in a carbonaceous groundmass but did not figure any sections. Drew (2004) sectioned specimen NHM.F14744 (*Ophiderpeton brownriggii*) and noted the presence of carbon-rich pockets in the bone with concentric ring patterns with differing sulphur content. Bone replacement has been attributed to acidic bottom waters of the Jarrow channel remobilising apatite (Rayner, 1971; Drew, 2004). Rayner (1971) proposed that there were at least two stages of calcium phosphate mobilisation, followed by a phase of coalification. Drew (2004) also suggested that during diagenesis there would have been mobilisation of apatite in acidic bottom waters and that reprecipitation of apatite would encrust integumentary structures. These integumentary structures were then replaced with concentric carbon-pockets mentioned above. This was finally followed by the infill of void space by sphalerite. The absence of pyrite within the altered bone and its presence within the matrix led Drew (2004) to suggest that diagenesis of the skeletons and the matrix differed.

Replacement makes examination of the Jarrow tetrapods problematic. Manual preparation of specimens TCD.R252 (*Keraterpeton galvani*) and TCD.38352 (*Keraterpeton galvani*) has been effective in increasing the contrast between bone and matrix, yet the boundary between them is still indistinct. Many of the specimens from Jarrow are fragile and partially degraded from pyrite disease. This means that manual preparation is not an appropriately safe technique. Additionally, manual preparation may remove part of the soft body and scalation. Acid etching and latex peeling (*sensu* Baird, 1955) is a common technique for preparing coal seam tetrapods but it has been less effective on material from Jarrow. This is seen in the caudal region of specimen TCD.T83 (*Urocordylus wandesfordii*), which was prepared using acid etching by Bossy (1976). More modern techniques, such as micro-computed tomography (µCT), had not been used on the Jarrow tetrapods before the present study. Being able to differentiate the body fossil and the matrix is vital for the application µCT. If the body fossil and the matrix share similar mineralogical compositions, then the resulting CT-slices will not reveal contrast between them.

In this chapter the use of cathodoluminescense (CL) and associated SEM based EDAX analysis to examine the composition of the vertebra and the scalation of one of the aïstopods, *Ophiderpeton brownriggii*, is described. This provided information for the best way in which to apply µCT to the specimens. Additionally, laser ablation inductively coupled mass spectrometry (LA-ICP-MS) was used to date the apatite using U-Pb dating. CT-slices utilised in later chapters were used to highlight the taphonomy of the specimens.

3.2 Material and Methods

Osteoderms and a vertebra from a specimen of *Ophiderpeton brownriggii* (NMI.F16850) were mounted in epoxy resin and polished to approximately half-thickness. These were then imaged using cathodoluminescence (CL) and analyzed by energy-dispersive X-ray spectroscopy via scanning electron microscopy (SEM-EDX) at the iCRAG laboratory, Trinity College Dublin. Analyses were carried out using a Tescan TIGER MIRA3 field emission SEM, equipped with two Oxford XMax^n 150 mm^2 EDS detectors. The TIGER MIRA3 instrument utilizes the Oxford Instruments AZtec X-ray microanalysis software suite. The instrument was calibrated using a suite of appropriate mineral standards from the Smithsonian Institute (Jarosewich, 2002; Jarosewich et al., 1980) following the method of Ubide et al. (2017). Analytical biases using this setup for CaO, P_2O_5, F are typically < 1% (Ansberque et al., 2019; Ubide et al., 2017). For elemental Cl analysis the instrument was calibrated using natural scapolite (meionite) NMNH R6600 obtained from the Smithsonian Institute. Two quality control standards were used; a natural reference material fluorapatite,

NMNH 10402 (Jarosewich et al., 1980) and scapolite BB-1 (Kendrick, 2012; Kendrick et al., 2013) to verify accuracy. The observed analytical biases for Cl analyses were < 5 %. The detection limit for Cl utilizing this analytical setup is ~ 0.10 wt. %.

Apatite was also analysed by LA-ICP-MS at TCD. The analytical setup utilized a Teledyne Photon Machines G2 laser-ablation system, comprising a 193 nm ArF excimer laser and a Helex II active two-volume ablation cell, coupled to a Thermo Scientific iCAPQc ICP-MS. Analyses were conducted using a 35 µm spot size with Calcium the internal standard element. The repetition rate was 15 Hz with an energy density of 1.6 Jcm^{-2}. Oxide production rates were below 0.02%. The integration times for individual mass scans were 60 ms for mass 238, 10 ms for masses 232, 207, 206 and 202, and 5 ms for mass 204. Data reduction was completed using the VizualAge_UcomPbine DRS reduction scheme which makes use of the Iolite software package of Paton et al. (2011) and were corrected for variable common Pb. Following installation of VizualAge of Petrus and Kamber (2012), the additional files required for the VizualAge_UcomPbine DRS can be found at http://www.japetrus.net/va/UcomPbine/.

The analytical procedure for apatite U-Pb geochronology utilized repeated blocks of six apatite standards followed by 20 unknown samples using standard-sample bracketing. The six apatite standard analyses comprised: two analyses of the primary standard Madagascar apatite (ID-TIMS concordia age of 473 ± 0.7 Ma; Chew *et al*. (2014) and references therein); followed by two analyses of both Durango apatite (^{40}Ar–^{39}Ar of 31.44 ± 0.18 Ma; McDowellet al. 2005) and McClure Mountain apatite (weighted mean $^{207}Pb/^{235}U$ age of 523.51 ± 2.09 Ma; Schoene and Bowring, 2006) (Appendix 2).

Micro-computed tomography (µCT) was carried out using the Nikon XTH 225ST instrument of the Palaeobiology Research Group, University of Bristol on the following specimens: TCD.38352 - *Keraterpeton galvani*; NMI.F14879 - *Ophiderpeton brownriggii*; and TCD.38365 - *O. brownriggii*. The specimen scanned on the Nikon XTH225 ST instrument at the Amber Lab, Trinity College Dublin was TCD.T85 - *Lepterpeton dobbsii*. Scan parameters were: TCD.38352 - *Keraterpeton galvani* scanned at 225 kV, 165 uA with a 05mm Cu filter; NMI.F14679 - *Ophiderpeton brownriggii* scanned at 225kV, 120uA with a 1mm Cu filter; TCD.38363 - *Ophiderpeton brownriggii* at 225kV, 115 uA with a 1.5mm Cu filter; and TCD.T85b -*Lepterpeton dobbsii* scanned at 75kV, 214µA with no filter.

3.3 Geochemical Results

3.3.1 Cathodoluminescence

Cathodoluminescence of osteoderms and a vertebra from NMI.F16850 (*Ophiderpeton brownriggii*) conform to Drew's (2004) account, that bone no longer retains its typical internal vascular morphology. Instead bone has been replaced by angular carbon-rich grains, surrounded by smaller apatite crystals (Fig 3.1). Apatite (determined by Energy Dispersive Analysis of selected spots on the CL image) in the fossils are elongated sub-rectangular zoned crystals, with a lighter core enriched in Cl and a darker rim poorer in Cl (Table 3.1). Sphalerite and a K-rich clay also appear within the bone. Carbon-rich grains match that of the coal matrix. This suggest that they are coalified pockets. The matrix also contains apatite, but in less abundance than within the body fossil.

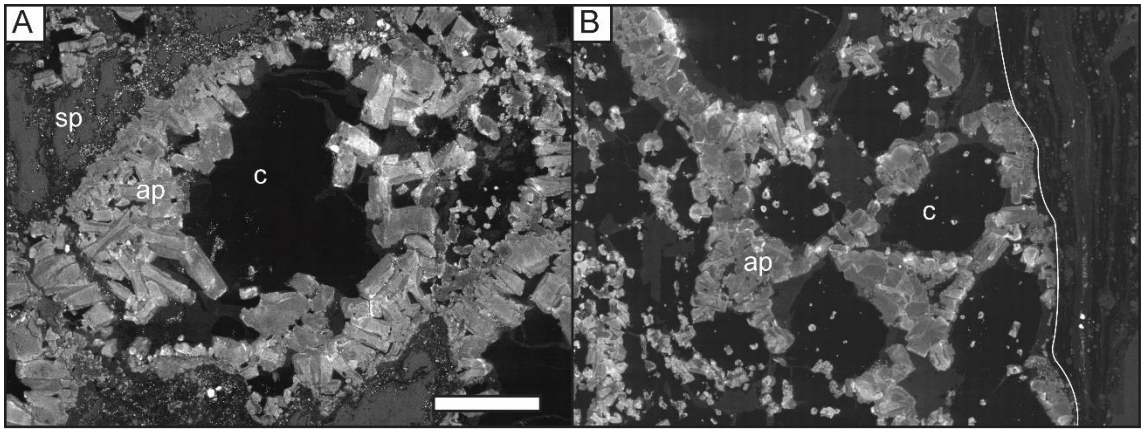

Figure 3.1. SEM cathodoluminescence image of (A) an osteoderm and (B) a vertebra of *Ophiderpeton brownriggii* NMI.F16850. The white line in B indicates the boundary between the vertebra and matrix. Abbreviations are ap, apatite, c, carbon-rich mass and sp, sphalerite. Scale bar = 100µm for A and 125µm for B.

Location on apatite	Cl%
Core-1	0.46
Core-2	0.74
Core-3	0.74
Rim-1	0.09
Rim-2	0
Rim-3	0

Table 3.1. Differences in Cl concentration between the core and rim of apatite crystals in the osteoderm of *Ophiderpeton brownriggii* NMI.F16850 (Fig. 3.1A).

3.3.2 LA-ICP-MS

The secondary standards, Durango apatite (n= 15) and McClure Mountain apatite (n= 15) yielded U-Pb TW concordia lower intercept ages of 31.0 ± 2.0 Ma (MSWD= 1.06) and 521 ± 22 (MSWD= 0.61), respectively. Apatite from NMI.F16850 provided a U-Pb TW of 308 ± 11.0 Ma (MSWD= 1.03) (Fig. 3.2).

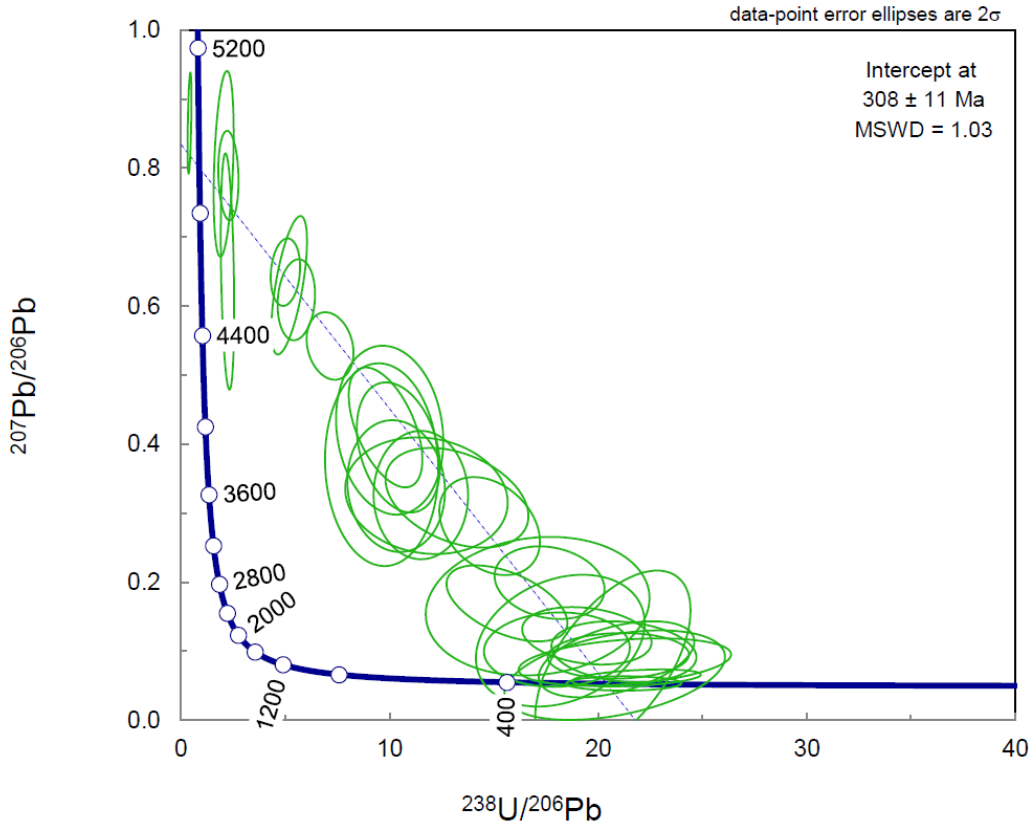

Figure 3.2. Terra Wasserburg plot of U-Pb dating of apatite from NMI.F16850 giving an age of 308 ± 11 Ma.

3.4 Discussion

3.4.1 Implications for the mechanisms of preservation

Cathodoluminescence reveals that the body fossils and matrix of the tetrapod specimens analysed from Jarrow have similar composition, with body fossils containing carbon-rich pockets surrounded by small apatite crystals and the matrix being composed of coal with small apatite crystals throughout. This is problematic for µCT, which works better where there is a difference in mineralogical composition between the area of interest (the body fossil) and the background (the matrix). However, there is a higher concentration of apatite in the body fossil than in the matrix (Fig. 3.1B, Fig. 3.3) and this allows for the overall body fossil to be made out. The high degree of alteration of the bone also creates problems for identifying

features within the bone in the CT-slices. Such features as the spinal nerve foramen in the vertebrae and lateral lines in the cranial bones can be difficult to identify. Recrystallisation of the bone also creates problems when trying to identify sutures between bones. Where a bone suture is not seen in a position where it would be expected, it can be difficult to judge whether this is a result of the bones fusing during life, or recrystallisation. Ideally multiple specimens of the same species need to be scanned. If a lack of bone sutures is consistent in all specimens it would be indicative of fusion during life. Specimens from the Jarrow assemblage are highly compressed. In many articulated specimens the palate and braincase are compressed between the mandibles and the cranial elements (Fig. 3.3B,C). In these cases, compression, recrystallization and coalification of the specimens results in the boundary between the palate, braincase and the "overlying" or "underlying" mandibles being very difficult to discern. Additionally, certain specimens are highly fractured, such as the aïstopod *Ophiderpeton brownriggii* (NMI.F14879). The degree of preservation appears to vary between specimens. *Keraterpeton galvani* (TCD.38352) (Fig. 3.3A) preserves clearly distinguishable bone sutures and even preserves the pitting of the dermal cranial bones in great detail. In contrast, *Ophiderpeton brownriggii* (TCD.38363) (Fig. 3.3C) preserves very little cranial detail. Preservation even varies within a single specimen. *O. brownriggii* (NMI.F14679) contains cheek elements in which lateral line pits can be identified, yet the midline elements are preserved as an amorphous mass (Fig. 3.3B). Apatite veins in the matrix intersect some specimens (Fig. 3.3B) which also hinders µCT analysis. Additionally, contrary to the observations of Drew (2004), pyrite can be found within body fossils (Fig. 3.3D). Specimens with high concentrations of pyrite within them produce the worst µCT images, as the contrast between coal and apatite is lessened. µCT works best when specimens preserve a 3D structure with a large contrast between different materials. Specimens from Jarrow clearly do not fit either criteria well. Yet, µCT has been effective in at least aiding in describing some of the specimens (Chapters 4-7).

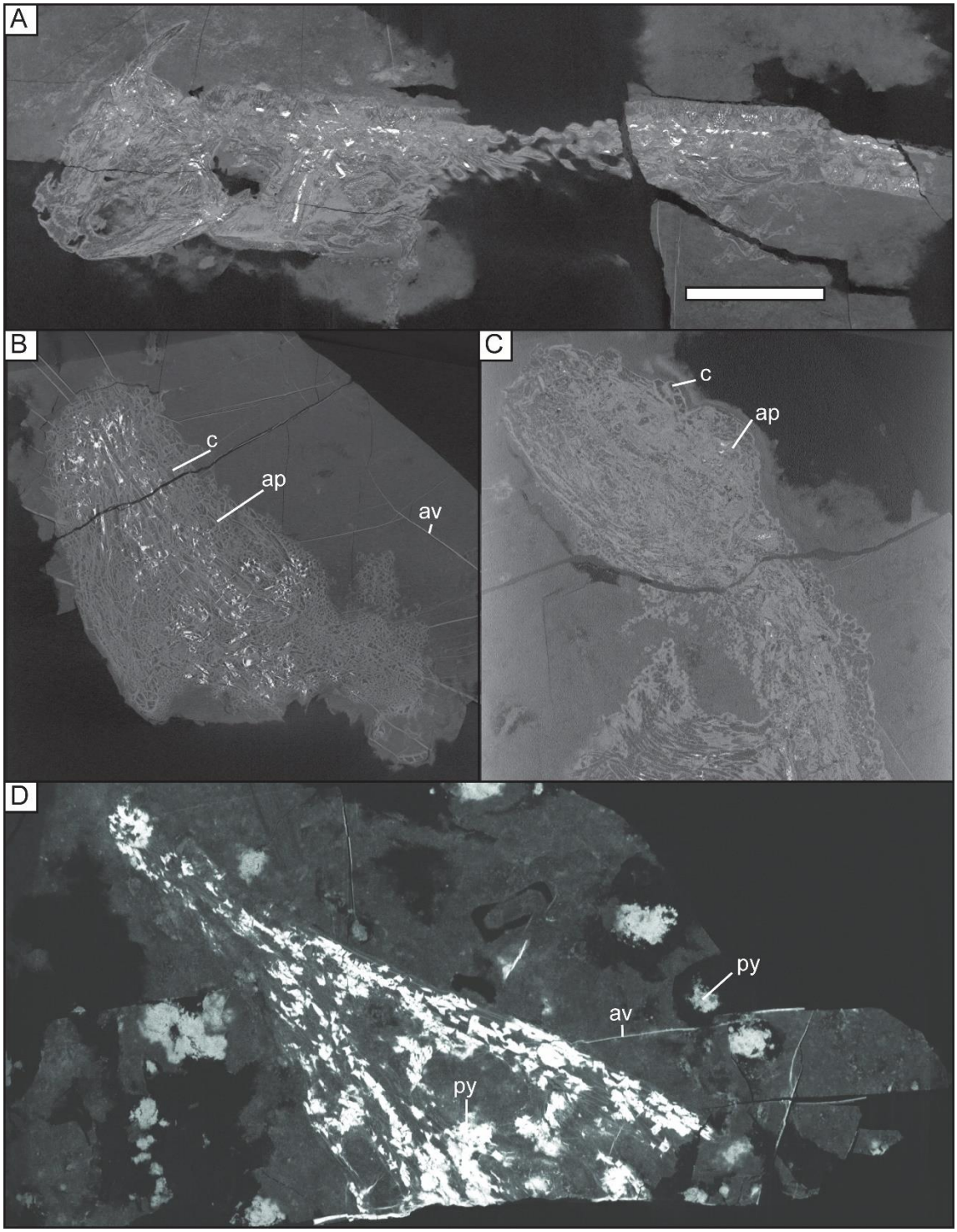

Figure 3.3 Computed tomography slices of (A) TCD.38352 *Keraterpeton galvani*, (B) NMI.F14879 *Ophiderpeton brownriggii*, (C) TCD.38365 *O. brownriggii* and (D) TCD.T85 *Lepterpeton dobbsii*. Abbreviations are ap, apatite, av, apatite vein, c, coal (high C content), py, pyrite. Scale bar = 20mm for A, 16mm for B, 10mm for C and 6mm for D.

3.4.2 Processes of alteration

The apatite crystals that replace the bone yield U-Pb ages of 308±11 Ma. The horizon of the Jarrow seam is at least as young as the middle part of the Langsettian, probably slightly

below the horizon of the Tonstein T75 from Belgium dated by Pointon et al. (2012) at approximately 317.6 Ma. Although the ages of the Jarrow apatite crystals are just within error of the estimated depositional age of the Jarrow seam (Higgs and O'Connor, 2005), the probability is that the reprecipitation of the apatite that replaces bone is younger. This suggests that the acid remobilisation model of Rayner (1971) and Drew (2004) is not correct. Coals in the Leinster Coalfield are anthracites and vitrinite reflection measurements suggest that the rocks have has been heated to 300-350ºC (Clayton *et al.*, 1989), placing them within the greenschist metamorphism facies. It should be noted that the nearly contemporary Pennsylvanian tetrapod assemblage at Linton, Ohio (Hook and Baird, 1988) was deposited in a similar environment to the Jarrow assemblage. Fossil fish and tetrapods from this assemblage preserve the original bone morphology (Hook and Hower, 1988). The Pennsylvanian coals in eastern Ohio are of very much lower thermal maturity than the Jarrow coal ($\%R_0 \sim 0.6 – 0.8$; Ruppel et al. 2014). This may suggest that metamorphism during deep burial, as suggested by Hook and Hower (1988), was the main factor that lead to bone replacement in the Jarrow tetrapods, and not the original acidic depositional environment. The age of maximum burial in the Leinster Coalfield is not known because the succession is truncated as a result of later uplift and erosion. In the Kish Basin, offshore Dublin, the youngest Carboniferous rocks are Asturian in age (Naylor et al. 1993). Assuming that the eroded succession of the Leinster Coalfield extended to the Asturian (late Moscovian), peak burial would have been at 306 -310 Ma (Gradstein *et al*. 2012). This suggests that the U-Pb dates from the apatite (308±11 Ma) reflect precipitation of apatite resulting in the alteration of bone of the Jarrow tetrapods during deep burial, rather than a consequence of acid dissolution during early diagenesis.

3.5 Conclusion

The preservation of the Jarrow assemblage is different from the approximately coeval Linton, Ohio assemblage, despite similar depositional environments. Osteoderms and a vertebra in *Ophiderpeton brownriggii* show that bone no longer retains its structure. It has been replaced by large carbon-rich pockets surrounded by small elongated zoned crystals of apatite. Sphalerite is also present within the body fossil. Body fossils from the Jarrow assemblage have a similar mineralogical composition to that of the surrounding matrix except that they have a higher concentration of apatite relative to the matrix. Pyrite also occurs within body fossils. The degree of detail revealed varies between specimens and within specimens. Despite the imperfect nature of the Jarrow material for study by µCT, this method has produced results which aided the descriptions in later chapters of this thesis. Apatite in the bones of tetrapods from the Jarrow assemblage have been dated using U-Pb dating. On balance, the ages of reprecipitated apatite crystals (308±11 Ma) is more likely to have occurred during deep burial

(probably during the Asturian/late Moscovian) rather than following acid dissolution during early diagenesis as suggested by Rayner (1971).

3.6 References

ANSBERQUE, C., MARK, C., CAULFIELD, J. T., & CHEW, D. M. 2019. Combined in-situ determination of halogen (F, Cl) content in igneous and detrital apatite by SEM-EDS and LA-Q-ICPMS: A potential new provenance tool. *Chemical Geology*, **524**, 406–420. doi.org/10.1016/j.chemgeo.2019.07.012.

BAIRD, D. 1955. Latex micro-molding and latex-plaster molding mixture. *Science*, **122**, 202.

BOSSY, K. V. H. 1976. Morphology, paleoecology and evolutionary relationships of the Pennsylvanian urocordylid nectrideans (Subclass, Lepospondyli, Class Amphibia). Unpublished PhD thesis, Yale University–Disertation abstracts, **37**, 2731.

CHEW, D. M., PETRUS, J. A. and KAMBER, B. S. 2014. U–Pb LA–ICPMS dating using accessory mineral standards with variable common Pb. *Chemical Geology*, **363**, 185–199.

CLAYTON, G., HAUGHEY, N., SEVASTOPULO, G. D. and BURNETT, R. 1989. *Thermal maturation levels in the Devonian and Carboniferous rocks in Ireland*. Geological Survey of Ireland, Dublin, 36 pp.

DREW, C. 2004. Skeletal and soft tissue taphonomy of the Jarrow amphibians from southeast Ireland. Unpulished Masters thesis, University of Bristol.

GRADSTEIN, F. M., OGG, J. G., SCHMITZ, M. D. & OGG, G. M. 2012. *The Geologic Time Scale*. Elsevier.

HIGGS, K. T. and O'CONNOR, G. 2005. Stratigraphy and palynology of the Westphalian strata of the Leinster Coalfield, Ireland. *Irish Journal of Earth Sciences*, **23**, 65–84.

HOOK, R. W. and BAIRD, D. 1988. An overview of the Upper Carboniferous Fossil Deposit at Linton, Ohio. *The Ohio Journal of Science*, **88**, 55–60.

— and HOWER, J. C. 1988. Petrography and taphonomic significance of the vertbrate-bearing cannel coal of Linton, Ohio (Westphalian D, Upper Carboniferous. *Journal of Sedimentary Petrology*, 58, 72–80.

HUXLEY, T. H. and WRIGHT, E. P. 1867. Royal Irish Academy On a Collection of Fossil Vertebrata , from the Jarrow Colliery, County of Kilkenny, Ireland. *Transactions of the Royal Irish Academy*, **24**, 351–370.

JAROSEWICH, E. 2002. Smithsonian Microbeam Standards. *Journal of Research of the National Institute of Standards and Technology*, **107**, 681. doi.org/10.6028/jres.107.054.

— NELEN, J. a, & NORBERG, J. 1980. Reference samples for electron microprobe analysis. *Geostanders Newsletter*. **4**, 43–47.

KENDRICK, M. A. 2012. High precision Cl, Br and I determinations in mineral standards using the noble gas method. *Chemical Geology*, ***292–293***, 116–126. doi.org/10.1016/j.chemgeo.2011.11.021.

— ARCULUS, R., BURNARD, P., & HONDA, M. 2013. Quantifying brine assimilation by submarine magmas: Examples from the Galápagos Spreading Centre and Lau Basin. *Geochimica et Cosmochimica Acta*, **123**, 150–165.doi.org/10.1016/j.gca.2013.09.012.

MCDOWELL, F. W., MCINTOSh, W. C. and FARLEY, K. A. 2005. A precise 40Ar–39Ar reference age for the Durango apatite (U–Th)/He and fission-track dating standard. *Chemical Geology*, **214**, 249–263.

MILNER, A. R. 1980. The tetrapod assemblage from Nýřany, Czechoslovakia. 439–496. *In* Panchen, A. L. (ed). *The terrestrial environment and the origin of vertebrates*. Academic Press, London.

NAYLOR, D., HAUGHEY, G., CLAYTON, G. and GRAHAM, J. R. 1993. The Kish Bank Basin, offshore Ireland. 845–855. *In*: PARKER, J.R. (ed). *Petroleum Geology of Northwest Europe: Proceedings of the 6th Conference*. Geological Society, London.

PETRUS, J. A. and KAMBER, B. S. 2012. VizualAge: A Novel Approach to Laser Ablation ICP-MS U-Pb Geochronology Data Reduction. *Geostandards and Geoanalytical Research*, **36**, 247–270.

POINTON, M. A., CHEW, D. M., OVTCHAROVA, M., SEVASTOPULO, G. D. and CROWLEY, Q. G. 2012. New high-precision U–Pb dates from western European Carboniferous tuffs; implications for time scale calibration, the periodicity of late Carboniferous cycles and stratigraphical correlation. *Journal of the Geological Society,* **169**, 713-721.

RAYNER, D. H. 1971. Data on the environment and preservation of Late Palaeozoic tetrapods. *Proceedings of the Yorkshire Geological Society*, **38**, 437–495.

RUPPEL, L.F., TRIPPI, M.H., HOWER, J.C., GRADY, W.C., and LEVINE, J.R. 2014. Thermal maturity patterns in Pennsylvanian coal-bearing rocks in Alabama, Tennessee, Kentucky, Virginia, West Virginia, Ohio, Maryland, and Pennsylvania, Chap. F.2. *In* RUPPEL, L.F., and RYDER, R.T., (eds*). Coal and petroleum resources in the Appalachian basin; Distribution, geologic framework, and geochemical character*. U.S. Geological Survey Professional Paper 1708, 13 p. dx.doi.org/10.3133/pp1708F.2.

SCHOENE, B. and BOWRING, S. A. 2006. U-Pb systematics of the McClure Mountain syenite: thermochronological contraints on the age of the $^{40}Ar/^{39}Ar$ standard MMhb. *Contributions to Mineralogy and Petrology*, **151**, 615-630.

UBIDE, T., GUYETT, P. C., KENNY, G. G., O'SULLIVAN, E. M., AMES, D. E., PETRUS, J. A., RIGGS, N., & KAMBER, B. S. 2017. Protracted volcanism after large impacts: Evidence from the Sudbury impact basin. *Journal of Geophysical Research: Planets*, **122**, 701–728. doi.org/10.1002/2016JE005085.

Chapter 4: *Ophiderpeton brownriggii* and *Peisterpeton milnerorum* gen. nov., sp. nov from the Jarrow Assemblage (Langsettian, Pennsylvanian), Ireland, described using micro-computed tomography.

4.1 Introduction

Aïstopods are a clade of highly derived tetrapodomorphs that first appeared in the Viséan (Wellstead, 1982, Milner, 1993, Anderson *et al*., 2003) and disappeared by the Early Permian (Baird, 1964; Lund, 1978). The most notable feature of the clade is their elongated bodies composed of holospondylus vertebrae, with up to 220 vertebrae in the most derived forms (Anderson, 2002). Aïstopods lacked limbs and a pelvic girdle, and pectoral girdles consist of sickle-shaped elements found loosely attached to the vertebral column. This gives them eel-like or snake-like appearance. Skulls are small and fenestrated around the cheek area (Lund, 1978; Carroll, 1998a; Pardo *et al*. 2017), marking the earliest known occurrence of skull fenestration within tetrapods.

Aïstopods were first described from the tetrapod assemblage at the Jarrow Colliery, Co. Kilkenny, Ireland by T.H. Huxley (Etheridge, 1866; Wright and Huxley, 1866; Huxley and Wright, 1867); two species were formally named, the larger blunt-snouted *Ophiderpeton brownriggii* Huxley in Wright and Huxley, 1866 and the smaller narrow-snouted *Dolichosoma emersoni* Huxley in Huxley and Wright, 1867. *O. brownriggii* was officially described from three figured specimens, two body fossils (TCD.T89 and TCD.T90) and one impression (TCD.T88) by Huxley in Huxley and Wright (1867), but had been named a year earlier (Etheridge, 1866; Wright and Huxley, 1866). A third aïstopod species was described from Jarrow as *Dolichosoma huxleyi* from a single specimen (NMI.F14679) (Lydekker, 1891), though this appears to be the only mention of *D. huxleyi* in the literature. Since the initial descriptions of the Jarrow aïstopods by Huxley and Lydekker, little work was undertaken on them until Milner (1993) described the cranial elements of *O. brownriggii* from a single isolated skull (NHMUK R8465). *O. brownriggii* was included in reviews of the aïstopods (Baird, 1964; Carroll, 1998a) but was excluded from a revaluation of the Ophiderpetontidae by Carroll (1998b).

The family Ophiderpetontidae was erected by Schwarz (1908) to incorporate *Ophiderpeton* Huxley in Huxley and Wright (1867) and *Oestocephalus* Cope (1868). Hancock

and Atthey (1868) described a second species of *Ophiderpeton* from Northumberland, England as *Ophiderpeton nanum*. Cope (1868, 1875) and Fritsch (1875, 1879) named several species of *Ophiderpeton* from the coal seams of Linton, Ohio and Nýřany, Czech Republic. These species of *Ophiderpeton* were reduced to a single species per locality by Romer (1930) and (Steen, 1931, 1938), who could not distinguish different species from the material from each assemblage. This left *Ophiderpeton amphiuminus* Cope (1868) and *Ophiderpeton granulosum* (Fritsch, 1880) as the only ophiderpetontids from the Linton and Nýřany assemblages respectively. Milner (1993) described *Ophiderpeton kirktonense* from East Kirkton, Scotland and restricted the genus *Ophiderpeton* to include only *O. brownriggii* and *O. kirktonense*, and suggested that *O. amphiuminus*, *O. nanum* and other named *Ophiderpeton* material should be placed within the genus *Oestocephalus*. Anderson's (2003a) review of the Ophiderpetontidae, considered *Oestocephalus granulosum* and *Oestocephalus vicinum* to be junior synonyms of *Oestocephalus amphiuminus*, as no differences between *Oestocephalus* specimens from Linton, Ohio, Mazon Creek, Illinois and Nýřany, Czech Republic were found. *Oestocephalus nanum* still remains a distinct valid species (Anderson, 2003a). Vaughin (1969) added the new species *Coloraderpeton brilli* to the Ophiderpetontidae. Phylogenetic analysis of the aïstopods reveals that the Ophiderpetontidae are paraphyletic, with *Ophiderpeton* being placed as a sister taxon to more derived ophiderpetontids, *Pseudophlegethontia* and *Phlegethontia* (Anderson *et al*. 2003). This makes the validity of the ophiderpetontids as a clade questionable. This led Anderson (2003a) to establish a new family, the Oestocephalidae for the more derived ophiderpetontids, comprising *Oestocephalus* and *Coloraderpeton.* Ophiderpetontids is still used informally to group Oestocephalidae and *Ophiderpeton*, together, despite oestocephalids sharing a closer common ancestor with *Phlegethontia* than with *Ophiderpeton* (Anderson, 2003b).

Traditionally aïstopods were classified within the sub-class Lepospondyli, a group of small, elongated Palaeozoic tetrapods with reduced limbs (Baird, 1965). Within this group, aïstopods represented the oldest and most specialised clade, with all other clades arising within the Late Mississippian and the Pennsylvanian (Baird, 1965). The evolutionary relationship of aïstopods has been disputed. Aïstopods have been placed both on the lissamphibians stem (Trueb and Cloutier, 1991; Vallin and Laurin, 2004) or on the amniote stem (Ruta, *et al.*, 2003). Recent imaging of the braincases of *Lethiscus stocki* (Pardo *et al.* 2017) and *Oestocephalus* (Pardo, *et al*., 2019) using micro-computed tomography (µCT) has revealed several plesiomorphic characteristics, placing aïstopods on the tetrapod stem, crownward of *Acanthostega* (Pardo, *et al*., 2017) or possible further down the stem (Pardo, *et al*., 2019). A stem-tetrapod placement is also supported by the jaw of *Andersonerpeton longidentatum*, which includes plesiomorphic characters such as pointed teeth on all coronoids, denticles on the adsymphyseal and a parasymphyseal fang pair (Pardo and Mann, 2018). Phylogenetic analysis

in Clack *et al*. (2019) placed aïstopods in a stem-tetrapod clade with colosteids, nectrideans, adelospondyls, *Aytonerpeton* and *Acherontiscus*

Given the lack of descriptions of the Jarrow aïstopods, it is imperative that they are redescribed to aid our understanding of early aïstopod evolution and the understanding of tetrapod evolution. Here micro-computed tomography has been carried out on four separate specimens identified as *O. brownriggii* to aid better morphological description. The specimens include the syntype TCD.T90, the figured specimen in Milner (1993) NHMUK R8465, a smaller, less mature specimen TCD.38363 and the type specimen of *Dolichosoma emersoni* NMI.F14679. All specimens are considered to represent *O. brownriggii*, with the exception of TCD.T90 which appears to be a previously unidentified new genus and species of Ophiderpetontidae here named *Peisterpeton milnerorum* gen. et. sp. nov.

4.2 Material and Methods

Micro-computed tomography was carried out on NMI.F14679 *Ophiderpeton brownriggii*, TCD.T90 *Peisterpeton milnerorum* and TCD.38363 *Ophiderpeton brownriggii* using the Nikon XTH 225ST from the Palaeobiology Research Group, University of Bristol and on NHMUK R8465 *Ophiderpeton brownriggii* using the Nikon Metrology HMX ST 225 at the Imaging and Analysis Centre, Natural History Museum, London. The scanning parameters are as follows: NHMUK R8465 *Ophiderpeton brownriggii* scanned at 100kV, 340uA with a 1.5mm Al filter; NMI.F14679 *Ophiderpeton brownriggii* scanned at 225kV, 120uA with a 1mm Cu filter; TCD.T90 *Peisterpeton milnerorum* scanned at 225kV, 187uA with a 2mm Cu filter; TCD.38363 *Ophiderpeton brownriggii* was scanned twice, for the cranium at 225kV, 115 uA with a 1.5mm Cu filter, and for the trunk scanned at 225kV 170uA with a 1.5mm Cu filter.

Resulting TIF-stacks were converted into PNG files and imported into the freeware SPIERS (Sutton *et al.*, 2012). Fossils were virtually separated from the matrix using the masking function.

Museum abbreviations are: FMNH, Field Museum of Natural History; NHMUK, Natural History Museum, United Kingdom; NMI, National Museum of Ireland; TCD, Trinity College Dublin, Geological Museum.

A systematic description of the taxa was formed. The systematic section includes a synonym list with the notation v representing that the author has viewed the specimens mentioned in previous works (*sensu* Matthews, 1973).

4.3 Systematic Palaeontology

Infraclass TETRAPODOMORPHA Ahlberg, 1991

Order AÏSTOPODA Miall, 1875

Family OPHIDERPETONIDAE Schwarz, 1908

Diagnosis— Aïstopods with blunt snout and orbits positioned anteriorly. Temporal fenestra is closed with weak suturing between the jugal and quadratojugal. Mandible articulates to the cranium posterior of the occipital condyle. Transverse process originates from the centrum and does not contact the neural arch.

Genus *PEISTERPETON* gen. nov.

Type Species— *Peisterpeton milnerorum* sp. nov.

Diagnosis—Ophiderpetontid aïstopod with a pineal foramen. Skull table width 25% of the skull table length except at the waisted parietals where it is 20%. Mandible slightly concave along its dorsal margin. Lacks large osteoderms along the cheek region.

PEISTERPETON MILNERORUM sp. nov.

(Figs. 4.1-4.3)

v. 1866 *Ophiderpeton brownriggii* Huxley *in* Wright and Huxley:**.

v. 1867 *Ophiderpeton brownriggii*; Huxley *in* Huxley and Wright:365, pl. 22, figs. 3

Etymology— "*Peist*" from the Irish for serpent (péist) and "-erpeton" from the Greek for crawler; *milnerorum* in honour of Dr Andrew and Dr Angela Milner who have worked extensively on the Jarrow tetrapods.

Diagnosis—Same as for genus.

Holotype—TCD.T90 (Figured in Huxley and Wright, 1867, plate 22, figure 3.)

Type Locality—Clogh, County Kilkenny, Ireland.

Type Horizon—Jarrow (No. 4) Coal Seam, Coolbaun Coal Formation, Langsettian: Pennsylvanian.

Description

TCD.T90 is dorso-ventrally flattened, preserving the skull, mandibles and 10 articulated vertebrae in ventral view. Posterior to the 10th vertebra the block of coal in which it is preserved is broken, hindering any identification of further postcranial elements.

Cranium

In dorsal view the ventral margin of the right side of the cranium is partially tucked under the rest of the cranium, while the ventral margin of the left side is exposed. 3D preservation is better in the posterior midline elements of the skull compared to those of the rostral, orbital and cheek regions. The skull table is waisted along the parietal to accommodate the temporal fenestra. The temporal fenestra is hard to distinguish in TCD.T90 as compression has distorted its shape and forced palatal elements to "infill" it. The snout of TCD.T90 comprises approximately half of the length of the skull table (Fig. 4.1A, C). The snout is highly fractured and compressed making the identification of individual elements nearly impossible. A lateral bone extension into the left orbit probably represents the dorsal process of the postorbital. The exact morphology of frontals, nasals and prefrontals cannot be seen due to the fracturing. The most anterior midline elements that can be readily identified are the parietals. Their anterior margins are not clearly visible, but posteriorly they are better preserved. The parietals are paired elements which make up approximately 22% of the length of the skull table. Midway between their posterior and anterior margins is a pineal foramen. The lateral margin of each parietal forms the dorsal margin of the temporal fenestra. The parietals contact the postparietals along their postero-medial margin and the supratemporal along their posterior-lateral margin. The parietal-supratemporal contact is positioned anterior of the parietal-

postparietal contact which gives the parietal a medial posterior projection. The supratemporal composes the posterior-dorsal margin of the temporal fenestra and contacts the postparietal along its medial margin, preventing the parietal from contact with the tabular. The posterior margin of the skull table is made up of the postparietals medially and the tabulars laterally. The postparietals extend anteriorly to approximately the midpoint of the supratemporal.

No premaxilla can be found near the anterior margin of the snout. This is common in aïstopods where the premaxilla is displaced. It is unclear whether part of the posterior end of the premaxilla is present close to the left maxilla. Here this bone housing teeth is interpreted as just the maxilla. The maxilla forms the ventral margin of the orbit. It extends posteriorly and tapers just posterior to the level of the pineal foramen. There are at least four maxillary teeth associated with the left maxilla. They are disarticulated and displaced lateral to the left maxilla. The right maxilla houses a single articulated tooth. The disarticulated teeth in the left maxilla are widely spaced but it is not clear whether this can be taken to suggest that the teeth were widely spaced in life. Teeth are curved posteriorly towards their apex. A jugal is present, articulated to the dorsal margin of the right maxilla. The jugal has a dorsal rounded process which probably forms the postero-ventral margin of the orbit. It has a long posterior process which extends backwards as far as the maxilla and makes up the anterior half of the ventral margin of the temporal fenestra (Fig. 4.1B, D). The posterior half of the ventral margin of the temporal fenestra is made up of the quadratojugal which contacts the jugal and maxilla anteriorly. The quadratojugal is a long robust element which extends posterior to the occipital condyle to articulate with the lower jaw. The suture between the quadrate and the quadratojugal cannot be distinguished. On either side of the skull table, the squamosal is difficult to distinguish. On the left side it appears to contact the tabular and supratemporal and forms the posterior margin of the temporal fenestra. It contacts the quadratojugal along its ventral margin, which extends from the posterior margin of the temporal fenestra to a position just posterior to the occipital condyle. Posterior to the tabulars and postparietals is the occipital complex. It is highly fractured preventing the identification of constituent elements apart from the condyle which juts out posteriorly to articulate with the atlas.

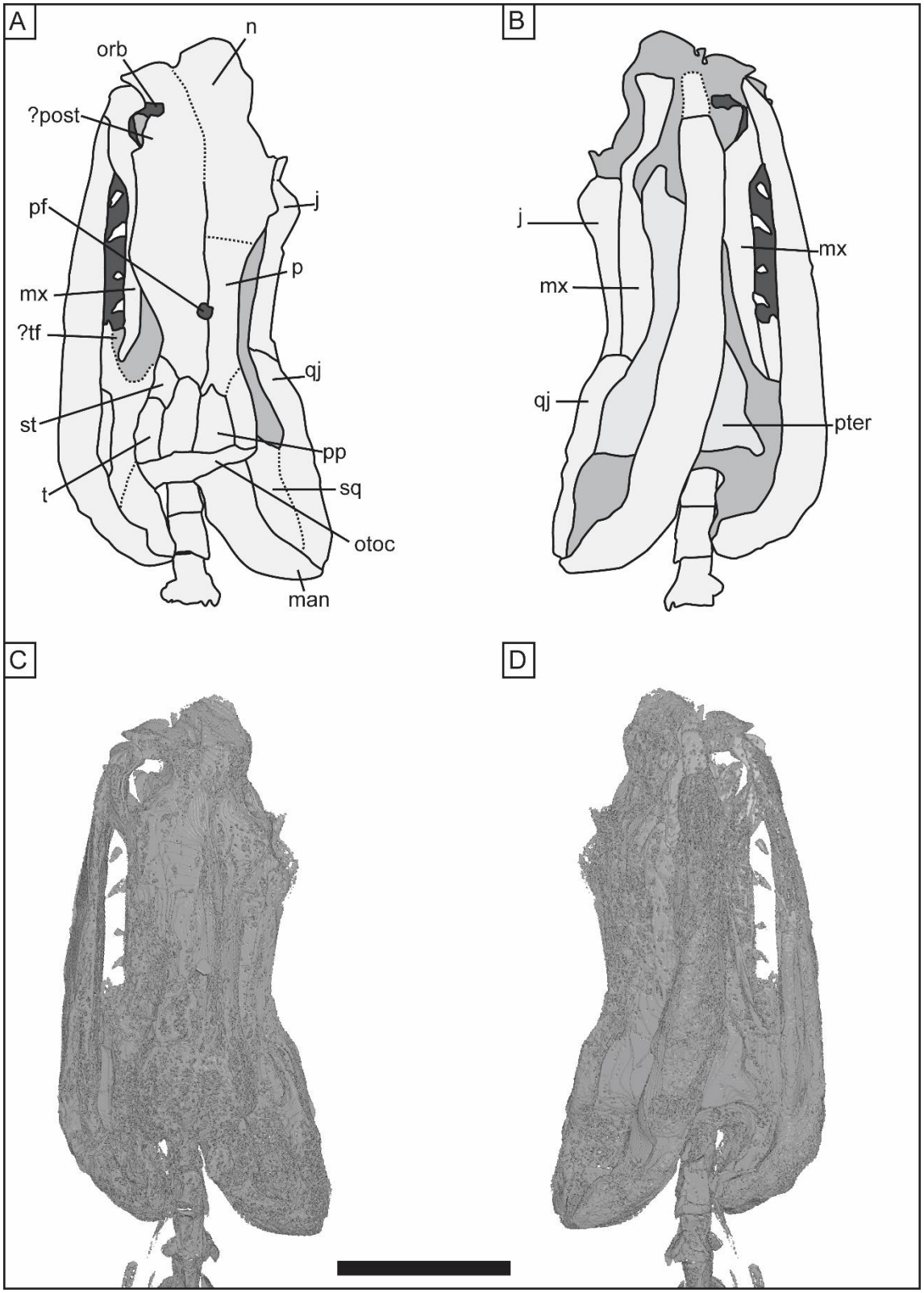

Figure 4.1. Cranium of TCD.T90 *Peisterpeton milnerorum* in (A and C) dorsal view and (B and D) ventral view. Abbreviations: j, jugal; man, mandible; mx, maxilla; n, nasal; orb, orbit; otoc, occipital complex, p, parietal; pf, parietal foramen; ?post, postorbital?; pp, postparietal; pter, pterygoid; qj, quadratojugal; sq, squamosal; st, suptratemporal; t, tabular; ?tf, temporal fenestra?. Scale bar = 10mm.

Palate

The morphology of the pterygoids is more clearly distinct posteriorly and less so anteriorly (Fig 4.1B, D). The pterygoids have a nearly straight posterior margin. Here pterygoids attain their greatest width. A postero-lateral process seen in the left pterygoid contacts the quadratojugal but does not extend posteriorly to the articulation with the quadrate. The morphology of the quadrate rami is unknown. The medial margins of the pterygoids and the parasphenoid are not visible as the right mandible has been compressed into them. The pterygoids thin and extend at least as far anteriorly as the posterior margin of the orbits. An ectopterygoid, palatine and vomer are observable on the right side of the palate (Fig. 4.2). The ectopterygoid is an elongated element that extends posteriorly at least to the level of the posterior margin of the maxilla and houses seven alveoli for palatal denticles, arranged in a curved line. The ectopterygoid contacts the palatine anteriorly midway along the length of the jugal. The palatine is also an elongated element with a row of eight palatine denticle alveoli which are arranged in a straight line. The vomer is a thin curved element with at least six palatal denticle alveoli. It appears to be disarticulated from the palatine on the right side. The left vomer is observable in the left side and has been displaced into the orbit.

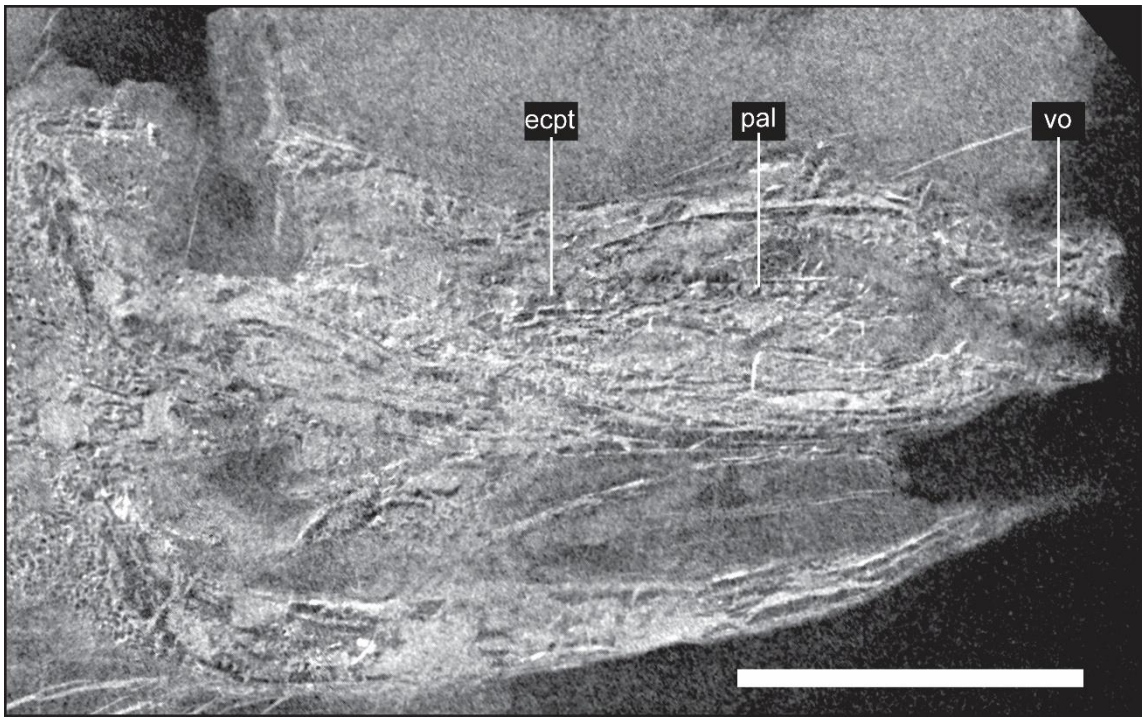

Figure 4.2. CT-slice of TCD.T90 *Peisterpeton milnerorum* showing part of the palate. Abbreviations: ecpt, ectopterygoid; pal, palatine, vo, vomer. Scale bar =10mm.

Lower Jaw

In ventral view, the lateral side of the posterior end of the right mandible is exposed. Anteriorly it is curved c.90^0 clockwise so that its dorsal surface is exposed (Fig. 4.1). This makes the right mandible appear thicker than the left, whose medial surface is exposed (Fig. 4.3A, B). Mandibles are slightly concave along their dorsal surface with a postero-dorsal projection forming the jaw articulation. The left mandible is highly flattened making the identification of elements in dorsal view problematic. In lateral view the deep transverse recess of the articular is exposed in the left mandible. Sutures between the articular, surangular and angular are not visible. The dentary makes up 80% of the dorsal surface of the mandible anteriorly. There is a recess between the dentary and the angular on the left mandible, but the absence of a similar recess in the right mandible indicates that this is not a natural feature and may be due to the angular being displaced dorsally over the dentary and surangular. Anterior to this recess, the angular tapers out so that the dentary composes the entire lateral surface of the mandible anteriorly. There is slight anticlockwise curvature anteriorly in the left mandible exposing the anterior end of the splenial. In medial view the transverse groove of the articular, which accommodates the quadrate for jaw articulation, is partially covered by the prearticular. The prearticular extends ventro-anteriorly from the articular. Anteriorly the prearticular is split by the Meckelian foramen. The ventral process of the prearticular extends c. 6% of the length of the Meckelian foramen along its ventral side, while its dorsal process extends anterior to the Meckelian foramen. Both processes of the prearticular contact the splenial anteriorly, which makes up the majority of the ventral margin of the Meckelian foramen and the rest of the medial surface of the mandible anteriorly. A row of seven small alveoli on the medial side of the dorsal surface of the right mandible, posterior to the symphyses, probably indicates the presence of a coronoid, with alveoli representing denticle sites. It is not possible to determine whether there is a single coronoid or more.

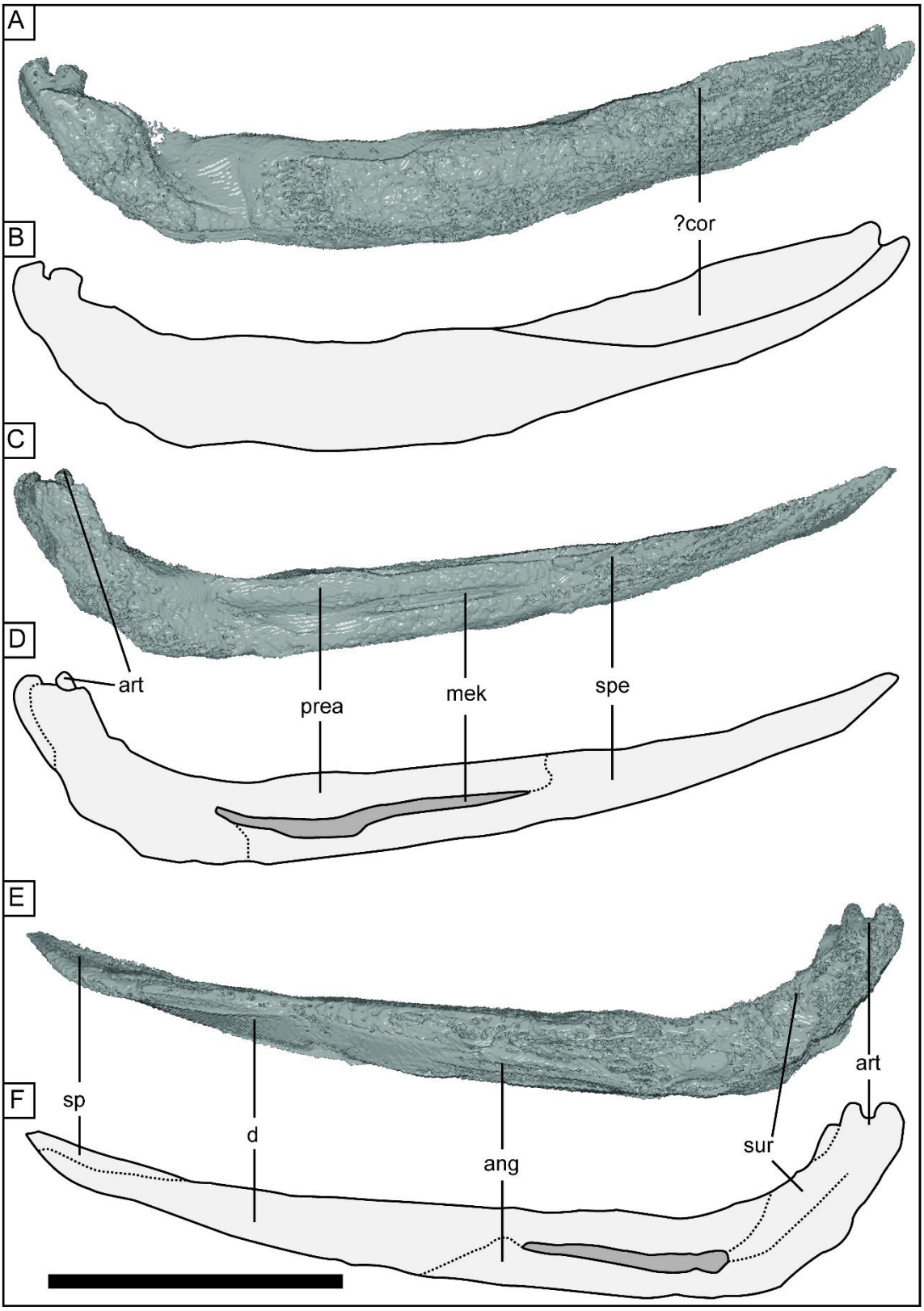

Figure 4.3. Mandible of TCD.T90 *Peisterpeton milnerorum* showing (A-B), the left mandible in lateral view, (C-D), the left mandible in ventral view and (E-F) the left mandible in lateral view. Abbreviations: ang, angular; art, articular; ?cor, coronoid?; d, dentary; mek, Mekilian foramen; prea, prearticular; sp, spenial; sur, surangular. Scale bar = 10mm.

Axial Skeleton

Ten articulated vertebrae are preserved posterior to the cranium in TCD.T90. Vertebrae conform to the aïstopod pattern and are amphicoelous with waisted centra. Centra have a mid-ventral antero-posterior orientated ridge running along their ventral surfaces. Transverse processes extended posterio-laterally from the lateral midpoint of the centrum in each vertebra at an angle of c.30°. The transverse process does not thicken distally unlike *Ophiderpeton brownriggii* (see below). The exact nature of the contact between the neural arch and the centrum is difficult to discern, but it is likely that it is fused to the centrum as is typical of aïstopods. The neural spine has four projections, two anterio-lateral projections and two posterior-lateral projections terminating in the anteriorzygapophysis and the posteriorzygapophysis. Both the anteriorzygapophysis and the posteriorzygapophysis have horizontal articulation surfaces. A neural spine appears to be present but the presence of dorsal osteoderms in the CT slices hinders an interpretation of its morphology. All preserved vertebrae are of similar morphology with the exception of the atlas. The atlas is shorter with two small posteriorly orientated projections on the anterior margin of its centrum. Transverse processes are present on the centrum but no ribs appear to articulate with them. The presence of an odontoid process cannot be clearly established. The atlas articulates directly with the condyle and a proatlas is not present. Ribs associated with vertebra 5 lack a "K"-shape. It is uncertain whether this is also the case for more posterior ribs. The shape of the head of the rib is not visible. Rib length is slightly greater than the length of two vertebrae.

Appendicular skeleton

The pectoral elements of aïstopods are considered to consist of a fused clavicle and cleithrum (Anderson, 2002). A single pectoral element is present, visible immediately posterior to the posterior margin of the right mandible. It has the typical "sickle" shape seen in other aïstopods (Carroll, 1998a; Anderson, 2002).

Scalation

Sub-elliptical osteoderms cover the cheek region of TCD.T90 as far anteriorly as the posterior border of the temporal fenestra, leaving the majority of the temporal fenestra free of scalation. Sub-ovoid osteoderms also cover the dorsal margin of the postcranium and extend as far posteriorly as the natural breakage in the block (and thus likely carry on posteriorly). These osteoderms also form a covering down to the ventral side of the post-cranial region as far posteriorly as the 4th vertebra. There appears to be no major size variation among osteoderms

in different areas unlike in *O. brownriggii* (see below). Posterior to the 4th vertebra the skin outline is marked by tightly interlocked gastralia along the ventral margin of the specimen. Similar to the dorsal osteoderms, the gastralia extend as far posteriorly as the breakage. It is difficult to estimate the exact length of the gastralia, but several of them are slightly shorter than the vertebrae.

Remarks— TCD.T90 is the only identifiable specimen of *Peisterpeton milneri*. The Jarrow assemblage has c.25 specimens of aïstopods, the majority of which are represented solely by postcranial material. Many of these specimens, in turn, are represented by hollowed out fossils. It is difficult to distinguish from which of the three Jarrow aïstopods these specimens represent.

Genus *OPHIDERPETON* Huxley in Etheridge, 1866

Type Species—*Ophiderpeton brownriggii* Huxley *in* Wright, and Huxley, 1866.

Diagnosis—Ophiderpetontid aïstopod with a dorsal tuberculation covering the centre of ossification of the parietals. Here it is termed the pineal button as it is located where the pineal foramen would be expected. Highly waisted parietals changing the skull table width to length from 50% to 27%. Squamosal is robust.

OPHIDERPETON BROWNRIGGII Huxley *in* Wright, and Huxley, 1866

(Figs. 4.4-4.11)

v 1866 *Ophiderpeton brownriggii* Huxley *in* Wright and Huxley, 1866:167.

v 1867 *Ophiderpeton brownriggii*; Huxley *in* Huxley and Wright, 1867:364, pl. 22, figs. 1–4

v 1891 *Dolichosoma huxleyi* Lydekker, 1891:60

v 1994 *Ophiderpeton brownriggi*; Milner, 1993:366, fig. 4

Syntypes—TCD.T88 (Figured in Huxley and Wright 1867, plate 22, figure 4.); TCD.T89 (Figured in Huxley and Wright 1867, plate 22, figure 1).

Topotypes—NHMUK R 8465, NMI.F14679 and TCD.38363

Type Locality—Clogh, County Kilkenny, Ireland.

Type Horizon—Jarrow (No. 4) Coal Seam, Coolbaun Coal Formation, Langsettian: Pennsylvanian.

Diagnosis— *Ophiderpeton* with broad squamosal that contacts the skull table along the lateral margins of the tabular and supratemporal.

Description

NHMUK R 8465 and NMI.F14679 are the two largest specimens of *Ophiderpeton brownriggii* and are here considered to be the most mature forms. NHMUK R 8465 is a dorso-ventrally flattened cranium with articulated mandibles. Two vertebrae are preserved posteriorly. It is mostly free of the matrix allowing for observation of both the dorsal and ventral sides. NMI.F14679 is a cranium with articulated mandibles in ventral view and an articulated vertebral column with c.55 vertebrae. The specimen is currently broken into three blocks and the matrix is brittle in parts. It had been conserved by applying a plastic casing around the outer edges and on the base of the specimen. The breakage probably happened after conservation work as the breaks include the plastic casing. TCD.38363 is the longest and most complete specimens of *O. brownriggii* in ventro-lateral view. It shows a cranium with articulated mandibles and vertebral column with c.69 vertebrae. Given the fact that its cranium is smaller than that of other described specimens, it is considered to be of a less mature individual. The holotype TCD.T89, the only specimen here that was not scanned, preserves a smaller specimen of *O. brownriggii,* similar to TCD.38363. It is preserved in lateral view with the disarticulated skull roof dorsal to the mandibles and is exposed in dorsal view. It has an articulated vertebral column containing c.50 vertebrae.

Cranium

The cranium of NHMUK R 8465 has a blunt snout, anteriorly positioned orbitals and temporal fenestra which causes a constriction in the skull table along the parietals. The mandibles articulate with the suspensorium, composed of the squamosal, quadratojugal and quadrate (*sensu* Carroll, 1998a), posterior to the occipital condyle. The length of the of the cranium from the suspensorium to the anterior tip of the rostrum is 45.6mm, while the skull table length is 34.1mm. The snout makes up 36% of the skull table. The paired nasals are situated at the anterior end of the skull table and overlie the premaxilla in NHMUK R 8465 (Fig. 4.4A, B). The midline through the nares is at an angle of 25° to the midline through the frontal and has probably been shifted during post-mortem decay and burial. The right nasal appears to make up the anterior corner of the nares, but is mostly excluded by the prefrontal. The frontals contact the nasals along their posterior margin with a slightly interdigating suture. The paired frontals are more than twice the length of the nasals. The anterior half of the frontals appear to be less wide than the nasals. The midline area of the frontals is hard to discern anteriorly. The frontals expand laterally along their posterior half. In NHMUK R 8465 the frontals contact the parietals along their posterior margin along an interdigating suture. The frontal-parietal sutures extend to the anterodorsal corner of the temporal fenestra. The parietal-frontal contact in TCD.38353 is different from that in NHMUK R 8465 as the frontals have a posterior extension along their lateral side into the parietal (Fig. 4.5A). The extension does not extend as far posteriorly as the pineal "button" (see below). The parietals are the longest elements of the skull table in NHMUK R 8465. A dorsal swelling is present on the midline at the centre of ossification for the parietals of NHMUK R 8465 and TCD.38363 and is here termed the pineal button. No pineal foramen is present in this button. The parietals form the dorsal margin of the temporal fenestra. Where the posterior margin of the temporal fenestra begins to extend ventro-posteriorly the skull table expands laterally. The parietals do not widen sideways with the skull table and are excluded from the posterior margin of the temporal fenestra by the supratemporal. Posterior of the parietals and the supratemporal are the paired postparietals which compose the majority of the posterior margin of the skull roof. The tabular makes up the lateral most corner of the posterior margin of the skull. A contact between the supratemporal and the postparietal excludes the parietal from contacting the tabular.

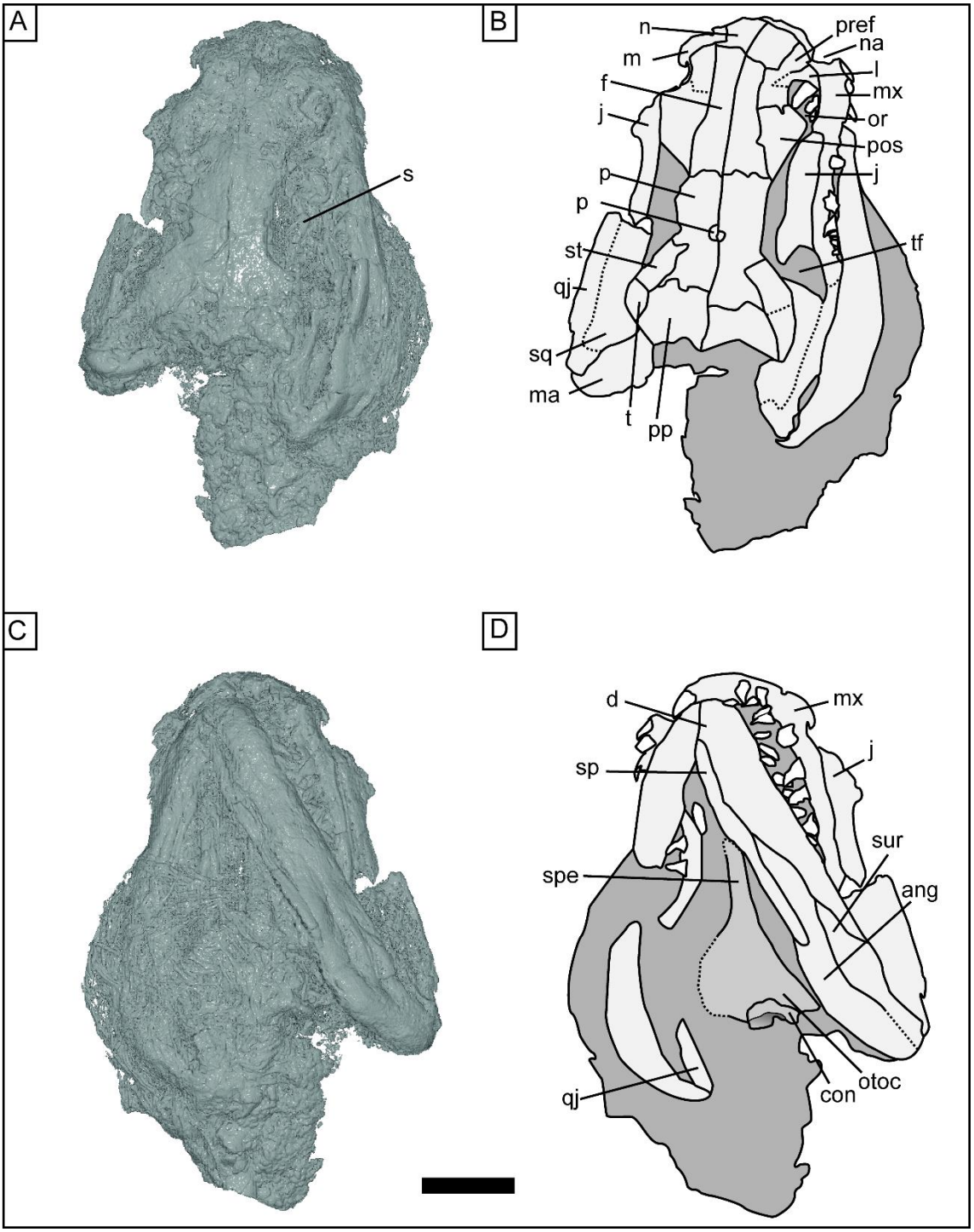

Figure 4.4. The skull of NHMUK R 8465 *Ophiderpeton brownriggii* in (A-B), dorsal view and (C-D), ventral view. Abbreviations: ang, angular; con, condyle; d, dentary; f, frontal; j, jugal; l, lacrimal; man, mandible; mx, maxilla; n, nasal; na, nares; orb, orbit; otoc, occopital condyle; p, parietal; pb, parietal "button"; post, postorbital; pp, postparietal; pref, prefrontal; qj, quadratojugal; s, scute; sp, spenial; spe, sphenoid; sq, squamosal; sur, surangular; st, supratemporal; t, tabular; tf, temporal fenestra. Scale bar = 10mm.

The lacrimal is a triangular element that forms the anterior and ventro-anterior margin of the orbit. In NHMUK R 8465 it contacts the prefrontal along its anterior margin. As a result of postmortem displacement, the prefrontal excludes the lacrimal from contacting the nasal. It

is unclear whether and to what extent the nares receive a contribution from the lacrimal. In NMI.F14679 there is an unidentified bone between the lacrimal and the maxilla. It is unclear whether it is part of the lacrimal or part of a different cranial element and it appears to merge seamlessly with the other indistinguishable cranial elements dorsally (Fig. 4.6). This unidentified element appears to exclude the maxilla from the ventral orbital margin. This appears to be the result of disarticulation and movement more than a record of the original bone positioning as the maxilla in NHMUK R 8465 makes up the ventral orbital margin. The prefrontal is a crescentic element. It forms a smooth contact with the frontal along its posterodorsal margin and appears to be notched at the frontal-nasal contact (Fig. 4.4A, B). It extends ventro-anteriorly to make up the dorsal margin of the nasal. Posterior of the lacrimal the prefrontal makes up the dorsal margin of the orbits. It contacts the postorbital along its posterior margin along a smooth sutural line. There is a small posterior projection of the prefrontal into the postorbital. The postorbital forms a smooth contact with the frontal and has a ventral curved extension which forms the posterodorsal boundary of the orbit. Posterior to this ventral extension, the postorbital tapers posteriorly where it contacts the anterior margin of the temporal fenestra. The right jugal of NHMUK R 8465 is displaced slightly posteriorly and shows its lateral side in dorsal view. The left jugal is overturned and overlain by the postorbital and its lateral side is visible in ventral view. The jugal is an elongated element which forms a smooth ventral contact with the maxilla. It expands dorsally from its anterior most part, with this expansion making up the ventro-posterior margin of the orbit. Posterior of the dorsal extension, the dorsal margin of the jugal is concave. The posterior end of the jugal is bifurcated with a posterodorsal and ventro-posterior extension. The former extension is far more robust than the latter. This posterodorsal extension would probably narrow the temporal fenestra. In NHMUK R 8465 and NMI.F14679 the jugal and maxilla are displaced from the quadratojugal. This leaves a gap in the ventral wall of the temporal fenestra. However, the temporal fenestra is not actually open. The presence of part of the jugal in contact with the quadratojugal on the left side of NMI.F14679 (Fig. 4.6) suggests that the jugal and quadratojugal contact one another. Due to the high frequency of breakages observed between these bones it is thought that this contact was porbably weak. Four small openings on the lateral face of the jugal of NMI.F14679 (Fig. 4.6) are here interpreted as openings for the lateral line system. The boundary between the squamosal and the quadratojugal is difficult to discern. The quadratojugal forms a long robust extension from the mid-point of the temporal fenestra to a point posterior to the condyle. Posteriorly, it extends slightly ventro-posteriorly to articulate with the mandible. There is no identifiable suture between the quadrate and quadratojugal. Bone in the transverse groove of the articular of the lower jaw in NMI.F14679 marks the only part of the quadrate that can certainly be identified. The base of the temporal fenestra is made up of the quadratojugal along its posterior half of its margin and the jugal along its anterior half. The squamosal sits between the

quadratojugal and the skull table. It forms the posterior margin of the cheek region and the posterior margin of the temporal fenestra. It is a broad bone with a ridge running along parallel to the quadratojugal. It contacts the tabular and supratemporal dorsally.

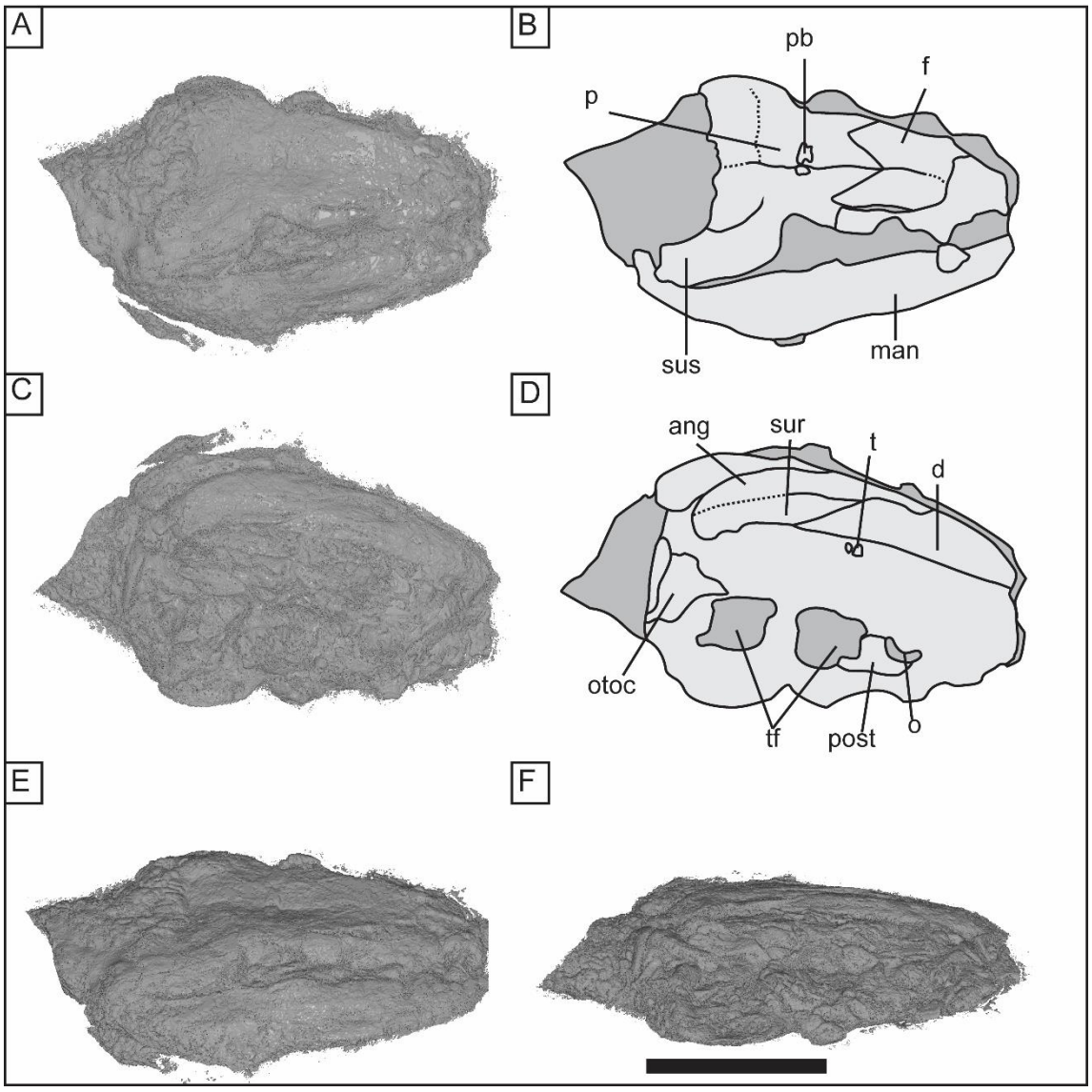

Figure 4.5. Skull of TCD.38363 *Ophiderpeton brownriggii* in A,B dorsal view, C,D, ventral view, E, dorso-lateral view and F, ventro-lateral view. Abbreviations: ang, angular; d, dentary; f, frontal; man, mandible; o, orbit; otoc, otoccipital condyle; p, parietal; p, parietal "button"; post, postorbital; sus, suspensorium; sur, surangular; t, tooth; tf, temporal fenestra. Scale bar = 13mm.

The premaxilla of NHMUK R 8465 is a robust element which makes up the flat blunt anterior margin of the cranium. It does not extend posteriorly along the midline and curves posteriorly at the anterio-lateral margin of the skull (Fig. 4.4). The boundary between the premaxilla and the maxilla is placed ventral of the nares as the premaxilla in NMI.F14679 appears to have broken off at this part (Fig. 4.6). The premaxilla of NHMUK R 8465 and

NMI.F14679 house four teeth each. This is unlikely to present the original number as there is space for between 8-10 teeth. The maxilla is similarly a robust element that extends posteriorly from its contact with the premaxilla ventral of the nares. It contacts the lacrimal and the jugal along its dorsal margin and forms the ventral margin of the orbit and the postero-ventral margin of the nares. The maxilla tapers abruptly directly posterior of the posterior margin of the jugal. The left maxilla of NHMUK R 8465 houses seven teeth while the right maxilla of NHMUK R 8465 and the left maxilla of NMI.F14679 both house 8 teeth. A single alveoli posterior of the last observable tooth on the left maxilla of NMI.F14679 indicates that it could house up to nine. Premaxillary/maxillary teeth are curved posteriorly towards their apex and preserve pulp cavities.

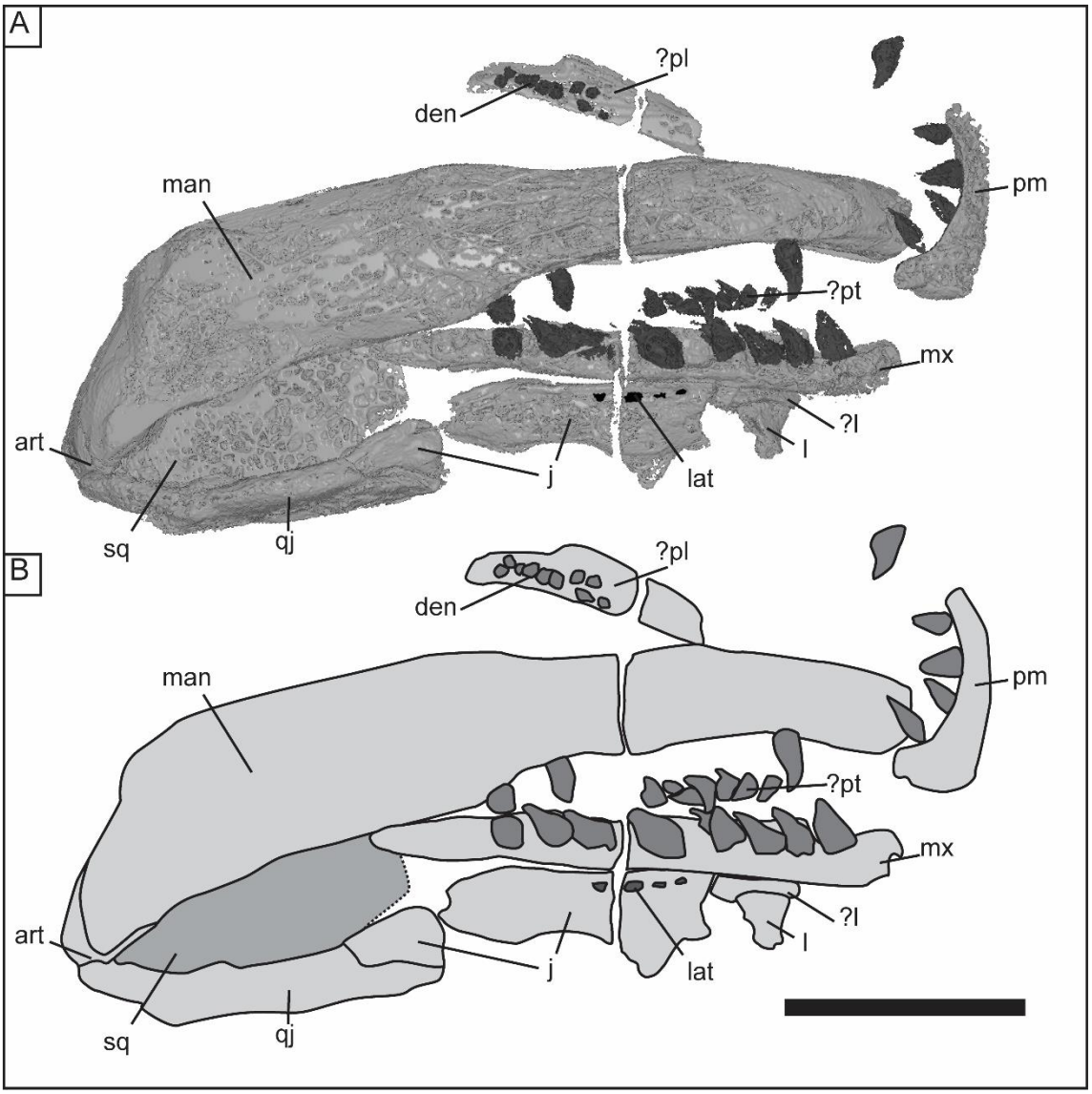

Figure 4.6. Skull of NMI.F14879 *Ophiderpeton brownriggii* in ventral view. Abbreviations: art, articular; den, denticles; j, jugal; l, lacrimal; ?l, lacrimal; lat, lateral line foramen; man, mandible; mx, maxilla; ?pl, palatine?; pm, premaxilla; ?pt, palatal teeth?; qj, quadratojugal; sq, squamosal. Scale bar = 10mm.

Palate

A palatal element is seen in NMI.F14679 and contains a two intersecting rows of palatal denticles with ten denticles in total (Fig. 4.6). It is uncertain whether the element represents a ectopterygoid, vomer or a palatine but it is here considered to represent a palatine because of its position midway along the skull. An antero-medial process seen below the left squamosal of NMI.F14679 originates at the quadrate-articular articulation and probably represents a posterior projection of the pterygoid.

Mandible

The mandible of *Ophiderpeton brownriggii* lacks a retroarticular process (Figs 4.6 and 4.7). The articular is best seen in the left mandible of NMI.F14679 which preserves the lateral side in ventral view. Here the articular composes dorso-posterior most element of the mandible. It has an anterior and ventro-anterior process which run along the dorsal surface of the surangular and the posterior surface of the angular respectfully before tapering out (Fig. 4.6). The preceding lateral mandible elements are observable in the left mandible of the less mature TCD.38363 (Fig. 4.5). The surangular, anterior to the articular, extends along the ventral margin of the mandible and tapers anteroventral to this margin between the dentary and the angular. This makes the ventral margin of the surangular make up 50% the length of the mandible. The angular is a long element that makes up the posterior margin of the mandible and expands two-thirds the length of the mandible anteriorly to contact that dentary. The dentary composes the remaining anterior part of the mandible. In the more mature NHMUK R 8465 the dentary makes up 70% of the dorsal margin (Fig. 4.4) as opposed to 60% in TCD.38363 (Fig. 4.5) indicating that the dentary is relatively longer in more mature forms. Eight recurved teeth are associated with the left dentary in NHMUK R 8465. Teeth appear to be widely spaced. At least five teeth-like structures are seen within the dentary (Fig. 4.8). These likely represent replacement teeth. On the dentary of the right mandible of NHMUK R 8465 there are three associated dentary teeth. Posterior of the posteriormost tooth is a row of four smaller teeth (Fig. 4.7B, D). The posteriormost tooth is recurved and may represent a dentary tooth. The other three however are small tightly packed straight teeth. They probably represent accessory teeth. An isolated tooth smaller than the dentary teeth on the medial side of the mandible anterior of the surangular may indicate the presence of a posterior coronoid (Fig. 4.7D). The morphology of the coronoid cannot be distinguished. It is unsure whether there is a single coronoid, or three as is the case for *Andersonerpeton* (Pardo and Mann, 2018).

The medial surface of the mandibles of NHMUK R 8465, NMI.F14679 and TCD.38363 are all difficult to model as this side of the mandible tends to be compressed against the palate/dorsal elements obscuring identification of individual elements. The most informative mandible for detail of the medial side is the right mandible of NHMUK R 8465 (Fig. 4.7C, D). Ventral of the articular, the prearticular extends ventro-anteriorly. It is uncertain to what extent this extension goes. Ventral of the prearticular there is a large Meckelian fossa. Anterior to the Meckelian fossa there is a long element, considered to be the splenial. More anteriorly elements are hard to distinguish.

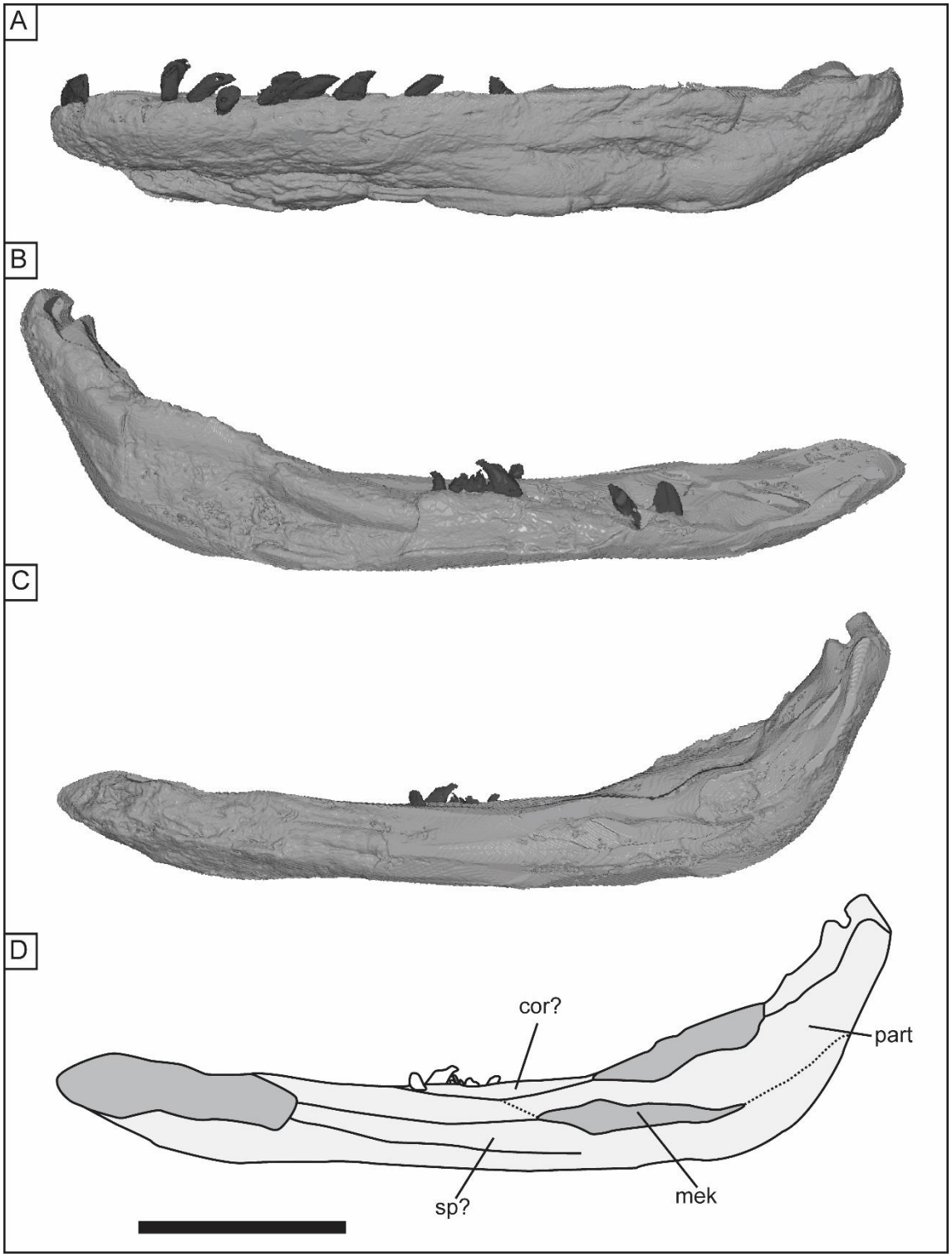

Figure 4.7. Mandible of NHMUK R 8465 showing A, left mandible in lateral view, B, right mandible in lateral view, C,D left mandible in ventral view. Abbreviations: cor?, coronoid?; mek, Mekilian foramen; part, prearticular; sp?, splenial?. Scale bar = 5mm.

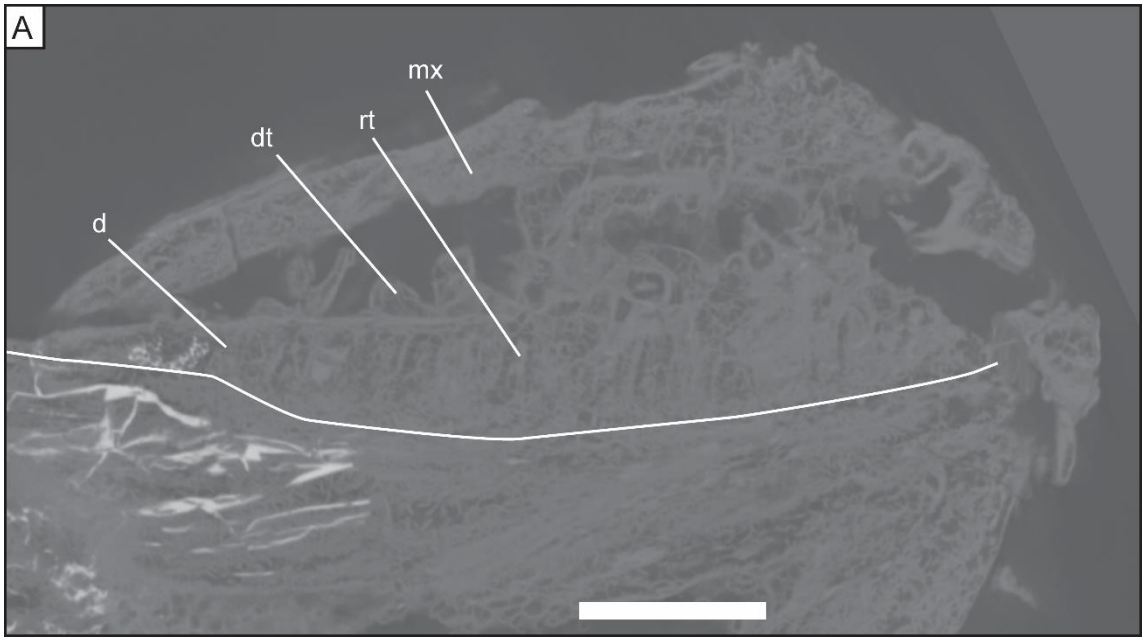

Figure 4.8. CT-slice of NMI.F14879 *Ophiderpeton brownriggii* showing possible replacement teeth in the dentary. Abbreviations: d, dentary; dt, dentary tooth, mx, maxilla, rt, replacement tooth. Scale bar = 5mm.

Appendicular skeleton

The pectoral girdle of *Ophiderpeton brownriggii* has an uneven sigmoidal shaped cleithrum/fused cleithrum and clavicle. This gives it the typical sickle shape seen in aïstopods (proximal handle and distal blade sections). In NMING.F14879 the pectoral element is an elongate curved process with a straight proximal (handle) portion. It thickens along the curve proximally, until it straightens out and begins to thin (Fig. 4.9A). The curved section (blade) curves away from the anterior of the body. It appears to be completely ossified throughout. Two pectoral girdles in TCD.38365 extend ventrally from the anterior portion of vertebra 4. This suggests that in life the pectoral elements were oriented so that their long axes was dorso-ventral.

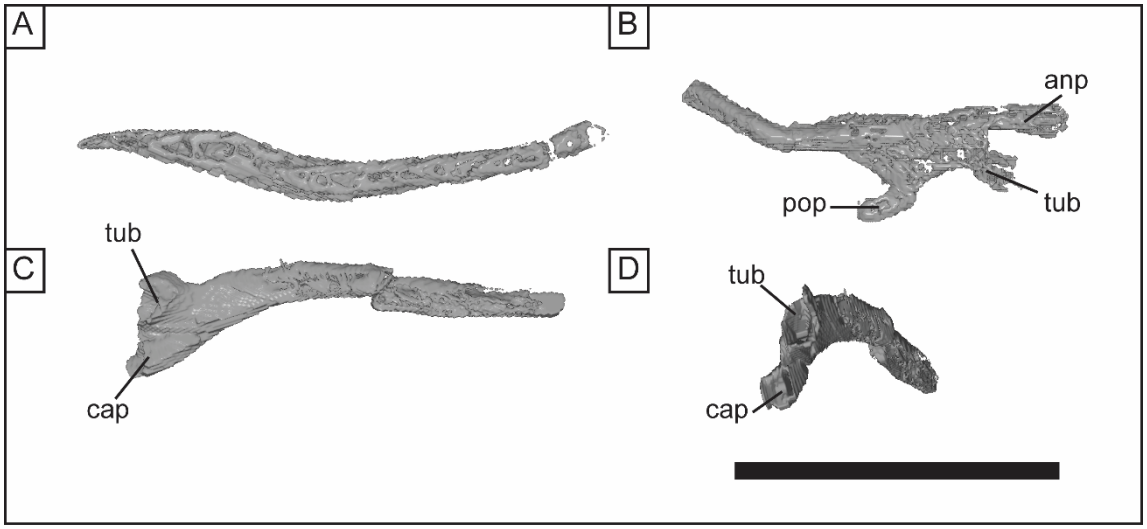

Figure 4.9. Ribs and shoulder girdle of NMING.F14879 showing (A), shoulder girdle lateral view, (B), K-shape rib near vertebra 7, and double-headed rib associated with vertebra 3 in (C), ventral view and (D), proximal view. Abbreviations: anp, anterior process; cap, capitulum; pop, posterior process; tub, tuberculum. Scale bar = 10mm.

Axial Skeleton

TCD.38363 preserve the longest complete trunk with approximately 69 vertebrae with the posterior most 22 vertebrae lacking ribs. Vertebra sizes diminish in these ribless vertebrae posteriorly, but it is uncertain whether the column includes all the vertebrae of the vertebral column as the posterior most vertebrae are slightly disarticulated. Aïstopods up to 93cm have been reported by the mid-1800's coal workers from Jarrow (Huxley and Wright, 1867) which might indicate that *Ophiderpeton brownriggii* had more vertebrae in its column. On the other hand these reported aïstopods could have belonged to the other two genera of Jarrow aïstopod. No haemal spines can be identified in TCD.38363 or in any of the other specimens of *O. brownriggii* so the ratio of ribbed to non-ribbed caudal vertebrae is currently unknown. Vertebrae are holospondylus, amphicoelous and are waisted towards the centre of the centrum restricting the notochord (Fig. 4.10A-J). The centra of the trunk vertebrae are hourglass shaped with an anterior-posterior ridge running along the ventral margin. The notochordal foramen on the posterior articular surface is relatively larger than the anterior foramen and is more susceptible to compression in NMI.F14679. Transverse processes extended posterior-laterally from the midpoint of the lateral side of each centrum with an angle of c.35° in the trunk vertebrae of NMI.F14679 (Fig. 4.10E-J). The transverse process of vertebra 4 in NMI.F14679 is bifurcated with a postero-ventral parapophysis and postero-lateral diapophysis that are not fully separate. There is a foramen on each transverse process which marks the articulation site for the capitulum and tuberculum respectively. A dorso-ventrally thin process extends posteriorly from the diapophysis. The angle between the transverse process and the centrum

changes to c.60° at vertebra 7. Transverse process on vertebra 7 and all preceding vertebrae show only a single rib articulation face. Neural arches are composed of a single element fused to the centra. They are low with anterior and posterior zygapophysial extensions beyond the edges of the centra giving the vertebra a “butterfly wing pattern” in dorsal view (Fig. 4.10K). The dorsal surface of the anterior zygopophysis articulates with the ventral surface of the posterior zygopophysis (Fig. 4.10L). A thin low neural spine runs along most of the antero-posterior length of the neural arch.

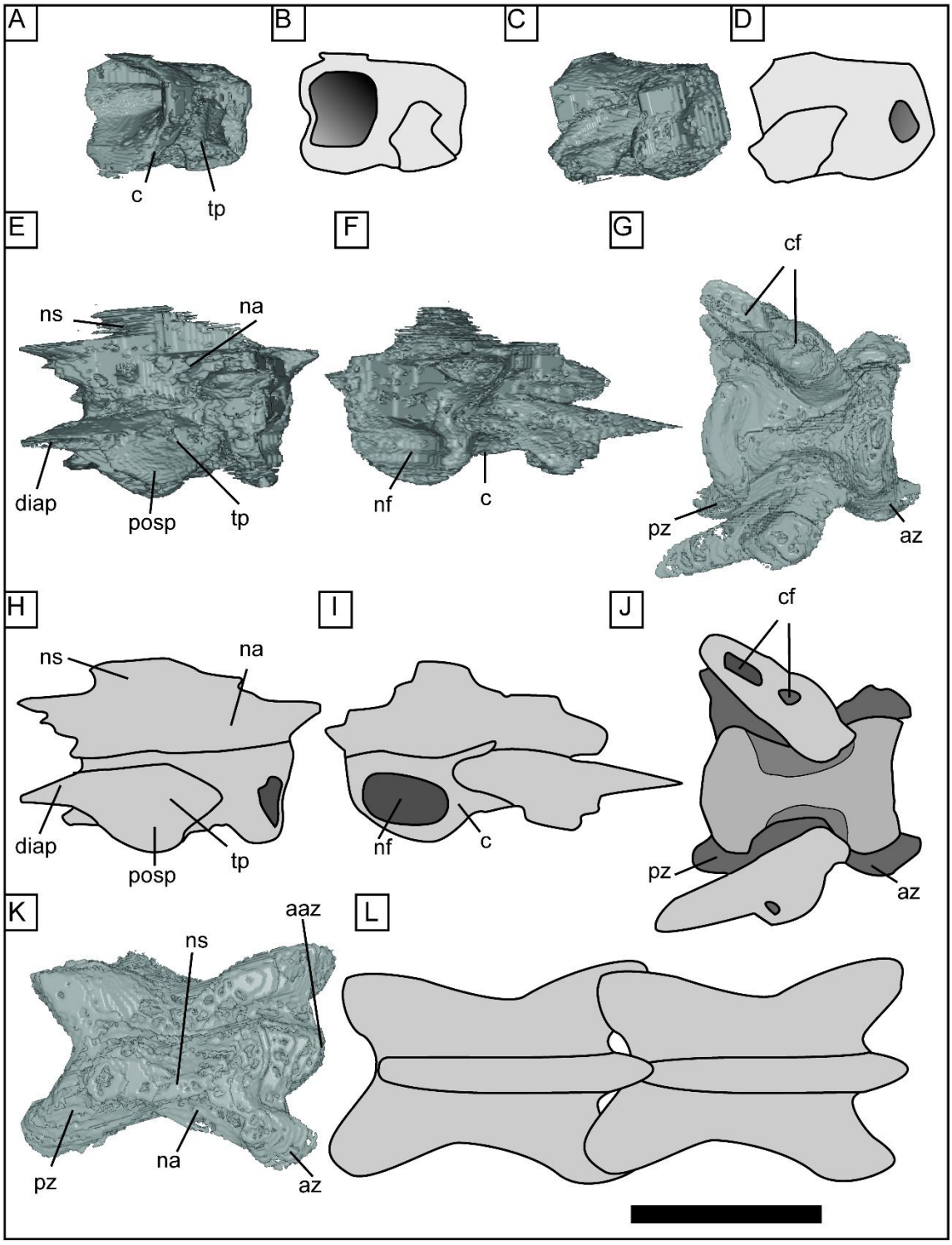

Figure 4.10. Vertebrae of NMI.F14879 *Ophiderpeton brownriggii* showing vertebra 1/atlas in (A-B), posterior-lateral view and (C-D), anterio-lateral view, vertebra 4 in (E, H) lateral view, (F, I), anterio-lateral view and (G, J) ventral view, vertebra 7 in dorsal view and (L), vertebrae 7, 8 in dorsal view. Abbreviations: aaz, accessory anterior zygopophysis; az, anterior zygopophysis; c, centrum; cf, capitulum facet; diap, diapophysis, na, neural arch; nf, notachordal foramen; ns, neural spine; posp, parapophysis; pz, posterior zygopophysis; tp, transverse process; tuf, tuberculum facet. Scale bar = 7mm.

The atlas is marginally smaller than the trunk/cervical vertebrae. It possesses a posterior notochordal foramen, and a more restricted anterior foramen (Fig. 4.10C,D). Transverse process and posterior zygopophysis typical of the vertebra 3-6 are present on the atlas but the exact morphology or presence/absence of anterior zygopophysis cannot be established.

The atlas lacks ribs despite its well-developed transverse processes. Ribs first appear on the 3rd vertebra in TCD.38363 and on the 2nd vertebra in NMI.F14679. Ribs on vertebrae 3-6 are double-headed with the capitulum and tuberculum attached by a web of bone (Fig. 4.9C). Both the capitulum and tuberculum have hollow depressions on their articulating surfaces (Fig. 4.9D). The posterior shaft is generally 2.5 the length of the associated vertebra. Rib morphology changes at the 7th vertebra and for all preceding vertebra and has the typical "K"-shaped morphology seen in other aïstopods (Anderson, 2002; 2003a). A anterior process forms the costal process, while the tuberculum extends anterior only half the length of the costal process and articulates with the transverse process (Fig. 4.9B). The rib thickens posterior of the meeting of the anterior process and the tuberculum. Posterior of this thickening there is a small curved posterior process. The main shaft of the rib is as long as the length between the anterior and posterior process.

Scalation

Posterior to the cranium the dorsal skin of TCD. 38363 is outlined by the presence of ovoid to rhombic osteoderms which extend posteriorly as far as vertebra 23 and probably extend along the full length of the body (Fig. 4.11A, B). However more posterior osteoderms are not observable as the area is covered in matrix. Osteoderms extend from the dorsal surface to the ventral surface anterior to vertebra 5 and on the anterior sides of the pectoral girdles. These ventral osteoderms appear to be slightly smaller than the dorsal osteoderms and extend as far anteriorly as the posterior one-third portion of the mandible. A coating of osteoderms is also present on the cheek region of NHMUK R 8465, with large, up to 4mm long sub-ovoid osteoderms covering the temporal region. Posterior to the pectoral elements of TCD. 38363 the ventral osteoderms are replaced by tightly interlocking elongated gastralia (Fig. 4.11A,B). Gastralia are distinguished from osteoderms by their morphology which comprises elongated wheat-shaped scales relative to the ovoid osteoderms, Gastralia appear to cover a larger area relative to the associated dorsal osteoderms and like the osteoderms extend posteriorly as far as observable in vertebra 23 and probably even further. Posterior to the pectoral girdles, the ventral gastralia and the dorsal osteoderms do not appear to contact one another along the flanks.

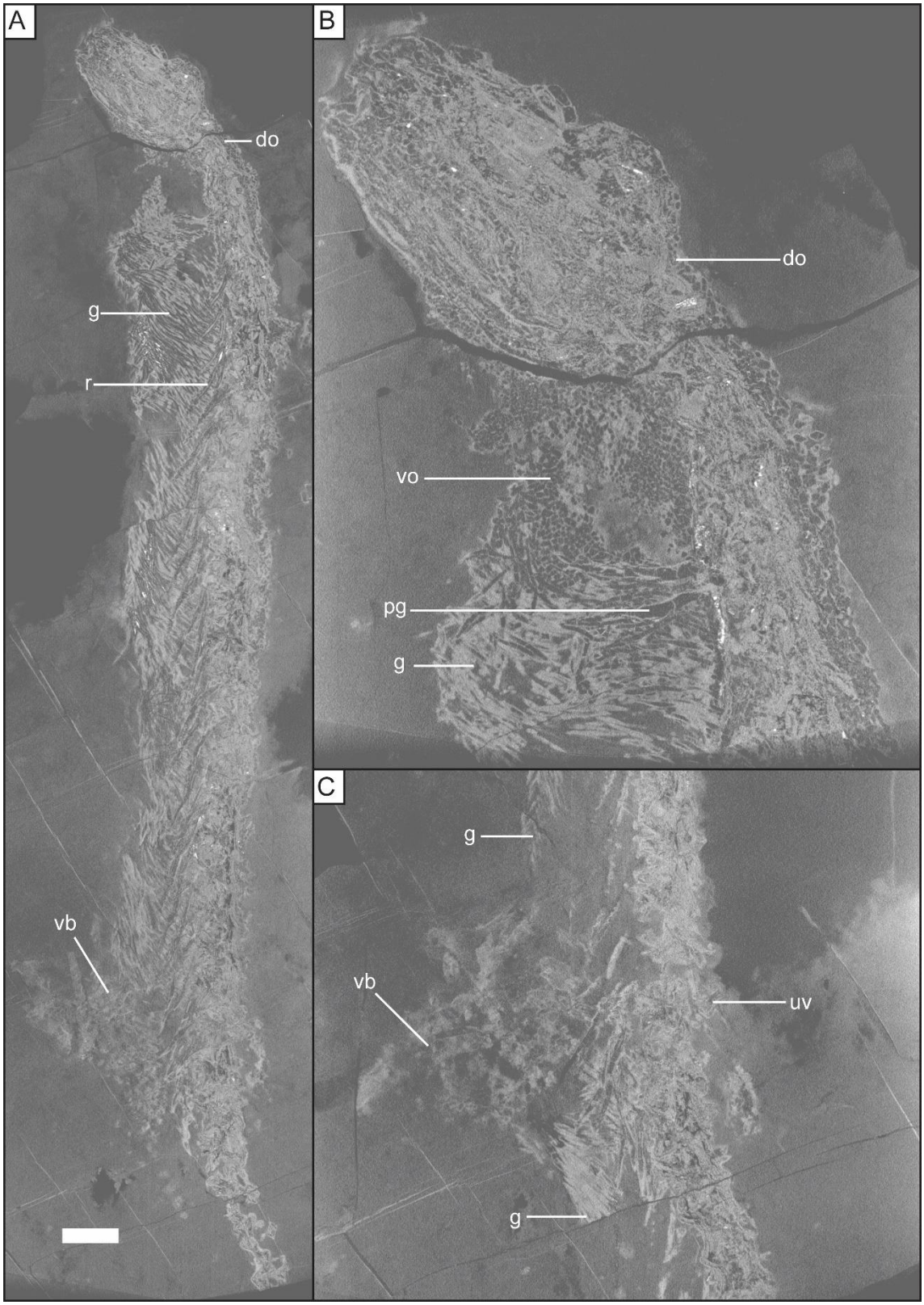

Figure 4.11. CT-slices of TCD.38363 *Ophiderpeton brownriggii* showing (A) full length of the body that was scanned, (B) close up of the skull, shoulder girdles and scalation directly posterior of skull and (C) close up of amorphous ventral mass. Abbreviations: do, dorsal osteoderms, g, gastralia, pg, pectoral girdle, uv, *Urocordylus* vertebrae, vb, ventral breakage, vo, ventral osteoderms. Scale bar = 10mm for A, 4mm for B, and 5mm for C.

Ventral to vertebra 19-21 in TCD. 38363 the ventral gastralia disappear and are replaced by a ventral extrusion of an amorphous mass which appears different from the surrounding matrix in the CT-slices (Fig. 4.11A, C). Some structured features can be made out including two long structures and several sub-spherical features but what these represent is unknown. This feature may have been caused by a post-mortem gas build up within the body which was then "blown out" during compaction. Three articulated caudal vertebrae belonging to *Urocordylus wandesfordii* partially overlie the right lateral surface of vertebra 20 (Fig. 4.11C). During compression these vertebrae may have caused rupture allowing for the innards to spill out. It is not likely that the vertebrae of *U. wandesfordii* represent stomach contents as they lie on the outer side of the ribs. Also, *U. wandesfordii* is almost certainly far too large a prey for such an immature *O. brownriggii* as TCD.38363.

4.4 Discussion

4.4.1 Comparative anatomy

TCD.T90 is the only one of the three original syntypes of *Ophiderpeton brownriggii* redescribed above and is here transferred to the new species *Peisterpeton milnerorum*, with NHMUK R 8465, NMI.F14679 and TCD.38363 still assigned to *O. brownriggii*. This is due to the similarity between the above mentioned *O. brownriggii* specimens and TCD.T89, the principal specimen Huxley and Wright (1867) used for the original description of *O. brownriggii*. Similarities include a wide posterior skull table (Fig. 4.12), similar to NHMUK R 8465 but unlike the thinner skull table in TCD.T90. Additional similarities include a robust dorso-ventrally deep mandible seen also in NHMUK R 8465, NMI.F14679 and TCD.38363. Since the original description, the area containing the skull table of TCD.T89 has been broken off and comparison can only be made with plate 22, figure 1 in Huxley and Wright (1867). Nether a pineal foramen nor a pineal button can be identified in the figure.

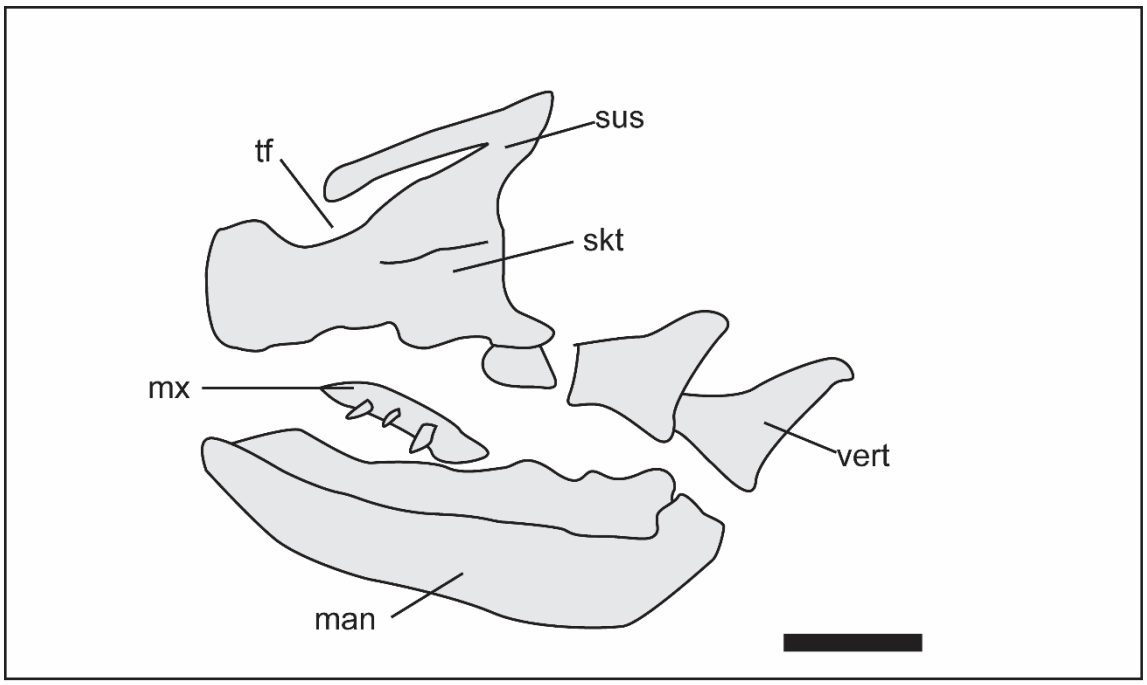

Figure 4.12. Skull of TCD.T89 *Ophiderpeton brownriggii* based on Huxley and Wright (1867) plate 22, figure 1. Abbreviations are: man, mandible; mx, maxilla; skt, skull table; sus, suspensorium; tf, temporal fenestra; vert, vertebra. Scale bar = 10mm.

P. milnerorum has many typical ophiderpetontid characteristics including anteriorly positioned orbits, a closed temporal fenestra with weakly articulated jugal-quadratojugal, no parietal-tabular contact, mandibles articulating posterior to the occipital condyle (also seen in *Coloraderpeton brilli* (Anderson, 2003a)) and a dense covering of dorsal osteoderms and ventral gastralia. It is distinguished from the genus *Ophiderpeton* by lacking a wide skull table posterior to the temporal fenestra, which is the condition in *O. brownriggii* and *O. kirktonense*, more gracile mandibles and at least from *O. brownriggii* by the presences of a pineal foramen instead of a pineal button; the function of the latter is unknown.

Milner (1993) identified a prefrontal, postfrontal and postorbital in NHMUK R 8465 (*O. brownriggii*) and in *O. kirktonense*. The postfrontal and postorbital in of NHMUK R 8465 are here considered to represent a single cranial element considered to be the postorbital. All other aïstopods have at most two dorsal orbital elements, the prefrontals and either the postfrontals (Anderson, 2002, 2003a, 2003b) or the postorbitals (Pardo, *et al*. 2017). Here the dorso-posterior element of the orbit is termed the postorbital in keeping with the most resent published homology of this bone (Pardo, *et al*. 2017). Milner (1993) identified the postorbital of *O. kirktonense* as lying along the dorsal surface of the posterior extension of the jugal, making up the ventro-anterior margin of the temporal fenestra. This is not seen in any other aïstopods, with the postorbital making up the anterodorsal margin of the temporal fenestra (Anderson, 2003b; Pardo, *et al*. 2017). This postorbital is probably just an additional part of the

jugal. Once considered part of the jugal, it gives the jugal the slight concave dorsal margin seen in of *O. brownriggii*. This would suggest that *Ophiderpeton* is not unique among the aïstopods in retaining a postorbital and a postfrontal. However, the author has not seen the specimen NMS G 1988.3.1p *Ophiderpeton kirktonense*, so it cannot be positively identified as part of the jugal.

A contact between the parietal and tabular is absent in *O. brownriggii* and *P. milnerorum* because the postparietal and the supratemporal are in contact. This is unlike the condition in *Oestocephalus* and *Coloraderpeton* in which a parietal-tabular contact is facilitated by a posterior projection of the parietal (Anderson, 2003a). This feature may be useful for distinguishing ophiderpetontids from oestocephalids but is of little use when distinguishing other aïstopods from ophiderpetontids giving the presence of a parietal-tabular contact in the basal *Lethiscus stocki* (Pardo, *et al*., 2017) and its absence in the derived *Pseudophlegethontia turnbullorum* (Anderson, 2003b). This suggests this characteristic has evolved independently in ophiderpetontids and more derived aïstopods. The posterior projection of the parietal does seem to be an apomorphy of the oestocephalids. Carroll (1998b) mentioned that the lack of a parietal-tabular contact in ophiderpetontids was similar to the condition of primitive tetrapodamorpha but again due to the presence of this contact in *L. stocki*, it is likely to be the result of convergence rather than representative of a shared unchanged trait.

A closed fenestra surrounded by the jugal, quadratojugal, squamosal, supratemporal, parietal and postorbital in *L. stocki* (Pardo, *et al*., 2017) suggests that this is the basal condition for aïstopods. Both *O. brownriggii* and *P. milnerorum* have closed temporal fenestra, though the common occurrence of breakage between the jugal-quadratojugal may suggest a weak contact between the bones. This could be a step towards the formation of an open fenestra, facilitated by no contact between the jugal and the quadratojugal in oestocephalids. An open fenestra is seen in all other more derived aïstopods (Anderson, 2002, 2003b)

Specimens of ophiderpetontids document the least number of observable vertebrae within the column (*O. brownriggii* 69, and *O. kirktonense*, 37) though this is not considered to be representative of the actual vertebral count in life. The number of vertebrae increases crownwards in the phylogeny of aïstopods (Anderson, 2003a) suggesting that ophiderpetontids probably had more than the 79 vertebrae seen in the basal *L. stocki*. The centra of ophiderpetontids are typical of the aïstopod condition with a waisted hourglass shape. Lateral zygopophyses appears to be characteristic of all aïstopod vertebrae (Zidek and Baird, 1978; Carroll, 1998b, 1998a; Anderson, 2002, 2003a, 2003b) though the presence of an anterior projection between the anterior zygopophyses appears to be unique to *O. brownriggii*. The position of the transverse process in ophiderpetontids and oestocephalids may be used to

distinguish between the two, as in oestocephalids it originates from both the neural arch and the centrum (Anderson, 2003a), while in ophiderpetontids it originates only from the centrum. The centrum of *Oestocephalus nanum* (Boyd, 1982) originates from the centrum and this suggests that it is an *Ophiderpeton*. "*Oestocephalus*" *nanum* is here transferred from the genus *Oestocephalus* to the genus *Ophiderpeton*. This makes *Oestocephalus* a monospecific genus. This taxonomic change is alluded to by Pardo *et al*. (2019) in which the Newsham aïstopod (*O. nanum*) is referred to as belonging to *Ophiderpeton* rather than *Oestocephalus*.

Coloraderpeton has previously been considered to be the only aïstopod with two rib articulations on each transverse process, though the parapophysis is considered to be non-functional and actually may be homologous with the posterior spinous process seen in *Oestocephalus* (Anderson, 2003a). This is similar to *Pseudophlegethontia* which has a diminished non-functional parapophysis (Anderson, 2003b). The presence of double-headed ribs with articulation depressions on both the tuberculum and capitulum in *O. brownriggii* marks the first record of double-headed rib articulation to the transverse process in aïstopods. Double-headed ribs have not been reported in any other ophiderpetontid, though with the exception of *O. nanum* this is likely due to the poor preservation of the fossils. K-shaped ribs have previously been considered to be absent in *O. brownriggii* (Milner, 1993; Anderson, *et al*., 2003) but this is not the case in *O. nanum*. The presence of K-shaped ribs on the 4th vertebra of *O. nanum* distinguishes it from *O. brownriggii*, which has articulated double-headed ribs on this vertebra. The presence or absence of K-shaped ribs is not determinable in either *O. kirktonense* or *P. milnerorum*. This observation implies that *L. stocki* is the only aïstopod definitely lacking K-shaped ribs.

Pectoral elements found in other aïstopods tend to fall between the third and sixth vertebrae (Anderson, 2002) and they are situated on the fourth vertebra in *O. brownriggii*. Aïstopods have "sickle" shaped pectoral girdles with a proximal or "handle" section and the distal or "sickle" sections. These are considered the cleithrum and clavicles respectively in *Phlegethontia* (Anderson, 2002) where both thickening and breakage between the two sections may indicate a plane of weakness along a suture line. In the pectoral elements of NMING.F14879 and TCD.38365 no suture lines can readily be identified within the μCT slices. The elements contain several cross-cutting fractures which could be mistaken for sutures, none of which intersects the boundary between the "sickle" and "handle" sections or are present in the same location in both elements in the same individual.

Scalation patterns in ophiderpetontids and oestocephalids are similar in showing dorsal osteoderms running the length of the vertebral column and with larger osteoderms covering the temporal fenestra and with ventral tightly interlocking elongated gastralia (Carroll, 1998a;

Anderson, 2003b). With the exception of larger osteoderms on the cheek region, this pattern of scalation is also seen in *L. stocki* (Anderson, *et al*., 2003) suggesting it represents the basal condition in aïstopods. The dorsal osteoderms in *L. stocki* are disarticulated so it is not clear whether large osteoderms in the fenestra were actually absent in life. This contrasts to the derived condition seen in *Pseudophlegethontia* and *Phlegethontia* which lack dorsal osteoderms and have widely spaced gastralia. Soft tissue outlines are also preserved in FMNH PR 624 *Phlegethontia longissima* showing that skin outline appears anteriorly, just dorsal of the mandible similar to the situation in TCD.38363 *O. brownriggii* (Fig. 4.11A,B).

4.4.2 Ophiderpetontidae

The Family Ophiderpetontidae traditionally included all blunt-snouted aïstopods with anterior placed orbits (Carroll, 1998a, 1998b) including *Ophiderpeton*, *Oestocephalus* and *Coloraderpeton*. (Anderson, *et al*. 2003) found that the traditional classification of ophiderpetontids to be a paraphyletic group with *Ophiderpeton* falling on the stem below a dichotomy between *Oestocephalus* and *Coloraderpeton* on one side and *Pseudophlegethontia* and *Phlegethontia* on the other. Anderson (2003a) erected the Family Oestocephalidae to include *Coloraderpeton* and *Oestocephalus*, within a larger paraphyletic ophiderpetontids. Pardo, *et al*. (2019) considered the ophiderpetontids as a separate family to the oestocephalids. Here the Family Ophiderpetontidae is designated for *O. brownriggii*, *O. kirktonense*, *O. nanum* and *Peisterpeton milnerorum* while the family Oestocephalidae is considered comprise of *Coloraderpeton brilli* and *Oestocephalus amphiuminus*.

4.4.3 Aïstopod physiology

Lateral line systems were only first reported in aïstopods in *Lethiscus stocki* by Pardo, *et al*. (2017) who also identified a spiracle indicative of a mostly aquatic if not entirely aquatic lifestyle. Prior to this discovery, aïstopods were considered to be terrestrial (Milner, 1993) or semi-terrestrial (Milner, 1987). The presence of lateral line systems in NMING.F14879 *O. brownriggii* indicates that lateral lines may also have been more widespread within aïstopods and supports the interpretation of an aquatic lifestyle. This lifestyle would explain the high frequency of aïstopod specimens in the aquatic Jarrow assemblage as terrestrial articulated organisms would be considered rarer elements and other dominant taxa from Jarrow have aquatic adaptions (i.e. lateral lines in *Keraterpeton galvani* and a tail adapted for aquatic locomotion in *K. galvani* and *Urocordylus wandesfordii*). An aquatic adaptation would also

explain the presence of aïstopods in more coastal deposits such as Montceau-les-Mines (Germain, 2008) and Mazon Creek (Anderson, 2003b).

Larger osteoderms along the temporal fenestra, seen in the mature specimen of *O. brownriggii* (NHMUK R 8465 and NMI.F14679), probably acted as a layer of protection for the mandible adductors not protected by the cranial bones. The absence of these osteoderms in the less mature TCD. 38363 follows the pattern of back to front appearance of osteoderms during ontogeny seen in *Oestocephalus (*Anderson, 2003a). The presence of ventral osteoderms between the pectoral girdle and the skull, as opposed to gastralia, which occur directly posterior to the pectoral girdle, may suggest a different function for this area. In this area, the osteoderms extend further ventrally compared to the gastralia. As osteoderms and gastralia appear articulated and show the body outline, this indicates that the area between the pectoral girdle and the skull was thicker than that of the rest of the body.

The lack of a retroarticular in aïstopods suggests the lack of a mandibularis depressor attached to the mandible and cranium. Instead the pectoral girdle may have aided in jaw opening as is seen in basal actinopterygians where mandible depression is facilitated by the sternohyoideus, which attaches from the mandible to the pectoral girdle, and the obliquus inferioris which moves the pectoral girdle posteriorly (Lauder, 1980). Aïstopods may have used suction feeding to catch prey. When the jaws were opened, the area between the pectoral girdle and the skull might have created differential pressure, sucking in nearby prey. This is a widespread method of aquatic predation in Recent Neopterygii (Elshoud-Oldenhave, 1979; Liem, 1980; Muller and Osse, 1984; Ferry-Graham and Lauder, 2001).

TCD.38363 preserves the pectoral region, which lacks any evidence of an interclavicle, nor is an interclavicle seen in any other Jarrow specimens. The interclavicle supposedly seen in *O. nanum* (Boyd, 1982) may not actually belong to it and may be from a different tetrapod, later washed in. Similar to the situation with the *U. wandesfordii*, caudal vertebrae are overlapping in specimen TCD. 38363. All other aïstopod specimens lack evidence for an interclavicle (Carroll, 1998b, 1998a; Anderson, 2002, 2003b, 2003a; Anderson, *et al*. 2003).

The amorphous mass within the region of vertebrae 19-21 in TCD. 38363 may represent part of the stomach content though its exact composition cannot be discerned. Similar stomach outlines are possibly seen ventral of vertebrae 21-30 in FMH PR 624 *Phlegethontia longissima* marked by darker pigmentation (Anderson, 2002).

4.5 Conclusion

Ophiderpeton brownriggii has been redescribed with the aid of µCT and 3D rendering as part of a review of Huxley's original Jarrow tetrapods with the aim of establishing the true diversity of the Jarrow assemblage, and as a contribution to the understanding of early tetrapod evolution and investigation of early tetrapod physiology.

O. brownriggii is characterised by a wide skull table, its width measuring 20-25% of its length (smaller widths represent the temporal fenestra which emarginates on the parietal giving the skull table a waisted appearance) and a pineal button. The postcranium of *O. brownriggii* shows typical aïstopod features including K-shaped ribs, which are now considered characteristic of all aïstopods with the exception of the basal *Lethiscus stocki*. Vertebrae possess transfers process which originate only from the centrum, unlike the transverse processes of *Oestocephalus*. This distinction is used to transfer "*Oestocephalus*" *nanum* to the genus *Ophiderpeton*, which now has three recognised species, *O. brownriggii*, *O. kirktonense* and *O. nanum*.

A new species, *Peisterpeton milneri*, is identified from one of Huxley's syntypes, TCD.T90. It is characterised by a slightly slimmer skull than *Ophiderpeton*, the lack of a pineal button and more slender mandibles more akin to those of *Oestocephalus*.

The Family Ophiderpetontidae is here resurrected to accommodate *O. brownriggii*, *O. kirktonense*, *O. nanum* and *P. milnerorum*. It is distinguished from the oestocephalids by the presence of a closed temporal fenestra and no parietal-tabular contact.

Despite degradation of the anatomy of the Jarrow specimens through post-depositional, including deep burial and low-grade metamorphism, certain details on the physiology of aïstopods can be interpreted including the presence of internal lateral lines in NMI.F14879 *O. brownriggii*, supporting the interpretation of an aquatic mode of life and the soft body outlines in TCD.38363 (marked by osteoderms and gastralia) demonstrating the presence of a body pouch directly posterior of the cranium. Possible stomach contents were identified in the region of vertebrae 19-21.

4.6 References

AHLBERG, P. E. 1991. A re-examination of sarcopterygian interrelationships, with special reference to the Porolepiformes. *Zoological Journal of the Linnean Society*, **103**, 241–287.

ANDERSON, J. S. 2002. Revision of the Aïstopod Genus *Phlegethontia* (Tetrapoda: Lepospondyli). *Journal of Paleontology*, **76**, 1029–1046.

— 2003a. Cranial anatomy of *Coloraderpeton brilli*, postcranial anatomy of *Oestocephalus amphiuminu*s, and reconsideration of Ophiderpetontidae (Tetrapoda: Lepospondyli: Aistopoda). *Journal of Vertebrate Paleontology*, **23**, 532–543.

— 2003b. A new Aïstopod (Tetrapoda: Lepospondyli) from Mazon Creek, Illinois. *Journal of Vertebrate Paleontology*, **23**, 79–88.

— CARROLL, R. L. and ROWE, T. B. 2003. New information on *Lethiscus stocki* (Tetrapoda : Lepospondyli : Aistopoda) from high-resolution computed tomography and a phylogenetic analysis of Aistopoda. *Candian Journal of Earth Science*, 40, 1071–1083. doi: 10.1139/E03-023.

BAIRD, D. 1964. The aistopod amphibians surveyed, *Brevoria*, **206**, 1–17.

— 1965. Paleozoic Lepospondyl Amphibians. *American Zoologist*, **5**, 287–294.

BOYD, M. J. 1982. Morphology and relationships of the Upper Carboniferous aïstopod amphibian *Ophiderpeton nanum*. *Palaeontology*, **25**, 209–214.

CARROLL, R. L. 1998a. Order Aïstopoda Miall 1875. 163–182. *In* WELLNHOER (ed). *Encyclopedia of Paleoherpetology*. Verlag Dr.Friedrich Pfeil, München, 206 pp.

— 1998b. Cranial anatomy of ophiderpetontid aistopods: Palaeozoic limbless amphibians. *Zoological Journal of the Linnean Society*, **122**, 143–166.

CLACK, J. A., RUTA, M., MILNER, A. R., MARSHALL, J. E. A., SMITHSON, T. R. and SMITHSON, K. Z. 2019. *Archerontiscus caledoniae*: the earliest heterodont and durophagous tetrapod. Rpyal Society Open Science, **6**, 182087. doi.org/10.1098/rsos.182087.

COPE, E. D. 1868. Synopsis of the extinct Batrachia of North America. *Proceedings of the Academy of Natural Science of Philadelphia*, **20**, 208–221.

— 1875. Synopsis of the extinct Batrachia Reptilia and Aves of North America, Part1. *Report*

of the Geological Society of Ohio, **2**, 351–411.

ELSHOUD-OLDENHAVE, M. J. W. (1979). Prey capture in the pike-perch, *Stizostedion lucioperca* (Teleostei, Percidae): A structural and functional analysis. *Zoomorphology*, **93**, 1–32.

ETHERIDGE, R. 1866. On the discovery of several new Labyrinthodont reptiles in the coal measures of Ireland. *Geological Magazine*, **3**, 4–5.

FERRY-GRAHAM, L. A., and LAUDER, G. V. 2001. Aquatic prey capture in fishes: A century of progress and new directions. *Journal of Morphology*, **245**, 99–119.

FRITSCH, A. 1875. *Über die Fauna der Gaskohle des Pilsner und Rakonitzer Beckens.* Prague: Sitzungsberichte der Böhemischen Gesellschaft der Wissenschaften.

— 1879. *Fauna der Gaskohle und der Kalksyeine der Permformation Böhmens. Band 1. Heft 1.* Prague.

— 1880. *Fauna der Gaskohle und der Kalksteine der Permformation Böhmens. Band 1. Heft 2.* Prague.

GERMAIN, D. 2008. A new phlegethontiid specimen (Lepospondyli, Aistopoda) from the Late Carboniferous of Montceau-les-Mines (Saône-et-Loire, France). *Geodiversitas*, **30**, 669–680.

HANCOCK, A. and ATTHEY, T. 1868. Notes on the remains of some reptiles and fishes from the shales of the Northumberland coal field. *Annals and Magazine of Natural History*, **4**, pp. 226–278.

HUXLEY, T. H. and WRIGHT, E. P. 1867. Royal Irish Academy On a Collection of Fossil Vertebrata , from the Jarrow Colliery, County of Kilkenny, Ireland. *Transactions of the Royal Irish Academy*, **24**, 351–370.

LAUDER, G. V. 1980. Evolution of the Feeding Mechanism in Primitive Actinopterygian Fishes : A Functional Anatomical Analysis of *Polypterus* , *Lepisosteus*, and *Amia*. *Journal of Morphology*, **317**, 283–317.

LIEM, K. F. 1980. Adaptive significance of intra- and interspecific diVerences in the feeding repertoires of cichlid fishes. *American Zoologist*, **20**, 295–314.

LUND, R. 1978. Anatomy and relationships of the family Phlegethontiidae (Amphibia, Aistopoda). *Annals of the Carnegie Museum*, **47**, 53–79.

LYDEKKER, R. 1891. *Catalogue of Fossil Mammals, Birds, Reptiles, and Amphibians in the*

Science and Art Museum: Dublin, Science and Art Museum. British Museum (Natural History), London.

MATTHEWS, S. C. 1973. Notes on open nomenclature and on synonymy lists. *Palaeontology*, **16**, 713-719.

MIALL, L. C. 1875. Report of the committee on the structure and classification of the labyrinthodonts. *Report of the 44th Meeting of the British Association for the Advancement of Science*, **1874**,149–92.

MILNER, A. C. 1993. The aïstopod amphibian from the Viséan of East Kirkton, West Lothian, Scotland. *Transactions of the Royal Society of Edinburgh: Earth Sciences*, **84**, 363–368. doi: 10.1017/S0263593300006167.

MILNER, A. R. 1987. The Westphalian tetrapod fauna; some aspects of its geography and ecology. *Journal of the Geological Society*, **144**, 495–506. doi: 10.1144/gsjgs.144.3.0495.

MULLER, M., and OSSE, J. W. M. 1984. Hydrodynamics of suction feeding in fish. *Transactions of the Zoological Society London*, **37**, 51–135.

PARDO, J. D., SZOSTAKIWSKYJ, M. and ANDERSON, J. S. 2017. Hidden morphological diversity among early tetrapods. *Nature*, **546**, 642–645.

— and MANN, A. 2018. A basal aïstopod from the earliest Pennsylvanian of Canada, and the antiquity of the first limbless tetrapod lineage. *Royal Society Open Science*, **5**, p. 181056.

— HOLMES, R. B. and ANDERSON, J. S. 2019. An enigmatic braincase from Five Points, Ohio (Westphalian D) further supports a stem tetrapod position for aïstopods. *Earth and Environmental Science Transactions of the Royal Society of Edinburgh*, **109**, 1–10.

ROMER, A. S. 1930. The Pennsylvanian tetrapods of Linton, Ohio. *Bulletin of the American Museum of Natural History*, **59**, 77–147.

RUTA, M., COATES, M. I. and QUICKE, D. L. J. 2003. Early tetrapod relationships revisited. *Biological Reviews*, **78**, 251–345.

SCHWARZ, H. 1908. Uber die Wirbelsaule und die Rippen Holospondyler Stegocephalen (Lepospondyli Zittel). *Beiträge zur Geologie und Palaäontologie Österreich-Ungarn*, **21**, 63–105.

STEEN, M. C. 1931. The British Museum collection of Amphibia from the Middle Coal Measures of Linton, Ohio. *Proceedings of the Zoological Society of London*, **4**, 849–891.

—1938. On the fossil Amphibia from the Gas Coal of Nýřany and other deposits in Czechoslovakia. *Proceedings of the Zoological Society of London*, **108**, 205–283.

SUTTON, M. D., *GARWOOD, R. J., SIVETER, D. J. and SIVETER, D. J.* 2012. SPIERS and VAXML; A software toolkit for tomographic visualisation and a format for virtual specimen interchange. *Palaeontologia Electronica*, **15**, 1–14.

TRUEB, L. and CLOUTIER, R. 1991. A phylogenetic investigation of the inter- and intrarelationships of the Lissamphibia(Amphibia: Temnospondyli). 223–313. *In* SCHULTZE, H. and TRUEB, L. (eds). *Origins of the Higher Groups of Tetrapods-Controversy and Consensus.* Cornell University Press, Ithaca.

VALLIN, G. and LAURIN, M. 2004. Cranial morphology and affinities of *Microbrachis*, and a reappraisal of the phylogeny and lifestyle of the first amphibians. *Journal of Vertebrate Paleontology*, **24**, 56–72.

VAUGHN, P. P. 1969. Upper Pennsylvanian vertebrates from the Sangre de Cristo Formation of Central Colorado. *Los Angeles County Museum Contributions in Science*, **164**, 1–28.

WELLSTEAD, C. F. 1982. A Lower Carboniferous aïstopod amphibian from Scotland. *Palaeontology*, **25**, 193–208.

WRIGHT, E. P. and HUXLEY, T. H. 1866. On a collection of fossils from the Jarrow Colliery Kilkenny, Ireland, *Geological Magazine*, **3**, 165–171.

ZIDEK, J. and BAIRD, D. 1978. *Cercariomorphus* Cope, 1885, identified as the aistopod amphibian *Ophiderpeton*. *Journal of Paleontology*, **52**, 561–564.

Chapter 5: The enigmatic "*Dolichosoma*" *emersoni* (Aïstopoda, Tetrapodomorpha) from the Jarrow Assemblage, described using micro-computed tomography.

5.1 Introduction

Dolichosoma emersoni is one of the two original aïstopods described from Jarrow by Huxley (*in* Huxley and Wright, 1867). Huxley (*in* Huxley and Wright, 1867) previously noted that he considered *D. emersoni* to be an ontogenetic variant of *Ophiderpeton brownriggii*, but then reassigned it to a separate species because of its smaller skull that tapers anteriorly, a slender ramus of the mandible and short ribs with bifurcated proximal ends (Huxley and Wright, 1867). Since the original description, the holotype has not been properly prepared or redescribed (Baird, 1964; Carroll, 1998). Unfortunately, the holotype of *D. emersoni* TCD.T86 is currently misplaced. It was transferred, along with 23 other Jarrow specimens, from the Geological Museum, Trinity College Dublin, to the National Museum of Ireland (NMI) in 1959 as there were fears that the former repository would have to shut down (Wyse Jackson and Monaghan, 1995). These specimens were officially transferred back to the Geological Museum in 1994 (Wyse Jackson and Monaghan, 1995) but were not relocated until 2016. During this repatriation the holotype could not be identified among any of the Jarrow specimens at the NMI. McGinnis (1967) mentioned that the holotype had been mounted in paraffin wax in a baking tray by 1925 by which time the skull had already been destroyed by pyrite decay. The absence of work on the holotype and ?syntypes has led to some taxonomic problems of the relationship of *D. emersoni* and the narrow snouted aïstopod *Phlegethontia* (Carroll 1998).

Following the description of *D. emersoni*, Cope, (1871, 1874) described a similar small aïstopod from Linton, Ohio, with an anteriorly tapering snout. It was named *Phlegethontia linearis* and was the type genus of the family Phlegethontiidae (Cope, 1875). Fritsch, (1875, 1879) described several additional species of *Dolichosoma* from Nýřany, Czech Republic. Lydekker (1890) erected the family Dolichosomatidae which was later used to include *Dolichosoma*, *Phlegethontia* and the family Molgophidae (Lydekker, 1890). Lydekker (1891) identified a new species of *Dolichosoma*, *D. huxleyi*, but this has been shown to be a mature specimen of *O. brownriggii* (see Chapter 4). Later Romer (1930) removed *Phlegethontia* from Dolichosomatidae and re-erected the family Phlegethontiidae. *Dolichosoma* was then transferred into Phlegethontiidae, given the priority of the latter over Dolichosomatidae (Turnbull and Turnbull, 1955). Kuhn (1961) noted that the genus name *Dolichosoma* was

already occupied by an extant beetle (Stephens, 1830), which had priority. To resolve this, Kuhn (1961) erected the genus *Dolichosomatites* for "*Dolichosoma*" and placed it within the family Dolichosomatitidae; this replacement appears to have been largely ignored in the literature and was omitted in later reviews of the aïstopods (Baird, 1964; Carroll, 1998). Baird (1964) considered that *Dolichosoma* and *Phlegethontia* are probably the same and placed the Nýřany "*Dolichosoma*" *longissima* Fritsch, 1875 into the genus *Phlegethontia*. This restricted "*Dolichosoma*" to the Jarrow assemblage. Baird (1964) also mentioned the poor preservation of the holotype of "*D*". *emersoni* and the lack of an appropriate description by Huxley, rendering "*D*". *emersoni* into a *nomen nudum* as noted in Anderson, (2002). Placement of "*Dolichosoma*" in the Phlegethontiidae was also supported by Carroll (1998). A recent review of *Phlegethontia* omitted the Jarrow "*Dolichosoma*" (Anderson, 2002).

Resolving the relationship between "*D*". *emersoni* and *Phlegethontia* is important not just for resolving taxonomic issues but also for understanding aïstopod evolution and ecology. With the exception of the basal *Lethiscus stocki*, aïstopods were traditionally divided into the larger broad-snouted Ophiderpetontidae and the smaller narrow-snouted Phlegethontiidae (Carroll, 1998). Anderson (2003a) and Anderson *et al*. (2003) demonstrated that narrow-snouted types share a closer common ancestor with the more derived broad-snouted types. This suggested a transition from the basal *Ophiderpeton* to the more derived *Phlegethontia*. However, these analyses lacked information on "*Dolichosoma*", which marks the first occurrence of the narrow-snouted aïstopods and predates the more derived broad snouted aïstopods *Oestocephalus* and *Coloraderpeton*. It is important to understand whether "*Dolichosoma*" fits into this stepwise transition or has a different placement.

Although the holotype is missing, additional specimens from Jarrow can be used for a redescription of "*D*". *emersoni*. NHMUK.R8466 is the only specimen identified that contains the cranial region and it is from this specimen that the description below was made. µCT was applied to the specimen to allow for 3D rendering. "*D*". *emersoni* is shown to be distinct from all previously described aïstopods and is here treated as the type species of the genus *Dolichosomatites* Kuhn, 1961.

5.2 Methods and Material

Micro-computed tomography was carried out on NHMUK.R8466 *Dolichosomatites emersoni* using the Nikon Metrology HMX ST 225 at the Imaging and Analysis Centre, Natural History Museum, London. Two scans were carried out, one on the cranial region, the other on the vertebral column, up to the level of vertebra 40. Both were scanned at: 160 kV, 125 uA with a 1 mm Cu filter.

Resulting TIF-stacks were converted into PNG files and imported into SPIERS (Sutton *et al.*, 2012). Using the masking function in SPIERS, the fossil was virtually isolated from the matrix.

Museum abbreviations are: NHMUK, Natural History Museum, United Kingdom; NMI, National Museum of Ireland; TCD, Trinity College Dublin, Geological Museum.

5.3 Systematic Palaeontology

Infraclass TETRAPODOMORPHA Ahlberg, 1991

Order AÏSTOPODA Miall, 1875

Family DOLICHOSOMATITIDAE Kuhn, 1961

Diagnosis— Aïstopod with a triangular skull, widest at the occiput and tapering anteriorly. Paired frontals, parietals and postparietals. Temporal fenestra closed. Mandibles robust and jaw articulation is aligned with the occipital condyle.

Genus *DOLICHOSOMATITES* Kuhn, 1961

Diagnosis— Dolichosomatitidae aïstopod with posterior cranial width (measured from the left to right suspensorium) to cranial length ratio of 1:1.38.

Type Species— *Dolichosomatites emersoni* (Huxley *in* Huxley and Wright, 1867)

DOLICHOSOMATITES EMERSONI (Huxley *in* Huxley and Wright, 1867)

(Figs. 5.1-5.4)

1867 *Dolichosoma emersoni*; Huxley *in* Huxley and Wright, 1867:366, pl. 21, figs. 3

1891 *Dolichosoma emersoni* Lydekker, 1891:60

1961 *Dolichosomatites emersoni* Kuhn, 1961

1965 *Dolichosoma emersoni*; Baird, 1964:4

1998 *Dolichosoma emersoni*; Carroll *in* Carroll, Bossy, Milner, Andrews and Wellstead, 1998:181

Holotype—TCD.T86 (Figured in Huxley and Wright 1867, plate 21, figure 3.); currently missing.

Topotypes— NHMUK.R8466 and TCD.38350

Type Locality—Clogh, County Kilkenny, Ireland.

Type Horizon—Jarrow (No. 4) Coal Seam, Coolbaun Coal Formation, Langsettian: Pennsylvanian.

Diagnosis—Same as for genus.

Description

NHMUK.R8466 consists of a skull articulated to a vertebral column in dorsal view. The vertebral column consists of 43 articulated vertebrae. Anterior of the narial region the skull is masked by a concretion which appears in the µCT images to have replaced the fossil. The mandibles lie directly under the skull aligned with the upper jaw. Posteriorly the vertebral column and the surrounding matrix have been broken off so that the full length of the vertebral column is unknown. The body outline is marked by gastralia posterior to the occiput and continuing posteriorly to the break in the vertebral column.

Cranium

The cranium of NHMUK.R8466 is triangular with a preserved length of 10 mm along the midline but it is interrupted anteriorly by a concretion (Fig. 5.1). It is likely that the cranium was slightly longer than recorded. It is widest at the occiput, at 9 mm, and narrows anteriorly. The width of the skull table at the occiput is 6.5 mm. Compression has displaced the suspensorium and cheek elements to the same plane as the skull table elements. No element that can be confidently determined as the premaxilla have been identified. The area where the premaxilla would be expected to occur is within the concretion. The maxilla is best seen on the left side of the skull, were it extends from the nares posteriorly along 57% of the preserved skull length. The right maxilla is broken posteriorly. The left maxilla houses six teeth while the right houses four. Teeth are curved posteriorly and widely space throughout the maxilla. A triangular lacrimal is visible on the left side and posterior of the nares. It is situated on top of the maxilla. Dorso-medial to the lacrimal is a prefrontal. The prefrontal tapers into a posterior process. It is displaced so that the posterior process impinges on the orbit. The anterior end of the prefrontal is slightly bifurcated, showing an anterior and a ventral process. These process, between them, form a curved anteroventra margin which probably made up part of the margin of the nares. An orbit is visible only on the left side of the cranium in dorsal view. A bone of unknown homology is present along the dorso-medial margin of the orbit. It forms a long strut like process. Posterior of the orbit is a triangular postorbital. It minimally contributes to the anterodorsal margin of the orbit. It is relatively long in the medio-lateral plane (so dorso-ventrally deep in life) suggesting that the cheek region was deep. The exact morphology of the jugal is uncertain; it appears as a more elongate bone in the right side of the cranium and contacts the quadratojugal posteriorly. This contact between the quadratojugal and the jugal closes the temporal fenestra so that the quadratojugal and the jugal make up its ventral margin. The squamosal is best seen in the right side of the cranium. It is a triangular element and is situated on the dorso-medial margin of the posterior end of the quadratojugal. It contacts the tabular and possibly the supratemporal along the dorso-medial margin. The posterior margin of the skull table consists of the tabulars laterally and the postparietals medially. The tabulars appear to be excluded from entering the margin of the temporal fenestra by the inferred supratemporal. The identification of a supratemporal in NHMUK.R8466 is uncertain. A ridge along the lateral margin of the postparietals probably houses the supratemporal. The supratemporals suture is inferred here by the presence of matching pyrite infills in the µCT slices. If this is the case, then the supratemporal would have restricted the postparietal from contacting the temporal fenestra margin. The parietals contact the postparietals and the inferred supratemporal along their posterior margins. There is no contact between the parietals and the tabulars. Together the paired parietals have an anteroposterior elongated diamond shape. A

centre of ossification is located at the centre of the parietals, but it is not clear whether a pineal foramen is present here. The parietals both have an anterior extension along the midline into the frontal so that the frontal-parietal contact aligned with the midpoint of the orbit and extends to the posterior margin of the orbit contact laterally. The left parietal contacts the postorbital along the latter's dorso-medial margin and enters the margin of the temporal fenestra. The frontals are paired. Their anterior-most morphology has been lost due to the presence of the concretion. The left frontal is broken so that along the its lateral half, part of it juts up dorsally. Anterio-lateral of the right frontal is a subcircular bone, here interpreted to be the nasal.

Palate

In ventral view much of the palate is hidden by osteoderms. Two isolated paired anterio-posteriorly elongated bones are present anterior, between the two lower jaws. The right bone appears to preserve two denticles (Fig. 5.2). These are here interpreted as the vomers. The occipital complex is a single fused element and is visible posterior of the skull table in dorsal view. Part of the condyle is also visible in ventral view. It is partially articulated with the atlas.

Mandible

NHMUK.R8466 preserves two robust mandibles that articulate with the cranium at the level of the condyle. The lateral face of the right mandible is exposed in ventral view (Fig. 5.2). The surangular is partially obscured by the quadratojugal. It extends from the posterior margin of the mandible to 29% of the length anteriorly. Anterior to the surangular, the dentary makes up the rest of the lateral face of the mandible. The angular is located ventro-medial of the surangular. It contacts the splenial anteriorly but the nature of this contact is uncertain. It is inferred as being midway along the length of the mandible. The boundary between the splenial and the dentary is also uncertain anteriorly. The splenial extends as far anteriorly as the dentary.

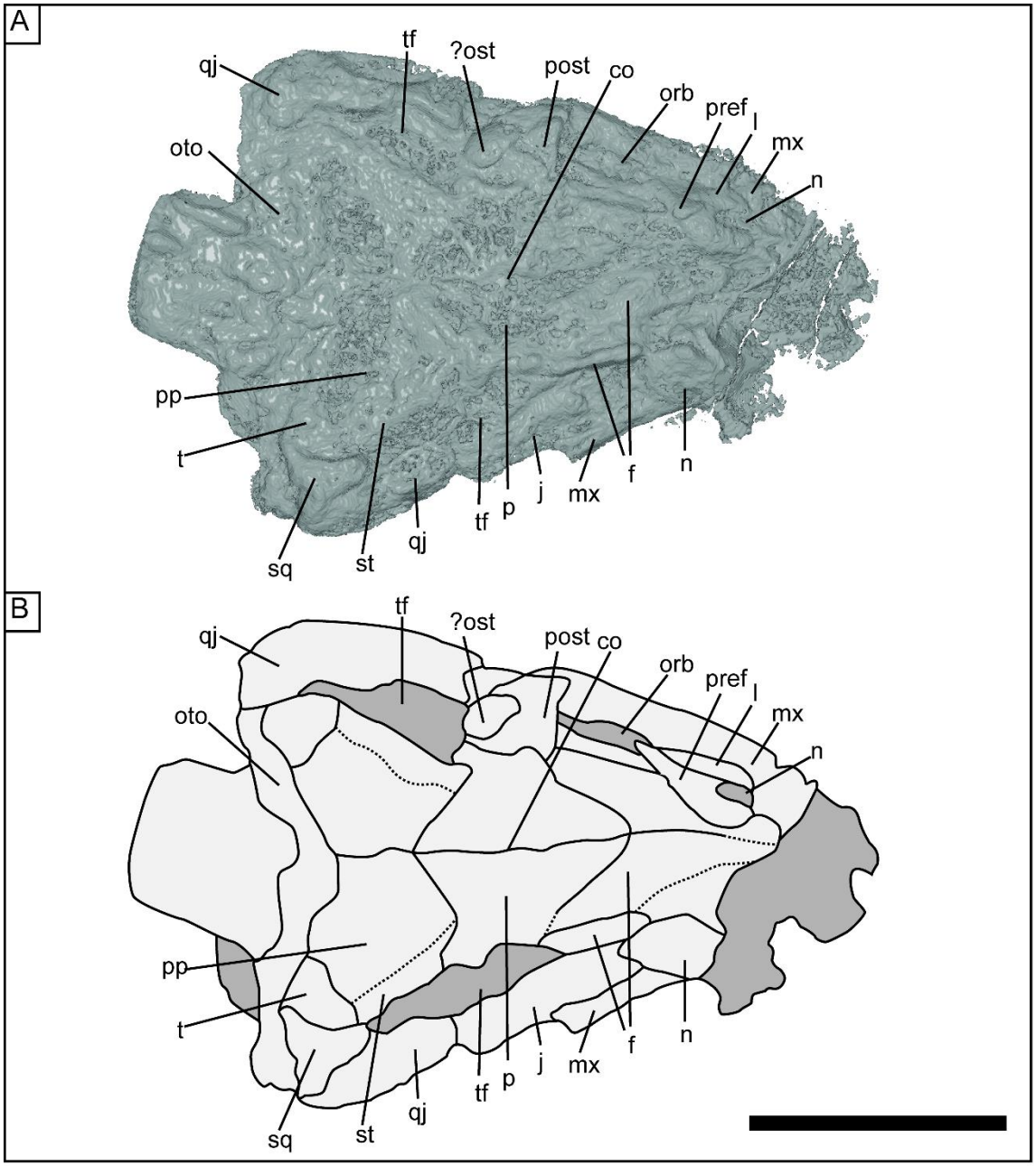

Figure 5.1. Skull of *Dolichosomatites emersoni* NHMUK.R8466 in dorsal view, showing (A) 3D rendering and (B) sketch. Abbreviations: f, frontal; j, jugal; l, lacrimal; mx, maxilla; n, nasal; na, nares; otoc, occipital complex; orb, orbit; ?ost, ?osteoderm; p, parietal; co, centre of ossification; post, postorbital; pp, postparietal; pref, prefrontal; qj, quadratojugal; sq, squamosal; st, supratemporal; tf, temporal fenestra. Scalebar = 5 mm.

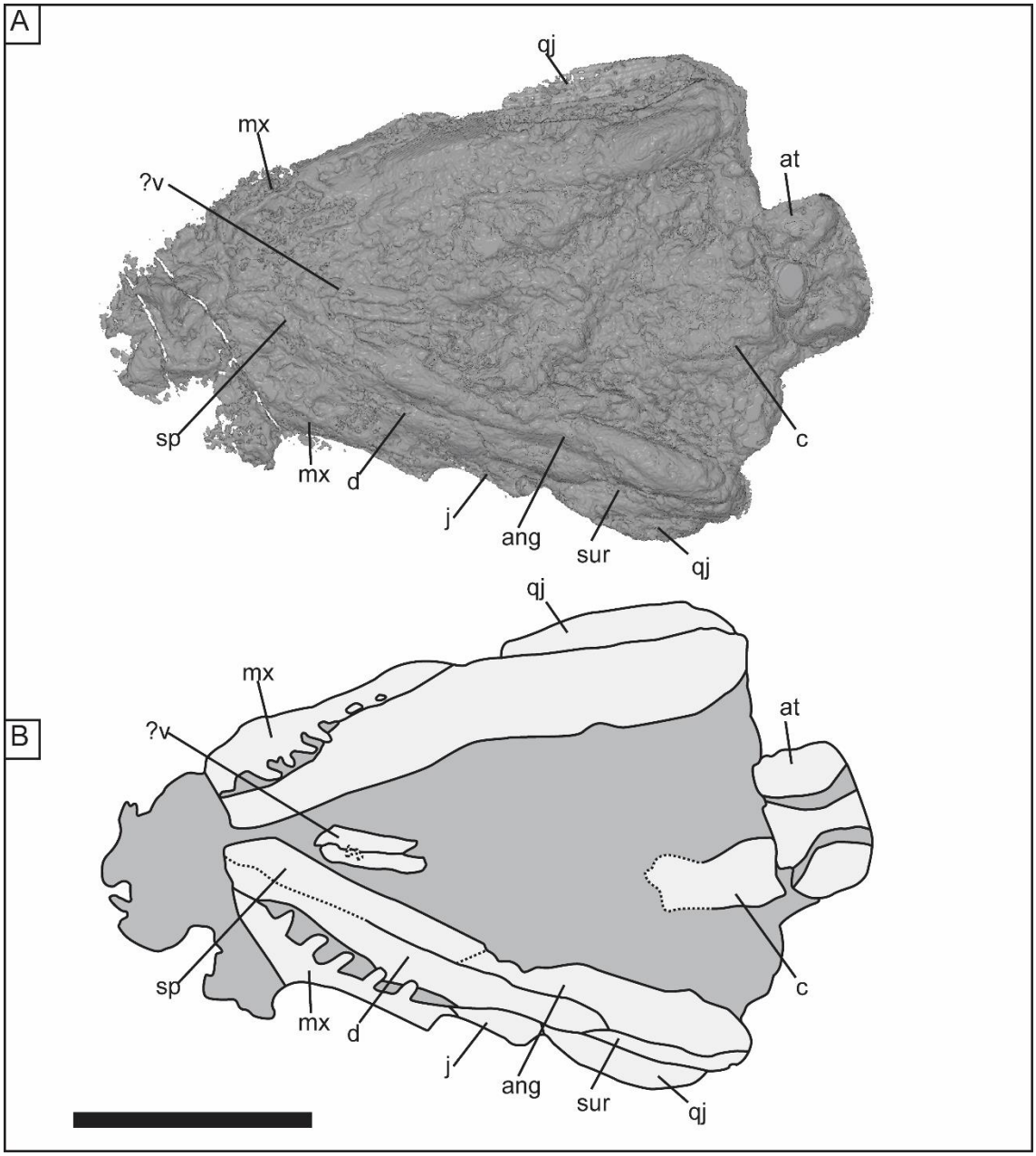

Figure 5.2. Skull of *Dolichosomatites emersoni* NHMUK.R8466 in ventral view, showing (A) 3D rendering and (B) sketch. Abbreviations: ang, angular; at, atlas; c, condyle; d, dentary; j, jugal; mx, maxilla; qj, quadratojugal; sp, splenial; sur, surangular; ?v, vomer. Scalebar = 5mm.

Appendicular Skeleton

A single pectoral element is preserved lateral to vertebra 5 on the left side. It lacks the "sickle" shape outline seen in the pectoral elements of aïstopods, but it can still be divided into a "handle" and "blade" region (*sensu* Anderson, 2002). This morphology is consistent with the cleithrum/fused cleithrum and clavicle in *Phlegethontia* (Anderson, 2002). The proximal handle region is relatively straight and robust (Fig. 5.3E). It is 36% the length of the blade region. It meets the blade region at an angle of c.170°. There is no apparent boundary or suture between

the handle and blade regions; both are identified only by their change in morphology. The blade region is slightly curved with a concave anterior margin. Its distal end tapers into a point.

Axial Skeleton

NHMUK.R8466 has 43 articulated vertebrae which are highly compressed dorso-ventrally. Vertebrae are typical of aïstopods (Carroll, 1998; Anderson, 2002, 2003a, 2003b) being holospondylus and amphicoelous (Fig. 5.3A-D). The centra are waisted towards their midpoint, giving them an hourglass shape and restricting the notochord. In ventral view there is an antero-posterior ridge running along the midline. Due to compression the openings of the articular faces have been flattened. The articulation faces are thickened along their ventral to lateral margins. In vertebrae 1-9 the transverse process extends postero-laterally from each centrum at an angle of c.70^{o} Transverse processes originate just posterior of the midpoint of each centra. This changes in vertebra 10 and all preceding posterior vertebrae in which the transverse processes extend at an angle of 90^{o}. In vertebra 10-43 the transverse processes originate just anterior of the midpoint of each centrum. In no vertebrae does the transverse process appear to originate or partially originate from the neural arch. The neural arches are low and composed of a single element fused to the centrum. The neural arches have paired posterior and anterior zygapophyses extensions, each of which extends postero-laterally and antero-laterally respectively. All zygapophysial extensions extend beyond the margin of their associated centrum. The articulation surfaces of the zygapophyses are horizontal with the anterior zygopophysis of one vertebra underlying the posterior zygopophysis of the preceding vertebra. The posterior zygapophysial extensions of each vertebra are more extensive than the anterior zygapophysial extensions. A thin neural spine extends in an antero-posteriorly direction along the dorsal margin of the neural arch. The neural spines of NHMUK.R8466 have been compressed so that they now preserved flattened onto the left side of the neural arch. The neural spine does not contact the anterior or posterior margins of each neural arch. Neural arches reach their greatest height dorsally around 33% along the antero-posterior length of the neural arch.

Despite the atlas showing transverse processes, ribs only appear on vertebra 2. Ribs associated with vertebrae 2-8 are double-headed and lack a K-shape morphology. The ribs of vertebrae 9-16 are difficult to identify, but by vertebra 17, ribs are distinctly K-shaped. These ribs articulate to the transverse process via the tuberculum. They have anterior processes at right angles to the tuberculum. Posterior to the tuberculum, the rib is divided into a short posterior process on the medial side and a rib shaft that extends just beyond the midpoint of the next posterior vertebra.

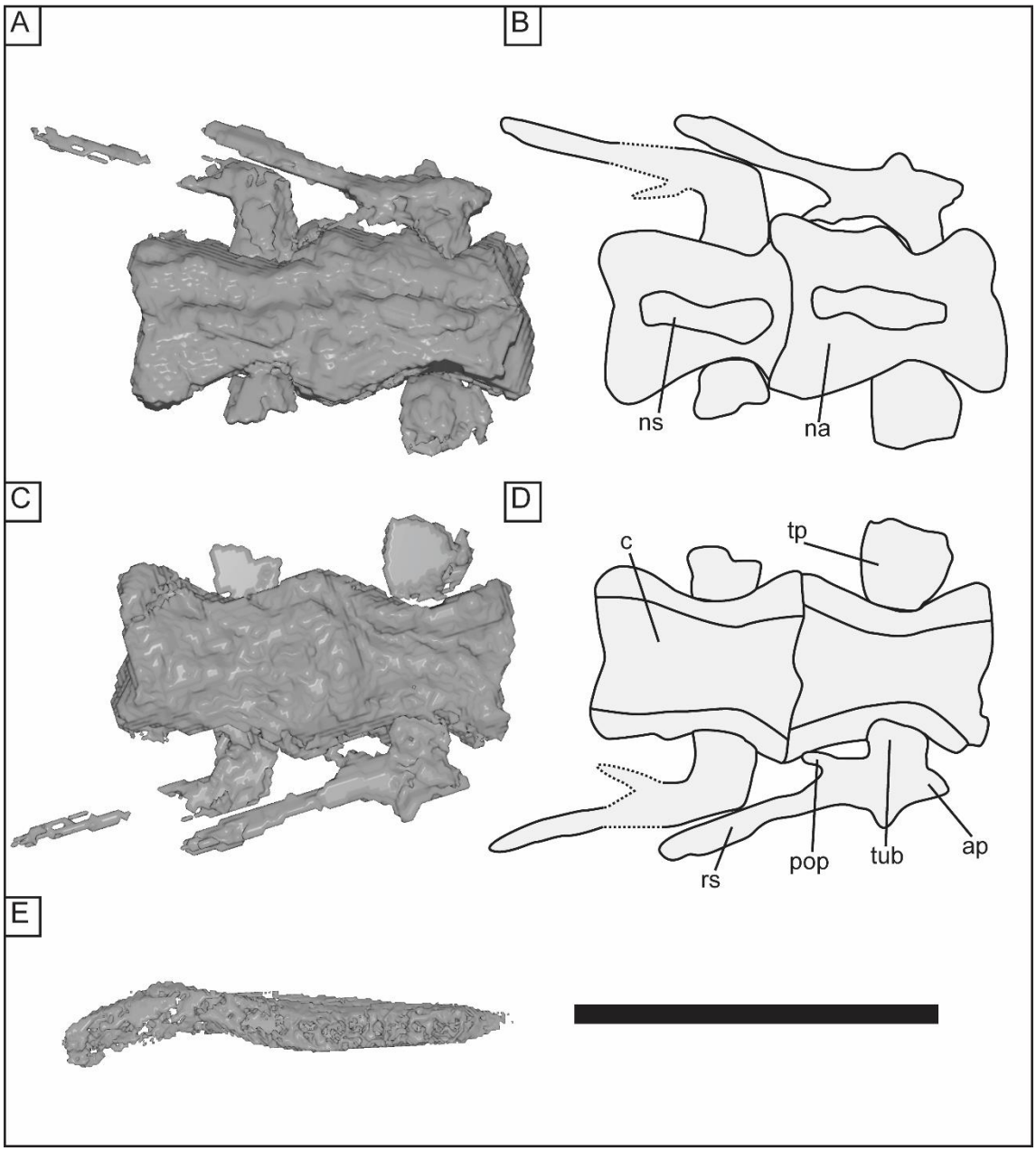

Figure 5.3. Axial skeleton and pectoral element of *Dolichosomatites emersoni* NHMUK.R8466 showing vertebra 31 and vertebra 32 in (A, B) dorsal view and (C, D) ventral view, and (E) pectoral element in medial view. Abbreviations: ap, anterior process; c, centrum; na, neural arch; ns, neural spine; pop, posterior process; rs, rib shaft; tp, transverse process; tub, tuberculum. Scalebar = 7mm A-D and 5mm for E.

Scalation

Gastralia are present along the ventral outline of NHMUK.R8466, appearing first at vertebra 2 and extending as far as vertebra 43. Posterior to vertebra 43, the block is broken so the exact posterior extent of the gastralia is uncertain. Gastralia are elongated, posteriorly curved scales that are tightly packed and they meet in a chevron pattern along the ventral midline. Dorsal osteoderms are present in the form of tightly packed small sub-ovoid scales

(Fig. 5.4). They extend as far anteriorly as the posterior half of the temporal fenestra and extend as far posteriorly as vertebra 22. Posterior of vertebra 22 there are no osteoderms, but this could be a result of accidental removal during manual preparation of the specimen. A single large bone posterior of the left postorbital in NHMUK.R8466 has been identified as possible being an osteoderm. It has a similar morphology to cheek osteoderms seen in NHMUK R 8465 *Ophiderpeton brownriggii* (see Chapter 4). If correctly identified it would be markedly larger than those seen posterior of it.

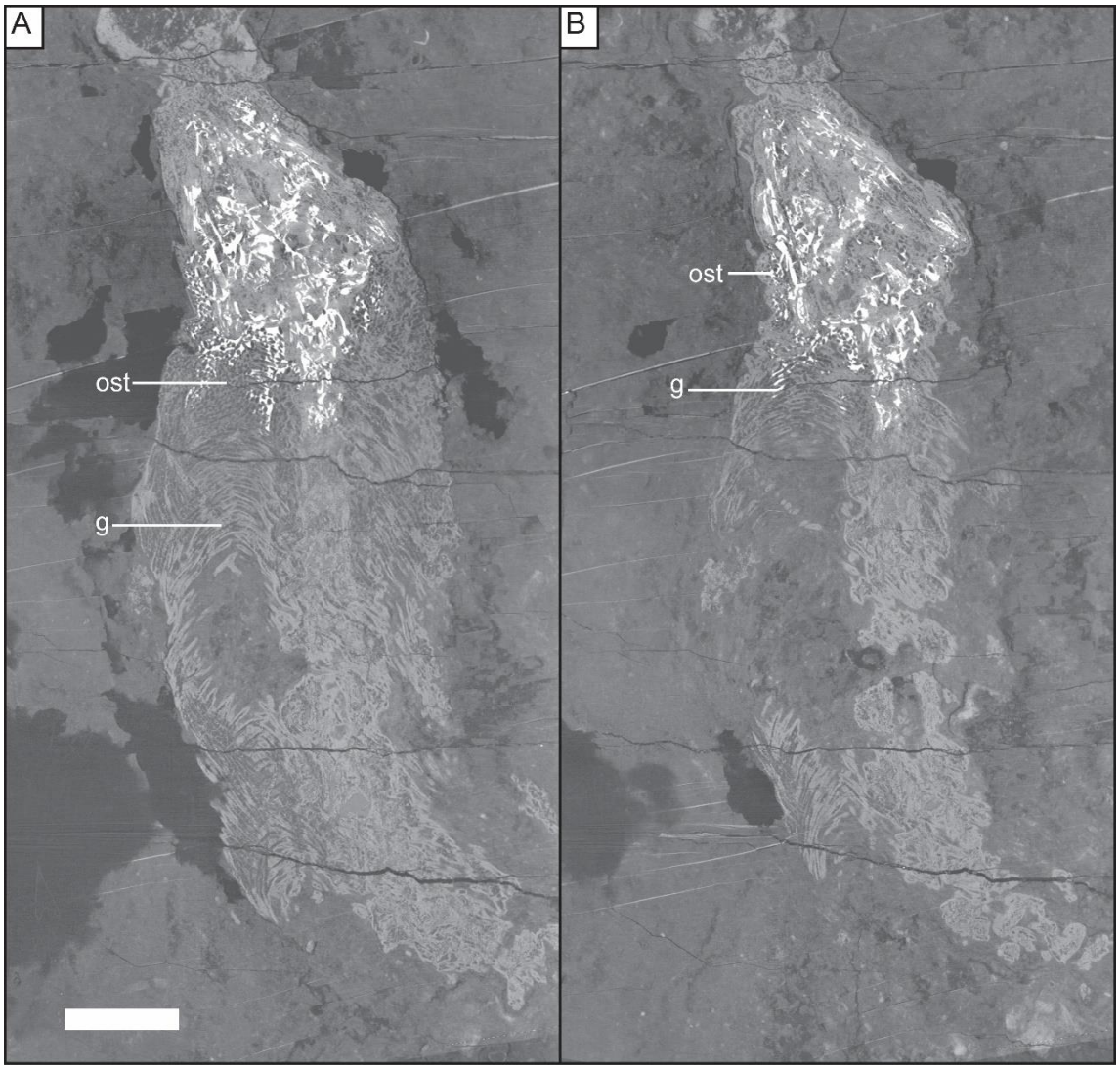

Figure 5.4. CT slices of *Dolichosomatites emersoni* NHMUK.R8466 showing scalation posterior of the skull. Abbreviations are g, gastralia; ost, osteoderms. Scalebar = 5mm

5.4 Discussion

5.4.1 Comparative anatomy

NHMUK.R8466 resembles the triangular cranium of Huxley's original description of the holotype TCD.T86 of "*Dolichosoma*" *emersoni*, which "tapers from the occiput to the snout, so as to have the form of an isosceles triangle" (Huxley and Wright, 1867). K-shaped ribs are also present which Huxley noted (Huxley and Wright, 1867). The mandible of NHMUK.R8466 does not however match the original description: Huxley described the mandible of TCD.T86 as being a "very slender ramus" (Huxley and Wright, 1867).

The overall triangular skull of *Dolichosomatites emersoni* approximately matches that of the derived *Pseudophlegethontia* (Anderson, 2003a) and *Phlegethontia* (Anderson, 2002), which is the reasons why it has been considered a Phlegethontiid (Carroll, 1998). However, the bone arrangement in the cranium is markedly different. The possession of a fused frontal bearing the pineal foramen and an absence of parietals and postparietals posteriorly in *Phlegethontia* (Anderson, 2002) contrasts with *Dolichosomatites* which has both postparietals and parietals and bears paired frontals. This lack of posterior cranial midline elements in *Phlegethontia* exposes most of the occipital complex. The occipital complex in NHMUK.R8466 is only partially visible in dorsal view directly posterior of the skull table. The anterior projection of the parietals along the midline onto the frontals in *Dolichosomatites* is similar to the situation in *Pseudophlegethontia* (Anderson, 2003a) and in *Ophiderpeton brownriggii* TCD.38363. The posterior margin of the skull table differs in *Pseudophlegethontia* and *Dolichosomatites*. In *Pseudophlegethontia*, the tabulars and postparietals extend posterior to the suspensorium (Anderson, 2003a). In *Dolichosomatites* the posterior margin of the tabulars and postparietals is at the same level as the suspensorium.

Although the exact morphology of the quadratojugal is difficult to observe in NHMUK.R8466, it appears to extend further anteriorly than the quadratojugal of *Pseudophlegethontia* (Anderson, 2003a). The temporal fenestra is closed in *Dolichosomatites* with the ventral margin being made up of nearly equal proportions of the jugal and quadratojugal which contact along the mid-length of the fenestra. This is also the case in *Lethiscus* (Pardo, *et al*., 2017), *Ophiderpeton* and *Peisterpeton* (see Chapter 4). The temporal fenestra in *Pseudophlegethontia* and *Phlegethontia* are open (Anderson 2002, 2003a). A closed temporal fenestra appears to be plesiomorphic in aïstopods with the more basal *Lethiscus* and Ophiderpetontidae retaining this morphology and the more derived Oestocephalidae, Pseudophlegethontiidae and the Phlegethontiidae all having an open temporal fenestra. Therefore, the presence of a closed temporal fenestra and the retention of paired midline

elements in *Dolichosomatites* suggests that it is a more basal aïstopod and confirming that it differs from the Pseudophlegethontiidae and the Phlegethontiidae.

5.4.2 Dolichosomatites and Ophiderpeton

The majority of aïstopod specimens from the Jarrow assemblage, many of which are external moulds, preserve only the vertebral column and scalation, many of which are external moulds. Specimens preserving skulls are less common. Though the skulls of *Dolichosomatites* and *Ophiderpeton* are evidently different, the postcranium requires discussion. The postcranium of *Dolichosomatites* and *Ophiderpeton* are very similar, both in the axial skeleton and in the scalation. In the vertebrae of *Dolichosomatites* the transverse process originates from the centrum, as is the case in *Ophiderpeton* (Chapter 4). The angle at which the transverse process extends laterally may be used to distinguish *Dolichosomatites* and *Ophiderpeton* vertebrae from one another. In *Dolichosomatites* the transverse processes extend laterally at an angle of c.90° (in vertebra 10 and all subsequent vertebrae), while in *Ophiderpeton* they extend posterior-laterally at an angle of c.60°. The presence of a medial accessory articulation in *Dolichosomatites* is not visible. This is due to the tightly packed nature of the vertebral column which hinders observation in the CT-slices. With the exception of this one characteristic, the vertebrae of *Dolichosomatites* and *Ophiderpeton* are nearly indistinguishable. Both *Dolichosomatites* and *Ophiderpeton* possess double-headed ribs anteriorly and K-shaped ribs. More posteriorly rib morphology changes from double-headed ribs to K-shaped ribs by vertebra 7 in *Ophiderpeton*, and possibly by vertebra 10 in *Dolichosomatites*.

Scalation patterns in *Dolichosomatites* and *Ophiderpeton* are also very similar with tightly packed ventral gastralia and small sub-ovoid dorsal osteoderms. One key difference is the absence of larger osteoderms around the cheek region in *Dolichosomatites* (with the exception of one possible large osteoderm). The cheek region of *Ophiderpeton* contains these larger osteoderms (Chapter 4), although they are not present in less mature *Ophiderpeton*. Despite the similarity in the postcranium of *Dolichosomatites* and *Ophiderpeton*, it is unlikely that the former represents an ontogenetic variant of the latter. This is mostly due to the major difference in skull morphology, and secondly because specimen NHMUK.R8466 exhibits complete scalation anteriorly and thus is not an immature individual as dorsal scalation is known to ossify posteriorly and gradually ossify anteriorly with maturity in aïstopods (Anderson, 2003b). The similarities between the two taxa lead to difficulties when trying to identify the aïstopods vertebral columns in the Jarrow assemblage. Given the small sizes of *Dolichosomatites* it could be argued that all vertebral columns with “large” vertebrae are *Ophiderpeton*. This is not a robust argument and the converse is even less convincing because

vertebral columns with “small” vertebrae could be either *Ophiderpeton* or *Dolichosomatites*. Therefore, it is not currently possible to resolve the affinity of aïstopod specimens known only from the vertebral column.

5.4.3 Aïstopod assemblages through time

The traditional splitting of aïstopods into blunt-headed forms (i.e. *Ophiderpeton*) and narrow-headed forms (i.e. *Phlegethontia*) indicated a low level of disparity and diversity throughout the clade. Recent reviews of the aïstopods by Anderson (2002, 2003a, 2003b) and Anderson, *et al*. (2003) highlighted this misconception by naming a new transitional form (Anderson, 2003a) and indicating that the basal *Lethiscus* does not fit this traditional pattern (Anderson, *et al*. 2003). The most recently described aïstopod from the Pennsylvanian, *Andersonerpeton* (Pardo and Mann, 2018), does not fit into either grouping of aïstopod. *Andersonerpeton* is represented by a single mandible with more plesiomorphic characteristic than *Lethiscus*. When dealing with aïstopod disparity and evolution through time, the Jarrow assemblage has been generally overlooked.

Aïstopods first appeared in the geological record in the Viséan and are represented by two species (Fig. 5.5), the older of which is the basal *Lethiscus* (Wellstead, 1982; Anderson, *et al*. 2003) the younger, *Ophiderpeton kirktonense* (Milner, 1993). Both are represented only by a single specimen. There is then a gap in the geological record with no aïstopod material from the Serpukhovian stage (Fig. 5.5). The next occurrence of aïstopods is in the late Bashkirian (Langsettian) of the Jarrow assemblage. This is the earliest known occurrence in the geological record of a biota containing more than one aïstopod species. It is also the first assemblage with more than one specimen of each taxon. The sudden appearance of new and diverse tetrapods in the earliest Pennsylvanian is not limited to aïstopods. The Tournasian and Viséan has traditionally been considered to contain low tetrapod diversity during a period called “Romer’s Gap”. Recent tetrapod discoveries from early Mississippian deposits (Smithson *et al.*, 2012; Clack *et al.*, 2016) suggest this low diversity signal is the result of a lack of fossils finds, making Romer’s Gap an obsolete concept. Currently, our understanding of aïstopod evolution during the Mississippian suffers from this lack of discovered material. This will hopefully be rectified in the future with the additional collecting of new material.

To date, no assemblage has produced more than three separate species of aïstopods. Therefore, Jarrow and the later Mazon Creek and Linton preserve the most diverse aïstopod assemblages, although there are notable differences between the three biotas. The aïstopods preserved at Jarrow all represent plesiomorphic forms with a closed temporal fenestra. It is not until the Moscovian that the more derived Oestocephalidae, Pseudophlegethontiidae and the

Phlegethontiidae appear (Anderson, 2002, 2003a, 2003b). There appears to be a replacement of *Ophiderpeton*-type aïstopods near the Bashkirian-Moscovian boundary. This means that Mazon Creek, Linton and Nýřany preserve a more disparate fauna of aïstopods including at least one oestocephalids and one phlegethontiid each. By the Kasimovian, the only known aïstopods to be been found are phlegethontiids, which persist until the Middle Permian before the whole clade became extinct.

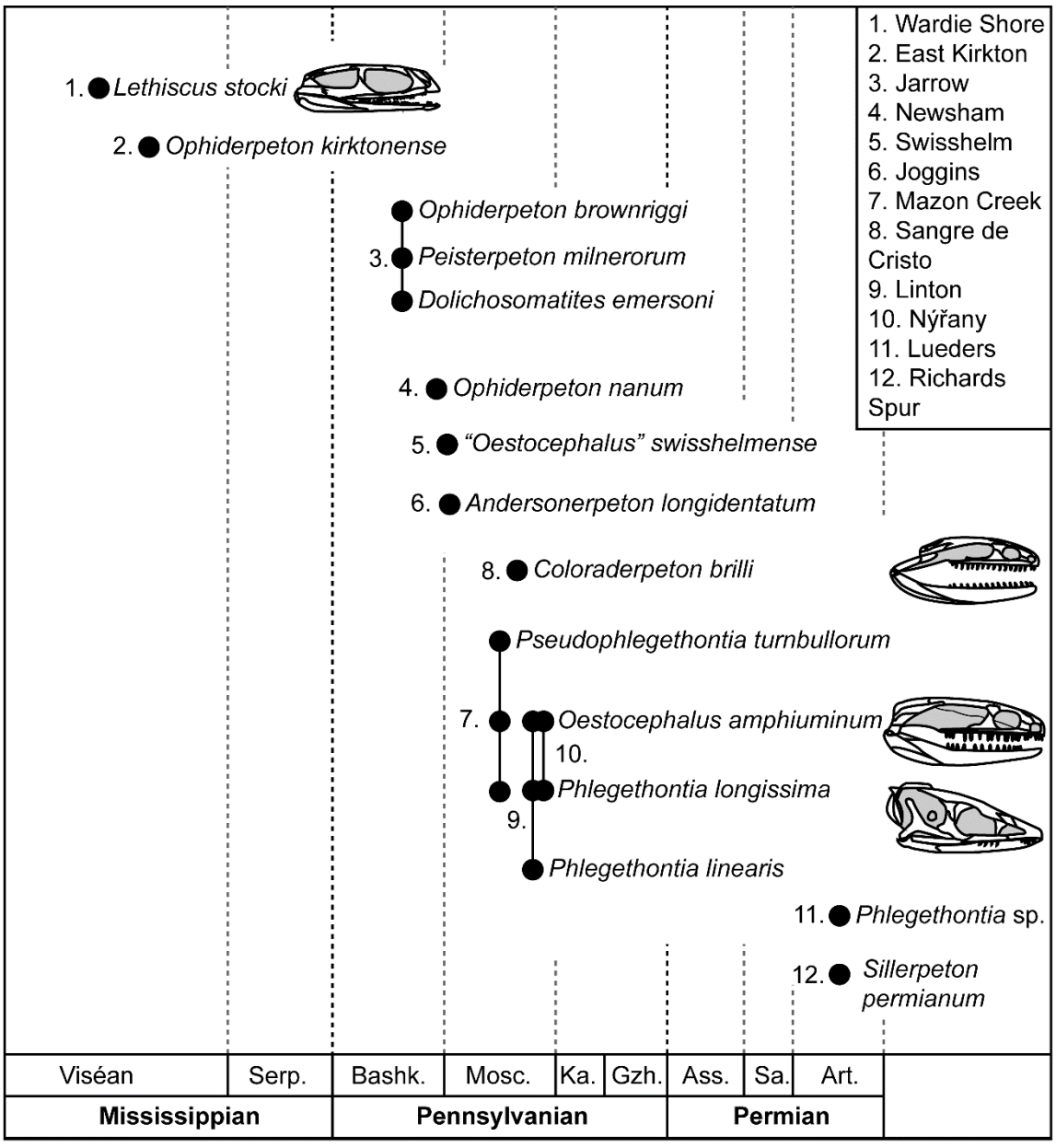

Figure 5.5. List of all known aïstopods occurrences and their ages. Skulls adapted from Anderson (2002, 2003b) and Pardo, *et al.* (2017).

5.5 Conclusion

In this chapter μCT has applied to the neotype of the aïstopod "*Dolichosoma*" *emersoni* NHMUK.R8466 in order to provide new data and clarify taxonomic issues.

"*Dolichosoma*" *emersoni* is here described and formally transferred to the genus *Dolichosomatites* as *Dolichosomatites emersoni*. *D. emersoni* is a small aïstopod with a triangular skull that tapers anteriorly and paired frontals, parietals and postparietals. The temporal fenestra is closed due to a contact between the jugal and the quadratojugal. Vertebrae are typical of aïstopods and closely resemble those of *Ophiderpeton*. K-shaped ribs are present. Scalation is composed of tightly packed ventral gastralia and small sub-ovoid osteoderms. All these characteristics suggest that *D. emersoni* shares a closer relationship to the basal aïstopods *Lethiscus* and *Ophiderpeton*.

D. emersoni was traditionally considered as part of the derived Phlegethontiidae aïstopods. However, this does not appear to be the case as *D. emersoni* lacks derived aïstopod characters such as fused frontals and the absence of parietals and postparietals. The Jarrow assemblage is now known to contain at least three aïstopod species. Unlike later assemblages, which contain members of both the Oestocephalidae and the Phlegethontiidae, the Jarrow aïstopods all appear to represent plesiomorphic members of the clade. This suggests that there is a faunal change of aïstopods close to the Bashkirian-Moscovian boundary, with more derived forms replacing "primitive" forms.

5.6 References

AHLBERG, P. E. 1991. A re-examination of sarcopterygian interrelationships, with special reference to the Porolepiformes. *Zoological Journal of the Linnean Society*, **103**, 241–287.

ANDERSON, J. S. 2002. Revision of the Aïstopod Genus *Phlegethontia* (Tetrapoda: Lepospondyli). *Journal of Paleontology*, **76**, 1029–1046.

— 2003. A new Aïstopod (Tetrapoda: Lepospondyli) from Mazon Creek, Illinois. *Journal of Vertebrate Paleontology*, **23**, 79–88.

— 2003b. Cranial anatomy of *Coloraderpeton brilli*, postcranial anatomy of *Oestocephalus amphiuminu*s, and reconsideration of Ophiderpetontidae (Tetrapoda: Lepospondyli: Aistopoda). *Journal of Vertebrate Paleontology*, **23**, 532–543.

— CARROLL, R. L. and ROWE, T. B. 2003. New information on *Lethiscus stocki* (Tetrapoda : Lepospondyli : Aistopoda) from high-resolution computed tomography and a phylogenetic analysis of Aistopoda. *Candian Journal of Earth Science*, 40, 1071–1083. doi: 10.1139/E03-023.

BAIRD, D. 1964. The aistopod amphibians surveyed, *Brevoria*, **206**, 1–17.

CARROLL, R. L. 1998a Order Aïstopoda Miall 1875. 163–182. *In* WELLNHOER (ed). *Encyclopedia of Paleoherpetology*. Verlag Dr.Friedrich Pfeil, München, 206 pp.

CLACK, J. A., BENNET, C. E., CARPENTER, D. K., DAVIES, S. J., FRASER, N. C., KEARSEY, T. I., MARSHALL, J. E. A., MILLWARD, D., OTOO, B. K. A., REEVES, E. J., ROSS, A. J., RUTA, M., SMITHSON, K. Z., SMITHSON, T. R. and WALSH, S. A. 2016. Phylogenetic and environmental context of a Tournaisian tetrapod fauna. *Nature Ecology and Evolution*, **1**, 0002. doi:10.1038/s41559-016-0002.

COPE, E. D. 1871. General observations on the extinct Batrachian fauna of the Carboniferous of Linton, Ohio. *Proceedings of the American Philosophical Society*, **12**, 177.

—1874. Supplement to the extinct Batrachia and Retilia of North America, I, Catalogue of the air breathing vertebrata from the Coal Mesures of Linton, Ohio. *Transactions of the American Philosophical Society*, **15**, 261–278.

— 1875. Synopsis of the extinct Batrachia Reptilia and Aves of North America, Part1. *Report of the Geological Society of Ohio*, **2**, 351–411.

FRITSCH, A. 1875. *Über die Fauna der Gaskohle des Pilsner und Rakonitzer Beckens.* Prague: Sitzungsberichte der Böhemischen Gesellschaft der Wissenschaften.

—1879. *Fauna der Gaskohle und der Kalksyeine der Permformation Böhmens. Band 1. Heft 1.* Prague.

HUXLEY, T. H. and WRIGHT, E. P. 1867. Royal Irish Academy On a Collection of Fossil Vertebrata , from the Jarrow Colliery, County of Kilkenny, Ireland. *Transactions of the Royal Irish Academy*, **24**, 351–370.

KUHN, O. 1961. *Die familien der rezenten und fossilen Amphibien und Reptilien.* Meisenbach, Bamberg.

LYDEKKER, R. 1890. *Catalogue Of The Fossil Reptilia and Amphibia in the British Museum (Natural History), Part IV. Containing the orders Anomodontia, Ecaudata, Caudata, And Labyrinthodontia; And Supplement*. British Museum (Natural History), London.

— 1891. *Catalogue of fossil mammals, birds, reptiles, and amphibians in the Science and Art Museum*. Science and Art Museum, Dublin:.

MCGINNIS, H. J. 1967. The osteology of *Phlegethontia*, a Carboniferous and Permian aïstopod amphibian. *University of California Publications in Geological Sciences*, **71**, 1–46.

MIALL, L. C. 1875. Report of the committee on the structure and classification of the labyrinthodonts. *Report of the 44th Meeting of the British Association for the Advancement of Science*, **1874**,149–92.

MILNER, A. C. 1993. The aïstopod amphibian from the Viséan of East Kirkton, West Lothian, Scotland. *Transactions of the Royal Society of Edinburgh: Earth Sciences*, **84**, 363–368. doi: 10.1017/S0263593300006167.

PARDO, J. D., SZOSTAKIWSKYJ, M. and ANDERSON, J. S. 2017. Hidden morphological diversity among early tetrapods. *Nature*, **546**, 642–645.

— and MANN, A. 2018. A basal aïstopod from the earliest Pennsylvanian of Canada, and the antiquity of the first limbless tetrapod lineage. *Royal Society Open Science*, **5**, p. 181056.

ROMER, A. S. 1930. The Pennsylvanian tetrapods of Linton, Ohio. *Bulletin of the American Museum of Natural History*, **59**, 77–147.

SMITHSON, T. R., WOOD, S. P., MARSHALL, J. E. A. and CLACK, J. A. (2012) Earliest Carboniferous tetrapod and arthropod faunas from Scotland populate Romer's Gap. *PNAS*, **109**, 4532–4537.

STEPHENS, J. F. 1830. *Illustrations of British Entomology, Volume 3*. Baldwin and Cradock, London. 362 pp.

SUTTON, M. D., *GARWOOD, R. J., SIVETER, D. J. and SIVETER, D. J.* 2012. SPIERS and VAXML; A software toolkit for tomographic visualisation and a format for virtual specimen interchange. *Palaeontologia Electronica*, **15**, 1–14.

TURNBULL, W. D. and TURNBULL, P. F. 1955. A recently discovered *Phlegethontia* from Illinois. *Fieldiana: Zoology*, **37**, 523–535.

WELLSTEAD, C. F. 1982. A Lower Carboniferous aïstopod amphibian from Scotland. *Palaeontology*, **25**, 193–208.

WYSE JACKSON, P. N. and MONAGHAN, N. T. 1995. Transfer of the Huxley and Wright (1867) Carboniferous amphibian and fish material to Trinity College, Dublin from the National Museum of Ireland. *Journal of Paleontology*, **69**, 602–603.

Chapter 6: A review of the Jarrow Urocordylidae (Nectridea, Tetrapoda) using micro-computed tomography.

6.1 Introduction

Nectridea is an order of small early tetrapods characterized by holospondylus vertebrae with fan-like neural and haemal spines with crenulated dorsal and ventral margins respectively and long, laterally flattened tails. The various genera were important aquatic members of the Pennsylvanian coal swamp ecosystems, being represented by several species at Jarrow, Ireland, Linton, Ohio, Nýřany, Czech Republic and Newsham, England. and also occurring in the red bed fluvial deposits of the early Permian (Huxley and Wright, 1867; Milner, 1980; Bossy and Milner, 1998).

Nectrideans comprise three families, all of which are first known from the early Pennsylvanian. The Diplocaulidae are characterized by having horn-like elongated posterior extensions of the tabulars. In Pennsylvanian forms these extensions may have been attached, via soft tissue, to anterior extensions of the cleithrum (Milner, 2019). This attachment was lost in later Permian forms, with the tabular extensions being more laterally oriented giving the skulls a boomerang-like shape, as in *Diplocaulus* (Willison, 1909; Olson, 1972; Rinehart and Lucas, 2001; Germain, 2010). The Scincosauridae have characters indicating a terrestrial mode of life, including ossified carpals/tarpals, L-shaped humeri and a co-ossified loadbearing pelvis (Milner, 1980). Diplocaulids and scincosaurids are sister families (Milner and Ruta, 2009) with Urocordylidae as a more outlying group. Urocordylids are characterized by longer tails relative to other nectrideans (up to two thirds the length of their trunk region). These tails have much higher haemal and neural arches compared to diplocaulids and scincosaurids. This makes the tail dorso-ventrally tall. Urocordylids are divided further into the subfamilies Sauropleurinae and Urocordylinae (Bossy and Milner, 1998). Sauropleurines have elongated snouts, formed by anterior extension of the nasal and premaxilla, with fused frontals giving the skull an arrow shape. The maxilla forms the ventral orbital margin. Urocordylines lack this anterior snout extension and instead have broad blunt skulls with paired frontals and a lacrimal-jugal contact excluding the maxilla from the orbit margin.

Nectrideans were first reported from the Jarrow assemblage by Huxley in Huxley and Wright (1867) who described three species: the diplocaulid *Keraterpeton galvani*; the urocordyline *Urocordylus wandesfordii*; and the sauropleurine *Lepterpeton dobbsii*. This was quickly followed by the identification of the urocordylid *Sauropleura* (now two species, a

sauropleurine, *Sauropleura pectinata* and a urocordyline, *Ctenerpeton remex*, (Bossy and Milner, 1998) from the Linton assemblage by Cope (1868), an indeterminate *Urocordylus* from the Newsham tetrapod assemblage (Hancock and Atthey, 1870) and *Sauropleura scalaris* from Nýřany, Czech Republic (Fritsch, 1881). The Orders Nectridea, Aïstopoda and Microsauria were established by Miall to classify those early tetrapods with holospondylus vertebrae (Miall, 1875). This was followed by the erection of the families Urocordylidae and Scincosauridae by Lydekker in Nicholson and Lydekker (1889), the first of which included the diplocaulid *K. galvani*, an assignment later amended by (Romer, 1930). Romer (1966) considered that the three Jarrow nectrideans should be accommodated in three nectridean families, the Urocordylidae, the Keraterpetontidae and the Lepterpetontidae. Since then *L. dobbsii* has been reassigned to the urocordylids (Bossy and Milner, 1998). Urocordylids were revised by Bossy (1976) and formed part of revisions of the nectrideans by Milner (1980) and Bossy and Milner (1998).

Traditionally nectrideans have been assigned to the subclass Lepospondyli together with the aïstopods, microsaurs, lysorophians, adelospondyls and the *Archerontiscus*. This is based primarily on vertebra being composed of a single co-ossified centrum and neural arch and on their general small sizes. Lepospondyls have traditionally been considered either to be on the lissamphibian stem (termed the lepospondyl hypothesis according to which modern amphibians originated from lepospondyls) (Vallin and Laurin, 2004; Germain, 2008) or on the amniote stem (the temnospondyl hypothesis) (Ruta, *et al*., 2003; Ruta and Coates, 2007, Pardo *et al*. 2017). Most workers support the temnospondyl hypothesis, with the lepospondyls situated on the amniote stem. However, lepospondyls have long been suspected to be polyphyletic (Thompson and Bossy, 1970; Milner *et al.*, 1986; Panchen and Smithson, 1988). Recent cladistic analysis supports a stem-tetrapod placement for aïstopods and a place among the amniotes for the recumbirostra "microsaurs" (Pardo, *et al*. 2017; Clack, *et al*. 2019) indicating lepospondyl polyphyly.

Not only is the Jarrow biota the first historical record of nectrideans but also marks the first geological appearance of the clade. The diverse assemblage (three genera in two families) indicates that nectrideans probably originated in the Mississippian, possibly from a terrestrial ancestor (Bossy and Milner, 1998). A recent review of *K. galvani* from Jarrow by Milner (2019) revealed previously unknown characters in the nectrideans including the presence of a basiobranchial. In the present study micro-computed tomography and 3D modelling have been applied to understand better the anatomy of the other two Jarrow nectrideans, *Urocordylus wandesfordii* and *Lepterpeton dobbsii*.

6.2 Material and Methods

Micro-computed tomography was carried out on *Urocordylus wandesfordii* (specimen NMI.F14716 using the Nikon XTH 225ST of the Palaeobiology Research Group, University of Bristol and on TCD. 38354 using the Nikon XTH225 ST at the Amber Lab, Trinity College Dublin) and on *Lepterpeton dobbsii* (TCD.T85b) using the Nikon XTH225 ST at the Amber Lab, Trinity College Dublin. The scanning parameters were as follows: NMI.F14716 scanned at 220kV, 264µA with a 0.5mm copper filter; TCD. 38354 was scanned in two runs with scanning parameters of 180kV, 57µA and 160kV, 86µA both with no filter; TCD.T85b was scanned at 75kV, 214µA with no filter; Resulting TIF stacks were converted into PNG files an imported into SPIERS (Sutton *et al.*, 2012). Bones were indentified and isolated using the 'curve to mask' function in order to produce 3D models.

Museum repository abbreviations are: NMI, National Museum of Ireland; MCZ, Museum of Comparative Zoology, Harvard University, Cambridge, Boston, USA; TCD, Trinity College Dublin, Geological Museum.

6.3 Systematic Palaeontology

Class TETRAPODA Goodrich, 1930

Order NECTRIDEA Miall, 1875

Family UROCORDYLIDAE Lydekker in Nicholson and Lydekker, 1889

Subfamily SAUROPLEURINAE Bossy and Milner, 1998

Diagnosis— (Adapted from Bossy and Milner, 1998). Urocordylidae nectrideans with narrow tables and elongated snouts formed by anterior extensions of the premaxilla and nasals. Nares directly anterior to the orbits. Frontals fused. Mandibles articulation at the level of the occipital condyle.

Genus *LEPTERPETON* Huxley in Etheridge, 1866

Type Species— *Lepterpeton dobbsii* Huxley *in* Wright and Huxley, 1866

Diagnosis— Sauropleurinae nectridean with a maximum skull length of 20mm. Maxilla plus premaxilla make up 77% of the length of the skull. Mandible articulation at the level of the condyle. Twenty precaudal vertebrae and 32-34 caudal vertebrae. Caudal vertebrae with haemal and neural spines of a similar morphology.

LEPTERPETON DOBBSII Huxley *in* Wright and Huxley, 1866

(Figs 6.1-6.3)

Diagnosis— Same as for genus.

v 1866 *Lepterpeton dobbsii* Huxley *in* Wright and Huxley, 1866: p. 169.

v 1867 *Lepterpeton dobbsii* Huxley *in* Huxley and Wright, 1867: p. 362, pl. 21, figs. 1–2.

1998 *Lepterpeton dobbsii* Huxley Bossy and Milner *in* Carroll, Bossy, Milner, Andrews and Wellstead, 1998: p. 115.

Holotype—TCD.T85a and TCD.T85b part and counterpart (Figured in Huxley and Wright, 1867, plate 21, figures 1-2.)

Type Locality—Clogh, County Kilkenny, Ireland.

Type Horizon—Jarrow (No. 4) Coal Seam, Coolbaun Coal Formation, Langsettian: Pennsylvanian.

Description

TCD.T85a and TCD.T85b preserve part and counter part of the holotype of *Lepterpeton dobbsii*. TCD.T85a at one time recorded the complete length of *L. dobbsii* with the trunk and cranial regions being preserved as moulds and the caudal region preserved as a complete body fossil. This is the specimen figured by Huxley and Wright (1867; plate 21, figure 1.). Unfortunately, the specimen has degraded badly since its first description, with the

caudal region being lost as well as part of the left leg and digits (Fig. 6.1). The rest of the specimen is in a poor state, having apparently broken into three. The specimen is currently surrounded with wax in a modified tray which was a common method of slowing down pyrite decay in Jarrow specimens during the 1950-1960s in TCD and the NMI. TCD.T85b preserves the body fossil of the cranial region with mandibles corresponding to the mould in TCD.T85a. It preserves the entire snout and as far posterior as the mandibular-cranial articulation on the left side. The right side is broken posterior of the orbit. All other posterior parts of the skeleton have been lost through breakage. It is preserved in ventro-lateral view with part of the right side of the cranium folded under the rest of the skull. The skull itself has been largely replaced with pyrite (Fig. 6.2).

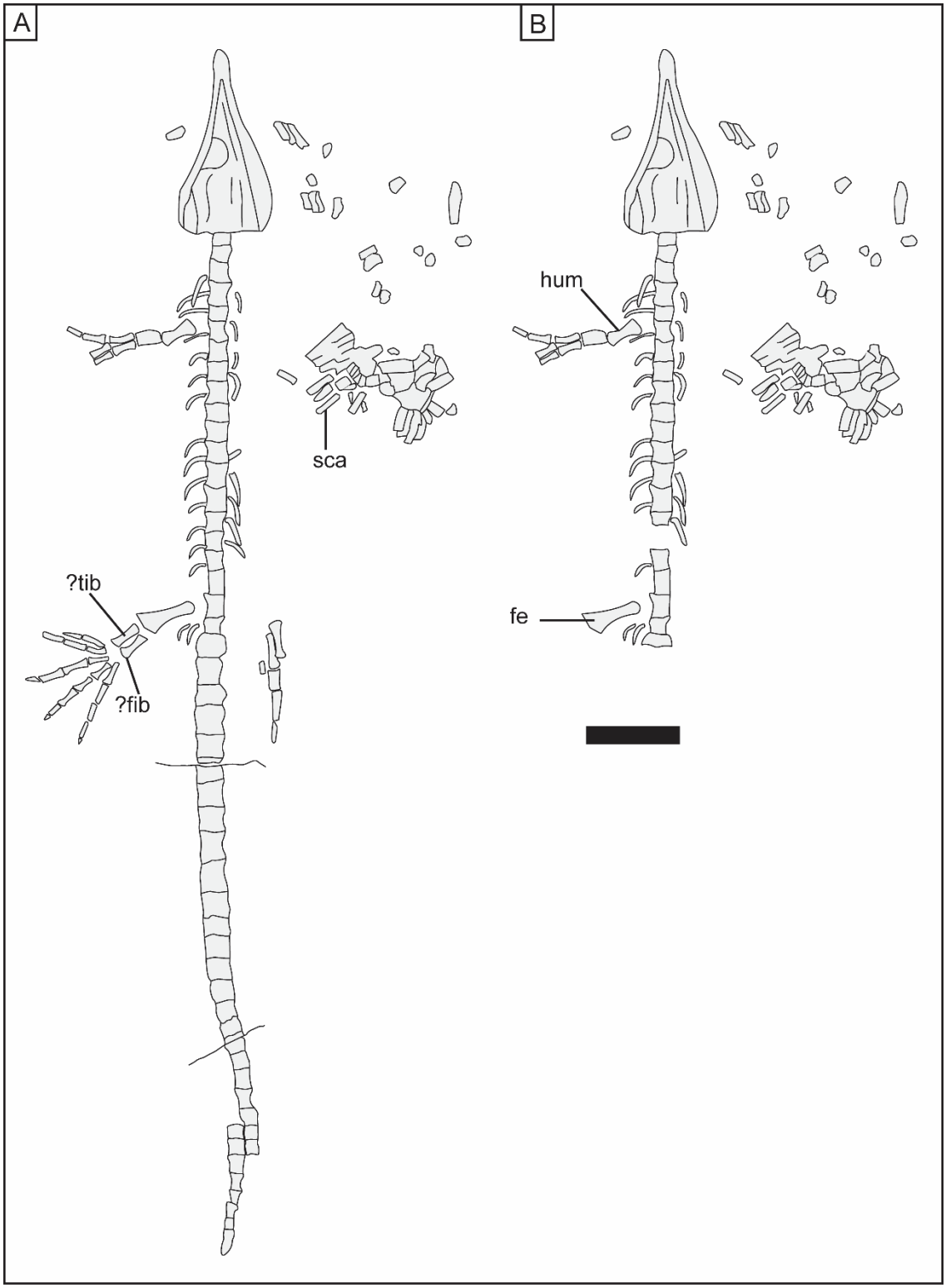

Figure 6.1. Complete fossil of TCD.T85a *Lepterpeton dobbsii* in dorsal view showing (A), drawing of the specimen from the original description by Huxley and Wright (1867), and (B), drawing of the current state of specimen. A, adapted from Huxley and Wright (1867: p.362, pl. 21, fig. 1). Abbreviations: fe, femur; ?fib, ?fibula; hum, humerus; sca, scalation; ?tib, ?tibula. Scalebar = 10mm.

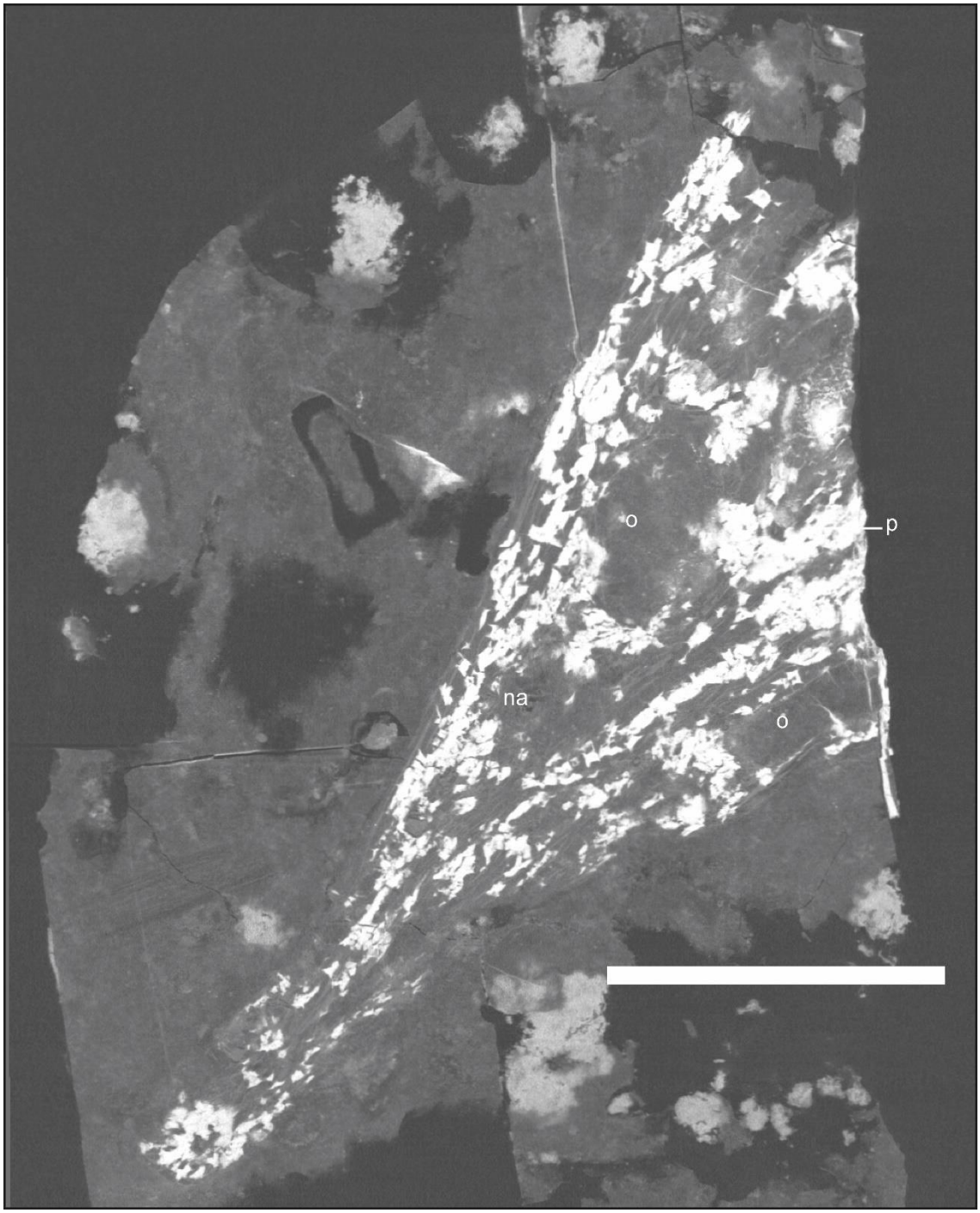

Figure 6.2. µCT slice of TCD.T85b *Lepterpeton dobbsii*. Abbreviations: na, nares, o, orbit, p, pyrite. Scale bar = 5mm.

Cranium

The skull is 20mm long from the mandible articulation to the anterior margin of the premaxilla. It is narrowest anteriorly and expands laterally towards the posterior end. The skull is widest along the posterior margin where it measures c. 8mm (measured from Huxley and Wright, 1867; plate 21, figure 1). These gives the skull an angular shape (Fig. 6.3). The snout

makes up 68% of the length of the cranium, contributed to by anterior projection of the premaxilla and the nasals. The premaxilla is an anteriorly elongate element which makes up 40% of the length of the cranium. Although the boundary between the nares and the premaxilla is difficult to discern it appears that midway along its length the premaxilla appears to close out the nares to become the only cranial element anteriorly (Fig. 6.3B). The premaxilla anteriorly appears to form a bulbous area (Fig. 6.3B). It is not clear whether this is original or the result of the underlying mandibular elements causing the appearance of a thickening. The premaxilla extends posteriorly to form the anteroventral margin of the nares. The boundary between the premaxilla and the maxilla is not clear although it probably lies ventral to the nares with the maxilla making up part, if not most, of the ventral margin of the nares. The maxilla extends posteriorly, making up part of the ventral margin of the orbits and tapers laterally (due to compression) to the inferred posterior margin of the jugal (Fig. 6.3B). The combined length of the maxilla and premaxilla makes up 77% of the skull length. Posterior of the left nares is a triangular bone which lies medial to the maxilla and is here considered to represent the lacrimal. It forms the posterior margin of the nares and the anterior margin of the orbit. The prefrontal lies dorsomedial to the lacrimal; it is a crescentic bone with a concave lateral margin and a convex medial margin. It expands anteriorly where it forms the posterodorsal margin of the nares (Fig. 6.3B). Posteriorly it forms a small part of the dorso-anterior margin of the orbit. The jugal makes up the ventral half of the posterior margin of the orbit. It is a triangular bone, only slightly larger than the lacrimal, although its posterior extent is uncertain. An emargination of the posterodorsal border of the orbit probably represents part of the postorbital which has been displaced slightly anteriorly post-mortem. There is no evidence of a ventral extension of the postorbital. Although the exact morphology of both the postorbital and the postfrontal is not clear, the nearly complete orbit suggests the presence of a postfrontal (Fig. 6.3B). Similarly, posterior to the jugal the squamosal and quadratojugal are probably still preserved (given the lack of major disarticulation) but cannot be confidently distinguished. It appears at least that in life the squamosal and quadratojugal would have been deep in a dorso-ventral direction resulting in a deep cheek region in *L. dobbsii*. The midline elements cannot be distinguished from one another but there appears to be at least a boundary between them and more lateral elements on the left side of the cranium (Fig. 6.3B). The boundaries between the nasals, frontal and parietals cannot be readily identified. Based on the similar sauropleurine *Sauropleura pectinatus*, the nasals probably extended not further posteriorly than the posterior margin of the nares and the frontal was probably unpaired.

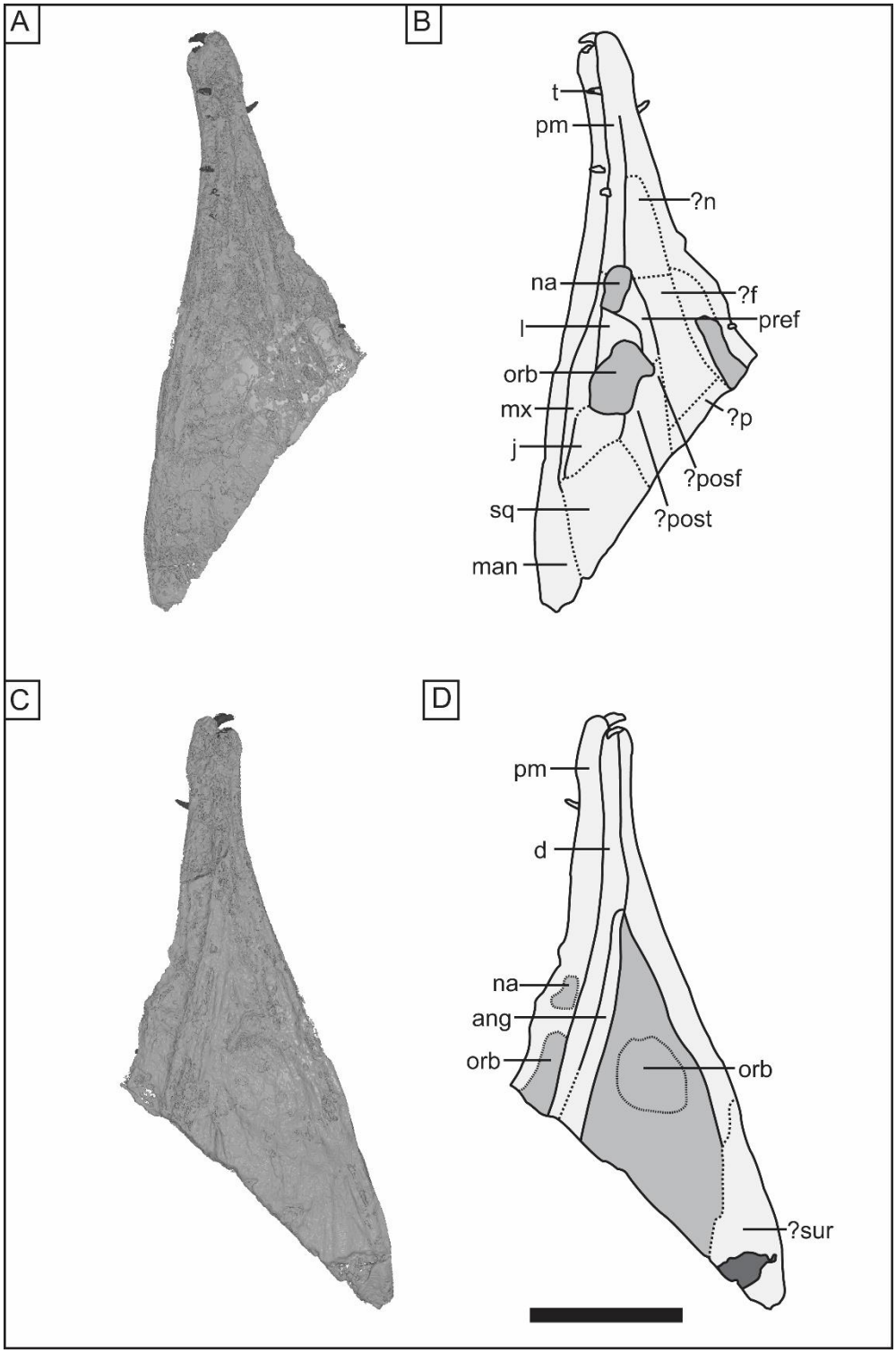

Figure 6.3. 3D model and sketch of TCD.T85b *Lepterpeton dobbsii* in (A, B) dorsal view, and (C, D), ventral view. Abbreviations: ang, angular; den, dentary; ?f, ?frontal; j, jugal; l, lacrimal; man, mandible; mx, maxilla;?n, nasal; na, nares; orb, orbit; ?p, ?parietal; pm, premaxilla; ?posf, ?postfrontal; ?post, ?postorbital; pref, prefrontal; sq, squamosal; ?sur, ?surangular; t, teeth. Scalebar = 5mm.

Palate

Individual palatal elements cannot be identified from the µCT slices of TCD.T85b. The presence of a "sheet" of bone overlying the left orbit in ventral view probably represents part of the pterygoid which has been crushed and tightly appressed against the orbit margin (Fig. 6.3D). Although the exact morphology of the pterygoid cannot be ascertained it is likely that it is laterally extended because of its areal extent in ventral view. In the µCT slices at least, two denticles are present in the bone, close to the crushed right orbit. It is uncertain whether this bone is part of the pterygoid, palatine or ectopterygoid, but it does indicate the presence of denticles on at least one of the palatal elements, which is a feature typical of sauropleurines. Since no denticles are observed in the left pterygoid, it is probable that either or both the palatine and ectopterygoid bore denticles.

Mandible

The mandibles are best seen in ventral view and can be observed both in the µCT scans (fig. 6.3C,D) and on the surface of the specimen under a binocular microscope. The right mandible is slightly displaced medially and exposes the lateral surface in ventral view. The left mandible appears to be compressed into the same plane as the overlying cranial bones. Mandibles are elongate and narrow, and the right mandible appears to be slightly curved near its midpoint, making the lateral margin concave (fig. 6.3D). Posterior to the left orbit the mandible appears to expand to over twice the height of the right mandible. This area is probably the surangular, but its exact morphology is difficult to establish. The right mandible preserves both the dentary and the angular, but the posterior extent of these bones is lost due to breakage. The angular occupies about c.70% of the length of the mandible from its posterior extremity.

Dentition

Teeth are curved posteriorly and appear to be laterally flattened, though this latter feature may be a result of compression. No two teeth appear side by side in either the dentary or the maxilla and premaxilla so no estimate of total tooth count can be made.

Appendicular Skeleton

A pectoral girdle is not preserved. The left forelimb is preserved in TCD.T85a as a mould consisting of the humerus, a single zeugopod element, two metacarpals and four phalanges. The humerus has expanded proximal and distal ends, with a waisted midpoint. There is slightly more expansion on the proximal end as opposed to the distal end. The bone is relatively straight from its proximal to its distal margin. Both margins are convex. Between the humerus and the metacarpals there is a hollow elongate bone with similar width as the humerus. This is probably one of the autopod elements. Further distal are two metacarpals which are elongate bones roughly 80% the length of the humerus. Three phalanges are preserved in articulation with the metacarpals and show similar lengths. The anterior most phalange also preserves a second phalange which is half the size of all the others.

TCD.T85a originally preserved a complete left hindlimb as well as the fibula, tibia, a possible metatarsal and three phalanges of the right limb. Unfortunately, all that is now left is the femur from the right hindlimb. It is here described from the specimen itself while the rest of the limb is described from the original figured limb in Huxley and Wright (1867, pl. 21 fig. 1). Huxley's figure is the only image of the specimen, prior to it being damaged, known to the author. The femur is expanded towards its distal margin, which is at least twice as wide as the shaft. The distal margin is oriented at about 90° degrees to the long axis of the shaft. This changes to approximately 60° posteriorly. The proximal end does not show a similar expansion and has a curved proximal margin. The tibia is tentatively interpreted as the more anterior of the two preserved zeugopod elements. It is approximately half the size of the femur with slightly concave distal and proximal margins, both oriented at about 80° to the long axis of the shaft. The proximal margin is rotated clockwise, while the distal margin is rotated anticlockwise. The fibula has a narrower shaft than the tibia but has a similar length. The distal and proximal margins are oriented at approximately 80-70° to the long axis. There is no evidence of ossified tarsals. The phalangeal arrangement is 1-2-3-4-4 though it is worth noting that the second digit lacks a distal-most phalange with a triangular distal tip (seen in all the other digits) indicating that the distal-most phalanx may be missing. This would indicate a digit arrangement of 1-3-3-4-4.

Axial Skeleton

The detailed morphology of the vertebrae is hard to discern in TCD.85a but the figures in Huxley and Wright (1867, pl. 21 fig. 2) and Bossy and Milner (1998, fig.61G,H) appear to show holospondylus vertebrae with crenulated dorsal margins on the neural arches. Even though neural arches in the figures do not show accessory articulations characteristic of nectrideans, such articulations were almost certainly present. The transverse process of the

trunk vertebrae extend straight laterally from the centrum. Haemal arches in the caudal vertebra appear to be crenulated and have a very similar morphology to their associated neural arches (Bossy and Milner, 1998). Based on Huxley and Wright (1867, pl. 21 fig. 1) there were 19 precaudal vertebrae and between 33 and 35 caudal vertebrae (Fig 6.1). Ribs are short and curve posteriorly. It is uncertain if this is genuine curvature or the result of compaction. Ribs appear to be absent from the first to the cervical vertebrae.

Scalation

A collection of variably articulated scales ranging in shape from elongate rectangles to circular occur on the lateral margin of the right side of the body. Scales appear to have a slightly raised ridge along their peripheral margins.

Subfamily UROCORDYLINAE Bossy and Milner, 1998

Diagnosis— (Adapted from Bossy and Milner, 1998). Urocordylid nectrideans with a broad blunt snout. Frontals paired. Two to three pairs of accessory apophyses between the neural arches. Tail very deep and roughly two-thirds the length of the precaudal region. Caudal vertebrae bearing haemal spines lack ribs. Interclavicle round to rhombic.

Genus *UROCORDYLUS* Huxley *in* Wright and Huxley, 1866

Type Species— *Urocordylus wandesfordii* Huxley *in* Wright and Huxley, 1866

Diagnosis— Broad snouted urocordylid. Jugal-lacrimal contact. Nares placed laterally relative to the frontals. Parietals joined by interdigitating sutures with frontals anteriorly. Trunk vertebrae with only one additional accessory articulation. Caudal vertebrae with neural spines and haemal spines making up 36% and 34% of the vertebral centrum height, respectively. Caudal region contains 81 caudal vertebrae. Ribs double-headed. Ventral osteoderms interlock in a chevron pattern and cover the trunk region.

UROCORDYLUS WANDESFORDII Huxley *in* Wright and Huxley, 1866

(Figs 6.4-6.10)

Diagnosis— Same as for genus.

v 1866 *Urocordylus wandesfordii* Huxley *in* Wright and Huxley, 1866: p.167.

v 1867 *Urocordylus wandesfordii* Huxley *in* Huxley and Wright, 1867: p.359, pl. 20. fig. 1.

1998 *Urocordylus wandesfordii* Huxley Bossy and Milner *in* Carroll, Bossy, Milner, Andrews and Wellstead, 1998: p. 121.

Holotype—TCD.T83 (Figured in Huxley and Wright, 1867, pl. 20, fig. 1.). Counterpart of holotype is MCZ 2189.

Type Locality—Clogh, County Kilkenny, Ireland.

Type Horizon—Jarrow (No. 4) Coal Seam, Coolbaun Coal Formation, Langsettian: Pennsylvanian.

Description

The cranium and trunk region of *Urocordylus wandesfordii* is described principally from NMI.F14716 and TCD.38354 with information on the caudal region based on TCD.T83 and TCD.38354. NMI.F14716 preserves a specimen of *U. wandesfordii* in dorsal view (Fig. 6.4) with an articulated trunk region including the pectoral region. The cranium is articulated to the trunk. However, several cranial elements are disarticulated and displaced around the cranium. Two caudal vertebrae are also displaced anteriorly to the cranium and five articulated caudal vertebrae are followed by four disarticulated caudal vertebrae. TCD.38354 preserves a less mature individual that is completely disarticulated, with several caudal and trunk vertebrae and disarticulated cranial and mandible elements. TCD.T83, the holotype of *U. wandesfordii* (part of the holotype figured by Huxley and Wright, 1867, pl. 20. fig. 1), is a mould of the partially disarticulated cranium and the body fossil of the partially disarticulated trunk region. Posterior to the trunk there is a complete row of articulated caudal vertebrae.

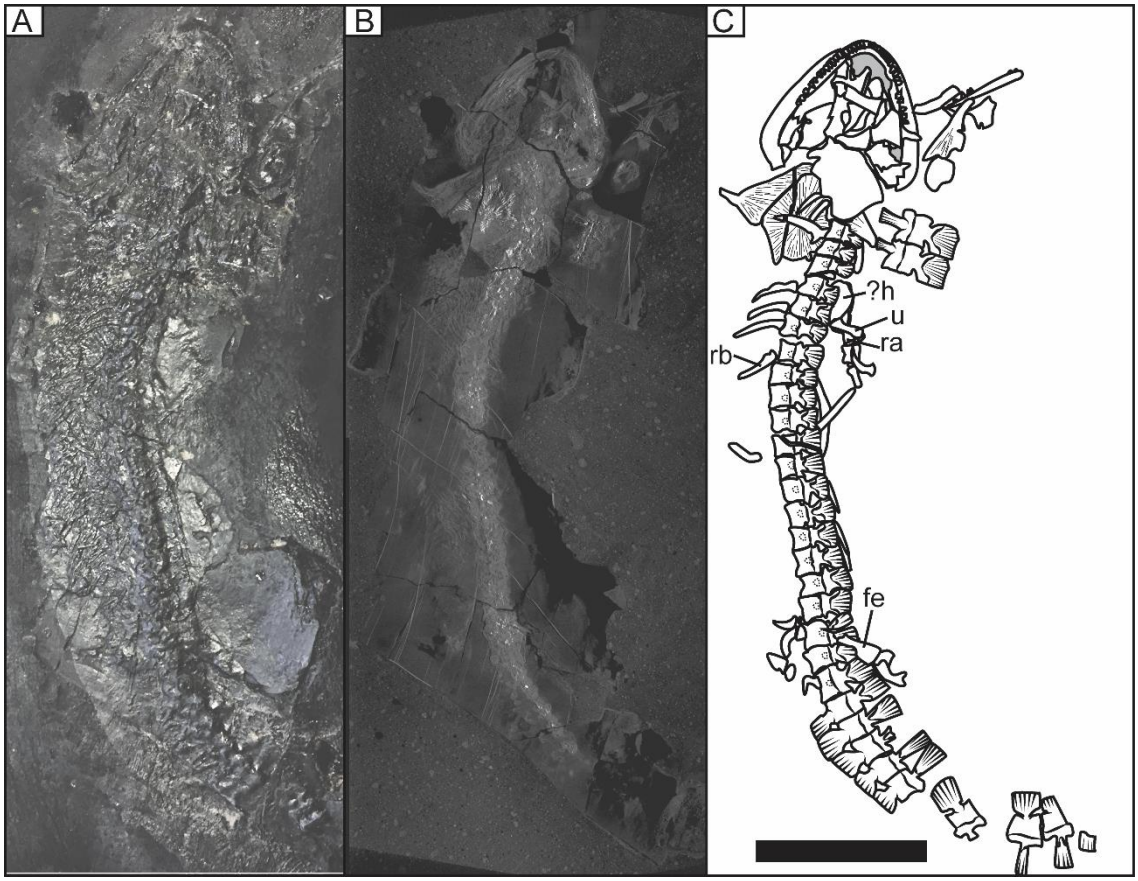

Figure 6.4. NMI.F14716 *Urocordylus wandesfordii* showing (A), specimen in dorsal view, (B), µCT slice and (C), sketch of specimen. Abbreviations: fe, femur; ?h, humerus; ra, radius; rb, rib; u, ulna. Scalebar = 40 mm

Cranium

In NMI.F14716, the boundary between the maxilla and the premaxilla cannot be seen (Fig. 6.5). The maxilla extends posteriorly to at least just over half the length of the mandible and possibly even further because the dentary of both mandibles preserves two to three teeth posterior of the termination of the maxilla. The premaxilla/maxilla preserved between the two mandibles shows no teeth. A displaced part of a maxilla, lateral to the right of the skull, is approximately half of the length of the mandibles. The displaced maxilla tapers towards one end suggesting this may be the posterior direction. Six teeth are preserved in the mandible, a single pair anteriorly and four tightly packed teeth posteriorly. Medial to the left maxilla is an articulated triangular lacrimal, with a break going through it. It appears that the lacrimal makes up at least the ventral half of the anterior orbital margin. No detail of the morphology of the nares can be seen in NMI.F14716. The lacrimal is in contact posteriorly with an anterior extension of the jugal (Fig. 6.5). This contact excludes the maxilla from part of the margin of the orbit. The jugal forms the ventral and postero-ventral margin of the orbit, where it reaches its greatest depth, and tapers posteriorly. At its dorso-ventral thickest section it bears a ventral

groove from its dorsal margin. This is to accommodate the posterior extension of the postorbital. The jugal contacts the quadratojugal with an interdigating boundary, approximately 60% of the skull length from the posterior end. It is as dorso-ventrally thick as the posterior extension of the jugal. Medial of the jugal and quadratojugal is the squamosal, which extends as far anteriorly as the dorsal extension of the jugal and as far posteriorly as the posterior margin of the quadratojugal.

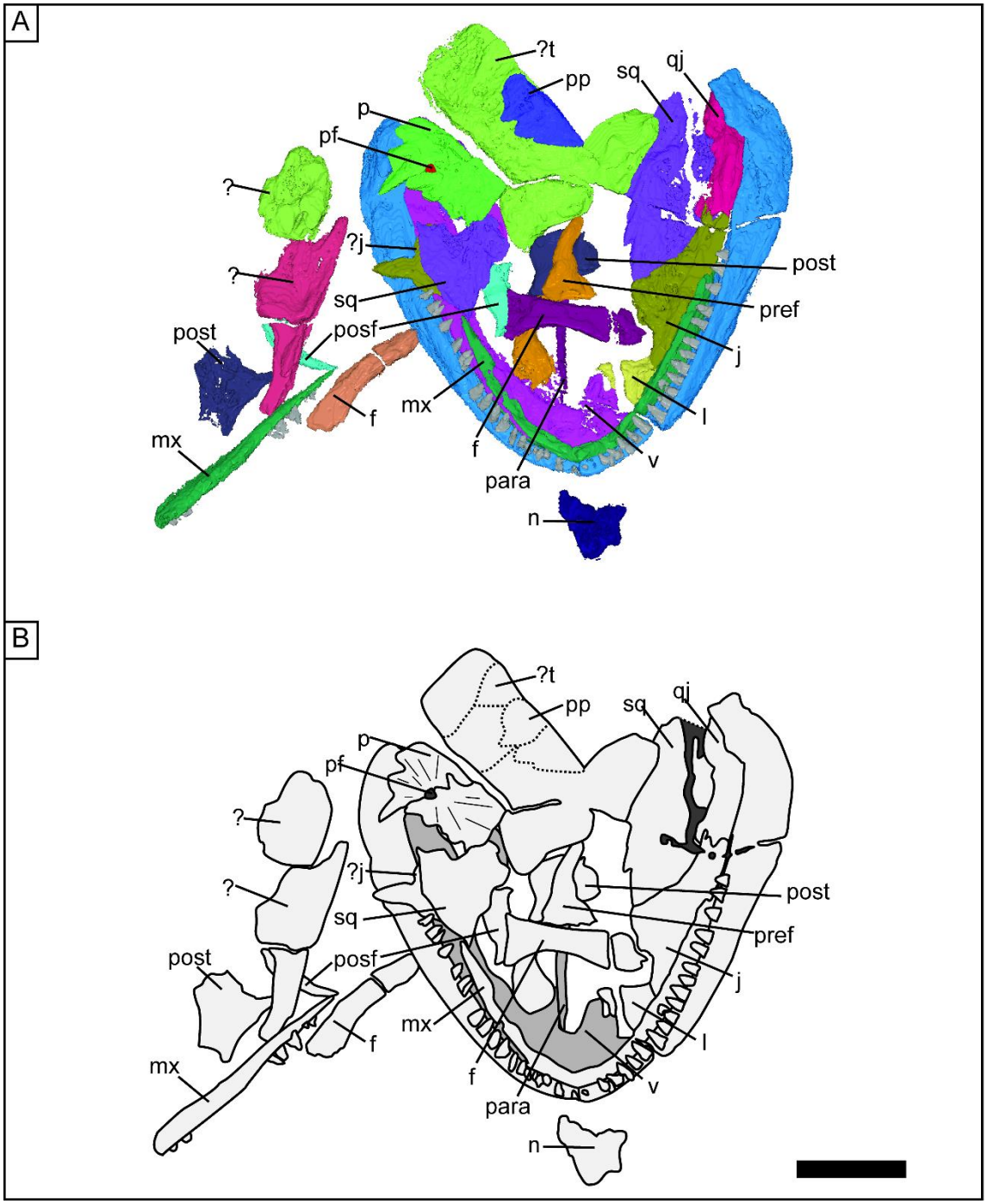

Figure 6.5. Skull of NMI.F14716 *Urocordylus wandesfordii* in dorsal view showing (A), 3D rendering and (B), sketch. Abbreviations: ?, unidentified bone; f, frontal; ?f, ?frontal; j, jugal; ?j, jugal?; l, lacrimal; mx, maxilla; n, nasal; p, parietal; para, parasphenoid; pf, parietal foramen; posf, postfrontal; post, postorbital; pp, postparietal; pref, prefrontal; qj, quadratojugal; sq, squamosal; ?t, tabular; v, vomer. Scalebar = 10mm.

The squamosal contacts a cluster of unidentified bones medially which form the midline elements of the posterior skull table (Fig. 6.5). Two triangular bones along the posterior margin of this cluster are identified as paired postparietals. Postero-lateral of the right postparietal there is another raised triangular bone, probably a tabular. Antero-lateral to the right of this cluster, and separated by a fracture, are two paired parietals with a pineal foramen

near their anterior margin. Both parietals have interdigating sutures with one another and along their anterior margin although no bone is in contact with them anteriorly. The right parietal has a long anterior extension from its anterior margin. Between the separated parietals and the postparietals is the posterior extremity of the parietals, which contacts the postparietals along a slight interdigating suture. This is typical of the parietal morphology of urocordylids which show a greater degree of extension posterior of the pineal foramen (Bossy and Milner, 1998). It is likely that the supratemporals are also present but no confident identification could be made. All known nectrideans have a parietal-tabular contact, while the supratemporal and tabular both contact the cheek region in urocordylids (with the exception of *P. marshii*) (Milner, 1980, Bossy and Milner, 1998). Therefore, a supratemporal could be inferred as lying directly anterior of the tabular. It is possible, but speculative, that it would be a long element because of the need to accommodate a parietal-tabular contact. Two disarticulated postparietals are present in TCD.38354 (Fig. 6.6A, B). Both are relatively small with triangular shapes matching the morphology in NMI.F14716. It is unlikely that they are tabulars as they lack the ventral rounded articular site for the opisthotic, characteristic of nectrideans (Bossy and Milner, 1998).

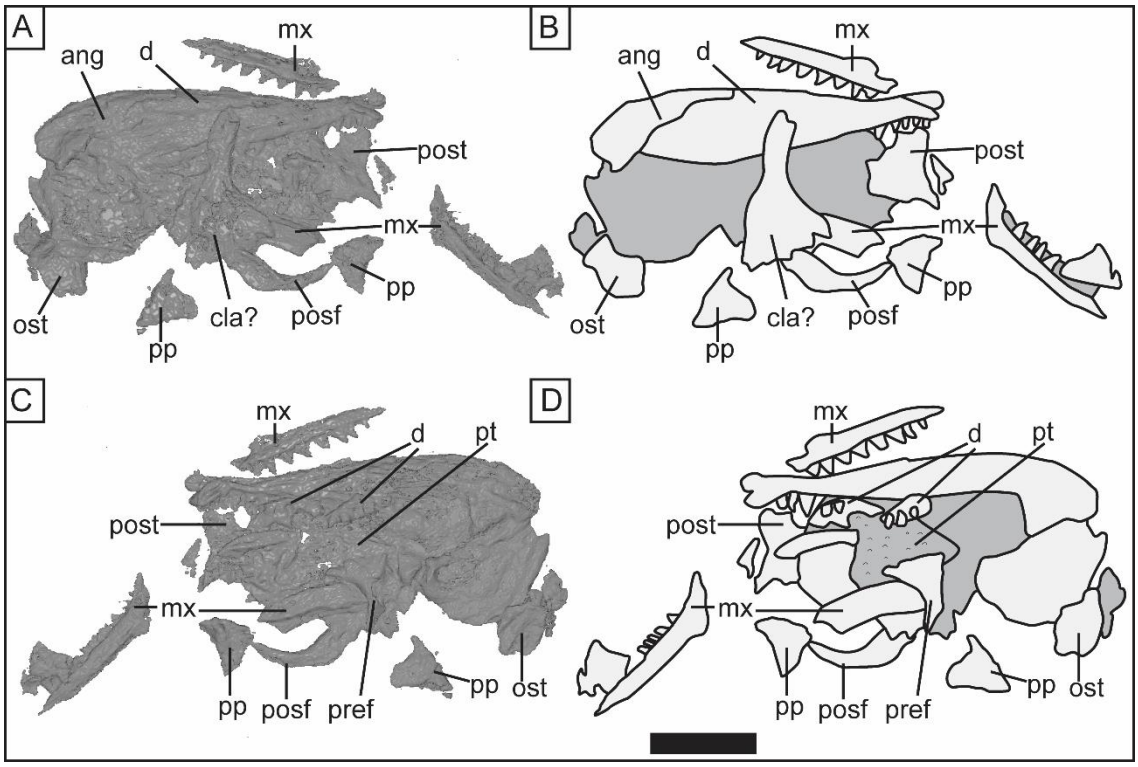

Figure 6.6. TCD.38354 *Urocordylus wandesfordii* showing (A), 3D rendering of exposed surface, (B), sketch of exposed surface, (C), 3D rendering of underside and (D), sketch of underside. Abbreviations: ang, angular; cla? ?clavicle; d, dentary; mx, maxilla; ost, osteoderm; posf, postfrontal; post, postorbital; pp, postparietal; pt, pterygoid. Scalebar = 5mm.

Anterior to the cranium is an unidentified bone (Fig. 6.5). Lateral to the right mandible are disarticulated elements including the maxilla mentioned above. The posterior most element is unidentified and has been highly altered by pyrite. Anterior to this is a bone composed of a long shaft which expands posteriorly into a blade. The blade expands posterior-laterally from the shaft and terminates in a W-shaped antero-posterior margin. Again, the identity of this bone is uncertain. It may be a clavicle or a tabular of *Keraterpeton galvani* (Milner, 2019). The shaft is separated from the blade by a fracture through the specimen. This bone covers an element identified here as the postfrontal. A second postfrontal is identified between the mandibles. The postfrontal are crescentic with smooth lateral and medial margins. Similar postfrontals are seen in TCD.38354 (Fig. 6.6). They expand slightly towards their putative posterior extremity. Lateral to the postfrontal covered by the putative *K. galvani* bone in NMI.F14716 is a roughly triangular element with a smooth lateral border (Fig. 6.5). This triangular bone has an antero-posterior most extent along its lateral border and has a medial process. This element is identified as the postorbital, with the medial process being the dorsal postorbital process that fits into the ventral groove of the jugal. This is typical of the morphology of the postorbitals in nectrideans (Bossy and Milner, 1998). A second postorbital is seen towards the centre of the cranium under a prefrontal. Medial to the maxilla is a slightly curved element here considered to be the frontal. Two disarticulated prefrontals are present in the cranium. Both are curved with an expanded triangular base towards the possible anterior end. This triangular base probably accommodates part of the lacrimal, a common feature in nectrideans (Bossy and Milner, 1998). Directly anterior to the cranium is an isolated triangular bone here identified as a single nasal (Fig. 6.5). This bone has a similar morphology to the nasals of the Urocordylinae *Ptyonius marshii* (Bossy and Milner, 1998).

Palatal Elements

Part of the left vomer is preserved antero-medial to the lacrimal in NMI.F14716 (Fig. 6.7). It preserves four denticles in a row. Medial to the vomer there is a long splint-like bone which is oriented antero-posteriorly and extends from the anterior-most margin to the midpoint of the cranium. This is probably the cultriform process of the parasphenoid, which has been displaced anteriorly. Below the right maxilla in NMI.F14716, the palatine is preserved (Fig. 6.7). The geometry of the suture between the palatine and the vomer is not clear. The posterior suture between the palatine and the pterygoid is also not clear. Part of the posterior-lateral extension of the pterygoid is seen on the left side of NMI.F14716. Here the pterygoid extends and contacts the articulation zone of the left mandible. It is likely that the quadrate is also preserved but the distinction between the two cannot be made confidently. Lateral to the

pterygoid is an opening, possibly representing part of a compressed interpterygoid vacuity. Part of the pterygoid is also preserved in TCD. 38354 showing a tuberculated ventral surface with unorganised denticles.

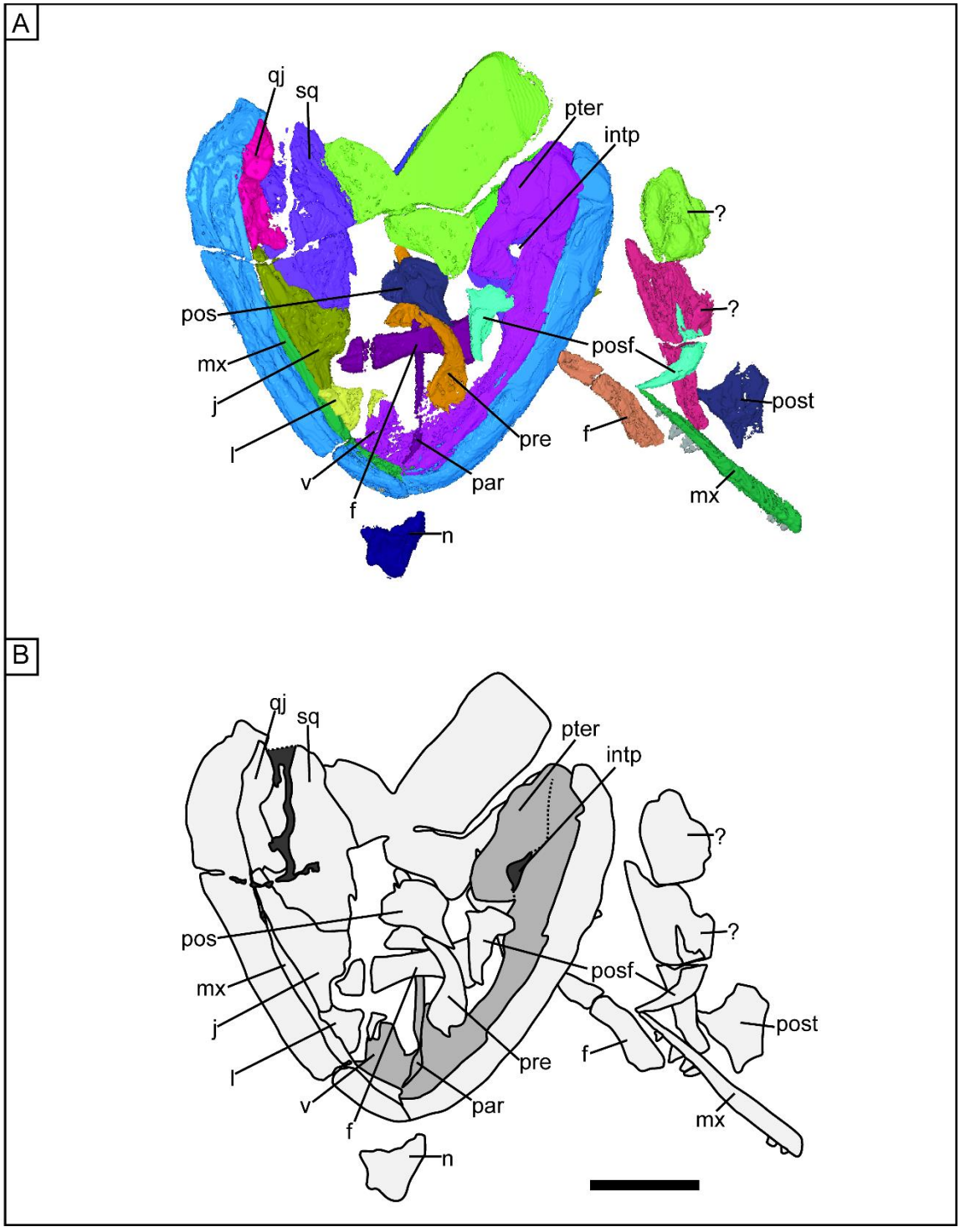

Figure 6.7. Skull of NMI.F14716 *Urocordylus wandesfordii* in ventral view showing (A), 3D rendering and (B), sketch. Abbreviations: ?, unidentified bone; f, frontal; ?f, ?frontal j, jugal; ?j, jugal?; l, lacrimal; mx, maxilla; n, nasal; para, parasphenoid; posf, postfrontal; post, postorbital; pref, prefrontal; qj, quadratojugal; sq, squamosal; v, vomer. Scalebar = 10mm.

Mandibles

Both mandibles are preserved in articulation in NMI.F14716. They are “hockey-stick shaped” with a dorsally extending posterior end (Fig. 6.8). A sub-rectangular retroarticular process is positioned posterior of the articular. Anterior of the zone of articulation the dorsal margin is concave in both the left and right mandible, but this may be the result of post-mortem compression. In the left mandible, the surangular occurs as a posterodorsal extension on the lateral side. It contacts the dentary dorsally which makes up 85% of the dorsal margin of the mandible. The dentary on the right mandible houses 20 teeth while that on the left mandible houses 17. The angular makes up the posterior and the posteroventral margin of the mandible. It extends anteriorly for about 52% of the length of the mandible and contacts the dentary anterodorsally. The dentary of the left mandible is incomplete anteriorly in NMI.F14716. The splenial is exposed on the lateral side of the jaw, anterior to the angular. The medial side is best observed in the left mandible of NMI.F14716. The angular is exposed on the medial side and makes up the postero-dorsal bone. The boundary between it and the articular cannot be discerned. The anterior extent of the angular is also difficult to discern. It appears to bifurcate, with the dorsal anterior process contacting the dentary and the anteroventral process contacting the splenial. The prearticular forms an elongated thin bone which partially overlies the anteroventral process of the angular medially and extends anterodorsally along the dorsal margin of the splenial to contact the dentary anteriorly. Anterior to this, the splenial makes up the ventral margin of the mandible while the dentary makes up the dorsal margin. Both bones participate in the symphysis.

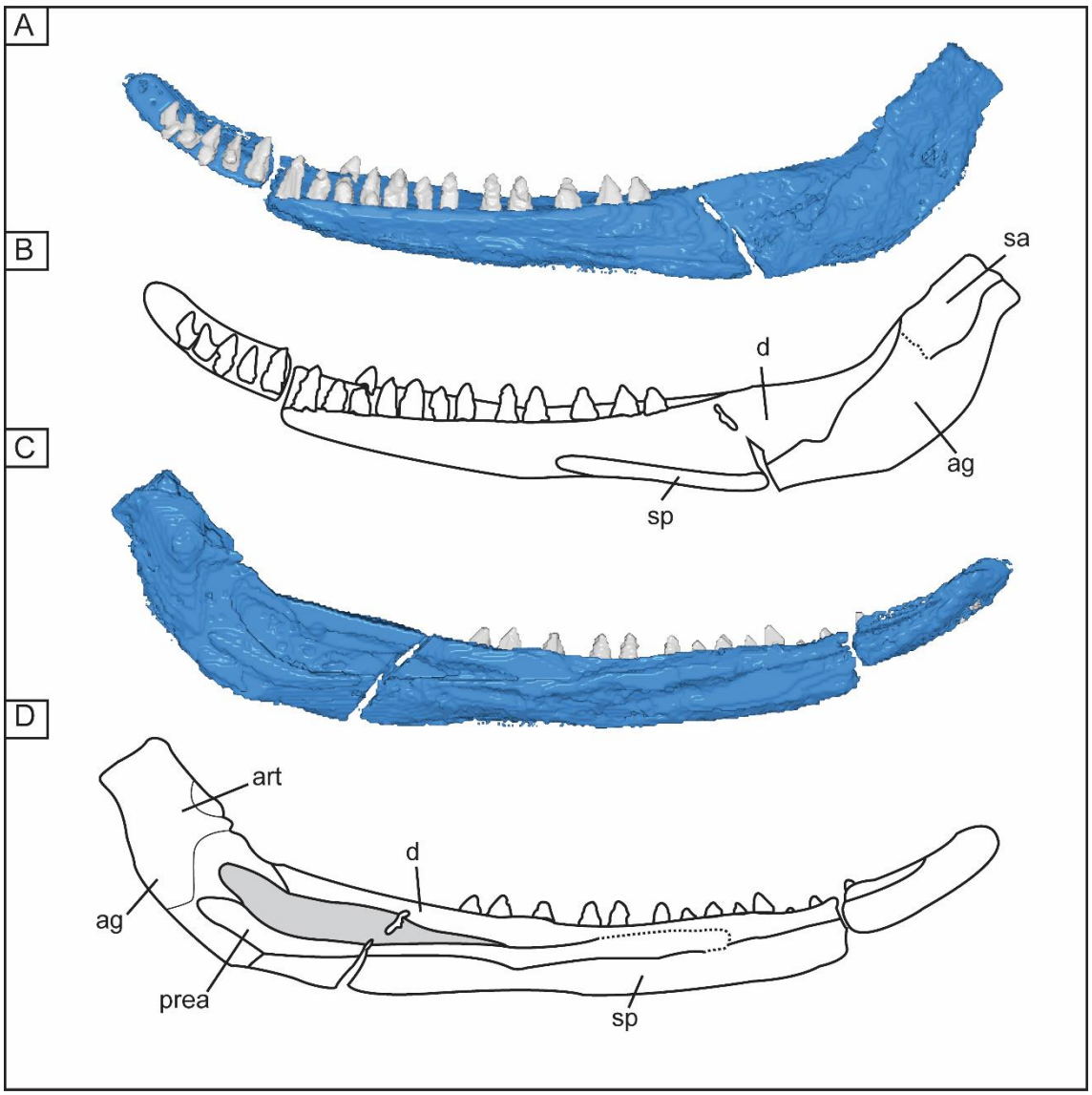

Figure 6.8. Left mandible of NMI.F14716 *Urocordylus wandesfordii* showing (A), 3D rendering in lateral view, (B), sketch in lateral view, (C), 3D rendering in medial view, (D), sketch in medial view. Abbreviations are: ag, angular; art, articular; d, dentary; pre, prearticular; sa, surangular; sp, splenial. Scalebar = 10mm.

Appendicular skeleton.

An interclavicle, two clavicles and a single cleithrum are preserved in NMI.F14716 (Fig. 6.9). The interclavicle is a roughly diamond-shaped thin blade with an anterior-posterior long axis. It is laterally thickest at 40% along its anterior-posterior length. The ventral surface of the interclavicle is sculptured with grooves and ridges that radiate out from the midpoint centre of ossification of the laterally thick area. The right clavicle in NMI.F14716 is incompletely preserved. The left clavicle is fully preserved. The clavicle is composed of a dorsal stem and a ventral blade. The blade expands ventro-medially from the stem. The blade of the clavicle is just short of the length of the interclavicle. The blade is sculptured similarly to

the interclavicle with groves and ridges radiating from the base of the stem. The stem lacks this ornamentation. It extends dorsally with a circular cross-section. The stem is at a 60° angle to the blade, although this may not represent the original orientation of the blade. The cleithrum is a curved elongated element that tapers ventrally to a point. Dorsally, the stem is occupied by a small anterior-posterior expansion. The stem shows dorso-ventrally oriented grooves.

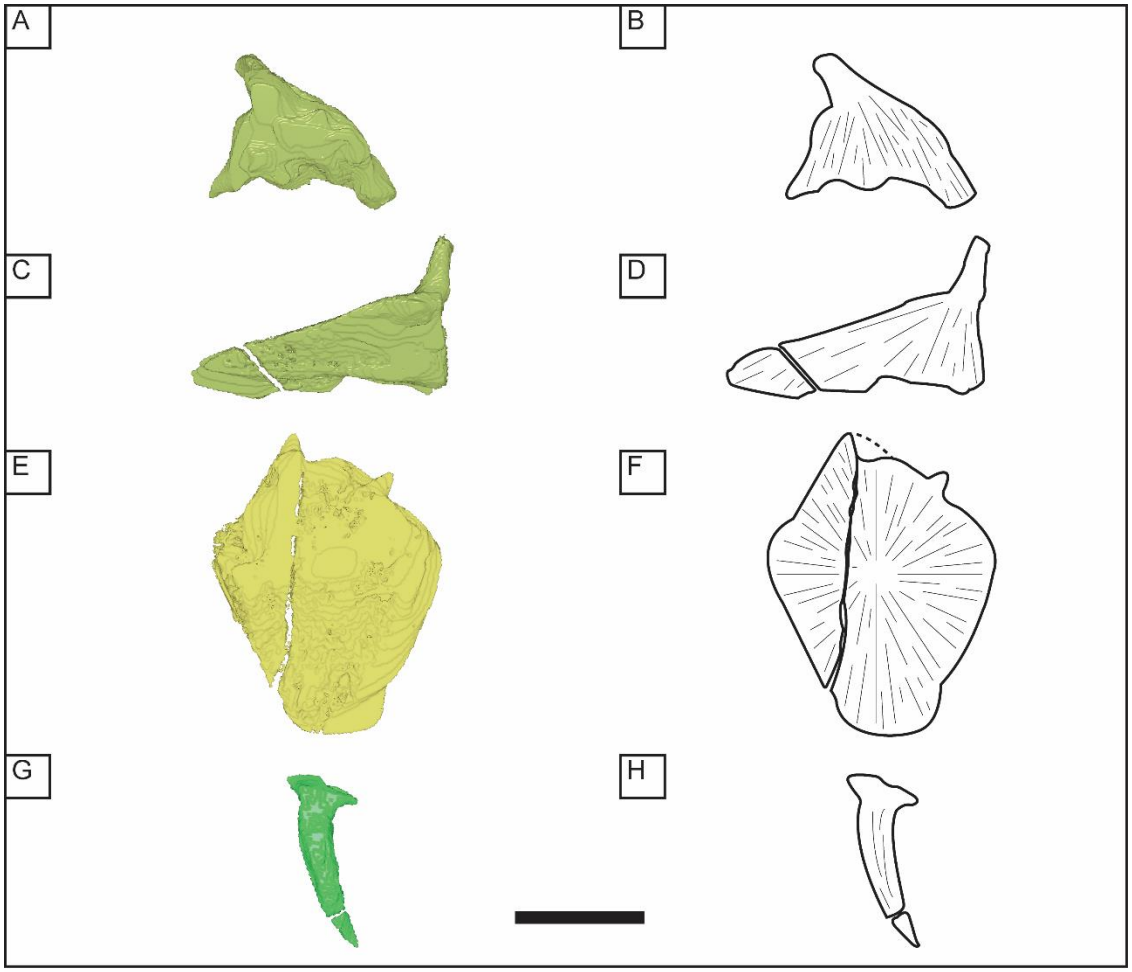

Figure 6.9. Shoulder girdle elements of NMI.F14716 *Urocordylus wandesfordii* the right clavicle as (A), 3D rendering, (B), sketch both in dorsal view, the left clavicle as (C), 3D rendering, (D), sketch both in dorso-lateral view, the interclavicle as (E), 3D rendering, (F), sketch, both in ventral view and the cleithrum as (G), 3D rendering, (H), sketch both in lateral view. Scalebar = 10 mm.

A single humerus is preserved on the right side of NMI.F14716, but part of it cannot be distinguished from the adjacent vertebrae (Fig. 6.4C). Bossy and Milner (1998, p. 97) described the humerus as having a "semi-lunar shaft" with the humerus head having a "rather thin, curved surface, the plane of which is twisted only slightly relative to that of the distal end". Lateral to the humerus in NMI.F14716 there is an ulna and radius which overlay one another in a cross pattern (Fig. 6.4C). The ulna and radius have similar lengths and are roughly 60% of the length of the humerus. The ulna shows similar-sized expansions proximally and distally. The margin

of the proximal end is straight and oriented at approximately 80° to the long axis of the shaft. The border of the distal end has a convex margin and is oriented at angle of 90° to the shaft. The shaft of the ulna is flattened, though it is unclear whether this a result of compression. The radius has a similar shaft width to the ulna. It also shows similar proximal extremities, with the proximal margin being flat and at a 90° angle to the shaft length. The distal margin of the radius is one and half times larger than the proximal margin and is oriented at 90° to the shaft length. The distal margin is concave. Distal of the ulna and radius, three metacarpals and two phalanges are preserved. A complete autopod is not preserved in either NMI.F14716, TCD. 38354 or in TCD.T83. An inferred phalangeal formula of 2-3-4-3-2 was reported by Bossy and Milner (1998) based on the holotype TCD.T83 and its counterpart MCZ 2189.

Likewise, no pectoral elements are present in NMI.F14716, TCD. 38354 or in TCD.T83. Bossy and Milner (1998) reported a pectoral girdle with a unipartite ilium, a sub-circular pubis and posteriorly elongated ischium with the acetabular region spreading straddling the three bones. The femur is slightly longer than the humerus. It has a relatively narrower shaft with expanded distal and proximal ends. The proximal and distal margins are straight and oriented at 80° and 90° to the shaft. Only the proximal half of the tibia is preserved in NMI.F14716. The tibia and fibula are preserved as impressions in TCD.T83. The distal margin of the tibia is half as wide as the proximal margin. The fibula shows similar lengths with proximal and distal margins approximately 90° to the shaft. TCD.T83 has a phalangeal formula of at least 2-2-2-1. Only the anterior (first number) digit preserves a distal triangular phalange indicating it preserves the whole digit. An inferred autopod arrangement of 2-3-4-4-2 was reported by Bossy and Milner (1998).

Axial Skeleton

Urocordylus wandesfordii has approximately 102 vertebrae; 20 presacral, one sacral and 81 caudal. Vertebrae are holospondylus with the neural arch fused to the centrum. Centra appear square in lateral view with laterally bulbous ridges extending dorso-posteriorly, ventro-posteriorly and ventro-anteriorly (Fig. 6.10B-E). These ridges form two crescentic depression on the posterior end and along the ventral margin of the centra. There is a groove between the neural arch of the caudal vertebrae in TCD. 38354 (Fig. 6.10B, C). The neural arch is just over 20% the height of the centrum (excluding the neural spine). It extends further laterally than the centrum and has an anterior projection which extends beyond the centrum and houses the anterior zygapophyses and a secondary articulation called the zygantrum. The posterior end of the neural arch extends no further than the posterior most extension of the centrum. The detail of the articulation surfaces of the anterior and posterior zygapophyses are difficult to discern. A

posterior projection of the neural arch here probably represents the zygosphene. The neural arch of the trunk and sacral vertebrae occupies 77% of the anterior-posterior length of the centrum and expands to cover this entire length dorsally. This narrows in caudal vertebrae where it makes up 45% at the base and 75% dorsally. The neural arch makes up 30% of the dorsal-ventral height of the trunk and sacral vertebrae and 34% of that of the caudal vertebrae. Neural arches are crenulated along their dorsal margins with "grooves" extending ventrally over more than half the length of the neural arch. The transverse process originates from the midpoint of the lateral surface of the centrum in the trunk and sacral vertebrae. It extends laterally from the centrum at c.90° and is thickest at its point of origin on the centrum. Well-developed haemal arches and spines appear on the third caudal vertebrae. Haemal arches are approximately 60% the height of their associated vertebrae. Ventrally the haemal spine forms a "fan" spanning the anterior-posterior length of the centrum. It has a thickened anterior and posterior margin which extends the height of the spine. It is crenulated in the same fashion as the neural arches with grooves running dorsally from the ventral margin. Haemal spines appear to overlap in many causes, suggesting that there was probably a degree of articulation between the haemal spine of one vertebra and the preceding vertebra. By the 37th caudal vertebra the haemal and neural spines begin to narrow antero-posteriorly. The crenulated pattern is lost in the neural spine from caudal vertebra 44 and in the haemal spine from caudal vertebra 50. By caudal vertebra 65 neural and haemal arches are absent and the rest of the vertebral column is composed of cylindric centra which diminish in length posteriorly.

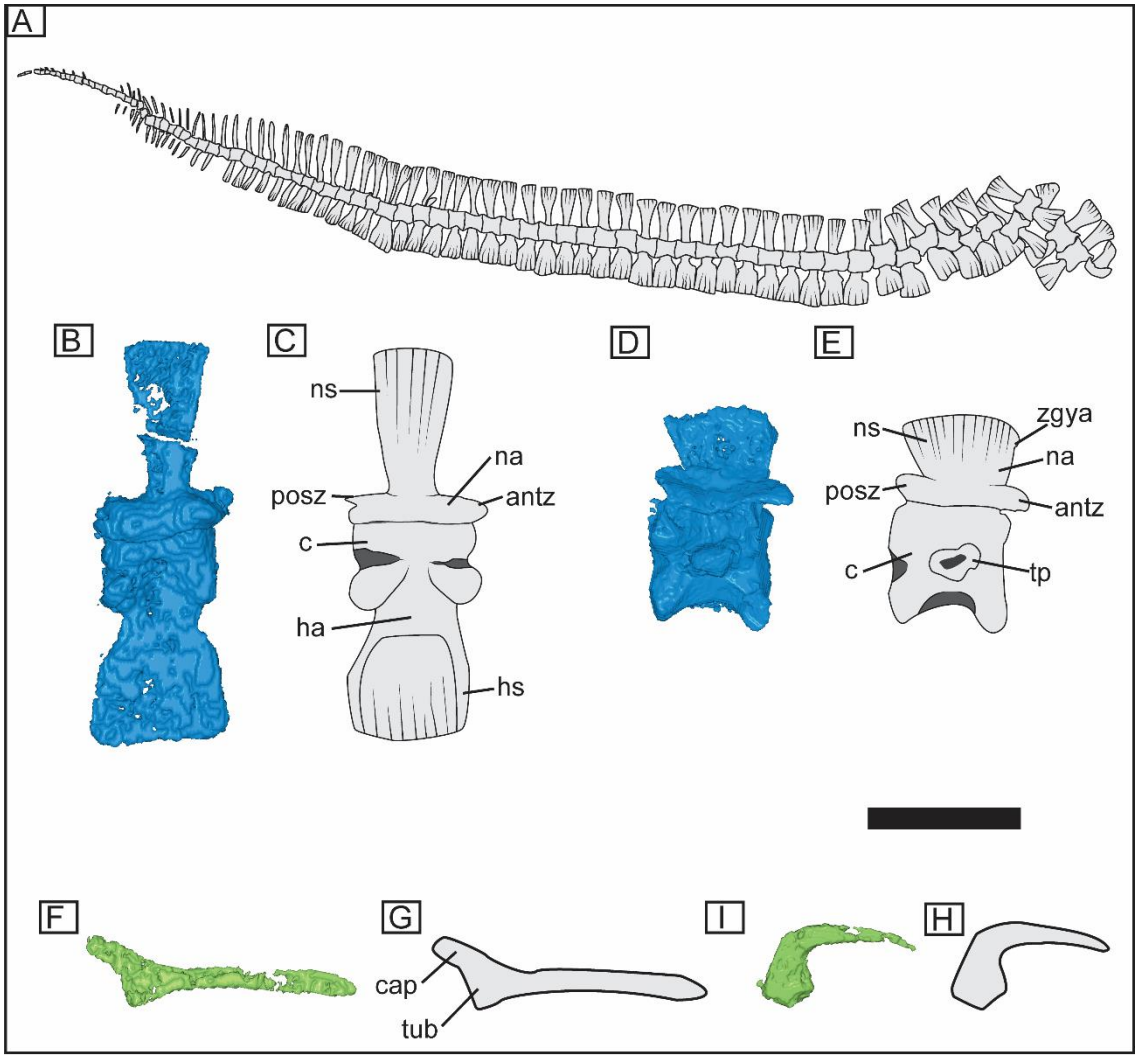

Figure 6.10. showing (A), the caudal section of TCD.T83 *Urocordylus wandesfordii* in lateral view, and (B-H), the parts of the axial skeleton of TCD.38354 *Urocordylus wandesfordii* including an anterior caudal vertebra (B), 3D rendering and (C), sketch, both in lateral view; a trunk vertebra (D), 3D rendering and (E), sketch, both in lateral view; an anterior trunk rib (F), 3D rendering and (G), sketch; and a sacral rib (I), 3D rendering and (H), sketch. Abbreviations: antz, anterior zygapophyses; c, centrum; cap, capitulum; ha, haemal arch; hs, haemal spine; na, neural arch; ns, neural spine; posz, posterior zygapophyses; tp, transverse process; tub, tuberculum; zgya, zygosphene. Scale bar = 40mm for A and 5mm for B-H.

Trunk ribs are double-headed with both a capitulum and tuberculum. The tuberculum articulates with the transverse process of a single centrum. It is not clear whether the capitulum is free or whether it articulates with the preceding centrum. In TCD. 38354 the capitulum does not extend as far as the preceding centrum, so this is unlikely. However, this specimen represents an immature condition. Ribs are the length of three centra. The capitulum and tuberculum approach each other on proceeding ribs posteriorly. Sacral and caudal ribs are single-headed and L-shaped.

Scalation

The trunk of NMI.F14716 shows a complete set of ventral gastralia from the pectoral girdle posterior to the pelvic girdle. Gastralia are as long as the centra and tightly interlocked in a chevron pattern. A single osteoderm is preserved in TCD. 38354.

6.4 Discussion

6.4.1 Comparative anatomy

The cranium of *Lepterpeton dobbsii* is characteristic of the sauropleurines with an elongated snout, formed by the extension of the premaxilla and nasal, nares directly anterior to the orbit and the ventral orbital margin made up of the maxilla. Other expected shared characters, including a fused frontal (see description) are hard to make out. An elongated snout could be considered to be the plesiomorphic condition within sauropleurines given its presence in *L. dobbsii*, *Sauropleura scalaris* (Bossy and Milner, 1998), *Crossotelos annulatus* (Bossy and Milner, 1998), and *Montcellia longicaudata* (Gand *et al.*, 2012). Such extensive elongation is not seen in *S. scalaris*, though it has more anterior extension than that in the urocordylines.

The caudal vertebrae of the sauropleurines show disparate morphologies. The anterior caudal vertebrae of *S. pectinata* (Bossy and Milner, 1998, fig. 61F) are similar to the caudal vertebrae of the urocordyline *Urocordylus wandesfordii* with a height of c.17mm in the former and c.22mm in the latter. *S. pectinata* and *U. wandesfordii* have similar thin caudal neural spines which expand anterio-posteriorly dorsally and haemal spines longer than the haemal arches. In fact, the caudal vertebrae of *S. pectinata* are more similar to the caudal vertebrae of *U. wandesfordii* than the caudal vertebrae of the other two urocordylines are to those of *U. wandesfordii*. Both *Ctenerpeton remex* and *Ptyonius marshii* have longer haemal arches relative to the haemal spines. The neural spine of *P. marshii* has a smaller dorsal neural spine extension relative to both *U. wandesfordii* and *S. pectinata*. Because of the destruction of the caudal section in the holotype of *L. dobbsii* TCD.T85a, it is impossible to interpret the detailed morphology of the caudal vertebrae. An anterior caudal vertebra was figured in Bossy and Milner (1998, figure 61H) and is probably described from Bossy, (1976), whose thesis was completed after the pyrite destruction of TCD.83a as indicated by the presence of a latex peel showing the caudal region missing. It is possible that the figured vertebra was from a second specimen of *L. dobbsii* (MCZ 2193), though this specimen could not be located by the author during a trip to the MCZ. Based on the figures of Bossy and Milner (1998, figure 61H) and Huxley and Wright (1867, plate 21, figure 1-2) the neural and haemal spines do not resemble

the dorso-ventral elongated morphologies in *S. pectinata* and the urocordylines, which have a height of c.3mm and both neural and haemal spines of similar morphology. Shorter caudal vertebrae are also seen in *M. longicaudata* (Gand *et al*., 2012, figure 22).

L. dobbsii is the stratigraphically oldest sauropleurine, being Langsettian in age. *Sauropleura* spp. range from Asturian to Lower Permian, and *M. longicaudata* is Stephanianin age and *C. annulatus* Lower Permian. Despite being the older, *L. dobbsii* may not represent the plesiomorphic condition for the sauropleurines. The shortened snout of *Sauropleura scalaris* and the *Urocordylus*-like caudal vertebra in *Sauropleura* suggest a closer affinity between *Sauropleura* and the urocordylines than with any other of the sauropleurines. This is probably the result of one of two scenarios. The first is that *L. dobbsii* does represent the basal condition in sauropleurines and that similarities between *Sauropleura* and the urocordylines result from convergence; the second is that *Sauropleura* is actually representative of the basal condition of sauropleurines and that snout elongation and shortening of the caudal vertebrae represents derived states. This latter scenario would give rise to a ghost lineage spanning at least from the Langsettian to the Asurian of more basal sauropleurines. This scenario would agree with the hypothesis that *U. wandesfordii* represents a more primitive nectridean than *L. dobbsii* (Bossy and Milner, 1998). Neither scenario can be tested until a phylogenetic analysis is carried out on inter-nectridean relationships.

The urocordylids retain the largest number of cranial elements, with the diplocaulids lacking supratemporals and the scincosaurids being the most derived forms with cranial anatomy lacking supratemporals and postparietals. This is in contrast to the interpretation of Bossy and Milner (1998) who indicated that the vertebral column of scincosaurids is representative of basal nectrideans having transverse processes placed anteriorly along their centrum, similar to stem-amniotes. This in turn is not supported by the late appearance of the scincosaurids (Asturian), though this could be a result of terrestrial organism preserving less frequently than aquatic ones. If *U. wandesfordii* is representative of the basal condition of nectrideans, this would indicate that territorialisation evolved independently in nectrideans. It is thought that the nectrideans were secondarily aquatic (Bossy and Milner, 1998), despite many early limbed Pennsylvanian tetrapods, including nectrideans, retaining aquatic adaptions.

6.5 Conclusion

Lepterpeton dobbsii and *Urocordylus wandesfordii* are two of the three nectrideans originally described by Huxley in Huxley and Wright (1867). They were the first members of the clade to be described and also mark the first appearance of nectrideans in the geological record. Relative to the third nectridean from the assemblage *Keraterpeton galvani*, they have

remained understudied until now. µCT has been used here to document previously unobservable cranial and palatal features. The skull of TCD.T85b (*L. dobbsii*) is articulated but is highly pyritised, resulting in poor µCT images rendition. Despite this, the orbital and upper jaw elements are described in detail. The skull of NMI.F14716 (*U wandesfordii* is) disarticulated, yet still preserves the majority of the cranial elements. The palate is not as well preserved. The braincase is not present in any of the specimens. µCT images of NMI.F14716 *U wandesfordii* has provided the description of the midline elements (nasals, frontals, parietals and postparietals). Understanding the anatomy of *L. dobbsii* and *U. wandesfordii* is important for our understanding of the origin of nectrideans and for establishing inter-nectridean relationships. *L. dobbsii* represents the first occurrence of the Sauropleurinae, while *U. wandesfordii* represents the first occurrence of the Urocordylinae.

6.6 References

BOSSY, K. V. H. 1976. Morphology, paleoecology and evolutionary relationships of the Pennsylvanian urocordylid nectrideans (Subclass, Lepospondyli, Class Amphibia). Unpublished PhD thesis, Yale University–Disertation abstracts, **37**, 2731.

— and MILNER, A. C. 1998. Order Nectridea Miall 1875. 73–131. *In* WELLNHOER (ed). *Encyclopedia of Paleoherpetology*. Verlag Dr.Friedrich Pfeil, München, 206 pp.

CLACK, J. A., RUTA, M., MILNER, A. R., MARSHALL, J. E. A., SMITHSON, T. R. and SMITHSON, K. Z. 2019. *Archerontiscus caledoniae*: the earliest heterodont and durophagous tetrapod. Rpyal Society Open Science, **6**, 182087. doi.org/10.1098/rsos.182087.

COPE, E. D. 1868. Synopsis of the extinct Batrachia of North America. *Proceedings of the Academy of Natural Science of Philadelphia*, **20**, 208–221.

ETHERIDGE, R. 1866. On the discovery of several new Labyrinthodont reptiles in the coal measures of Ireland. *Geological Magazine*, **3**, 4–5.

FRITSCH, A. 1881. *Fauna der Gaskohle und der Kalksyeine der Permformation Böhmens, Band 1. Heft 3.* Prague.

GAND, G., BOURILLOT,R., BRIGAUD, B., STEYER, J. S. AND PEYROUSE, J. B. 2012. Les Amphibiens fossiles de Bourgogne (Temnospondyles et Lissamphibiens), *Revue Scientifique Bourgogne-Nature*, **11**, 47–69.

GERMAIN, D. 2008. *Anatomie des Lépospondyles et origine des Lissamphibiens*. Muséum national d'Histoire naturelle, Paris. 244 pp.

— 2010. The Moroccan diplocaulid: the last lepospondyl, the single one on Gondwana. *Historical Biology*, **22**, 4-39.

GOODRICH, E. S. 1930. *Studies on the structure and developmetn of vertebrates*. Macmillian and Co.

HANCOCK, A. and ATTHEY, T. 1870. Description of a labyrinthodont amphibian, a new generic form, obtained in the coal-shale at Newsham, near Newcastle upon Tyne. *Annals and Magazine of Natural History*, **6**, 56–65.

HUXLEY, T. H. and WRIGHT, E. P. 1867. Royal Irish Academy On a Collection of Fossil Vertebrata , from the Jarrow Colliery, County of Kilkenny, Ireland. *Transactions of the*

Royal Irish Academy, **24**, 351–370.

MIALL, L. C. 1875. Report of the committee on the structure and classification of the labyrinthodonts. *Report of the 44th Meeting of the British Association for the Advancement of Science*, **1874**,149–92.

MILNER, A. C. 1980. A review of the Nectridea (Amphibia). 377–405. *In* PANCHEN, A. L. (ed). *The terrestrial environment and the origin of vertebrates*. Academic Press, London.

— 2019. A morphological revision of Keraterpeton, the earliest horned nectridean from the Pennsylvanian of England and Ireland. *Earth and Environmental Science Transactions of the Royal Society of Edinburgh*, **109**, 237–253. doi: 10.1017/S1755691018000579.

— and RUTA, M. 2009. A revision of *Scincosaurus* (Tetrapoda, Nectridea) from the Moscovian of Nyrany, Czech Republic, and the phylogeny and interrelationships of nectrideans. *Special Papers in Palaeontology*, **81**, 71–89.

MILNER, A. R., SMITHSON, T. R., MILNER, A. C., COATES, M. I. and ROLFE, W. D. L. 1986. The search for early tetrapods. *Modern Geology*, **10**, 1–27.

OLSSEN, E. C. 1972. *Diplocaulus parvus* n. sp. (Amphibia; Nectridea) from the Chickasha Formation (Permian; Guadalupian) of Oklahoma. *Journal of Paleontology*, **46**, 656-659

PANCHEN, A. L. and SMITHSON, T. R. 1988. The relationship of early tetrapods. 1–32. *In* BENTON, M. J. (ed). *The Phylogeney and Classification of the Tetrapods. Volume 1*. Clarendon Press, Oxford.

PARDO, J. D., SZOSTAKIWSKYJ, M. and ANDERSON, J. S. 2017. Hidden morphological diversity among early tetrapods. *Nature*, **546**, 642–645.

RINEHART, L, F. and LUCAS, S. G. 2001. A statistical analysis of a growth series of the Permian nectridean Diplocaulus magnicornis showing two-stage ontogeny. *Journal of Vertebrate Paleontology*, **21**, 803–806.

ROMER, A. S. 1930. The Pennsylvanian tetrapods of Linton, Ohio. *Bulletin of the American Museum of Natural History*, **59**, 77–147.

—1966. *Vertebrte Paleontology*. Chicago University Press, Chicago.

RUTA, M. and COATES, M. I. 2007. Dates, nodes and character conflict: addressing the lissamphibian origin problem. *Journal of Systematic Palaeontology*, **5**, 69–122.

— — and QUICKE, D. L. J. 2003. Early tetrapod relationships revisited. *Biological Reviews*, **78**, 251–345.

SUTTON, M. D., *GARWOOD, R. J., SIVETER, D. J. and SIVETER, D. J.* 2012. SPIERS and VAXML; A software toolkit for tomographic visualisation and a format for virtual specimen interchange. *Palaeontologia Electronica*, **15**, 1–14.

THOMPSON, K. S. and BOSSY, K. H. 1970. Adaptive trends and relationships in early Amphibia. *forma et functio*, **3**, 7–31.

VALLIN, G. and LAURIN, M. 2004. Cranial morphology and affinities of *Microbrachis*, and a reappraisal of the phylogeny and lifestyle of the first amphibians. *Journal of Vertebrate Paleontology*, **24**, 56–72.

WILLISON, S. W. 1909. The Skull and Extemites of Diplocaulus. *Transactions of the Kansas Academy of Science*, **22**, 122-131

WRIGHT, E. P. and HUXLEY, T. H. 1866. On a collection of fossils from the Jarrow Colliery Kilkenny, Ireland, *Geological Magazine*, **3**, 165–171.

Chapter 7: Micro-computed tomography of the holotype of *Ichthyerpeton bradleyae* (Huxley in Wright and Huxley, 1866).

7.1 Introduction

The Langsettian (Pennsylvanian) Jarrow coal seam from northern Kilkenny, Ireland preserves a diverse assemblage of plant, fish and early tetrapod fossils of enormous historical and paleontological significance. Although it was not the first of the classic Westphalian tetrapod coal assemblages to be discovered, it was the first to be described in detail, with all other assemblages such as Linton, Ohio, described with reference to it (Milner, 1980). It is also the oldest of these assemblages (Milner, 1987), and thus important for our understanding of early tetrapod evolution and ecology at the start of the Pennsylvanian.

Huxley in Huxley and Wright, (1867) made the first formal description of tetrapods from Jarrow and erected seven new species. One of these, *Ichthyerpeton bradleyae*, was described from a single specimen (TCD.T87), including the trunk, the hindlimbs and the caudal region. As is the case of some of the other seven tetrapods, *I. bradleyae* was actually briefly described and remarked upon in Etheridge (1866) and Wright and Huxley (1866) before the formal description by Huxley in Huxley and Wright (1867). As a result, the genus *Ichthyerpeton* first appeared in the literature in Etheridge (1866), despite its name being credited to Huxley by Etheridge. The original descriptions focused on the presence of "horny scales" (Etheridge, 1866), covering the body, including most of the hindlimb (Wright and Huxley, 1866), the morphology of vertebrae with discoidal centra (Huxley and Wright, 1867) and the number of digits on the manus which varied from three (Etheridge, 1866) to five (Wright and Huxley, 1866). Lydekker (1890, 1891a) regarded *Erpetocephalus rugosum* (Huxley in Huxley and Wright, 1867), which was originally described from a single cranium, to be a junior synonym of *I. bradleyae*. However, this does not seem to have been generally accepted (Milner, 1980). Lydekker (1891a) placed *I. bradleyae* in the temnospondyl family Dendrerpetontidae and identified a second species from an isolated skull and mandible, later named *Ichthyerpeton hibernicum* (Lydekker, 1891b). Lydekker (1891b) also suggested a close affinity between *I. bradleyae* and the colosteid *Pholidogaster* based on post cranial material. A third species, *Ichthyerpeton squamosum*, was described from Linton, Ohio (Moodie, 1909) and later identified as an aïstopod. Romer (1947) considered *I. bradleyae* to be an embolomere and suggested that there may be an affinity between it and the anthracosaur vertebrae material described from Jarrow (Baily, 1879, 1884). In this case, the holotype of *I. bradleyae* would

represent an immature form of an animal similar to the anthracosaur *Pteroplax*. A placement among the anthracosaurs was suggested by Panchen (1970), who noted that the long body with short hindlimbs was Anthracosaur-like. However Panchen (1970) considered *I. bradleyae* to be a *nomen vanum*. The skulls of *E. rugosum* and *I. hibernicum* were redescribed by Milner (1980), who placed them in the temnospondyl genus *Dendrerpeton* as the species *D. rugosum*. Milner (1980) indicated that, although the trunk vertebrae of *I. bradleyae* are difficult to discern, they do not appear to be embolomerous. The presence of a long presacral column and the similarity of the holotype and specimens of colosteids from Jarrow led Milner (1980) to suggest that *I. bradleyae* may be a colosteid, but he also proposed that it may be a temnospondyl. Assignment to the colosteids was also supported by Clack and Milner (2015), although this was based on additional specimens supposedly from Jarrow and not from evidence derived from the holotype.

A common characteristic of specimens of tetrapods from the Jarrow assemblage is that despite the preservation of fully to partially articulated bodies and scale/skin impressions, in detail the quality of preservation is poor. Specimens tend to be highly compressed and a layer of matrix coating them means that the boundary between bone and matrix can be difficult to discern partly because the bones are replaced to a greater or lesser degree by carbonaceous material (Chapter 3) making them chemically similar to the host rock. Manual preparation of the holotype of *I. bradleyae* TCD. T87 would have been unsatisfactory because of the dense "coating" of scalation throughout the column. In this chapter, micro-computed tomography (µCT) has been applied to the entire length of the column of the holotype of *I. bradleyae* (specimenTCD.T87) to visualize the vertebrae column and associated elements surrounding it. This allows for a comprehensive redescription of the holotype and it is hoped this will allow for further comparison with it and other material attributed to *I. bradleyae*.

7.2 Materials and methods

TCD.T87 *Ichthyerpeton bradleyae* was scanned using the Nikon XTH 225 ST computed tomography scanner at the University of Bristol, UK. The scan was run at 220kV and 375uA with a 1mm plate of Cu in front of the source.

3D models of TCD.T87 were rendered using the freeware SPIERS (Sutton *et al.*, 2012). Individual elements were isolated using the masking function.

Specimens examined in this chapter are deposited in the following institutions: Natural History Museum London, United Kingdom (NHMUK), National Museum of Ireland, (NMI), Geological Museum, Trinity College Dublin (TCD).

7.3 Systematic Palaeontology

Infraclass TETRAPODOMORPHA Ahlberg, 1991

Order *incertae sedis*

Genus *ICHTHYERPETON* Huxley in Etheridge, 1866

Type species—*Ichthyerpeton bradleyae* Huxley in Wright and Huxley, 1866

Diagnosis— Elongated tetrapod with trunk, sacral and caudal vertebrae. Vertebrae each composed of a single centrum and bearing ribs in the trunk region. Centra are rectangular in lateral view with the long axis dorso-ventrally oriented. Trunk ribs approximately three times the length of the centra. Covering of scales with thin ventral trunk gastralia, dorsal ?ovoid trunk scutes and rectangular scales covering the caudal region.

ICHTHYERPETON BRADLEYAE Huxley, in Wright and Huxley, 1866

(Figs 7.1–7.5)

1866 *Ichthyerpeton* sp.; Huxley in Etheridge, 1866: p. 4.

1866 *Ichthyerpeton bradleyae* Huxley in Wright and Huxley, 1866: p. 168.

1867 *Ichthyerpeton bradleyae* Huxley; Huxley and Wright, 1867: p. 367, pl. 23, fig. 1.

1890 *Ichthyerpetum bradleyae* Lydekker; Lydekker, 1890: p. 344.

1891 *Ichthyerpetum bradleyae* Lydekker; Lydekker, 1891a: p. 58.

1970 *Ichthyerpeton bradleyae* Huxley; Panchen, 1970: p. 63.

2015 *Ichthyerpeton bradleyae* Huxley; Clack and Milner, 2015: p. 48.

Holotype—Articulated vertebrae and hind limbs (TCD.T87).

Type Locality—Clogh, County Kilkenny, Ireland.

Type Horizon—Jarrow (No. 4) Coal Seam, Coolbaun Coal Formation, Langsettian: Pennsylvanian.

Diagnosis— Same as for genus.

Description

The holotype (TCD.T87) is preserved in a rectangular block of coaly shale. The block has been broken so that only the trunk, pelvic region and part of the caudal region of *Ichthyerpeton bradleyae* are present. The fossil is compressed laterally, measures 240 mm in length and as a result of post-mortem effects is arched dorsally midway along its length giving it a crescentic shape (Fig. 7.1).

Axial Skeleton

Each vertebra is composed of a single centrum with the centra here numbered serially from anterior to posterior. The vertebral column is made up of 38 articulated centra, seen in lateral view and three disarticulated centra seen in articular view in the caudal region (Fig. 7.2). Presacral, sacral or caudal elements of the centra cannot be confidently distinguished because neither neural arches nor haemal arches are preserved. The anterior most centrum shows only its posterior margin, with the anterior end being lost due to the breakage in the block. In lateral view the centra are rectangular with a height to length ratio of c.2:1 in centra 1-29. There is in an increase in height in centra 30-32 giving a ratio to c.2.5:1. This is followed by a decrease in height in centra 33-38, which have similar sizes to centra 1-29. The ventral margin of each centrum shows an emargination, giving the margin a W-shape (Fig. 7.3A-H). The lateral margins of the articulated centra are difficult to discern. There appears to be a depression between the edges of the articulated surface on the lateral sides. Between centra 7-8, 13-15, 16-17, 18-22, 23-27 and 35-36 there is an "intercentral gap" between the posterior articular face of the anterior centrum and the anterior articular face of the next centrum (Fig. 7.3). This intercentral gap is seen only in the ventral half of each centrum, which results in a decrease in the anterio-posterior length in the ventral half of the centrum compared with the dorsal half. This is most apparent between centra 21-22. The intercentral gap is wider towards the centre of each centrum and becomes smaller laterally. It is difficult to establish if this intercentral gap is present between centra anterior of the 7th centrum. It appears to be absent in all centra following the 27th centrum with the exception of centra 35-36. In the intercentral gap between the centra

20-21 there is a sub-spherical bone (Fig. 7.3 G,H). A similar bone is seen on the ventral margin of the centrum 22 (Fig. 7.3 G,H). Apart from these the other intercentral gaps do not contain any fossilised bone indicating that the gap may not have accommodated hard tissue during life. The morphology of the centra in articular view can be ascertained from the three disarticulated centra in the caudal region, but is impossible to make out in the articulated centra because of the high degree of lateral compression. The best information is from the anterior most disarticulated centrum (Fig. 7.4A-B). In articular view, it is discoidal with a central foramen for the notochord. The dorsal surface shows the most lateral expansion with thickening of the bone along the dorso-lateral margin. This thickening gives the dorsal margin a concave surface. In contrast, the ventral half of the centrum has a smooth convex margin. The ratio of the diameter of the centrum (measured from the dorsal to ventral margins) to that of the foramen which housed the notochord is 3:1. The surface of the articular face slopes inwards towards the foramen after 25% of the radius from the periphery. A process of bone that extends laterally from one of the dorso-laterally thickened margins probably represents the transfer process although this is not seen in the adjacent margin.

Ribs in the trunk region are generally difficult to discern, especially the details of morphology of the rib head and distal ends. Centra 6,7, 11 and 12 all have articulated ribs indicating that all centra in the preserved trunk region housed ribs (and therefore centra were not divided into intercentra or pleuracentra). Two of the longest trunk ribs are preserved ventral of the centrum 15 and dorsal of centrum 21, each of them being as long as three centra. Vertebrae 31-34 lack ribs. It is not clear whether this is a result of taphonomy. By vertebra 34 rib morphology changed with an initial ventro-anterior projection from the centrum followed by a sharp curve of c.60° giving the rib a posterior extension which is 150% the length of the centrum. The rib appears to be single-headed. It is not clear whether vertebra 34 marks the first occurrence of this rib morphology.

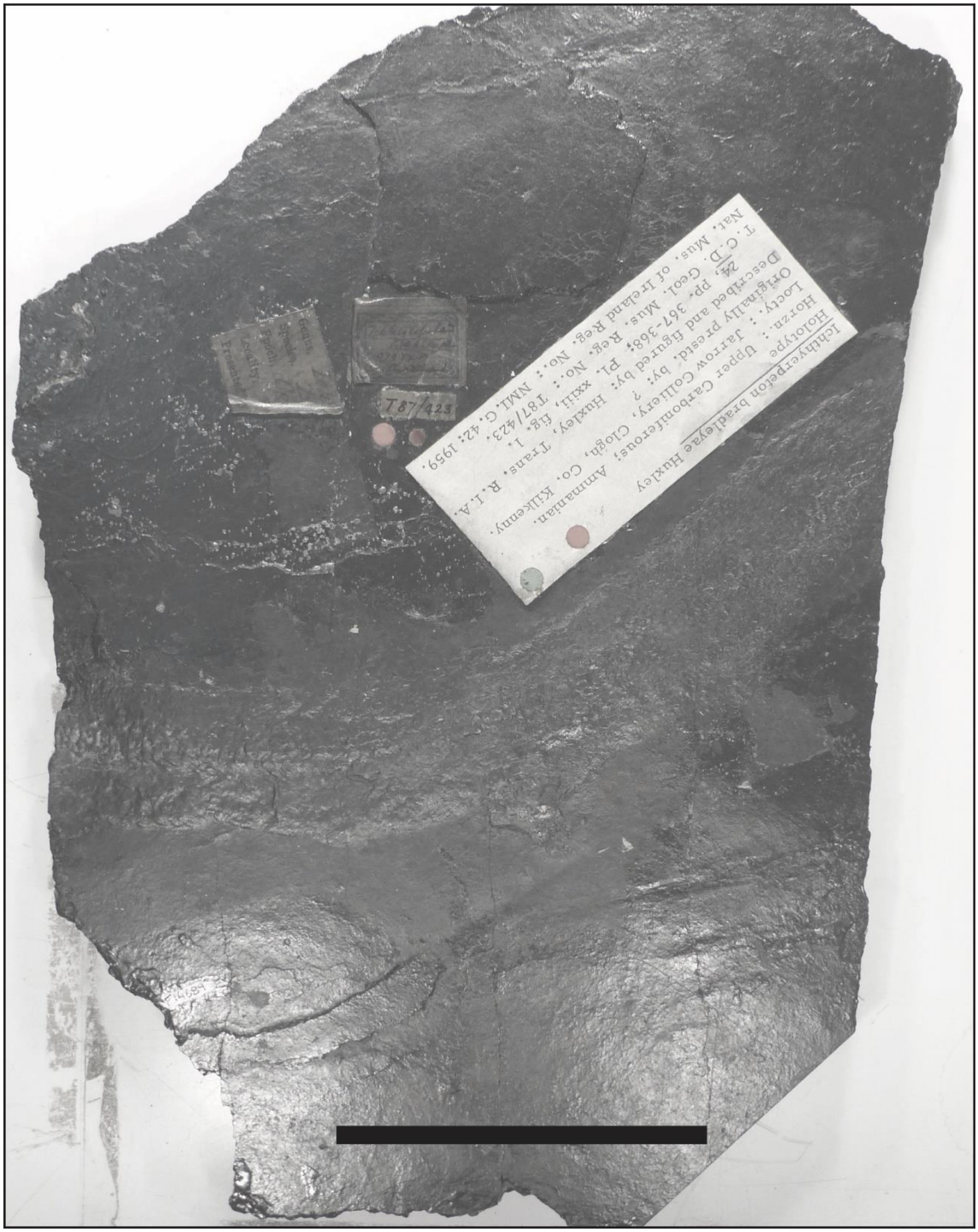

Figure 7.1. Photograph of the holotype of *Ichthyerpeton bradleyae* (TCD.T87). Scale bar = 100 mm.

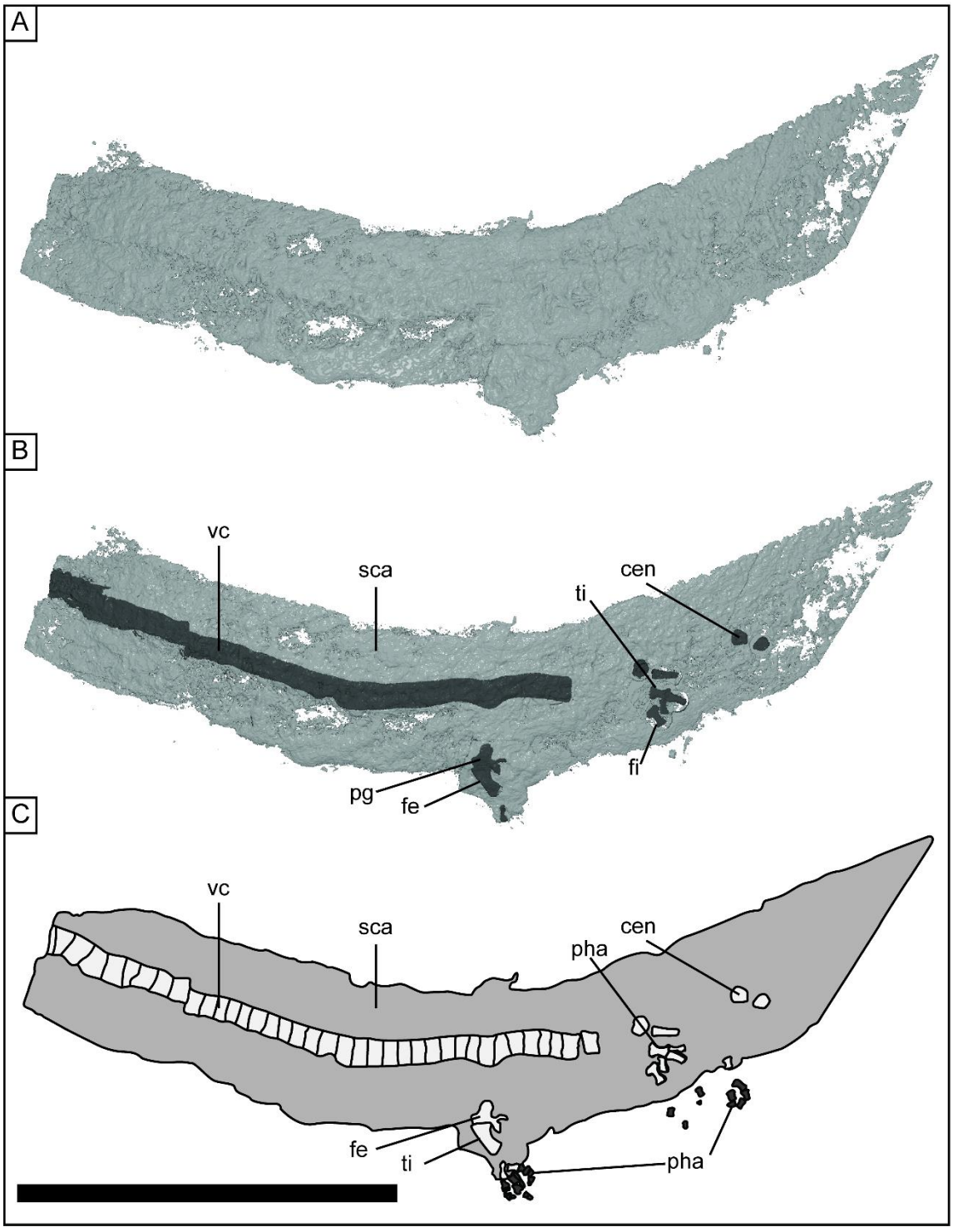

Figure 7.2. 3D models and sketch of TCD.T87 *Ichthyerpeton bradleyae* showing (A) 3D rendering of specimen, (B) 3D rendering made semi-transparent with identifiable elements highlighted in red and (C) sketch of specimen. Abbreviations are: cen, centrum; fe, femur; fi, fibula; pg, pelvic girdle; ph, phalanges; r; rib; ti, tibia; vc, vertebral column. Scale bar = 100 mm.

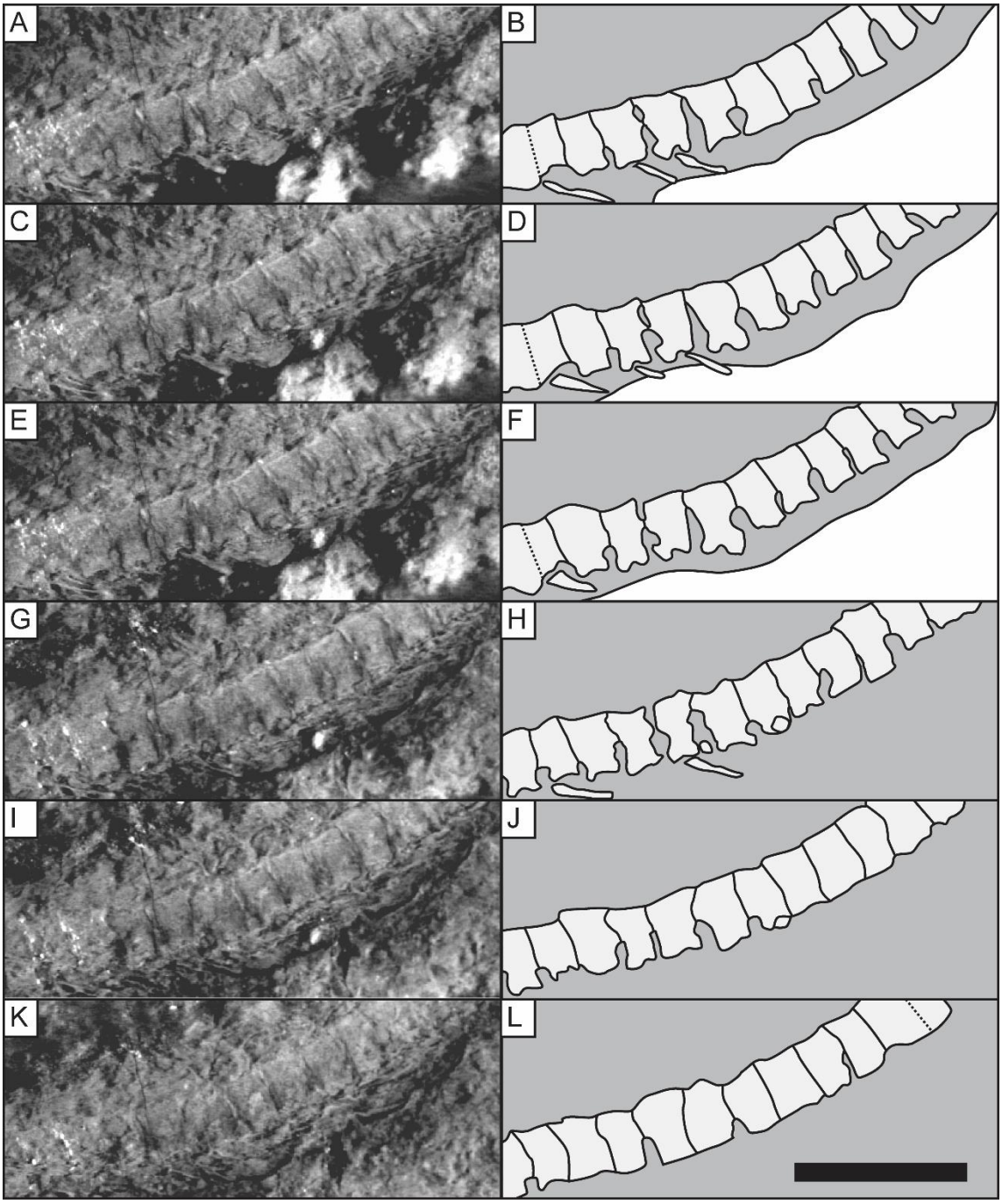

Figure 7.3. showing CT slices (A, C, E, G, I, K) and corresponding sketch (B, D, F, H, J, L) of centra 16-27 of TCD.T87 *Ichthyerpeton bradleyae*. Images show CT slices in descending order from the exposed surface through the column. Scalebar = 10 mm.

Appendicular Skeleton

Ventral of vertebrae 30-33 there is a protrusion of the scaly body outline, in which a femur, a tibia and at least 3 digits are partially preserved. The femur is exposed in flexor view (Fig. 7.2B,C). There is deep intertrochanteric fossa proximally (Fig 7.4G), where it is present along 40% of the length of the femur. The adductor blade is present anterior to the distal margin of the intertrochanteric fossa. The adductor blade juts out along the anterior margin. The fourth trochanter is also located along this margin, distal of the adductor blade. The femur is waisted distal of the fourth trochanter. There is an angle of c. 80° between the fibular and tibial facet.

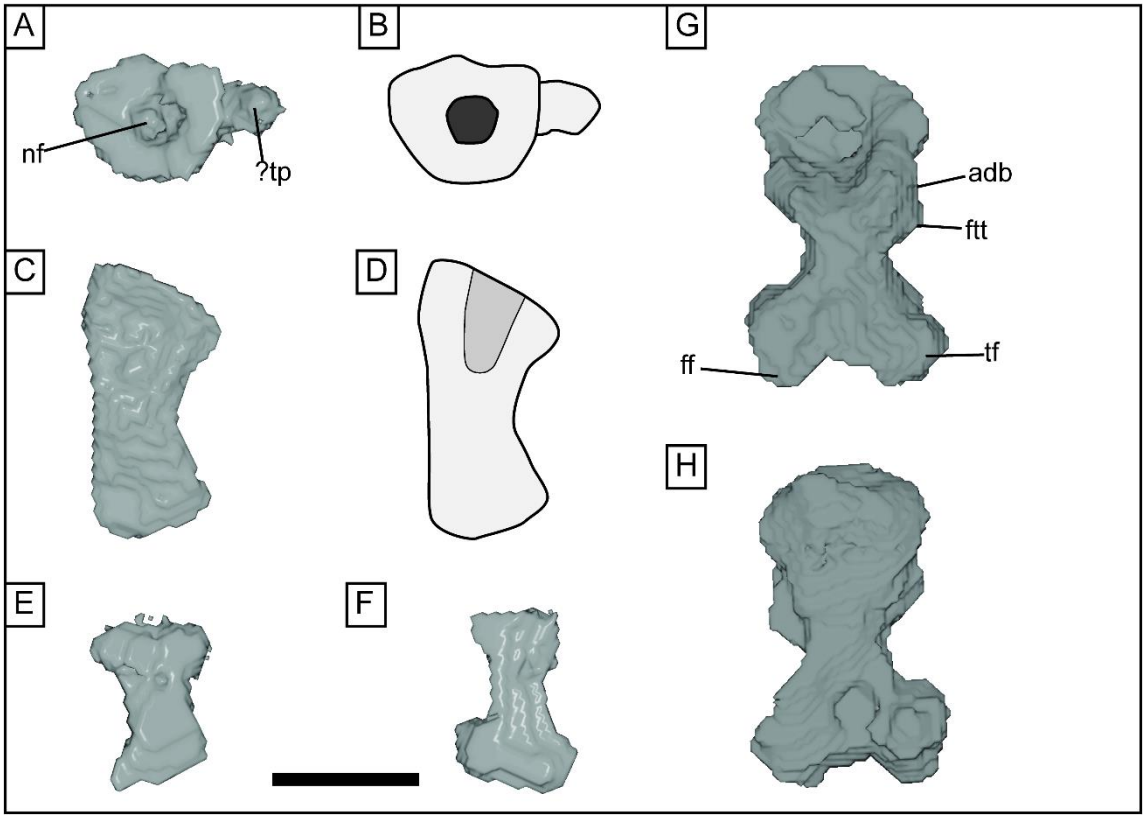

Figure 7.4. Isolated axial and appendicular elements of TCD.T87 *Ichthyerpeton bradleyae* showing (A, B) 39th centrum in articular view, (C, D) tibia, (E, F) phalange, and a femur in (F) flexor view and (H) extensor. Abbreviations are adb, adductor blade: ff, fibular fossa, ftt, fourth trochanter; nf, notochordal foramen; tf, tibial facet and ?tp, transverse process. Scale bar = 5mm.

Podial elements are preserved in two areas in TCD.T87, distal to the femur and tibia and in the caudal area. At least three digits are preserved ventral to the tibia in the projection of the scaly body. A single metatarsal is also preserved there. The anterior most digit is made up of four articulated phalanges with the distal most phalanx being triangular (Fig. 7.2B,C), indicating that it is the most distal section of this digit. The second digit also consists of four phalanges. The third digit has five phalanges. All three digits end in triangular phalanx. The

second set of digits occurs in the caudal region, dorsal of the disarticulated pleuracentra. There two metatarsals (Fig 7.4 E,F) are preserved with three phalanges (Fig. 7.2B,C). Posterodorsal of these there are nine disarticulated phalanges, four of them, including a distal triangular element representing a single digit. A small subtriangular element beside these phalanges may represent a distal tarsal. It is unlikely, despite its shape, to be a distal phalanx as it appears to be too small. Without an articulated hindlimb it is hard to interpret this putative distal tarsal with any confidence. It is likely that pelvic girdle and the limb elements all represent elements from the left side of the body. This would suggest that *Ichthyerpeton bradleyae* had a five-digited manus.

Scalation

TCD.T87 shows the body outline covered in scales throughout, including in an outward projection associated with hindlimb elements (Fig. 7.5). Scalation appears to be variable throughout the specimen. Along the ventral side of the trunk, scales are elongated and arranged in rows which form a chevron pattern. Trunk scalation along the flanks and on the dorsal margin is difficult to distinguish both in the CT-slices and under a binocular microscope. Ovoid nodules along this section may indicate that scales had an ovoid or sub-ovoid shape. Directly posterior to the sacral vertebrae the scales are sub-rhombic and are arranged in dorso-ventral rows with a ridge along the posterior margin (Fig. 7.5B). Some individual scales show striations along their surface (Fig. 7.5C-D). These striations extend from the dorso-posterior corner of the scale outwards covering the rest of the scale anteriorly (Fig. 6.5D) and do not appear to intercept one another except at the dorso-posterior corner.

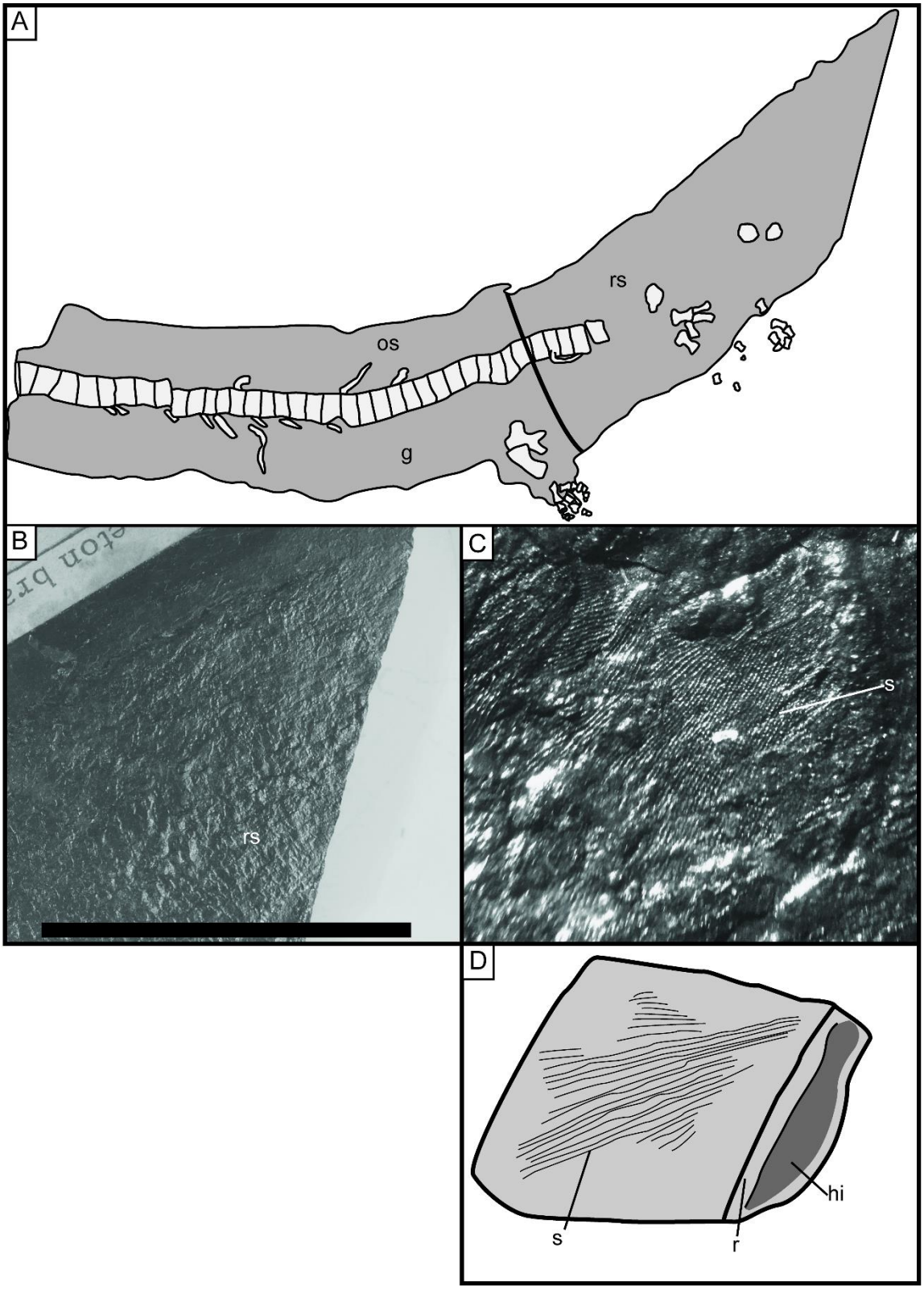

Figure 7.5. Images of the scalation in TCD.T87 *Ichthyerpeton bradleyae*. (A) drawing of entire specimen breaking up the three scalation zones; (B) close up photograph of caudal scalation; (C) photograph of striations in the caudal scale; and (D) a drawn reconstruction of a caudal scale. Abbreviations are: g, gastralia; hi, hollow indent; os, osteoderms/scutes; r, ridge; rs, rhombic scales; s, striations. Scale bar = 100mm for A, 50 mm for B and 1 mm for C and D.

Remarks.—TCD.T87 was the only specimen of *Ichthyerpeton bradleyae* described by Huxley in Huxley and Wright (1867), with all other specimens identified as *I. bradleyae* described later by other authors (Lydekker, 1890; Panchen, 1970). Therefore, there is a need to describe all other associated specimens to compare with TCD.T87. µCT slices of the holotype of *I. bradleyae* reveal more detail about the arrangement of centra in the vertebrate column than has previously been described, but the morphology of the lateral surfaces of the centra is still difficult to discern.

7.4 Discussion

7.4.1 Other specimens attributed to I. bradleyae

A detailed study of specimens, apart from the holotype, attributed to *I. bradleyae* needs to be undertaken to resolve whether they have been correctly identified. In this chapter a detailed redescription of the holotype only has been carried out. The comments below regarding other specimens that have been identified as *I. bradleyae* are based on a survey of the literature. NHMUK.R8433 was identified by Panchen (1970) as *I. bradleyae* but has since been redescribed as the temnospondyl *Procochleosaurus jarrowensis* (Sequeira, 1996). NHMUK.R.8454, NHMUK.R 8455 and NHMUK.R 8458 preserve three separate Jarrow tetrapods in ventral, dorsal and dorso-lateral view respectively and are currently considered to be *I. bradleyae* (Clack and Milner, 2015). They all appear to be similar and are probably from a single taxon. The vertebrae are discoidal but show larger notochordal openings than that seen in TCD.T87. All specimens lack the heavy scalation cover seen in TCD.T87. These three specimens may represent a new species of colosteid, as suggested by Clack and Milner (2015), but their affinity to the holotype of *I. bradleyae* is not clear. Specimen NHMUK R.8459 from Jarrow is composed of two parallel rows of discoidal vertebrae which are identified as *I. bradleyae* on the specimen label but were considered as belonging to a rhipidistian fish by Panchen (1970). This is a likely attribution since there are no rib articular surface on the centra. Specimen NHMUK.R. 8463 from Jarrow preserves a distorted skull and part of the vertebral column of a tetrapod. The vertebrae appear to be longer and less wide than those of NHMUK.R 8454 and NHMUK.R 8455 and appear more similar to the vertebra in TCD.T87 but this specimen lacks the scalation characteristic of *I. bradleyae* possibly as a result of non-preservation. Specimen TCD.38351 from Jarrow preserves the mould of the trunk region of a vertebrate that has been identified as *I. bradleyae*. This specimen is poorly preserved and anatomical detail is difficult to discern from it, but it is the only additional specimen that can possibly be attributed to *I. bradleyae* with confidence.

7.4.2 Comparative anatomy

New data on the vertebral column, hindlimbs and scalation permit some comparisons between *Ichthyerpeton bradleyae* and other early tetrapods. The femur, tibia, and podial elements are less informative. The vertebral column in the holotype of *I. bradleyae* lacks any information on the neural arch morphology. There are two possible explanations for this. The first is that the vertebrae of *I. bradleyae* are holospondylus with the neural arches fused to the centra. This is unlikely because within the trunk region there is no change in morphology of the centra dorsally that would suggest the presence of even a low neural arch. It is worth noting that the "intercentrum gap" seen throughout the column (Fig.7.3) does not imply the contrast between a ventral centrum and a more elongate dorsal neural arch. This is because the gap is not seen in all centra. The second explanation, which is favoured here, is that the neural arches became disarticulated from the vertebral column during decay and have since been lost. Although this seems unlikely because of the complete suite of articulated scalation throughout the specimen suggests minimal disarticulation, the absence of vertebral elements (with the exception of three isolated centra) in the caudal region indicates that the vertebral column has been disrupted in TCD.T87, while the scalation has remained relatively intact. This could suggest that neural arches were lost.

The presence of induvial ribs on each centra of *I. bradleyae* suggests that vertebrae are monospondylus. This means that there are several major tetrapod clades to which *I. bradleyae* certainly does not belong, including both colosteids and embolomeres, which it has traditionally been placed among. Colosteids have vertebrae composed of wedge shaped unpaired intercentra and paired pleurocentra, seen in *Colosteus scutellatus* (Hook, 1983) and *Greererpeton burkemorani* (Godfrey, 1989). Embolomeres are characterised by having vertebrae with discoidal intercentra and pleurocentra of equal sizes (Panchen, 1970), though centra are not always complete discs. Although the dorso-ventrally tall discoidal centra of *I. bradleyae* could be considered similar to those of embolomeres, such as *Carbonoherpeton carrolli* (Klembara, 1985) and *Pholiderpeton scutigerum* (Clack, 1987) and although the intercentra and pleurocentra of *Pholiderpeton scutigerum* also have an articulation surface morphology similar to those of *I. bradleyae*, with a notochordal foramen less than half the diameter of the intercentrum/pleurocentrum (Clack, 1987), the fact that the vertebrae of *I. bradleyae* are composed of a single centrum means that the traditional placement in either the colosteids (Clack and Milner, 2015) or the embolomeres (Panchen, 1970) cannot be supported. The arrangement of the centra of *I. bradleyae* does not fit the pattern seen in temnospondyls, which in most taxa are rhachitomous with each vertebra containing an intercentrum and paired pleurocentrum. The exception to this occurs in the more derived stereospondyl clade of temnospondyls, which only have a single central element in their vertebrae (Schoch and Milner,

2014). However, a close relationship between *I. bradleyae* and stereospondyls might be unlikely because the latter clade did not originate until the Permian (Warren and Marsicano, 2000). Rhachitomous vertebrae are seen also in the whatcheeriid *Pederpes* (Clack and Finney, 2005) ruling out an affinity with *I. bradleyae*. The vertebrae of stem-tetrapod *Crassigyrinus scoticus* have horseshoe shaped intercentrum, which are constricted along their midline in anterior trunk vertebrae (Panchen, 1985; Herbst and Hutchinson, 2019). Herbst and Hutchinson (2019) identified both paired and fused pleurocentra in *Crassigyrinus*, which are considered to sit dorsal of the notochord. Vertebrate morphology rules out an affinity between *I. bradleyae* and *Crassigyrinus* as vertebrae of the latter are diplospondylus and possibly rhachitomous morphology (Herbst and Hutchinson, 2019).

The monospondylus vertebrae of *I. bradleyae* best matches that of the "lepospondyls". "Lepospondyls" (aïstopods, nectrideans, "microsaurs" adelospondyls, lysorophians and *Acherontiscus caledoniae*) are a polyphyletic grouping of tetrapods (Pardo, *et al.*, 2017, Clack, *et al*., 2019) that are characterised by having spool-shaped centra which are fused in most taxa to the neural arch (Baird, 1965). The vertebrae of most of the clades within the "lepospondyls" have a single centrum. The exception to this is seen in some recumbirostran "microsaurs" which are diplospondylus (Carroll and Gaskill, 1978). In contrast to *I. bradleyae*, the centra of nectrideans, aïstopods, lysorophians and "microsaurs" are more elongated anterio-posteriorly as opposed to dorso-ventrally. The lack of neural arches, if confirmed, in *I. bradleyae* indicates they were probably weakly sutured to the centra, the opposite of the lepospondyl condition. *Adelospondyls* are traditionally considered to be lepospondyls (Carroll and Andrews, 1998). However, in this clade the neural arches are sutured, and not fused to the centra and the vertebrae contain only one centrum each. The centra are also more elongate along the anterio-posterior line. Additionally, adelospondyls lack any vestige of a pelvic girdle and associated limbs (Carroll and Andrews, 1998).

The morphology of the centra of *I. bradleyae* are similar to those of the smaller stem-tetrapod *Acherontiscus caledoniae* (Carroll, 1998; Clack *et al*. 2019). However, the vertebrae of *A. caledoniae* shows similar-sized intercentra and pleuracentra, similar to the embolomere condition. Additionally, the only known specimen of *A. caledoniae* lacks any evidence of a pelvic girdle and limbs. It is uncertain whether this is the result of post-mortem disarticulation. A recent review of *A. caledoniae* placed it in a clade with nectrideans, aïstopods, colosteids and adelospondyls. With the exception of the nectrideans (Clack, *et al*. 2019), all these clades have taxa characterised by elongated bodies and reduced limbs, with limb being absent in aïstopods.

It is difficult to deduce the relationship between the holotype of *I. bradleyae* and other early tetrapod clades. This is both as a result of the loss of information about parts of the

individual specimen TCD.T87 (such as lack of cranial elements) and the fact that what is preserved does not seem to be comparable to other early tetrapods. This makes *I. bradleyae* more enigmatic than previously thought. The Carboniferous was a period in which tetrapod body plans were becoming disparate as individual clades exploited new niches. The presence of vertebrae with a single centrum in early tetrapods was previously thought to occur only in "lepospondyls". With identification of polyphyly in the lepospondyls (Pardo *et al*., 2017) it is apparent that similar body plans evolved several times. *I. bradleyae* may represent a member of a separate clade, in which this vertebral arrangement also evolved. The clade made up of nectrideans, aïstopods, colosteids, adelospondyls and *A. caledoniae* (Clack *et al*. 2019) shows the closest affinity to *I. bradleyae*, as members of this clade all have elongated bodies (with the exception of the nectrideans) and reduced limbs (with no limbs in aïstopods) similar to the overall morphology of *I. bradleyae*

7.4.5 Jarrow anthracosaurs

Ichthyerpeton bradleyae does not conform to the embolomere condition. However, the Jarrow biota does include embolomere material. Huxley in Huxley and Wright (1867 p. 369) noted the presence of at least three more tetrapods, one of which resembles *Anthracosaurus*, and the other two which he named *Discospondylus* and *Brachyscelis*. Baily (1879, 1884) named, but did not figure, *Anthracosaurus edgei* from Jarrow, which is probably the *Anthracosaurus* identified by Huxley and Wright (1867). Due to the lack of figures, it is hard to identify these specimens in museum collections. Panchen (1970) mentioned that the only material from the TCD and the NMI collection which were attributed to *A. edgei* are the *Megalocephalus* skull described by Beaumont (1977) and material possible of megalicthyd fish vertebral columns. TCD.38359 preserves disarticulated curved ribs which may represent some material of *A.edgei*. NHMUK R.8456 was also considered to be *A. edgei* by Panchen (1970). *Discospondylus* is associated with the smaller embolomerous centra of NHMUK. R8470 (Panchen, 1970). Romer (1947) suggested that *I. bradleyae* may be juvenile member of the larger Jarrow anthracosaurs. This is unlikely as the centra of *I. bradleyae* appear to have a narrow range of size variation and a growth range of roughly 10mm in TCD.T87 to just under 30mm in NHMUK. R8470 is unlikely in an ossified column. NHMUK. R8470 does appear to show embolomerous material, so does not belong to *I. bradleyae*, and review of the Jarrow anthracosaur material is much needed.

7.5 Conclusion

Ichthyerpeton bradleyae is one of the seven tetrapod species originally described by Huxley in Huxley and Wright (1867), but unlike the other species, its affinities have remained problematic. This is because the holotype consists of the vertebral column, the hindlimb and the caudal region only and the apparently poor preservation of the fossil. The application of µCT has revealed previously unobserved anatomical features of the holotype of *I. bradleyae*. This allowed for the reconstruction of vertebrae as being composed of single discoidal centra. Each centrum has a closed notochordal foramen. The vertebral column lacks neural arches throughout. Vertebral characteristics do not support a placement of *I. bradleyae* within either colosteids or embolomeres. The relationship between *I. bradleyae* and other described early tetrapod clades remains difficult to discern. It is suggested that there may be an affinity between *I. bradleyae* and other clades with an undivided centrum, including aïstopods, nectrideans, and adelospondyls (Clack, *et al*., 2019). The holotype of *I. bradleyae* TCD.T87 and one other specimen, TCD.38351 are considered to be the only known specimens of *I. bradleyae*. All other specimens are attributed to rhipidistian fish or currently undescribed tetrapods.

7.6 References

AHLBERG, P. E. 1991. A re-examination of sarcopterygian interrelationships, with special reference to the Porolepiformes. *Zoological Journal of the Linnean Society*, **103**, 241–287.

BAILY, W. H. 1879. Notice of some additional labyrinthodont Amphibia and fish from the coal of Jarrow solliery, County of Kilkenny, Ireland. *Reports of the British Association for the Advancement of Science*, **48**, 530.

— 1884 Some additional notes on *Anthracosaurus edgei* (Baily sp.), a large sauro-batrachian from the lower Coal Measures, Jarrow colliery, near Castlecomer, County Kilkenny. *Reports of the British Association for the Advancement of Science*, **54**, 496–497.

BAIRD, D. 1965. Paleozoic Lepospondyl Amphibians. *American Zoologist*, **5**, 287–294.

BEAUMONT, E. H. 1977. Cranial Morphology of the Loxommatidae (Amphibia: Labyrinthodontia). *Philosophical Transactions of the Royal Society B: Biological Sciences*, **280**, 29–101. doi: 10.1098/rstb.1977.0099.

CARROLL, R. L. 1998. Order Undesignated. 183–185. *In* WELLNHOER (ed). *Encyclopedia of Paleoherpetology*. Verlag Dr.Friedrich Pfeil, München, 206 pp.

— and GASKILL, P. 1978. *The order Microsauria*. American Philosophical Society, Philadelphia, 211 pp.

— and ANDREWS, S. M. 1998. Order Adelospondyli Watson 1929. 149–162. *In* WELLNHOER (ed). *Encyclopedia of Paleoherpetology*. Verlag Dr.Friedrich Pfeil, München, 206 pp.

CLACK, J. A. 1987. *Pholiderpeton scutigerum* Huxley, an amphibian from the Yorkshire Coal Measures, *Philosophical Transactions of the Royal Society B: Biological Sciences*. **318**, 1–107.

— and FINNEY, S. M. 2005. *Pederpes finneyae*, an articulated tetrapod from the tournaisian of Western Scotland. *Journal of Systematic Palaeontology*, **2**, 311–346.

— and MILNER, A. R. 2015. *Handbook of Paleoherpetology, Part 3A1: Basal Tetrapoda.* Verlag Dr.Friedrich Pfeil, München, 93 pp.

— RUTA, M., MILNER, A. R., MARSHALL, J. E. A., SMITHSON, T. R. and SMITHSON, K. Z. 2019. *Archerontiscus caledoniae*: the earliest heterodont and durophagous tetrapod. Rpyal Society Open Science, **6**, 182087. doi.org/10.1098/rsos.182087.

ETHERIDGE, R. 1866. On the discovery of several new Labyrinthodont reptiles in the coal measures of Ireland. *Geological Magazine*, **3**, 4–5.

GODFREY, S. 1989. The Postcranial Skeletal Anatomy of the Carboniferous Tetrapod *Greererpeton burkemorani* Romer, 1969. *Philosophical Transactions of the Royal Society B: Biological Sciences*, **323**, 75–133.

HERBST, E. C. and HUTCHINSON, J. R. 2019. New insights into the morphology of the Carboniferous tetrapod *Crassigyrinus scoticus* from computed tomography. *Earth and Environmental Science Transactions of the Royal Society of Edinburgh*, **109**, 157-175.

HOOK, R. W. 1983. *Colosteus scutellatus* (Newberry), a Primitive Temnospondyl Amphibian from the Middle Pennsylvanian of Linton, Ohio. *American Museum Novitates*, **2770**, 1–41.

HUXLEY, T. H. and WRIGHT, E. P. 1867. Royal Irish Academy On a Collection of Fossil Vertebrata , from the Jarrow Colliery, County of Kilkenny, Ireland. *Transactions of the Royal Irish Academy*, **24**, 351–370.

KLEMBARA, J. 1985. A New Embolomerous Amphibian (Anthracosauria) from the Upper Carboniferous of Florence, Nova Scotia. *Journal of Vertebrate Paleontology*, **5**, 293–302.

LYDEKKER, R. 1890. *Catalogue Of The Fossil Reptilia and Amphibia in the British Museum (Natural History), Part IV. Containing the orders Anomodontia, Ecaudata, Caudata, And Labyrinthodontia; And Supplement*. British Museum (Natural History), London.

— 1891a. A labyrinthodont skull from the Kilkenny coal-measures. *Quarterly Journal of the Geological Society, London*, **47**, 343–347.

— 1891b. *Catalogue of Fossil Mammals, Birds, Reptiles, and Amphibians in the Science and Art Museum: Dublin, Science and Art Museum*. British Museum (Natural History), London.

MILNER, A. R. 1980. The temnospondyl amphibian Dendrerpeton from the Upper Carboniferous of Ireland. *Palaeontology*, **23**, 125–141.

— 1987. The Westphalian tetrapod fauna; some aspects of its geography and ecology. *Journal of the Geological Society*, **144**, 495–506. doi: 10.1144/gsjgs.144.3.0495.

MOODIE, R. L. 1909. A contribution to a monograph of the extinct Amphibia of North America. New forms from the Carboniferous. *Journal of Geology*, **17**, 38–82.

PANCHEN, A. L. 1970. *Encyclopedia of Paleoherpetology, Part 5, Batrachosauria, Part A*

Anthracosauria. Verlag Dr.Friedrich Pfeil, München.

—1985. On the Amphibian *Crassigyrinus scoticus* Watson from the Carboniferous of Scotland. *Philosophical Transactions of the Royal Society B: Biological Sciences*, **309**, 505–568.

PARDO, J. D., SZOSTAKIWSKYJ, M. and ANDERSON, J. S. 2017. Hidden morphological diversity among early tetrapods. *Nature*, **546**, 642–645.

ROMER, A. S. 1947. Review of the Labyrinthodontia. *Bulletin of the Museum of Comparative Zoology, Harvard University*, **99**, 1–368.

SCHOCH, R. R. and MILNER, A. R. 2014. *Encyclopedia of Paleoherpetology Part 3A ii, Temnospondyli*. Verlag Dr. Friedrich Pfeil, München.

SEQUIRA, S. E. K. 1996. A cochleosaurid amphibian from the Upper Carboniferous of Ireland. *Special Papers in Palaeontology*, **52**, 65–80.

SUTTON, M. D., *GARWOOD, R. J., SIVETER, D. J. and SIVETER, D. J.* 2012. SPIERS and VAXML; A software toolkit for tomographic visualisation and a format for virtual specimen interchange. *Palaeontologia Electronica*, **15**, 1–14.

WARREN, A. and MARSICANO, C. 2000. A Phylogeny of the Brachyopoidea (Temnospondyli, Stereospondyli). *Journal of Vertebrate Paleontology*, 20, 462–483.

WRIGHT, E. P. and HUXLEY, T. H. 1866. On a collection of fossils from the Jarrow Colliery Kilkenny, Ireland, *Geological Magazine*, **3**, 165–171.

Chapter 8: Conclusion.

8.1 Deposition and Preservation

The Jarrow fossil assemblage of diverse fish and early tetrapods in the south east of Ireland is of Langsettian (Early Pennsylvanian) age (Higgs and O'Connor, 2005) and thus is the oldest of the "Westphalian" coal swamp assemblages (Milner, 1987). The assemblage was apparently collected from towards the top of the No.4 Coal (the Jarrow Seam) (Fig. 2.2) and is localised to an area where the seam thickens, called the Jarrow Channel. In this area, which may have been atypical of the Jarrow seam as a whole the sediment preserved more amorphous organic matter (AOM) than the same beds outside of the channel (Fig. 2.6). The thickening of the Jarrow seam in the channel has been considered to be a result of it being deposited in an abandoned channel or oxbow lake (Hook and Ferm, 1985). This has lead to the idea that the Jarrow assemblage represents an autochthonous fauna, consisting of the fossils of animals living in and around the abandoned channel (Hook and Ferm, 1985). The presence of microconchids, in the Jarrow assemblage (Fig. 2.5) (albeit only two specimens) that are generally regarded as indicators of brackish to marine salinity, indicates that there was at least some wash-in material. The Linton, Ohio biota, of slightly younger Pennsylvanian age, also consists of an assemblage preserved in an abandoned channel, and it contains abundant microconchids (Hook and Baird, 1988) suggesting that at least for that assemblage there is a high degree of wash in. The fish fauna of the Jarrow assemblage is composed of taxa with known euryhaline adaptions, including *Ageleodus pectinatus*, *Saganodus*, *Megalichthys* and *Rhizodopsis* (Carpenter *et al.*, 2011, 2014, 2015; Ó Gogáin *et al.*, 2016). This indicates that the Jarrow assemblage probably represents an estuarine fauna, with taxa being washed into the abandoned channel and preserved. The Jarrow coal seam is considered to have been deposited in estuarine facies during a period of marine transgression (Fig. 2.5).

Rayner (1971) suggested that the bottom waters of the Jarrow channel were acidic and that during post-mortem burial of the tetrapods, this acid would have dissolved the bone. Rayner (1971) suggested that this is the reason that fossils from the Jarrow assemblage appear so poorly preserved with only a nebulous boundary between the body fossil and the matrix. Cathodoluminescence (Cl) imaging of the osteoderms and a vertebra of the aïstopods *Ophiderpeton brownriggii* show that the bone no longer retains its original structure. Instead bone has been replaced with large carbonaceous pockets surrounded by small elongated, zoned crystals of apatite and crystals of sphalerite (Fig. 3.1) This type of replacement has not been

recorded from other coeval vertebrate assemblages (Hook and Hower, 1988). U-Pb dating of the apatite gives a younger age than the depositional age of the Jarrow Seam (Fig. 3.2). Therefore, alteration in the bone was not a result of being dissolved by acidic waters and is here suggested to be a result of thermal alteration during deep burial.

8.2 Micro-computed tomography of the Jarrow fossil vertebrates

The replacement of bone, with material similar to the matrix (Fig. 3.1), and the high degree of compression means that the specimens from the Jarrow assemblage are not ideal for study by micro-computed tomography (µCT). However, the body fossils show different concentrations of apatite and bituminous material compared to the surrounding matrix and this can be resolved in µCT images. Recrystallisation of apatite has taken place and obscures detail of the bone, such as spinal nerves in the vertebra at one extreme of detail to concealing the sutures between bones at the other. In specimens where the skull has been dorso-ventrally flattened, recrystallisation has made the boundary between the mandibles, palate, braincase and cranial elements difficult to distinguish from one another, and even more so the bones associated with them. This is particularly problematic in the aïstopods NHMUK R 8465 *Ophiderpeton brownriggii* an TCD.38363 *Ophiderpeton brownriggii*. Both specimens preserve a complete skull which has been dorso-ventrally flattened so that the mandibles are nearly in the same plane as the cranial elements (Fig. 4.4, 4.5). Details of the exposed sides (both exposed to surface and the opposite side still encased in matrix in the specimen) can be readily made out. But closer to the midpoint of the dorsal and ventral surfaces, more bone morphology is obscured. All attempts to make out the braincase in this region have been unsuccessful as the CT-slices in this region show a confused mass. Therefore, when dealing with the description of the skulls of specimens from Jarrow, µCT results are generally limited to the cranial elements on one side and the mandibles on the other. Particularly in the aïstopods, scalation can also obscure the palate from being described in ventral view (Fig. 4.4). Despite the potential to remove these scales from 3D rendered models virtually, the uncertainty between the boundary of the scalation and the palate means that this cannot be satisfactorily done. Additionally, where a high concentration of pyrite is preserved within a specimen, the quality of the µCT scans is further reduced, for example in TCD.T85b *Lepterpeton dobbsii* (Fig 6.2).

Despite its limitations, µCT has proved useful in contributing to the descriptions of specimens of the Jarrow fossils.

8.3 Anatomy and systematic position of the Jarrow vertebrate fauna

The primary focus of this thesis was on the redescription of the tetrapods first described by Huxley in Huxley and Wright (1867), with the exception of *Keraterpeton galvani* and *Erpetocephalus rugosus*, which were part of recent studies (Milner, 1980; Milner, 2019). The tetrapods that were redescribed using µCT are *Ophiderpeton brownriggii* (Chapter 4), *"Dolichosoma" emersoni* (Chapter 5), *Lepterpeton dobbsii* and *Urocordylus wandesfordii* (Chapter 6) and *Ichthyerpeton bradleyae* (Chapter 7).

The first extensive description of the aïstopod *O. brownriggii* Huxley in Huxley and Wright (1867) is in Chapter 4, which includes new cranial, postcranial and scalation characteristics for the taxon (Fig. 4.4-4.10). A new genus of Ophiderpetontidae, *Peisterpeton milnerorum*, is described from one of the syntypes of *O. brownriggii* TCD.T90 (Fig. 4.1-4.3). Both *P. milnerorum* and *O. brownriggii* have fenestrated skulls with orbits placed anteriorly. *P. milnerorum* is distinguished from *O. brownriggii* by having a pineal foramen, a slimmer skull and lacking cheek scalation. *Oestocephalus nanum* is transferred to *Ophiderpeton*, based on the transverse process being restricted to the centrum, and the ophiderpetontids are here considered to include *O. brownriggii*, *O. kirktonense*, *O. nanum* and *P. milnerorum*. The identification of an internal lateral line system in the jugal of *O. brownriggii* supports the hypothesis that aïstopods where at least habitually aquatic.

The problematic taxonomy of the aïstopod "*Dolichosoma*" *emersoni* is dealt with in Chapter 5, in which it is formally transferred to *Dolichosomatites* Kuhn, 1961. It is described from a single specimen (NHMUK.R8466), as the holotype is missing, presumed destroyed. New characters which were identified, including paired frontals, parietals and postparietals (Fig. 5.1), do not support an affinity between *Dolichosomatites emersoni* and the derived *Phlegethontia*, as was originally supposed (Carroll, 1998). The presence of a closed temporal fenestra orbits midway along the length of the skull and an anteriorly tapering skull suggest an affinity with the basal *Lethiscus* (Anderson, *et al*., 2003; Pardo, *et al*., 2017). K-shaped ribs are not considered to be characteristic of derived aïstopods (Anderson, 2003), given their presence in the trunk of *D. emersoni* and *O. brownriggii* (Fig. 4.9 and Fig. 5.3). Based on the material investigated in Chapter 4 and 5, the Bashkirian Jarrow fauna contained at least three species of aïstopod, giving it the same number of aïstopod species as the Moscovian Mazon Creek and Linton faunas. There is a difference between the aïstopod faunas from the three localities as the older Jarrow fauna contains more basal aïstopods (*D. emersoni*, *O. brownriggi* and *P. milnerorum*) while the younger Mazon Creek and Linton faunas contain more derived Oestocephalids and Phaethontids. This suggests that there is a faunal change in aïstopods between the Bashkirian and Moscovian (Fig. 5.4).

Chapter 6 includes a review of the urocordylid nectrideans, *Lepterpeton dobbsii* and *Urocordylus wandesfordii*, from Jarrow. µCT revealed a notch in the jugal to accommodate the ventral extension of the orbit and a posterior extension of the parietals in *U. wandesfordii* (Fig. 6.5), which are characteristics of nectrideans and urocordylids respectably. The description of cranial elements from TCD.T85b was hindered by the presence of pyrite throughout the specimen (Fig. 6.2), but despite this morphology of parts of the lacrimal, postfrontal, postorbital and squamosal were described (Fig.6.3). Phylogenetic analysis is needed on intra-nectridean relationships in order to test the validity of the Sauropleurinae and the Urocordylinae.

Ichthyerpeton bradleyae is described for the first time since Huxley's description in Chapter 7. The vertebral column contains articulated centra, but neural arches were not found (Fig. 7.2). Single rib attachments to each centra indicate that the vertebrae are monospondylus, which does not support an affinity between *I. bradleyae* and either colosteids or embolomeres, with which it has traditionally been placed (Panchen, 1970; Clack and Milner, 2015). A femur, tibia and additional metatarsal and phalanges, which were previously unidentified, are described. A review of the literature and museum specimens indicates that only two specimens of *I. bradleyae*, TCD.T87 and TCD.38351, are known from the Jarrow Seam, with all other attributed material belonging to as yet undescribed material.

8.4 Future work

There are two tasks which will be vital for the future study of the Jarrow Assemblage. Firstly, phylogenies for the tetrapods should be produced. The position of aïstopods within a larger tetrapod phylogeny is based primarily on the basal *Lethiscus* (Pardo, *et al*., 2017; Clack *et al*., 2019) and characters identified from the Jarrow aïstopods (Chapters 4 and 5) do not add much in the way of new characters to aid investigating inter-tetrapod relationships. However, characters from *Dolichosomatites emersoni*, *Ophiderpeton brownriggi* and *Peisterpeton milnerorum* are vital for understanding intra-aïstopod relationships which appear to be more complex than previously thought (Anderson, *et al*., 2003). To investigate these relationships, phylogenetic analysis needs to be carried out on the aïstopods. A phylogenetic analysis also needs to be carried out on the nectrideans to test intra-nectridean relationships. Given that the Jarrow Assemblage marks the first occurrence of the nectrideans, characters from *Urocordylus wandesfordii* and *Lepterpeton dobbsii* will be important for investigating these relationships. Unlike the aïstopods, the nectrideans from Jarrow will be important for testing their recent placement on the tetrapod stem (Clack, *et al*. 2019). Unfortunately, *Ichthyerpeton bradleyae* does not have enough characters for a robust phylogeny.

µCT has proven to be a valid method for describing material from the Jarrow Assemblage. This thesis focused on previously described material. There are numerous specimens of tetrapods from Jarrow in the NHM and NMI which have not yet been described and which do not share an affinity to tetrapods described here. Further description of this material, using µCT, is vital for understanding the true diversity of the Jarrow Assemblage and for studying early tetrapod evolution and ecology.

8.5 References

ANDERSON, J. S. 2003. Cranial anatomy of *Coloraderpeton brilli*, postcranial anatomy of *Oestocephalus amphiuminu*s, and reconsideration of Ophiderpetontidae (Tetrapoda: Lepospondyli: Aistopoda). *Journal of Vertebrate Paleontology*, **23**, 532–543.

— CARROLL, R. L. and ROWE, T. B. 2003. New information on *Lethiscus stocki* (Tetrapoda : Lepospondyli : Aistopoda) from high-resolution computed tomography and a phylogenetic analysis of Aistopoda. *Candian Journal of Earth Science*, 40, 1071–1083. doi: 10.1139/E03-023.

CARPENTER, D. K., FALCON-LANG, H. J., BENTON, M. J. and NELSON, W. J. 2011. Fishes and tetrapods from the Pennsylvanian (Kasimovian) Cohn Coal Member of the Mattoon Formation, Illinois, USA: systematics, palaeoecology and palaeoenvironments. *Palaios*, **26**, 639–658.

— — — and HENDERSON E. 2014. Carboniferous (late Tournaisian) fish assemblages from the Isle of Bute, Scotland: systematics and palaeoecology. *Palaeontology*, **57**, 1215–1240.

— — — and GREY M. 2015. Early Pennsylvanian (Langsettian) fish assemblages from the Joggins Formation, Canada, and their implications for palaeoecology and palaeogeography. *Palaeontology*, **58**, 661–690.

CARROLL, R. L. 1998. Order Aïstopoda Miall 1875. 163–182. *In* WELLNHOER (ed). *Encyclopedia of Paleoherpetology*. Verlag Dr.Friedrich Pfeil, München, 206 pp.

CLACK, J. A. and MILNER, A. R. 2015. *Handbook of Paleoherpetology, Part 3A1: Basal Tetrapoda.* Verlag Dr.Friedrich Pfeil, München, 93 pp

— RUTA, M., MILNER, A. R., MARSHALL, J. E. A., SMITHSON, T. R. and SMITHSON, K. Z. 2019. *Archerontiscus caledoniae*: the earliest heterodont and durophagous tetrapod. Rpyal Society Open Science, **6**, 182087. doi.org/10.1098/rsos.182087.

HIGGS, K. T. and O'CONNOR, G. 2005. Stratigraphy and palynology of the Westphalian strata of the Leinster Coalfield, Ireland. *Irish Journal of Earth Sciences*, **23**, 65–84.

HOOK, R. W. and FERM, J. C. 1985. A depositional model for the Linton tetrapod assemblage (Westphalian D, Upper Carboniferous) and its palaeoenvironmental significance. *Philosophical Transactions of the Royal Society B: Biological Sciences*, **311**, 101–109.

— and and BAIRD, D. 1988. An overview of the Upper Carboniferous Fossil Deposit at Linton, Ohio. *The Ohio Journal of Science*, **88**, 55–60.

— and HOWER, J. C. 1988. Petrography and taphonomic significance of the vertbrate-bearing cannel coal of Linton, Ohio (Westphalian D, Upper Carboniferous. *Journal of Sedimentary Petrology*, 58, 72–80.

HUXLEY, T. H. and WRIGHT, E. P. 1867. Royal Irish Academy On a Collection of Fossil Vertebrata , from the Jarrow Colliery, County of Kilkenny, Ireland. *Transactions of the Royal Irish Academy*, **24**, 351–370.

KUHN, O. 1961. *Die familien der rezenten und fossilen Amphibien und Reptilien.* Meisenbach, Bamberg

— 2019. A morphological revision of Keraterpeton, the earliest horned nectridean from the Pennsylvanian of England and Ireland. *Earth and Environmental Science Transactions of the Royal Society of Edinburgh*, **109**, 237–253. doi: 10.1017/S1755691018000579.

MILNER, A. R. 1980. The temnospondyl amphibian Dendrerpeton from the Upper Carboniferous of Ireland. *Palaeontology*, **23**, 125–141.

— 1987. The Westphalian tetrapod fauna; some aspects of its geography and ecology. *Journal of the Geological Society*, **144**, 495–506.

Ó GOGÁIN, A., FALCON-LANG, H. J., CARPENTER, D. K., MILLER, R. F., BENTON, M. J., PUFAHL, P. K., RUTA, M., DAVIES, T. G., HINDS, S. J. and STIMSON, M. R. 2016. Fish and tetrapod communities across a marine to brackish salinity gradient in the Pennsylvanian (early Moscovian) Minto Formation of New Brunswick, Canada, and their palaeoecological and palaeogeographical implications. *Palaeontology*, **59**, 689–724. doi: 10.1111/pala.12249.

PANCHEN, A. L. 1970. *Encyclopedia of Paleoherpetology, Part 5, Batrachosauria, Part A Anthracosauria.* Verlag Dr.Friedrich Pfeil, München.

PARDO, J. D., SZOSTAKIWSKYJ, M. and ANDERSON, J. S. 2017. Hidden morphological diversity among early tetrapods. *Nature*, **546**, 642–645.

RAYNER, D. H. 1971. Data on the environment and preservation of Late Palaeozoic tetrapods. *Proceedings of the Yorkshire Geological Society*, **38**, 437–495.

Appendix 1

Museum Catalogue

Museum	Catalogue #	identification	Grouping
NMI	F.16844	*Ageleodus pectinatus*	
NMI	No Number, possibly F16889	*Ageleodus pectinatus*	Chondrichthyes
NMI	F.16859	*Xenacanthiformes indet.*	
NMI	F.16881	Elasmobranch indet.	
NHMUK	P.41851_4	*Gyracanthus sp.*	
NHMUK	P.43500	*Gyracanthus sp.*	
NHMUK	P.43499	*Gyracanthus sp.*	
NHMUK	P. 4181	*Gyracanthus sp.*	
NMI	F.16828	*Gyracanthus*	
NMI	F.16831	*Gyracanthus*	
NMI	F.16832	*Gyracanthus*	
NMI	F.16833	*Gyracanthus*	
NMI	F.16834	*Gyracanthus sp.*	
NMI	F.16835	*Gyracanthus sp.*	
NMI	F.16836	*Gyracanthus sp.*	Acanthodii
NMI	F.16837	*Gyracanthus sp.*	
NMI	F.16838	*Gyracanthus sp.*	
NMI	F.16849	*Gyracanthus sp.*	
NMI	F.16854	*Gyracanthus sp.*	
NMI	F.16857	*Gyracanthus sp.*	
NMI	F.16858	*Gyracanthus sp.*	
NMI	F.16860	*Gyracanthus sp.*	
NMI	F.16861	*Gyracanthus sp.*	
NMI	F.16864	*Gyracanthus sp.*	
NMI	F.16876	*Gyracanthus sp.*	
NHMUK	P.9604	*Myriolepis hibernica*	
NMI	F.16855	*Campylopleuron*	
NMI	F.16862	Actinopterygian indet.	Actinopterygii
TCD	38367	Actinop indet.	
TCD	38368	Palaeoniscoid-type fish	
NHMUK	P.3325d	*Megalichthys hibberti*	
NHMUK	P.41851_1	*Megalichthys hibberti*	
NMI	F.16840	*Megalichthys hibberti*	
NMI	F.16841	*Megalichthys hibberti*	
NMI	F.16842	*Megalichthys hibberti*	
NMI	F.16846	*Megalichthys hibberti*	Sarcopterygii
NMI	F.16847	*Megalichthys hibberti*	
NMI	F.16853	*?Megalichthys hibberti*	
NMI	F.16856	*Megalichthys hibberti*	
NMI	F.16868	*Megalichthys hibberti*	
NMI	F.16874	*Megalichthys hibberti*	

NMI	F.16878	*Megalichthys hibberti*	
NMI	F.16879	*Megalichthys hibberti*	
NMI	F.16880	*cf. Megalichthys hibberti*	
NMI	F.16882	*cf. Megalichthys hibberti*	
NMI	F.16884	*cf. Megalichthys hibberti*	
NMI	F.16886	*Megalichthys hibberti*	
TCD	38359	*cf. Megalichthys hibberti*	
TCD	38364	*cf. Megalichthys hibberti*	
NMI	F.16865	*Rhizodopsis sp.*	
NMI	F.16867	*Rhizodopsis sp.*	
TCD	38366	*Rhizodopsis sp.*	
NHMUK	P.41851_3	*Sagenodus* sp	
NHMUK	P.41684	Sagenodus sp	
NMI	F.14740	*Sagenodus* sp.	
NMI	F.16889b	*Sagenodus* sp.	
NHMUK	P.9607	*Rhabdoderma sp.*	
NHMUK	P.41851_2	*Rhabdoderma sp.*	
NMI	F.16863	*Rhabdoderma sp.*	
NHMUK	R.8459	Rhipitistian indet.	
NMI	F.16845	Sarcopterygian indet.	
NMI	F.16848	Sarcopterygian *indet.*	
NMI	F.16866	Sacropterygian indet.	
NMI	F.16869a	Sacropterygian indet.	
NHMUK	R.8465	*Ophiderpeton brownriggii*	
NMI	F.14762	*Ophiderpeton brownriggii*	
NMI	F.14879	*Ophiderpeton brownriggii*	
NMI	F.16850/16852	*Ophiderpeton brownriggii*	
TCD	T89	*Ophiderpeton brownriggii*	
TCD	T90	*Ophiderpeton brownriggii*	
TCD	T88	*Ophiderpeton brownriggii*	
TCD	38353	*Ophiderpeton brownriggii*	
NHMUK	R.8466	*"Dolichosoma" emersoni*	
NMI	F.14732	*"Dolichosoma emersoni"* + fish scales	
NMI	F.14733	*"Dolichosoma emersoni"* and *Gyracanthus*	Tetrapodomorpha
TCD	38350	? "*Dolichosoma" emersoni*	
NHMUK	R.8447	Aistopod indet.	
NHMUK	R.8448	Aistopod indet.	
NHMUK	R.8449	Aistopod indet.	
NHMUK	R.8462	Aistopod indet.	
NMI	F.14730	Aistopod indet.	
NMI	F.14731	Aistopod indet.	
NMI	F.14736	Aistopod indet.	
NMI	F.14737	Aistopod indet.	
NMI	F.14738	Aistopod indet.	
NMI	F.14739	Aistopod indet.	

NMI	F.14743	Aistopod indet.	
NMI	F.14888	Aistopod indet.	
TCD	38365	Aistopod indet.	
TCD	38360	Aistopod indet.	
NHMUK	R.8454	Colosteidae indet.	
NHMUK	R.8455	Colosteidae indet.	
NHMUK	R.8458	Colosteidae indet.	
NHMUK	R.8473+R.8451	Colosteid indet. + Embolomer indet.	
NMI	F.16890	Colosteid indet.	
NMI	F.14718	*Megalocephalus pachycephalus*	
NHMUK	R.8453	Procochleosaurus jarrowensis	Tetrapoda
NMI	F.14713	*Dendrerpeton rugosum*	
TCD	T84	*Dendrerpeton rugosum*	
NHMUK	R.8457	Keraterpeton galvani	
NHMUK	R.8460	Keraterpeton galvani	
NHMUK	R.8452	Keraterpeton galvani	
NHMUK	R.8472	Keraterpeton galvani	
NHMUK	R.8468	cf. Keraterpeton galvani	
NMI	F.14711	*Keraterpeton galvani*	
NMI	F.14712	*Keraterpeton galvani*	
NMI	F.14714	*Keraterpeton galvani*	
NMI	F.14715	*Keraterpeton galvani*	
NMI	F.14734	*Keraterpeton galvani*	
NMI	F.14735	*Keraterpeton galvani*	
NMI	F.14742	*Keraterpeton galvani*	
NMI	F.16888	*Keraterpeton galvani*	
TCD	R252	*Keraterpeton galvani*	
TCD	38352	*Keraterpeton galvani*	
NHMUK	R.8469	*Urocordylus wandesfordii*	
NHMUK	R.8471	cf. *Urocordylus wandesfordii*	
NMI	F.14691	*Urocordylus wandesfordii*	
NMI	F.14691	*Urocordylus wandesfordii*	
NMI	F.14716	*Urocordylus wandesfordii*	
NMI	F.14729	*Urocordylus wandesfordii*	
TCD	T83	*Urocordylus wandesfordii*	
TCD	38354	*Urocordylus wandesfordii*	
TCD	38363	*Urocordylus wandesfordii*	
TCD	T85	*Lepterpeton dobbsii*	
NMI	F.14741	*Anthracosaurus edgei*	
NMI	F.16891	*Anthracosaurus edgei*	
NMI	F.16870	*Ichthyerpeton bradleyae*	
TCD	T87	*Ichthyerpeton bradleyae*	
TCD	38351	*Ichthyerpeton bradleyae*	
NHMUK	R.9718	Anthracosaur indet.	
NHMUK	R.8470	Embolomere indet.	
NMI	F.16843	Embolomere indet.	

NMI	F.16869b	cf. Embolomere indet.	
NMI	F.16871	Embolomere indet.	
NMI	F.16875	cf. Embolomere indet.	
NMI	F.16887	Embolomere indet.	
NMI	F.18668	Embolomere indet.	
NHMUK	R.8456	Tetrapod indet.	
NHMUK	R.8461	Tetrapod indet.	
NHMUK	R.8463	Tetrapod indet.	
NHMUK	R.8464	Tetrapod indet.	
NHMUK	R.8467	Tetrapod indet.	
NHMUK	R.41851	Tetrapod indet.	
NMI	F.14717	Tetrapod indet.	
NHMUK	R.1851	Tetrapod misc.	Misc + Indet.
NMI	F.16869	Fish	
NMI	F.16872	Chordata indet.	
NMI	F.16873	Fish indet.	
NMI	F.16877	Strange pattern	
NMI	F.16883	S-shaped feature	
NMI	F.16885	Block. No fossil	
NMI	F.16889a	Block	
NMI	Unsure 1	Ribs	
TCD	T85	*Lepterpeton dobbsii* latex peel	
TCD	38355	No Fossil	
TCD	38357	*No fossil*	
TCD	38358	Unidentified	
TCD	38356	Unidentified	
TCD	38361	Bone indet.	
TCD	38361	Nothing here	
TCD	38362	Unidentified	
TCD	38369	Fish Remains	

Appendix 2

List of micro-computed tomography parameters. (Note all CT-slices, STL files and Spiers files from this study available from the author at ogogaina@tcd.ie)

NHMUK.R8466 *Dolichosomatites emersoni*

Scan Nane = AOG_Aistopod_R8465_01_ [2019-02-20 03.43.14]
Xray kV = 160
Xray uA = 125
Filter Thickness = 1.000
Filter Material = Copper
Projections = 3142
exposure = 1000 msec
gain = 0
brightness = 0
digitalGain = 0
binning = 0
accumulation = 0
FramesPerProjection = 4
Vertical Mortor pos = -104.25
Reconstruction Nane = AOG_Aistopod_R8465_01_.vol
Voxel Size = 0.0486502
Rec Dim X = 2000
Rec Dim Y = 2000
Rec Dim Z = 2000
Rec min = -331.71
Rec max = 1930.89
Rec Data Type = float
Rec Bits Per Element = 32

Scan Nane = AOG_Aistopod_R8465_02_ [2019-02-20 07.16.53]
Xray kV = 160
Xray uA = 125
Filter Thickness = 1.000
Filter Material = Copper
Projections = 3142
exposure = 1000 msec
gain = 0
brightness = 0
digitalGain = 0
binning = 0
accumulation = 0
FramesPerProjection = 4
Vertical Mortor pos = -42.85
Reconstruction Nane = AOG_Aistopod_R8465_02_.vol
Voxel Size = 0.0486521
Rec Dim X = 2000
Rec Dim Y = 2000
Rec Dim Z = 2000
Rec min = -390.82
Rec max = 938.08
Rec Data Type = float
Rec Bits Per Element = 32

Scan Stitching Parameters:
Final nb of files = 3188
Min = -1.900
Max = 70.000
Binning = 0
output_data_type = uint16
output_format = tif
Compression = none
jp2factor = 10
AOG_Aistopod_R8465_02_.vol & AOG_Aistopod_R8465_01_.vol :overlap = 540 skip = 100

Ichthyerpeton bradleyae TCD.T87


```
<?xml version="1.0" encoding="utf-8"?>
<CTProfile xmlns:xsi="http://www.w3.org/2001/XMLSchema-instance"
xmlns:xsd="http://www.w3.org/2001/XMLSchema">
  <DataSetName>T89_</DataSetName>
  <ManipulatorPosition>
    <AxisPosition>0.001</AxisPosition>
    <AxisPosition>93.37013</AxisPosition>
    <AxisPosition>613.1554</AxisPosition>
    <AxisPosition>251.2675</AxisPosition>
    <AxisPosition>0</AxisPosition>
  </ManipulatorPosition>
  <CTAxisOffset>0</CTAxisOffset>
  <SafePosition>
    <AxisPosition>-210.737</AxisPosition>
    <AxisPosition>22.3549328</AxisPosition>
    <AxisPosition>613.1554</AxisPosition>
    <AxisPosition>313.305756</AxisPosition>
    <AxisPosition>0</AxisPosition>
  </SafePosition>
  <XraySettings>
    <Settings>
      <kV>220</kV>
      <uA>375</uA>
    </Settings>
  </XraySettings>
  <XrayFilterMaterial>Copper</XrayFilterMaterial>
  <XrayFilterThickness>1</XrayFilterThickness>
  <requiresPreprocessing>false</requiresPreprocessing>
  <preprocessingType>-1</preprocessingType>
  <XrayHead>Reflection Rotating 225</XrayHead>
  <XrayHeadNumber>1</XrayHeadNumber>
  <ShadingCorrections>
    <CorrectionName>Aodhan</CorrectionName>
  </ShadingCorrections>
  <AutomaticShadingCorrection>false</AutomaticShadingCorrection>
  <FluxNormalisation>false</FluxNormalisation>
  <FluxNormalisationRect>
    <Location>
      <X>0</X>
      <Y>4</Y>
    </Location>
```

```
    <Size>
      <Width>81</Width>
      <Height>69</Height>
    </Size>
    <X>0</X>
    <Y>4</Y>
    <Width>81</Width>
    <Height>69</Height>
  </FluxNormalisationRect>
  <ImagingSettings binning="0" exposure="354" gain="4" brightness="0" digitalGain="0"
accumulation="0" WhiteToBlackLatency="20000" BlackToWhiteLatency="0"
WhiteToWhiteLatency="1000" lines="1">
    <transform>1</transform>
    <rotationCorrection>false</rotationCorrection>
    <imageOffsetX>24</imageOffsetX>
    <imageOffsetY>24</imageOffsetY>
    <imageSizeX>2000</imageSizeX>
    <imageSizeY>2000</imageSizeY>
    <defaultImagingMode>Histogram</defaultImagingMode>
  </ImagingSettings>
  <IntensifierField>0</IntensifierField>
  <IrisDemand>100</IrisDemand>
  <DetectorPixelSizeMM>0.2</DetectorPixelSizeMM>
  <MinimiseRingArtefacts>false</MinimiseRingArtefacts>
  <Reconstruct>false</Reconstruct>
  <ReconstructionQuality>100</ReconstructionQuality>
  <TallSampleRadius>0</TallSampleRadius>
  <UseTallSampleROI>false</UseTallSampleROI>
  <ReconstructionPCName>IT031713</ReconstructionPCName>
  <OptimiseProjections>true</OptimiseProjections>
  <Projections>3141</Projections>
  <FramesPerProjection>4</FramesPerProjection>
  <DatasetAcquisition>false</DatasetAcquisition>
  <TotalProjections>-1</TotalProjections>
  <NumberOfDatasets>1</NumberOfDatasets>
  <BeamHardeningPreset>0</BeamHardeningPreset>
  <BeamHardeningLUTFile />
  <NoiseReductionPreset>0</NoiseReductionPreset>
  <LinearInterpolation>false</LinearInterpolation>
  <MedianFilterSize>0</MedianFilterSize>
  <ProjectionImageEnhancement>None</ProjectionImageEnhancement>
  <CalculateCentreOfRotation>false</CalculateCentreOfRotation>
  <RunVolumeAnalysis>false</RunVolumeAnalysis>
  <VolumeGraphicsMacros />
  <ProfileName />
  <ProfileVersion>0</ProfileVersion>
  <ScanFlatPanel>false</ScanFlatPanel>
  <PanelScanImages>2</PanelScanImages>
  <FastPanelScan>false</FastPanelScan>
  <CentralCT>true</CentralCT>
  <VolumeOfInterest>
    <XStart>0</XStart>
    <XEnd>1999</XEnd>
    <YStart>0</YStart>
    <YEnd>1999</YEnd>
    <ZStart>0</ZStart>
```

```
   <ZEnd>1994</ZEnd>
  </VolumeOfInterest>
  <ApplyRodCorrection>false</ApplyRodCorrection>
  <Delay>
   <Hours>0</Hours>
   <Minutes>0</Minutes>
   <Seconds>0</Seconds>
  </Delay>
  <DualEnergy>false</DualEnergy>
</CTProfile>
```

Lepterpeton dobbsii TCD.T85b

```
<?xml version="1.0" encoding="utf-8"?>
<CTProfile xmlns:xsd="http://www.w3.org/2001/XMLSchema"
xmlns:xsi="http://www.w3.org/2001/XMLSchema-instance">
  <DataSetName>AOG</DataSetName>
  <ManipulatorPosition>
   <AxisPosition>0.001</AxisPosition>
   <AxisPosition>205.1432</AxisPosition>
   <AxisPosition>134.640289</AxisPosition>
   <AxisPosition>297.54425</AxisPosition>
   <AxisPosition>0</AxisPosition>
   <AxisPosition>0</AxisPosition>
  </ManipulatorPosition>
  <CTAxisOffset>0</CTAxisOffset>
  <SafePosition>
   <AxisPosition>0.928</AxisPosition>
   <AxisPosition>138.296127</AxisPosition>
   <AxisPosition>134.640289</AxisPosition>
   <AxisPosition>297.54425</AxisPosition>
   <AxisPosition>0</AxisPosition>
   <AxisPosition>0</AxisPosition>
  </SafePosition>
  <XraySettings>
   <Settings>
    <kV>75</kV>
    <uA>214</uA>
   </Settings>
  </XraySettings>
  <XrayFilterMaterial />
  <XrayFilterThickness>0</XrayFilterThickness>
  <requiresPreprocessing>false</requiresPreprocessing>
  <preprocessingType>-1</preprocessingType>
  <XrayHead>Reflection 225</XrayHead>
  <XrayHeadNumber>1</XrayHeadNumber>
  <ShadingCorrections>
   <CorrectionName>AOG</CorrectionName>
  </ShadingCorrections>
  <AutomaticShadingCorrection>false</AutomaticShadingCorrection>
```

```
  <FluxNormalisation>false</FluxNormalisation>
  <FluxNormalisationRect>
    <Location>
      <X>100</X>
      <Y>100</Y>
    </Location>
    <Size>
      <Width>100</Width>
      <Height>100</Height>
    </Size>
    <X>100</X>
    <Y>100</Y>
    <Width>100</Width>
    <Height>100</Height>
  </FluxNormalisationRect>
  <ImagingSettings binning="0" exposure="708" gain="4" brightness="0" digitalGain="0"
accumulation="0" WhiteToBlackLatency="20000" BlackToWhiteLatency="0"
WhiteToWhiteLatency="1000" lines="1">
    <transform>1</transform>
    <rotationCorrection>false</rotationCorrection>
    <imageOffsetX>24</imageOffsetX>
    <imageOffsetY>24</imageOffsetY>
    <imageSizeX>2000</imageSizeX>
    <imageSizeY>2000</imageSizeY>
    <defaultImagingMode>Histogram</defaultImagingMode>
  </ImagingSettings>
  <IntensifierField>0</IntensifierField>
  <IrisDemand>100</IrisDemand>
  <DetectorPixelSizeMM>0.2</DetectorPixelSizeMM>
  <MinimiseRingArtefacts>false</MinimiseRingArtefacts>
  <Reconstruct>false</Reconstruct>
  <ReconstructionQuality>100</ReconstructionQuality>
  <TallSampleRadius>0</TallSampleRadius>
  <UseTallSampleROI>false</UseTallSampleROI>
  <ReconstructionPCName>JN4022RECONPC</ReconstructionPCName>
  <OptimiseProjections>true</OptimiseProjections>
  <Projections>3085</Projections>
  <FramesPerProjection>1</FramesPerProjection>
  <DatasetAcquisition>false</DatasetAcquisition>
  <TotalProjections>-1</TotalProjections>
  <NumberOfDatasets>1</NumberOfDatasets>
  <BeamHardeningPreset>0</BeamHardeningPreset>
  <BeamHardeningLUTFile />
  <NoiseReductionPreset>0</NoiseReductionPreset>
  <LinearInterpolation>false</LinearInterpolation>
  <MedianFilterSize>0</MedianFilterSize>
  <ProjectionImageEnhancement>None</ProjectionImageEnhancement>
  <CalculateCentreOfRotation>false</CalculateCentreOfRotation>
  <RunVolumeAnalysis>false</RunVolumeAnalysis>
  <VolumeGraphicsMacros />
  <SafeFocusDisabled>false</SafeFocusDisabled>
```

```
  <ProfileName />
  <ProfileVersion>0</ProfileVersion>
  <ScanFlatPanel>false</ScanFlatPanel>
  <PanelScanImages>2</PanelScanImages>
  <FastPanelScan>false</FastPanelScan>
  <CentralCT>true</CentralCT>
  <VolumeOfInterest>
    <XStart>379</XStart>
    <XEnd>1588</XEnd>
    <YStart>239</YStart>
    <YEnd>1433</YEnd>
    <ZStart>0</ZStart>
    <ZEnd>1999</ZEnd>
  </VolumeOfInterest>
  <ApplyRodCorrection>false</ApplyRodCorrection>
  <Delay>
    <Hours>0</Hours>
    <Minutes>0</Minutes>
    <Seconds>0</Seconds>
  </Delay>
  <DualEnergy>false</DualEnergy>
  <HelicalScan>false</HelicalScan>
</CTProfile>
```


Ophiderpeton brownriggii NMI.F14879


```
<?xml version="1.0" encoding="utf-8"?>
<CTProfile xmlns:xsi="http://www.w3.org/2001/XMLSchema-instance"
xmlns:xsd="http://www.w3.org/2001/XMLSchema">
  <DataSetName>F14879_</DataSetName>
  <ManipulatorPosition>
    <AxisPosition>0</AxisPosition>
    <AxisPosition>161.731064</AxisPosition>
    <AxisPosition>251.950241</AxisPosition>
    <AxisPosition>171.723511</AxisPosition>
    <AxisPosition>0</AxisPosition>
  </ManipulatorPosition>
  <CTAxisOffset>0</CTAxisOffset>
  <SafePosition>
    <AxisPosition>-130.853</AxisPosition>
    <AxisPosition>147.374</AxisPosition>
    <AxisPosition>251.950241</AxisPosition>
    <AxisPosition>171.723511</AxisPosition>
    <AxisPosition>0</AxisPosition>
  </SafePosition>
  <XraySettings>
    <Settings>
      <kV>225</kV>
      <uA>120</uA>
    </Settings>
  </XraySettings>
  <XrayFilterMaterial>Copper</XrayFilterMaterial>
  <XrayFilterThickness>1</XrayFilterThickness>
  <XrayHead>Reflection Rotating 225</XrayHead>
```

```
  <XrayHeadNumber>1</XrayHeadNumber>
  <ShadingCorrections>
    <CorrectionName>Aodhan02</CorrectionName>
  </ShadingCorrections>
  <AutomaticShadingCorrection>false</AutomaticShadingCorrection>
  <FluxNormalisation>false</FluxNormalisation>
  <FluxNormalisationRect>
    <Location>
      <X>0</X>
      <Y>4</Y>
    </Location>
    <Size>
      <Width>81</Width>
      <Height>69</Height>
    </Size>
    <X>0</X>
    <Y>4</Y>
    <Width>81</Width>
    <Height>69</Height>
  </FluxNormalisationRect>
  <ImagingSettings binning="0" exposure="1415" gain="4" brightness="0" digitalGain="0"
accumulation="0" WhiteToBlackLatency="20000" BlackToWhiteLatency="0"
WhiteToWhiteLatency="1000" lines="1">
    <transform>1</transform>
    <imageOffsetX>24</imageOffsetX>
    <imageOffsetY>24</imageOffsetY>
    <imageSizeX>2000</imageSizeX>
    <imageSizeY>2000</imageSizeY>
    <defaultImagingMode>Histogram</defaultImagingMode>
  </ImagingSettings>
  <IntensifierField>0</IntensifierField>
  <IrisDemand>100</IrisDemand>
  <DetectorPixelSizeMM>0.2</DetectorPixelSizeMM>
  <MinimiseRingArtefacts>false</MinimiseRingArtefacts>
  <Reconstruct>false</Reconstruct>
  <ReconstructionQuality>100</ReconstructionQuality>
  <TallSampleRadius>0</TallSampleRadius>
  <UseTallSampleROI>false</UseTallSampleROI>
  <ReconstructionPCName>IT031711</ReconstructionPCName>
  <OptimiseProjections>true</OptimiseProjections>
  <Projections>3141</Projections>
  <FramesPerProjection>1</FramesPerProjection>
  <BeamHardeningPreset>0</BeamHardeningPreset>
  <BeamHardeningLUTFile />
  <NoiseReductionPreset>0</NoiseReductionPreset>
  <LinearInterpolation>true</LinearInterpolation>
  <MedianFilterSize>0</MedianFilterSize>
  <ProjectionImageEnhancement>None</ProjectionImageEnhancement>
  <CalculateCentreOfRotation>false</CalculateCentreOfRotation>
  <RunVolumeAnalysis>false</RunVolumeAnalysis>
  <VolumeGraphicsMacros />
  <ProfileName />
  <ProfileVersion>0</ProfileVersion>
  <ScanFlatPanel>false</ScanFlatPanel>
  <PanelScanImages>2</PanelScanImages>
  <DualEnergy>false</DualEnergy>
```

```
  <VolumeOfInterest>
    <XStart>0</XStart>
    <XEnd>1999</XEnd>
    <YStart>0</YStart>
    <YEnd>1999</YEnd>
    <ZStart>0</ZStart>
    <ZEnd>1999</ZEnd>
  </VolumeOfInterest>
  <ApplyRodCorrection>false</ApplyRodCorrection>
  <Delay>
    <Hours>0</Hours>
    <Minutes>0</Minutes>
    <Seconds>0</Seconds>
  </Delay>
</CTProfile>
```


Ophiderpeton brownriggii NHMUK R 8465


```
<?xml version="1.0" encoding="utf-8"?>
<CTProfile xmlns:xsi="http://www.w3.org/2001/XMLSchema-instance"
xmlns:xsd="http://www.w3.org/2001/XMLSchema">
  <ProfileName>JO_1900976_Inc_Cell</ProfileName>
  <ManipulatorPosition>
    <AxisPosition>-0.0014</AxisPosition>
    <AxisPosition>223.938232</AxisPosition>
    <AxisPosition>82.40423</AxisPosition>
    <AxisPosition>0</AxisPosition>
    <AxisPosition>-0.0180000011</AxisPosition>
    <AxisPosition>0</AxisPosition>
    <AxisPosition>0</AxisPosition>
    <AxisPosition>-37.95067</AxisPosition>
  </ManipulatorPosition>
  <CTAxisOffset>0</CTAxisOffset>
  <XraySettings>
    <Settings>
      <kV>100</kV>
      <uA>340</uA>
    </Settings>
  </XraySettings>
  <XrayFilterMaterial>Aluminium</XrayFilterMaterial>
  <XrayFilterThickness>1.5</XrayFilterThickness>
  <XrayHead>UltraFocus</XrayHead>
  <XrayHeadNumber>0</XrayHeadNumber>
  <ShadingCorrections>
    <CorrectionName>Shading</CorrectionName>
  </ShadingCorrections>
  <FluxNormalisation>false</FluxNormalisation>
  <FluxNormalisationRect>
    <Location>
      <X>1950</X>
      <Y>0</Y>
    </Location>
    <Size>
      <Width>49</Width>
      <Height>39</Height>
    </Size>
```

```
    <X>1950</X>
    <Y>0</Y>
    <Width>49</Width>
    <Height>39</Height>
  </FluxNormalisationRect>
  <IntensifierField>0</IntensifierField>
  <IrisDemand>100</IrisDemand>
  <ImagingSettings exposure="708" gain="0" brightness="0" digitalGain="0" binning="0"
WhiteToBlackLatency="0" BlackToWhiteLatency="0" WhiteToWhiteLatency="0" lines="0"
accumulation="0">
    <transform>1</transform>
    <imageOffsetX>24</imageOffsetX>
    <imageOffsetY>24</imageOffsetY>
    <imageSizeX>2000</imageSizeX>
    <imageSizeY>2000</imageSizeY>
    <defaultImagingMode>Histogram</defaultImagingMode>
  </ImagingSettings>
  <ScanFlatPanel>false</ScanFlatPanel>
  <PanelScanImages>2</PanelScanImages>
  <DetectorPixelSizeMM>0.2</DetectorPixelSizeMM>
  <MinimiseRingArtefacts>false</MinimiseRingArtefacts>
  <Reconstruct>false</Reconstruct>
  <ReconstructionPCName>CRL-378LJ5J</ReconstructionPCName>
  <DualEnergy>false</DualEnergy>
  <ReferenceImageFrames>0</ReferenceImageFrames>
  <OptimiseProjections>true</OptimiseProjections>
  <Projections>3142</Projections>
  <FramesPerProjection>4</FramesPerProjection>
  <VolumeOfInterest>
    <XStart>0</XStart>
    <XEnd>1999</XEnd>
    <YStart>0</YStart>
    <YEnd>1999</YEnd>
    <ZStart>0</ZStart>
    <ZEnd>1999</ZEnd>
  </VolumeOfInterest>
  <ReconstructionQuality>100</ReconstructionQuality>
  <BeamHardeningPreset>0</BeamHardeningPreset>
  <NoiseReductionPreset>-1</NoiseReductionPreset>
  <LinearInterpolation>false</LinearInterpolation>
  <MedianFilterSize>1</MedianFilterSize>
  <CalculateCentreOfRotation>true</CalculateCentreOfRotation>
  <ApplyRodCorrection>false</ApplyRodCorrection>
  <Delay>
    <Hours>0</Hours>
    <Minutes>1</Minutes>
    <Seconds>0</Seconds>
  </Delay>
</CTProfile>
```

Ophiderpeton brownriggii TCD.38363

Scan 1 (cranium):


```
<?xml version="1.0" encoding="utf-8"?>
<CTProfile xmlns:xsi="http://www.w3.org/2001/XMLSchema-instance"
xmlns:xsd="http://www.w3.org/2001/XMLSchema">
  <DataSetName>F14697_01_</DataSetName>
  <ManipulatorPosition>
    <AxisPosition>-0.002</AxisPosition>
    <AxisPosition>26.3912</AxisPosition>
    <AxisPosition>194.010635</AxisPosition>
    <AxisPosition>87.0553</AxisPosition>
    <AxisPosition>0</AxisPosition>
  </ManipulatorPosition>
  <CTAxisOffset>0</CTAxisOffset>
  <SafePosition>
    <AxisPosition>-183.519</AxisPosition>
    <AxisPosition>25.689867</AxisPosition>
    <AxisPosition>194.010635</AxisPosition>
    <AxisPosition>87.0553</AxisPosition>
    <AxisPosition>0</AxisPosition>
  </SafePosition>
  <XraySettings>
    <Settings>
      <kV>225</kV>
      <uA>115</uA>
    </Settings>
  </XraySettings>
  <XrayFilterMaterial>Copper</XrayFilterMaterial>
  <XrayFilterThickness>1.5</XrayFilterThickness>
  <XrayHead>Reflection Rotating 225</XrayHead>
  <XrayHeadNumber>1</XrayHeadNumber>
  <ShadingCorrections>
    <CorrectionName>Aodhan-5</CorrectionName>
  </ShadingCorrections>
  <AutomaticShadingCorrection>false</AutomaticShadingCorrection>
  <FluxNormalisation>false</FluxNormalisation>
  <FluxNormalisationRect>
    <Location>
      <X>0</X>
      <Y>4</Y>
    </Location>
    <Size>
      <Width>81</Width>
      <Height>69</Height>
    </Size>
    <X>0</X>
    <Y>4</Y>
    <Width>81</Width>
    <Height>69</Height>
  </FluxNormalisationRect>
```

```
  <ImagingSettings binning="0" exposure="2000" gain="4" brightness="0" digitalGain="0"
accumulation="0" WhiteToBlackLatency="20000" BlackToWhiteLatency="0"
WhiteToWhiteLatency="1000" lines="1">
    <transform>1</transform>
    <imageOffsetX>24</imageOffsetX>
    <imageOffsetY>24</imageOffsetY>
    <imageSizeX>2000</imageSizeX>
    <imageSizeY>2000</imageSizeY>
    <defaultImagingMode>Histogram</defaultImagingMode>
  </ImagingSettings>
  <IntensifierField>0</IntensifierField>
  <IrisDemand>100</IrisDemand>
  <DetectorPixelSizeMM>0.2</DetectorPixelSizeMM>
  <MinimiseRingArtefacts>false</MinimiseRingArtefacts>
  <Reconstruct>false</Reconstruct>
  <ReconstructionQuality>100</ReconstructionQuality>
  <TallSampleRadius>0</TallSampleRadius>
  <UseTallSampleROI>false</UseTallSampleROI>
  <ReconstructionPCName>IT031713</ReconstructionPCName>
  <OptimiseProjections>true</OptimiseProjections>
  <Projections>3141</Projections>
  <FramesPerProjection>1</FramesPerProjection>
  <BeamHardeningPreset>0</BeamHardeningPreset>
  <BeamHardeningLUTFile />
  <NoiseReductionPreset>0</NoiseReductionPreset>
  <LinearInterpolation>true</LinearInterpolation>
  <MedianFilterSize>0</MedianFilterSize>
  <ProjectionImageEnhancement>None</ProjectionImageEnhancement>
  <CalculateCentreOfRotation>false</CalculateCentreOfRotation>
  <RunVolumeAnalysis>false</RunVolumeAnalysis>
  <VolumeGraphicsMacros />
  <ProfileName />
  <ProfileVersion>0</ProfileVersion>
  <ScanFlatPanel>false</ScanFlatPanel>
  <PanelScanImages>2</PanelScanImages>
  <DualEnergy>false</DualEnergy>
  <VolumeOfInterest>
    <XStart>0</XStart>
    <XEnd>1999</XEnd>
    <YStart>0</YStart>
    <YEnd>1999</YEnd>
    <ZStart>0</ZStart>
    <ZEnd>1999</ZEnd>
  </VolumeOfInterest>
  <ApplyRodCorrection>false</ApplyRodCorrection>
  <Delay>
    <Hours>0</Hours>
    <Minutes>0</Minutes>
    <Seconds>0</Seconds>
  </Delay>
</CTProfile>
```

Scan 2 (body length):

<?xml version="1.0" encoding="utf-8"?>
<CTProfile xmlns:xsi="http://www.w3.org/2001/XMLSchema-instance"
xmlns:xsd="http://www.w3.org/2001/XMLSchema">
  <DataSetName>F14697_02_</DataSetName>
  <ManipulatorPosition>
    <AxisPosition>-0.001</AxisPosition>
    <AxisPosition>41.3</AxisPosition>
    <AxisPosition>294.6869</AxisPosition>
    <AxisPosition>87.0557861</AxisPosition>
    <AxisPosition>0</AxisPosition>
  </ManipulatorPosition>
  <CTAxisOffset>0</CTAxisOffset>
  <SafePosition>
    <AxisPosition>101.49</AxisPosition>
    <AxisPosition>41.7330666</AxisPosition>
    <AxisPosition>294.6869</AxisPosition>
    <AxisPosition>87.0557861</AxisPosition>
    <AxisPosition>0</AxisPosition>
  </SafePosition>
  <XraySettings>
    <Settings>
      <kV>225</kV>
      <uA>170</uA>
    </Settings>
  </XraySettings>
  <XrayFilterMaterial>Copper</XrayFilterMaterial>
  <XrayFilterThickness>1.5</XrayFilterThickness>
  <XrayHead>Reflection Rotating 225</XrayHead>
  <XrayHeadNumber>1</XrayHeadNumber>
  <ShadingCorrections>
    <CorrectionName>Aodhan-6</CorrectionName>
  </ShadingCorrections>
  <AutomaticShadingCorrection>false</AutomaticShadingCorrection>
  <FluxNormalisation>false</FluxNormalisation>
  <FluxNormalisationRect>
    <Location>
      <X>0</X>
      <Y>4</Y>
    </Location>
    <Size>
      <Width>81</Width>
      <Height>69</Height>
    </Size>
    <X>0</X>
    <Y>4</Y>
    <Width>81</Width>
    <Height>69</Height>
  </FluxNormalisationRect>
  <ImagingSettings binning="0" exposure="1415" gain="4" brightness="0" digitalGain="0"
accumulation="0" WhiteToBlackLatency="20000" BlackToWhiteLatency="0"
WhiteToWhiteLatency="1000" lines="1">
    <transform>1</transform>
    <imageOffsetX>24</imageOffsetX>
    <imageOffsetY>24</imageOffsetY>
    <imageSizeX>2000</imageSizeX>
    <imageSizeY>2000</imageSizeY>

```
    <defaultImagingMode>Histogram</defaultImagingMode>
  </ImagingSettings>
  <IntensifierField>0</IntensifierField>
  <IrisDemand>100</IrisDemand>
  <DetectorPixelSizeMM>0.2</DetectorPixelSizeMM>
  <MinimiseRingArtefacts>false</MinimiseRingArtefacts>
  <Reconstruct>false</Reconstruct>
  <ReconstructionQuality>100</ReconstructionQuality>
  <TallSampleRadius>0</TallSampleRadius>
  <UseTallSampleROI>false</UseTallSampleROI>
  <ReconstructionPCName>IT031713</ReconstructionPCName>
  <OptimiseProjections>true</OptimiseProjections>
  <Projections>3141</Projections>
  <FramesPerProjection>1</FramesPerProjection>
  <BeamHardeningPreset>0</BeamHardeningPreset>
  <BeamHardeningLUTFile />
  <NoiseReductionPreset>0</NoiseReductionPreset>
  <LinearInterpolation>true</LinearInterpolation>
  <MedianFilterSize>0</MedianFilterSize>
  <ProjectionImageEnhancement>None</ProjectionImageEnhancement>
  <CalculateCentreOfRotation>false</CalculateCentreOfRotation>
  <RunVolumeAnalysis>false</RunVolumeAnalysis>
  <VolumeGraphicsMacros />
  <ProfileName />
  <ProfileVersion>0</ProfileVersion>
  <ScanFlatPanel>false</ScanFlatPanel>
  <PanelScanImages>2</PanelScanImages>
  <DualEnergy>false</DualEnergy>
  <VolumeOfInterest>
    <XStart>0</XStart>
    <XEnd>1999</XEnd>
    <YStart>0</YStart>
    <YEnd>1999</YEnd>
    <ZStart>0</ZStart>
    <ZEnd>1999</ZEnd>
  </VolumeOfInterest>
  <ApplyRodCorrection>false</ApplyRodCorrection>
  <Delay>
    <Hours>0</Hours>
    <Minutes>0</Minutes>
    <Seconds>0</Seconds>
  </Delay>
</CTProfile>
```


Peisterpeton milnerorum TCD.T90


```
<?xml version="1.0" encoding="utf-8"?>
<CTProfile xmlns:xsi="http://www.w3.org/2001/XMLSchema-instance"
xmlns:xsd="http://www.w3.org/2001/XMLSchema">
  <DataSetName>T90_</DataSetName>
  <ManipulatorPosition>
    <AxisPosition>0</AxisPosition>
    <AxisPosition>164.747864</AxisPosition>
    <AxisPosition>270.4448</AxisPosition>
```

```
    <AxisPosition>77.3615</AxisPosition>
    <AxisPosition>0</AxisPosition>
   </ManipulatorPosition>
   <CTAxisOffset>0</CTAxisOffset>
   <SafePosition>
    <AxisPosition>-155.047</AxisPosition>
    <AxisPosition>144.6008</AxisPosition>
    <AxisPosition>270.4448</AxisPosition>
    <AxisPosition>77.3615</AxisPosition>
    <AxisPosition>0</AxisPosition>
   </SafePosition>
   <XraySettings>
    <Settings>
     <kV>225</kV>
     <uA>187</uA>
    </Settings>
   </XraySettings>
   <XrayFilterMaterial>Copper</XrayFilterMaterial>
   <XrayFilterThickness>2</XrayFilterThickness>
   <XrayHead>Reflection Rotating 225</XrayHead>
   <XrayHeadNumber>1</XrayHeadNumber>
   <ShadingCorrections>
    <CorrectionName>Aodhan-04</CorrectionName>
   </ShadingCorrections>
   <AutomaticShadingCorrection>false</AutomaticShadingCorrection>
   <FluxNormalisation>false</FluxNormalisation>
   <FluxNormalisationRect>
    <Location>
     <X>0</X>
     <Y>4</Y>
    </Location>
    <Size>
     <Width>81</Width>
     <Height>69</Height>
    </Size>
    <X>0</X>
    <Y>4</Y>
    <Width>81</Width>
    <Height>69</Height>
   </FluxNormalisationRect>
   <ImagingSettings binning="0" exposure="1415" gain="4" brightness="0" digitalGain="0"
accumulation="0" WhiteToBlackLatency="20000" BlackToWhiteLatency="0"
WhiteToWhiteLatency="1000" lines="1">
    <transform>1</transform>
    <imageOffsetX>24</imageOffsetX>
    <imageOffsetY>24</imageOffsetY>
    <imageSizeX>2000</imageSizeX>
    <imageSizeY>2000</imageSizeY>
    <defaultImagingMode>Histogram</defaultImagingMode>
   </ImagingSettings>
   <IntensifierField>0</IntensifierField>
   <IrisDemand>100</IrisDemand>
   <DetectorPixelSizeMM>0.2</DetectorPixelSizeMM>
   <MinimiseRingArtefacts>false</MinimiseRingArtefacts>
   <Reconstruct>false</Reconstruct>
   <ReconstructionQuality>100</ReconstructionQuality>
```

```
 <TallSampleRadius>0</TallSampleRadius>
 <UseTallSampleROI>false</UseTallSampleROI>
 <ReconstructionPCName>IT031711</ReconstructionPCName>
 <OptimiseProjections>true</OptimiseProjections>
 <Projections>3141</Projections>
 <FramesPerProjection>1</FramesPerProjection>
 <BeamHardeningPreset>0</BeamHardeningPreset>
 <BeamHardeningLUTFile />
 <NoiseReductionPreset>0</NoiseReductionPreset>
 <LinearInterpolation>true</LinearInterpolation>
 <MedianFilterSize>0</MedianFilterSize>
 <ProjectionImageEnhancement>None</ProjectionImageEnhancement>
 <CalculateCentreOfRotation>false</CalculateCentreOfRotation>
 <RunVolumeAnalysis>false</RunVolumeAnalysis>
 <VolumeGraphicsMacros />
 <ProfileName />
 <ProfileVersion>0</ProfileVersion>
 <ScanFlatPanel>false</ScanFlatPanel>
 <PanelScanImages>2</PanelScanImages>
 <DualEnergy>false</DualEnergy>
 <VolumeOfInterest>
  <XStart>0</XStart>
  <XEnd>1999</XEnd>
  <YStart>0</YStart>
  <YEnd>1999</YEnd>
  <ZStart>0</ZStart>
  <ZEnd>1999</ZEnd>
 </VolumeOfInterest>
 <ApplyRodCorrection>false</ApplyRodCorrection>
 <Delay>
  <Hours>0</Hours>
  <Minutes>0</Minutes>
  <Seconds>0</Seconds>
 </Delay>
</CTProfile>
```


Urocordylus wandesfordii NMI.F14716

Scan 1:


```
<?xml version="1.0" encoding="utf-8"?>
<CTProfile xmlns:xsi="http://www.w3.org/2001/XMLSchema-instance"
xmlns:xsd="http://www.w3.org/2001/XMLSchema">
 <DataSetName>T89_02A_</DataSetName>
 <ManipulatorPosition>
  <AxisPosition>0.001</AxisPosition>
  <AxisPosition>63.0618668</AxisPosition>
  <AxisPosition>397.923828</AxisPosition>
  <AxisPosition>253.973267</AxisPosition>
  <AxisPosition>0</AxisPosition>
 </ManipulatorPosition>
 <CTAxisOffset>0</CTAxisOffset>
 <SafePosition>
```

```
    <AxisPosition>-178.964</AxisPosition>
    <AxisPosition>2.53413343</AxisPosition>
    <AxisPosition>397.923828</AxisPosition>
    <AxisPosition>153.9455</AxisPosition>
    <AxisPosition>0</AxisPosition>
   </SafePosition>
   <XraySettings>
    <Settings>
     <kV>220</kV>
     <uA>264</uA>
    </Settings>
   </XraySettings>
   <XrayFilterMaterial>Copper</XrayFilterMaterial>
   <XrayFilterThickness>0.5</XrayFilterThickness>
   <requiresPreprocessing>false</requiresPreprocessing>
   <preprocessingType>-1</preprocessingType>
   <XrayHead>Reflection Rotating 225</XrayHead>
   <XrayHeadNumber>1</XrayHeadNumber>
   <ShadingCorrections>
    <CorrectionName>Aodhan-02</CorrectionName>
   </ShadingCorrections>
   <AutomaticShadingCorrection>false</AutomaticShadingCorrection>
   <FluxNormalisation>false</FluxNormalisation>
   <FluxNormalisationRect>
    <Location>
     <X>0</X>
     <Y>4</Y>
    </Location>
    <Size>
     <Width>81</Width>
     <Height>69</Height>
    </Size>
    <X>0</X>
    <Y>4</Y>
    <Width>81</Width>
    <Height>69</Height>
   </FluxNormalisationRect>
   <ImagingSettings binning="0" exposure="500" gain="4" brightness="0" digitalGain="0"
accumulation="0" WhiteToBlackLatency="20000" BlackToWhiteLatency="0"
WhiteToWhiteLatency="1000" lines="1">
    <transform>1</transform>
    <rotationCorrection>false</rotationCorrection>
    <imageOffsetX>24</imageOffsetX>
    <imageOffsetY>24</imageOffsetY>
    <imageSizeX>2000</imageSizeX>
    <imageSizeY>2000</imageSizeY>
    <defaultImagingMode>Histogram</defaultImagingMode>
   </ImagingSettings>
   <IntensifierField>0</IntensifierField>
   <IrisDemand>100</IrisDemand>
   <DetectorPixelSizeMM>0.2</DetectorPixelSizeMM>
   <MinimiseRingArtefacts>false</MinimiseRingArtefacts>
   <Reconstruct>false</Reconstruct>
   <ReconstructionQuality>100</ReconstructionQuality>
   <TallSampleRadius>0</TallSampleRadius>
   <UseTallSampleROI>false</UseTallSampleROI>
```

```
  <ReconstructionPCName>IT031711</ReconstructionPCName>
  <OptimiseProjections>false</OptimiseProjections>
  <Projections>2500</Projections>
  <FramesPerProjection>4</FramesPerProjection>
  <DatasetAcquisition>false</DatasetAcquisition>
  <TotalProjections>-1</TotalProjections>
  <NumberOfDatasets>1</NumberOfDatasets>
  <BeamHardeningPreset>0</BeamHardeningPreset>
  <BeamHardeningLUTFile />
  <NoiseReductionPreset>0</NoiseReductionPreset>
  <LinearInterpolation>false</LinearInterpolation>
  <MedianFilterSize>0</MedianFilterSize>
  <ProjectionImageEnhancement>None</ProjectionImageEnhancement>
  <CalculateCentreOfRotation>false</CalculateCentreOfRotation>
  <RunVolumeAnalysis>false</RunVolumeAnalysis>
  <VolumeGraphicsMacros />
  <ProfileName />
  <ProfileVersion>0</ProfileVersion>
  <ScanFlatPanel>false</ScanFlatPanel>
  <PanelScanImages>2</PanelScanImages>
  <FastPanelScan>false</FastPanelScan>
  <CentralCT>true</CentralCT>
  <VolumeOfInterest>
    <XStart>555</XStart>
    <XEnd>1651</XEnd>
    <YStart>570</YStart>
    <YEnd>1455</YEnd>
    <ZStart>0</ZStart>
    <ZEnd>1994</ZEnd>
  </VolumeOfInterest>
  <ApplyRodCorrection>false</ApplyRodCorrection>
  <Delay>
    <Hours>0</Hours>
    <Minutes>0</Minutes>
    <Seconds>0</Seconds>
  </Delay>
  <DualEnergy>false</DualEnergy>
</CTProfile>
```


Scan 2:


```
<?xml version="1.0" encoding="UTF-8"?>
-<CTProfile xmlns:xsd="http://www.w3.org/2001/XMLSchema"
xmlns:xsi="http://www.w3.org/2001/XMLSchema-instance">
<DataSetName>T89_02B_</DataSetName>
-<ManipulatorPosition>
<AxisPosition>0.001</AxisPosition>
<AxisPosition>156.78186</AxisPosition>
<AxisPosition>397.923828</AxisPosition>
<AxisPosition>253.974487</AxisPosition>
<AxisPosition>0</AxisPosition>
</ManipulatorPosition>
<CTAxisOffset>0</CTAxisOffset>
-<SafePosition>
<AxisPosition>-178.964</AxisPosition>
<AxisPosition>2.53413343</AxisPosition>
```

<AxisPosition>397.923828</AxisPosition>
<AxisPosition>153.9455</AxisPosition>
<AxisPosition>0</AxisPosition>
</SafePosition>
-<XraySettings>
-<Settings>
<kV>220</kV>
<uA>264</uA>
</Settings>
</XraySettings>
<XrayFilterMaterial>Copper</XrayFilterMaterial>
<XrayFilterThickness>0.5</XrayFilterThickness>
<requiresPreprocessing>false</requiresPreprocessing>
<preprocessingType>-1</preprocessingType>
<XrayHead>Reflection Rotating 225</XrayHead>
<XrayHeadNumber>1</XrayHeadNumber>
-<ShadingCorrections>
<CorrectionName>Aodhan-02</CorrectionName>
</ShadingCorrections>
<AutomaticShadingCorrection>false</AutomaticShadingCorrection>
<FluxNormalisation>false</FluxNormalisation>
-<FluxNormalisationRect>
-<Location>
<X>0</X>
<Y>4</Y>
</Location>
-<Size>
<Width>81</Width>
<Height>69</Height>
</Size>
<X>0</X>
<Y>4</Y>
<Width>81</Width>
<Height>69</Height>
</FluxNormalisationRect>
-<ImagingSettings lines="1" WhiteToWhiteLatency="1000" BlackToWhiteLatency="0"
WhiteToBlackLatency="20000" accumulation="0" digitalGain="0" brightness="0" gain="4"
exposure="500" binning="0">
<transform>1</transform>
<rotationCorrection>false</rotationCorrection>
<imageOffsetX>24</imageOffsetX>
<imageOffsetY>24</imageOffsetY>
<imageSizeX>2000</imageSizeX>
<imageSizeY>2000</imageSizeY>
<defaultImagingMode>Histogram</defaultImagingMode>
</ImagingSettings>
<IntensifierField>0</IntensifierField>
<IrisDemand>100</IrisDemand>
<DetectorPixelSizeMM>0.2</DetectorPixelSizeMM>
<MinimiseRingArtefacts>false</MinimiseRingArtefacts>
<Reconstruct>false</Reconstruct>
<ReconstructionQuality>100</ReconstructionQuality>
<TallSampleRadius>0</TallSampleRadius>
<UseTallSampleROI>false</UseTallSampleROI>
<ReconstructionPCName>IT031711</ReconstructionPCName>
<OptimiseProjections>false</OptimiseProjections>

<Projections>2500</Projections>
<FramesPerProjection>4</FramesPerProjection>
<DatasetAcquisition>false</DatasetAcquisition>
<TotalProjections>-1</TotalProjections>
<NumberOfDatasets>1</NumberOfDatasets>
<BeamHardeningPreset>0</BeamHardeningPreset>
<BeamHardeningLUTFile/>
<NoiseReductionPreset>0</NoiseReductionPreset>
<LinearInterpolation>false</LinearInterpolation>
<MedianFilterSize>0</MedianFilterSize>
<ProjectionImageEnhancement>None</ProjectionImageEnhancement>
<CalculateCentreOfRotation>false</CalculateCentreOfRotation>
<RunVolumeAnalysis>false</RunVolumeAnalysis>
<VolumeGraphicsMacros/>
<ProfileName/>
<ProfileVersion>0</ProfileVersion>
<ScanFlatPanel>false</ScanFlatPanel>
<PanelScanImages>2</PanelScanImages>
<FastPanelScan>false</FastPanelScan>
<CentralCT>true</CentralCT>
-<VolumeOfInterest>
<XStart>555</XStart>
<XEnd>1651</XEnd>
<YStart>570</YStart>
<YEnd>1455</YEnd>
<ZStart>0</ZStart>
<ZEnd>1994</ZEnd>
</VolumeOfInterest>
<ApplyRodCorrection>false</ApplyRodCorrection>
-<Delay>
<Hours>0</Hours>
<Minutes>0</Minutes>
<Seconds>0</Seconds
</Delay>
<DualEnergy>false</DualEnergy>
</CTProfile>

Urocordylus wandesfordii TCD.38354

Scan 1 (Cranium):

<?xml version="1.0" encoding="utf-8"?>
<CTProfile xmlns:xsd="http://www.w3.org/2001/XMLSchema"
xmlns:xsi="http://www.w3.org/2001/XMLSchema-instance">
  <DataSetName>AOG_UW</DataSetName>
  <ManipulatorPosition>
    <AxisPosition>-0.921</AxisPosition>
    <AxisPosition>40.6185341</AxisPosition>
    <AxisPosition>204.254578</AxisPosition>
    <AxisPosition>69.79224</AxisPosition>
    <AxisPosition>0</AxisPosition>
    <AxisPosition>0</AxisPosition>
  </ManipulatorPosition>
  <CTAxisOffset>0</CTAxisOffset>
  <SafePosition>
    <AxisPosition>-87.918</AxisPosition>

```
    <AxisPosition>0</AxisPosition>
    <AxisPosition>204.254578</AxisPosition>
    <AxisPosition>69.79224</AxisPosition>
    <AxisPosition>0</AxisPosition>
    <AxisPosition>0</AxisPosition>
   </SafePosition>
   <XraySettings>
    <Settings>
     <kV>160</kV>
     <uA>86</uA>
    </Settings>
   </XraySettings>
   <XrayFilterMaterial />
   <XrayFilterThickness>0</XrayFilterThickness>
   <requiresPreprocessing>false</requiresPreprocessing>
   <preprocessingType>-1</preprocessingType>
   <XrayHead>Reflection 225</XrayHead>
   <XrayHeadNumber>1</XrayHeadNumber>
   <ShadingCorrections>
    <CorrectionName>AOG16</CorrectionName>
   </ShadingCorrections>
   <AutomaticShadingCorrection>false</AutomaticShadingCorrection>
   <FluxNormalisation>false</FluxNormalisation>
   <FluxNormalisationRect>
    <Location>
     <X>100</X>
     <Y>100</Y>
    </Location>
    <Size>
     <Width>100</Width>
     <Height>100</Height>
    </Size>
    <X>100</X>
    <Y>100</Y>
    <Width>100</Width>
    <Height>100</Height>
   </FluxNormalisationRect>
   <ImagingSettings binning="0" exposure="500" gain="4" brightness="0" digitalGain="0"
accumulation="0" WhiteToBlackLatency="20000" BlackToWhiteLatency="0"
WhiteToWhiteLatency="1000" lines="1">
    <transform>1</transform>
    <rotationCorrection>false</rotationCorrection>
    <imageOffsetX>24</imageOffsetX>
    <imageOffsetY>24</imageOffsetY>
    <imageSizeX>2000</imageSizeX>
    <imageSizeY>2000</imageSizeY>
    <defaultImagingMode>Histogram</defaultImagingMode>
   </ImagingSettings>
   <IntensifierField>0</IntensifierField>
   <IrisDemand>100</IrisDemand>
```


Scan 2 (disarticulated postcranium):


```
?xml version="1.0" encoding="utf-8"?>
```

<CTProfile xmlns:xsd="http://www.w3.org/2001/XMLSchema"
xmlns:xsi="http://www.w3.org/2001/XMLSchema-instance">
  <DataSetName>AOG_UW2</DataSetName>
  <ManipulatorPosition>
    <AxisPosition>-1.285</AxisPosition>
    <AxisPosition>72.7514648</AxisPosition>
    <AxisPosition>458.776733</AxisPosition>
    <AxisPosition>57.6228027</AxisPosition>
    <AxisPosition>0</AxisPosition>
    <AxisPosition>-0.0003926991</AxisPosition>
  </ManipulatorPosition>
  <CTAxisOffset>0</CTAxisOffset>
  <SafePosition>
    <AxisPosition>-177.224</AxisPosition>
    <AxisPosition>0</AxisPosition>
    <AxisPosition>458.776733</AxisPosition>
    <AxisPosition>57.6228027</AxisPosition>
    <AxisPosition>0</AxisPosition>
    <AxisPosition>-0.0004908739</AxisPosition>
  </SafePosition>
  <XraySettings>
    <Settings>
      <kV>180</kV>
      <uA>57</uA>
    </Settings>
  </XraySettings>
  <XrayFilterMaterial />
  <XrayFilterThickness>0</XrayFilterThickness>
  <requiresPreprocessing>false</requiresPreprocessing>
  <preprocessingType>-1</preprocessingType>
  <XrayHead>Reflection 225</XrayHead>
  <XrayHeadNumber>1</XrayHeadNumber>
  <ShadingCorrections>
    <CorrectionName>AOG16</CorrectionName>
  </ShadingCorrections>
  <AutomaticShadingCorrection>false</AutomaticShadingCorrection>
  <FluxNormalisation>false</FluxNormalisation>
  <FluxNormalisationRect>
    <Location>
      <X>100</X>
      <Y>100</Y>
    </Location>
    <Size>
      <Width>100</Width>
      <Height>100</Height>
    </Size>
    <X>100</X>
    <Y>100</Y>
    <Width>100</Width>
    <Height>100</Height>
  </FluxNormalisationRect>
  <ImagingSettings binning="0" exposure="500" gain="4" brightness="0" digitalGain="0"
accumulation="0" WhiteToBlackLatency="20000" BlackToWhiteLatency="0"
WhiteToWhiteLatency="1000" lines="1">
    <transform>1</transform>
    <rotationCorrection>false</rotationCorrection>

```
  <imageOffsetX>24</imageOffsetX>
  <imageOffsetY>24</imageOffsetY>
  <imageSizeX>2000</imageSizeX>
  <imageSizeY>2000</imageSizeY>
  <defaultImagingMode>Histogram</defaultImagingMode>
</ImagingSettings>
<IntensifierField>0</IntensifierField>
<IrisDemand>100</IrisDemand>
<DetectorPixelSizeMM>0.2</DetectorPixelSizeMM>
<MinimiseRingArtefacts>true</MinimiseRingArtefacts>
<Reconstruct>true</Reconstruct
```